HYPOTHERMIC MACHINE PERFUSION OF CADAVERIC KIDNEYS: CLINICAL UTILITY, METABOLIC MECHANISMS AND METHODS OF OPTIMISATION

By

Kamlesh Vinodkumar Patel

MBChB, BMedSc (Hons), MRCS

A thesis submitted to the University of Birmingham for the degree of DOCTOR OF PHILOSOPHY

Institute of Metabolism and Systems Research

College of Medical and Dental Sciences

University of Birmingham

May 2020

UNIVERSITY OF BIRMINGHAM

Abstract

Hypothermic machine perfusion (HMP) is a dynamic method of preserving kidneys *ex vivo* with established clinical benefits over static cold storage (SCS). The aim of the first part of this thesis was to determine whether HMP influences clinical outcomes in the United Kingdom via registry analysis of a national dataset.

In the second part of this thesis, metabolic changes during HMP are explored using nuclear magnetic resonance (NMR) spectroscopy. Chapter 5 describes differences between HMP and SCS conditions using 1D ^{1}H NMR in a porcine donation after circulatory death (DCD) model.

Further experimental chapters use perfusion fluid supplemented with the metabolic tracer universally labelled [U^{13}-C] glucose to describe *de novo* aerobic and anaerobic metabolism in *ex vivo* kidneys during HMP. Novel developments in tracer-based NMR methodology are discussed early in the thesis.

In Chapter 6, perfusion fluid supplemented with [U^{13}-C] glucose was used to demonstrate several benefits of supplementing perfusion fluid with oxygen during HMP in a porcine DCD model.

In the final section, modified [U^{13}-C] glucose perfusion fluid demonstrated differences in *de novo* metabolism in sub-types of cadaveric kidneys prior to transplantation in a clinical study which also aimed to correlate metabolism with clinical outcome.

Acknowledgements

I would firstly like to thank my supervisors Dr Christian Ludwig and Mr Jay Nath for their advice and support during my PhD in addition to Mr Andrew Ready for his ongoing mentorship. Without the perseverance and direction of all three, our group's previous research would not have provided the basis for experiments in this thesis.

A special thanks goes to Thomas 'Chewbacca' Smith whose initial role as laboratory technician evolved to friend and PhD compatriot. Your day-to-day help and advice in the laboratory were invaluable in allowing me to perform experimental work.

I would also like to extend my thanks to the renal transplant surgeons at the Queen Elizabeth Hospital for their support of the project. I would like to thank statistician James Hodson and consultant pathologist Desley Neil for their assistance with data analysis and interpretation in addition to emergency theatre staff for facilitating 'back-bench' preparation of kidneys for machine perfusion out of hours. However, a special thanks goes to all organ donors, recipient patients and their families who consented to organs being used for research in addition to organ retrieval teams who procured those organs.

In addition to those aforementioned members of the laboratory group, I would like to thank those intercalating students, in particular Charlotte Turnbull and Will Ries, who assisted with laboratory experiments and sample preparation in addition to Alpesh Thakker who performed mass spectrometry experiments. I would like to thank Darren Perks and his colleagues at FA Gill, Wolverhampton for accommodating our ever-demanding requests for undamaged porcine kidneys.

I would like to thank our industry collaborators Peter Demuylder, Gunther Vanwezer and the rest of the team at Organ Recovery Systems for technical advice and for providing funding in addition to consumables for experimental work. I am grateful to University Hospital Birmingham Charities and the Kidney Patient Association who also provided funding for experimental work.

To my parents I am eternally grateful for providing me with the drive and determination to pursue a rewarding career and for cultivating the stamina required to complete a PhD. To my brothers, Kalpesh and Viresh, in addition to my sisters in-law, Veena and Jalpa, thank you for your continual encouragement. Last but not least, I would like to thank my wife Riya for providing much appreciated moral support since starting this PhD, and for bearing with me whilst completing the thesis write-up.

Published academic journal papers

The following papers were published as a result of work described in this thesis. Permission for inclusion in this thesis has been granted by the respective journals.

Nath J, Smith TB, **Patel K**, Ebbs SR, Hollis A, Tennant DA, Ludwig C, Ready AR. Metabolic differences between cold stored and machine perfused porcine kidneys: A 1H NMR based study. Cryobiology. 2017;74:115-20

Smith TB*, **Patel K***, Munford H, Peet A, Tennant DA, Jeeves M, Ludwig C. High-Speed Tracer Analysis of Metabolism (HS-TrAM). Wellcome Open Research. 2018; 3:5 (*denotes equal contribution)

Patel K, Nath J, Hodson J, Inston N, Ready A. Outcomes of donation after circulatory death kidneys undergoing hypothermic machine perfusion following static cold storage: A UK population-based cohort study. American Journal of Transplantation. 2018;18:1408–1414

Patel K, Smith TB, Neil D, Thakker A, Tsuchiya Y, Higgs EB, Hodges NJ, Ready AR, Nath J, Ludwig C. The effects of oxygenation on ex vivo kidneys undergoing hypothermic machine perfusion. Transplantation. 2019;103:318–327

Student supervision

During my PhD, I co-supervised two students (listed below) at the University of Birmingham who completed their intercalated BMedSci (hons) degrees in 2017.

Charlotte Turnbull	BMedSci	(1st)	completion July 2017
William Ries	BMedSci	(1st)	completion July 2017

Contents

List of figures

List of tables

List of abbreviations

Acetyl CoA	acetyl coenzyme A
a.m.u	atomic mass unit
ADP	adenosine diphosphate
AKI	acute kidney injury
AMP	adenosine monophosphate
AST	aspartate transaminase
ATP	adenosine triphosphate
AUC	area under the curve
BMI	body mass index
CI	confidence interval
CIT	cold ischaemic time
CMV	cytomegalovirus
COPE	Consortium for Organ Preservation in Europe
CRF	calculated reaction frequency
DBD	donation after brainstem death
DCD	donation after circulatory death
DGF	delayed graft function
DM	diabetes mellitus
DMSO	dimethyl sulfoxide
DNA	deoxyribonucleic acid
DSS	4,4-dimethyl-4-silapentane-1-sulfonic acid
EC	Euro-Collins
ECD	extended criteria donor
EDTA	ethylenediaminetetraacetic acid
ELISA	enzyme-linked immunosorbent assay
EM	electron microscopy
ESRD	end-stage renal disease
EVNP	*ex vivo* normothermic perfusion
FABP	fatty-acid-binding proteins
FAD	flavin adenine dinucleotide
FID	free induction decay
FT	fourier transform
GCMS	gas chromatography mass spectroscopy
GM-CSF	granulocyte-macrophage colony-stimulating factor
GSH	reduced glutathione
GST	glutathione-s-transferase

HCV	hepatitis C virus
HEPES	4-(2-hydroxyethyl)-1-piperazineethanesulfonic acid
HES	hydroxyethyl starch
HLA	human leukocyte antigen
HMP	hypothermic machine perfusion
HOC	hyper-osmolar citrate
HR-MAS	high resolution magic angle spectroscopy
HSQC	heteronuclear single quantum coherence
HTK	histidine-tryptophan-ketoglutarate solution
IGF	immediate graft function
INEPT	insensitive nuclei enhanced by polarization transfer
IQR	inter-quartile range
IRI	ischaemia reperfusion injury
KDRI	kidney donor risk index
KLF-2	Krüppel-like Factor 2
KPS-1	kidney perfusion solution-1
LDH	lactate dehydrogenase
MID	multiple ion detection
MS	mass spectroscopy
MTAC	Metabolic Tracer Analysis Core
NAD	nicotinamide adenine dinucleotide
NADH	nicotinamide adenine dinucleotide (reduced form)
NADP	nicotinamide adenine dinucleotide phosphate
NADPH	nicotinamide adenine dinucleotide phosphate (reduced form)
NGAL	neutrophil gelatinase-associated lipocalin
NHS	National Health Service
NHSBT	National Health Service Blood and Transplant
NICE	National Institute for Health and Care Excellence
NMR	nuclear magnetic resonance
NOESY	Nuclear Overhauser Spectroscopy
NRES	National Research Ethics Service
NRP	normothermic regional perfusion
PAS	Periodic acid–Schiff
PCT	proximal convoluted tubule
PEG	polyethylene glycol
PNF	primary non-function
POC	point of care
PPP	pentose phosphate pathway

RCT	randomised controlled trial
RF	radio frequency
RNA	ribonucleic acid
ROC	receiver operating characteristic
ROP	retrograde oxygen persufflation
ROS	reactive oxygen species
RPM	revolutions per minute
RR	renal resistance
RRT	renal replacement therapy
SCS	static cold storage
TBARS	thiobarbituric acid reactive substances
TCA	tri-carboxylic acid
TMNO	trimethylamine N-oxide
U-^{13}C	uniformly-labelled carbon 13
UK	United Kingdom
USA	United States of America
UW	University of Wisconsin
UW-MPS	University of Wisconsin Machine Perfusion Solution
WIT	warm ischaemic time

Chapter 1 : Introduction

Current practice in the field of Renal Transplantation is explored prior to description and discussion of hypothermic storage modalities, namely static cold storage and hypothermic machine perfusion. Following this, NMR spectroscopy and metabolism are discussed independently prior to exploring how NMR plays a role in the field of tracer-based metabolomics.

Renal Transplantation

Chronic Kidney Disease and the role of transplantation

Renal transplantation is considered the optimal treatment for patients with or approaching end stage renal disease (ESRD). The necessity to commence renal replacement therapy (RRT), including haemodialysis and peritoneal dialysis, defines ESRD (1, 2) with such dialysis modalities resulting in negative implications for quality of life (3, 4).

Renal transplantation confers several significant benefits compared to other forms of RRT including improvements to quality of life (5-7). Cohort studies also show a significant increase in patient survival (8-11), although such improvement in life expectancy is not consistently demonstrated for those over the age of 65 (12, 13). From a health economics perspective, renal transplantation is also cost-effective (14, 15) with the cost-benefit of renal transplantation estimated at £24,100 for every year a patient has a functioning graft compared to dialysis (16).

The first successful renal transplant was performed in 1954 between monozygotic twins (17) with the graft lasting for 8 years. Since then, transplantation outcomes have benefited from multiple medical advances (18) including advances in immunosuppression, donation from blood group incompatible donors, donation from circulatory death donors and laparoscopic donor nephrectomy being established as a surgical technique.

Cadaveric donation

Within the National Health Service Blood and Transplantation (NHSBT) framework in the United Kingdom, organs for transplantation are retrieved from both live donors and cadaveric donors. Cadaveric donors are divided into donation after brainstem death (DBD)

donors, formerly known as heart-beating donors, and donation after circulatory death (DCD) donors, formerly known as non-heart beating donors.

The number of renal transplants performed every year continues to increase with 3,596 renal transplants being performed in the UK between 1st April 2017 and 31st March 2018. Recent years have seen a near consistent increase in the number of organs transplanted from both DBD and DCD donors, yet despite these increasing numbers, the number of patients waiting for a renal transplant remains high. In April 2018, 5,011 patients were on the waiting list for a renal transplant (19).

Significant differences between DBD and DCD donors impact on graft quality, mainly as a result of exposure to warm ischaemia inherent to the retrieval of DCD organs but avoided in DBD donors.

DBD donors are those with an identifiable neurological insult causing damage such that patients are in an irreversible apnoeic coma, confirmed on brainstem testing. Such patients are considered dead from an ethical and legal perspective (20). The retrieval operation is commenced with an intact donor circulation. After gaining proximal and distal control, major blood vessels are cannulated prior to perfusion of abdominal viscera with chilled perfusion fluid and venting of perfusate through the inferior vena cava. Such rapid perfusion with chilled fluid, usually <10°C, cools organs whilst also clearing vasculature of blood products, thus preventing clots from forming within the organ. The aims of inducing hypothermia will be further discussed later in this chapter. The cold ischaemic time (CIT) extends from the initiation of cold perfusion until the restoration of warm circulation at the time of implantation (20). Figure 1a shows the DBD retrieval processes. DBD organs are not subject to warm ischaemia in stark contrast to the retrieval of DCD organs.

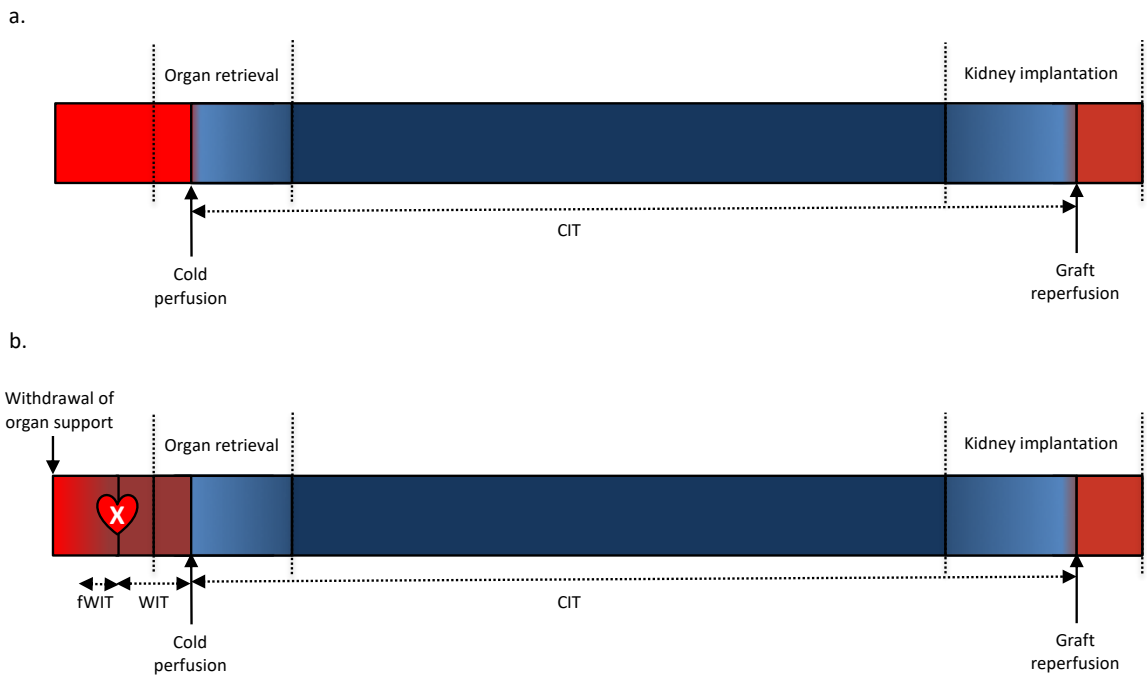

Figure 1. Schematic representation of the retrieval process for DBD(a) and DCD(b) kidneys showing the differences in visceral perfusion, starting with withdrawal of organ support for DCD organs, until graft reperfusion. Following withdrawal of organ support, kidneys experience a variable duration of functional warm ischaemic time (fWIT) prior to a period of warm ischaemic time (WIT) including a non-touch period prior to the retrieval operation commencing. The cold ischaemic time (CIT) for both DBD and DCD organs commences when abdominal viscera are cold perfused in-situ.

DCD organs are sub-classified as defined by the Maastricht criteria (21) which has been modified in recent years (22). This updated classification refers to the location of cardiac arrest and manner in which asystole is reached. In the UK, nearly all DCD organs are retrieved from Maastricht category III donors where circulatory arrest is expected. These donors have usually suffered severe irrecoverable neurological insult to the extent where further medical intervention is not thought to be of benefit, although such donors do not meet the criteria of brainstem death.

Following cessation of life-supporting treatment, typically inotropic and ventilatory support (23), organs are exposed to states of hypoxia and hypoperfusion before the donor reaches asystole. In the UK, once death is confirmed, the retrieval operation can commence following a five minute mandatory non-touch period although the duration of this period

varies internationally. The priority during subsequent laparotomy, performed according to national protocol (24), is arterial cannulation prior to re-perfusion of organs with chilled preservation fluid.

In countries such as Spain (25), France (26) and USA (27), additional DCD organs may be procured from uncontrolled donors in whom circulatory death was not expected but the cause of cardiac arrest is deemed to be non-reversible.

The warm ischaemic time (WIT) is defined as the time without perfusion and oxygen elapsed from the beginning of circulatory death to the start of organ perfusion either with cold flush or *in situ* normothermic perfusion (22). However, this does not reflect the period in which *in situ* organs are hypoperfused prior to asystole and therefore still exposed to warm ischaemic conditions. The definition of functional WIT (fWIT) makes reference to this period; fWIT begins when the systolic blood pressure drops below 50mmHg for at least two minutes after withdrawal of life sustaining treatment, continuing until the start of organ perfusion. Figure 1b shows the DCD retrieval processes with reference to asystole, WIT and fWIT.

As a result of the initial warm ischaemic insult during procurement, DCD organs are less tolerant of longer periods of cold ischaemia (28).This is reflected in the allocation system. Currently, one of each pair of DCD kidneys is allocated locally within 4 regions within the UK in an attempt to reduce CIT (19). In contrast DBD organs are allocated nationally via the NHSBT Kidney Allocation Scheme (19).

In contrast to organs such as the pancreas and lungs, the kidneys are surprisingly resilient to warm ischaemia, influencing the maximum recommended fWIT (30min and 60min vs 120min respectively) (29). Despite this resilience, it is recognised that any warm ischaemia

causes a degree of long-term functional damage with less than 20 minutes of warm ischaemia resulting in superior outcomes (30-32).

All cadaveric organs, whether DBD or DCD, vary in terms of quality with several factors identified to be independently associated with graft loss, namely donor age, cerebrovascular accident as the cause of death, renal insufficiency (serum creatinine >132 μmol/L) and a history of hypertension (33). These form the criteria for classification of sub-types of cadaveric donor as expanded criteria donors (ECD), also referred to as marginal organs or extended criteria donor organs (34). Organs are classified as ECD if the donor is aged over 60 or aged 50 to 59 with at least two of the other three co-morbidities (cerebrovascular cause of death, renal insufficiency, hypertension) (33). The simplicity of the dichotomous ECD classification benefits its use in the clinical setting to risk stratify organs.

Analysis of UK registry data determined donor risk factors determining graft outcome and patient survival following renal transplantation: donor age, history of hypertension, donor weight, length of stay in hospital and use of adrenaline. The risk factors were used to develop the UK Kidney Donor Risk Index (UK KDRI), a risk stratification tool to predict outcome for deceased donor kidneys. In the UK recent years have seen an increase in the number of organs transplanted from DCD and higher risk donors defined by UK KDRI (19, 35).

Outcomes following transplantation

Grafts are subject to a multitude of physiological insults during the transplantation process. As a consequence, a graft may exhibit immediate graft function (IGF) or delayed graft function (DGF).

When a graft fails to function immediately, patients may require dialysis in order to treat complications of renal failure, primarily hyperkalaemia, hyperuraemia and fluid overload. The requirement for dialysis in the first week following transplantation is most commonly used to define delayed graft function (DGF) (36) with the main benefit of this definition being the simplicity and relevance to everyday clinical practice. A minority of patients will remain reliant on dialysis due to primary non-function (PNF) of the graft. As with DGF, PNF includes non-functioning kidneys due to any cause. Figure 2 shows the development of possible outcomes following renal transplantation.

Long term outcomes following transplantation are described by rates of graft survival and patient survival. Graft survival is commonly defined as the time from transplantation until commencing renal replacement therapy or death (37).

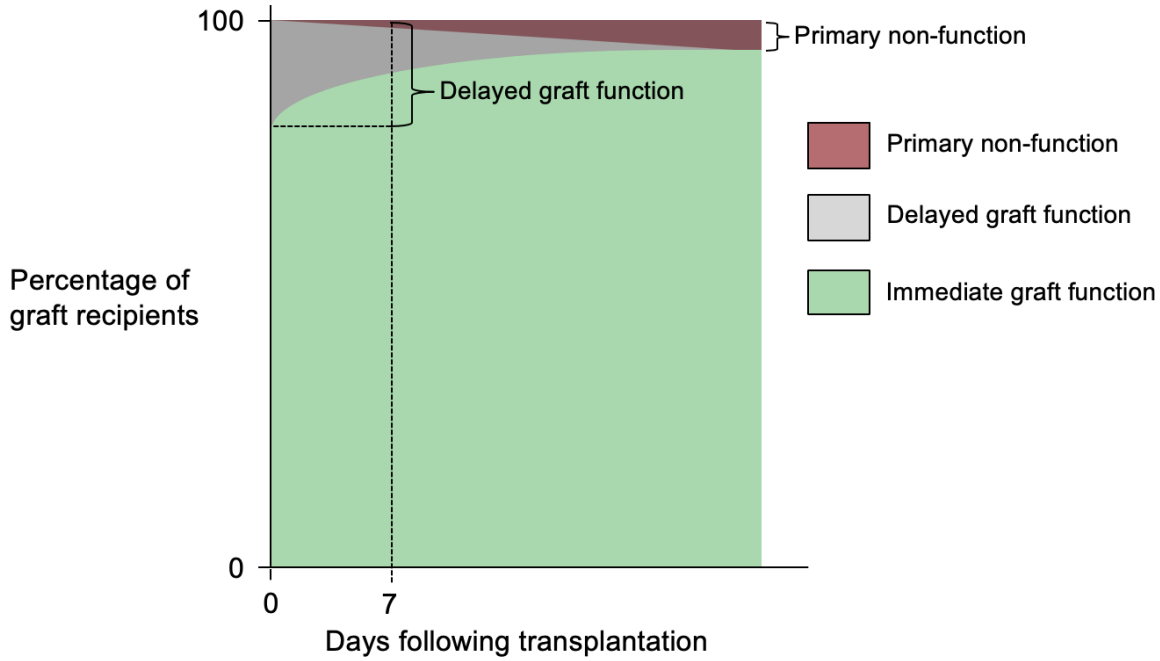

Figure 2. Clinical outcomes following renal transplantation (based on a figure by Bond et al.(38))

Consequences of DGF

In contrast with live donor kidneys which have a DGF rate of 4-9% (39), the rate of DGF in cadaveric kidneys is up to 56% (40). The presence of DGF has implications for patient, clinician and healthcare provider. In addition to post-operative dialysis sessions, DGF precipitates the need for transplant imaging and renal transplant biopsies, increasing the duration of hospital admission as a result. Aside from shorter-term concerns, the development of DGF is thought to have more serious implications including the development of acute rejection, negative implications for long term renal function, graft loss (41, 42) and death with a functioning graft (43). However, in DCD kidneys such association with longer term consequences does not hold true (44, 45).

Clinical course following transplantation from cadaveric donors

In keeping with other populations such as the USA (27), UK registry analyses have shown DCD organs experience nearly double the incidence of DGF compared to DBD organs with incidences of 48.5% and 24.9% reported respectively (28). This is perhaps unsurprising given the warm ischaemic insult these organs are subject to. Despite these higher rates of DGF compared to kidneys from DBD donors, DCD kidneys have comparable long-term outcomes with similar rates of graft survival and patient survival reported (46, 47). The same cannot be said for ECD organs. Such organs are associated with a worse long-term outcome regardless of whether the deceased donor sub-type is DBD or DCD (28). Despite this, due to the demand for cadaveric organs, the utilisation of ECD kidneys is increasing (19).

Of note, cold ischaemic time in static hypothermic conditions is a major determinant of many outcomes in cadaveric kidneys including DGF, PNF and graft survival (48),

especially in ECD and DCD organs (46). Such detrimental effects are particularly detrimental if CIT is prolonged (49).

Live donor transplantation involves a short CIT compared to cadaveric donation as a result of planned, usually same-site transplantation from relatively healthy individuals with low rates of DGF as a consequence (39). In contrast, donor factors, the retrieval process and logistical complexities in combination with the nature of emergency operating contribute to the inferior outcomes of cadaveric donation.

Organ Preservation

Since early work by Carrel and Lindbergh (50) performed even prior to the first successful renal transplant there has been interest in *ex vivo* organ perfusion. Initial interest in normothermic (51) and hypothermic methods of organ preservation faded away with the advent of static cold storage, a cheap, effective method of storing and transporting organs. In this chapter, hypothermic methods of organ preservation, namely static cold storage and hypothermic machine perfusion, are discussed. Normothermic perfusion is discussed later in Chapter 8.

Static Cold Storage

Figure 3 (a) Insulated box for transport of kidneys with attached tag showing laterality and transport information with (b) kidney contained internally surrounded by crushed ice

Static cold storage (SCS), the most common method of organ preservation worldwide (52), involves placing a kidney into an impermeable bag surrounded with chilled preservation fluid. This inner bag is surrounded by two bags, each containing chilled preservation fluid, then surrounded by ice in an insulated box (Figure 3). As a preservation modality SCS is simple and cheap.

The maintenance of hypothermia at 4°C reduces metabolism and enzyme activity within cells. At lower temperatures, freezing can occur resulting in coagulative necrosis on reperfusion. Whilst initial organ flush via the renal artery cools the kidney internally, subsequent maintenance of hypothermia occurs via heat transfer to surrounding fluid and ice.

In addition to the effects of hypothermia, the efficacy of SCS is in part due to changes effected by constituents of the surrounding preservation fluid, some of which attempt to counteract the detrimental effects of hypothermia and hypoxia. These effects, namely cell swelling, acidosis and the formation of reactive oxygen species (ROS), are key components of Ischaemia Reperfusion injury (IRI) discussed in more depth later in the introductory chapters.

Commercially available static cold storage preservation fluids

The composition of SCS preservation fluids varies widely yet the aims remain the same; to maintain intra-cellular fluid composition and prevent cell swelling using a combination of impermeants and colloids, to neutralise acidosis using buffers and to scavenge ROS. Table 1 shows the composition of key fluids used in SCS.

The elimination of magnesium from the first described Collins solution (53, 54) lead to the development of EuroCollins (EC) solution (55), commonly used in clinical practice for SCS until the early 1990's when it was replaced by Belzer's University of Wisconsin (UW) solution. Collins and EC solutions relied on glucose to maintain a high osmotic pressure with a Na^+/K^+ electrolyte composition reflecting intra-cellular fluid in an attempt to stop sodium influx which is responsible for cell swelling. However, the high glucose composition was deemed to be responsible for lactate accumulation rendering it an ineffective

impermeant. UW solution, now the commonly used industry gold standard for SCS (56), replaced glucose with the impermeants lactobionate and raffinose whilst maintaining a similar composition of electrolytes. Notably, UW includes ROS scavengers such as glutathione and allopurinol and hydroxyethyl starch (HES) as a colloid to provide significant oncotic pressure. However the choice of HES as a colloid within UW solution is contentious as it increases viscosity (57), consequently increasing aggregation of red blood cells (58, 59) which may contribute to patchy reperfusion patterns in the clinical setting (60). An alternative colloid, Polyethylene glycol (PEG), has been suggested as a less viscous alternative to HES (61).

Hyperosmolar citrate (HOC) in contrast, uses mannitol which acts as both a buffer and ROS scavenger. HOC also has an electrolyte composition which is dissimilar to both intra and extra-cellular fluid.

Several trials have compared the outcomes following the use of different SCS fluids, with one systematic review concluding that EC solution is associated with a higher incidence of DGF compared to preservation with UW or histidine-tryptophan-ketoglutarate solution (HTK) (62). In the UK, almost organs are transported to transplant centres in SCS conditions, relevant given its low cost and simplicity.

Table 1. Composition of SCS preservation fluids (table adapted from Maathius et al. 2008(66)). All concentrations in mM unless otherwise stated

	EC (55)	HOC (63)	UW (64)	HTK (65)
Colloids				
HES (g/l)	-	-	50	-
PEG-35 (g/l)	-	-	-	-
Impermeants				
Citrate	-	80	-	-
Glucose	195	-	-	-
Histidine	-	-	-	198
Lactobionate	-	-	100	-
Mannitol	-	185	-	38
Raffinose	-	-	30	-
Sucrose	-	-	-	-
Buffers				
Citrate	-	80	-	-
Histidine	-	-	-	198
K_2HPO_4	15	-	-	-
KH_2PO_4	43	-	25	-
$NaHCO_3$	10	-	-	-
NaH_2PO_4	-	-	-	-
Na_2HPO_4	-	-	-	-
Electrolytes				
Calcium	-	-	-	0.0015
Chloride	15	-	20	32
Magnesium	-	-	-	4
Magnesium sulphate	-	40	5	-
Potassium	115	79	120	9
Sodium	10	84	25	15
ROS Scavengers				
Allopurinol	-	-	1	-
Glutathione	-	-	3	-
Mannitol	-	185	-	38
Tryptophan	-	-	-	2
Additives				
Adenosine	-	-	5	-
Glutamic acid	-	-	-	-
Ketoglutarate	-	-	-	1

Hypothermic Machine Perfusion

Hypothermic machine perfusion (HMP) preceded SCS as a means of preserving ex-vivo kidneys but due to claims of equivalence of clinical outcome and higher costs, declined in usage, prior to its resurgence in the last 2 decades. As the name suggests, the key benefit of HMP is similar to SCS in that metabolism and other enzymatic pathways within cells are reduced by maintaining hypothermia.

The simple principle of HMP is the constant recirculation of chilled perfusion fluid through the kidney (67) at 1-8°C via a cannulated renal artery. Fluid leaves via the renal vein, flowing back into a reservoir. Organ Recovery System's LifePort® Kidney Transporter (Itasca, IL, USA, seen in Figure 4) is a non-oxygenating pressure-controlled device whereby a desired systolic pressure is maintained. The RM3 (Waters Medical Systems, Birmingham, AL, USA), a flow-controlled system, is another such device which delivers HMP. All HMP devices are small and portable with a simple user-friendly interface making them ideal for storage of kidneys within and during transport to transplant centres.

Debate remains over which device to use. One trial observed better short-term functional outcomes with less histological damage with Organ Recovery System's LifePort® Kidney Transporter compared to kidneys perfused with Waters RM3 flow-driven system (68). Since a NICE technology appraisal in 2009 (69), the LifePort® Kidney Transporter remains the only machine recommended for HMP in the UK. Standard clinical practice is to keep the systolic pressure constant at 30mmHg (40, 70-72), although some units change pressure settings dependant on perfusion parameters (73). This sub-physiological pressure is enough to re-instigate flow in capillary beds but not high enough to result in ultra-filtration which occurs at higher pressures (74).

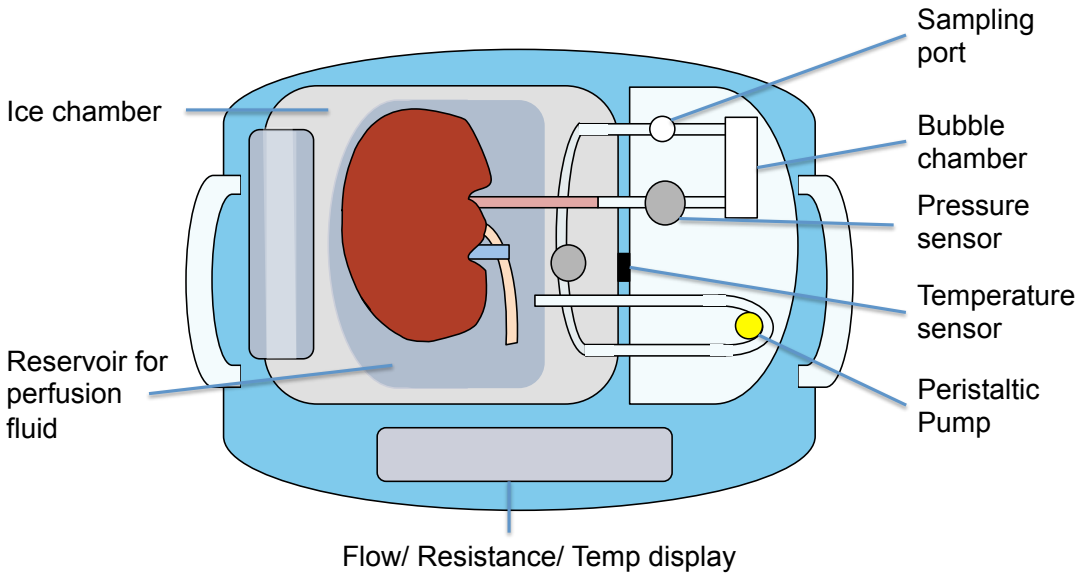

Figure 4. Schematic diagram of a LifePort® Kidney Transporter

Temperature regulation of perfusate at hypothermic temperatures is dependent on heat transfer between a reservoir of crushed ice/water and the disposable cartridge which sits within it which houses the kidney. The cartridge is covered with an inner sterile and outer plastic lid and connects to tubing which passes through the peristaltic pump, filter, sampling port, bubble chamber and pressure sensor. Measurements are provided for flow, resistance and actual pressure within the perfusion circuit. Figure 4 shows a schematic diagram showing the key components.

Two versions of the LifePort® Kidney Transporter are in clinical use with the newer version (1.1) updated with a few key features. The LifePort® 1.0 measures perfusate temperature at the interface between cartridge and ice reservoir, although this not the true temperature of circulating perfusate. The updated LifePort® 1.1 measures the temperature of the circulating perfusate itself. Added benefits include a more user-friendly interface enabling easier retrieval of perfusion parameters onto USB device and the measurement of systolic and diastolic pressure readings in the in-flow limb. Both devices are small and contains 4 rechargeable batteries making them easily portable between centres.

Figure 5. A range of portable devices commonly used for HMP: LifePort® Kidney Transporter 1.0 (a) and 1.1 (b), Kidney Assist, Organ Assist (c), Waters RM3 (d), and Waters Waves® (e).

Oxygenating HMP devices

The LifePort® Kidney Transporter v1.0 (Organ Recovery Systems, Itasca, IL, USA) and RM3 (Waters Medical Systems, Birmingham, AL, USA) featured in earlier research into HMP with newer devices incorporating updates dictated by the ever-evolving evidence

base for optimisation of HMP. Newer machines such as the Waves® preservation system (Waters Medical System, LLC; Rochester, MN, USA) and the Kidney Assist-transport (Organ Assist, Groningen, the Netherlands) incorporate a means of oxygenating circulating perfusion fluid into the HMP circuit.

Preservation fluids used for HMP

The solution most commonly used for HMP was formulated by Belzer and Southard at the University of Wisconsin (75). The solution, University of Wisconsin Machine Preservation Solution (UW-MPS), is a gluconate based solution incorporating the complex starch molecule HES similar to UW. The solution has a lower potassium content than UW, as the sodium/potassium ratio is reversed, in an attempt to reduce vasoconstriction. Notably UW-MPS includes 10mM glucose.

The constituents of UW-MPS are shown in Table 2. The perfusion fluid is available commercially as Belzer MPS® solution (Bridge to Life (Europe) ltd, London, UK) and Kidney Perfusion Solution (KPS-1, Organ Recovery Systems, Itasca, IL, USA).

Table 2. Constituents of UW-MPS (75)

Constituent	Amount in 1L (g)	Concentration (mM)
Calcium chloride (dehydrate)	0.068	0.5
Sodium hydroxide	0.70	n/a
HEPES (free acid)	2.38	10
Potassium phosphate (monobasic)	3.4	25
Mannitol (USP)	5.4	30
Glucose, beta D (+)	1.80	10
Sodium Gluconate	17.45	80
Magnesium Gluconate (D (-) gluconic acid, hemimagnesium salt)	1.13	5
Ribose, D (-)	0.75	5
Hydroxyethyl starch (HES)	50.0	n/a
Glutathione (reduced form)	0.92	3
Adenine (free base)	0.68	5
Sterile water for injection (SWI)	To 1L volume	n/a

Other solutions have been used during machine perfusion such as HTK (76), UW solution (77) and even cell culture medium (78) with varying results but UW-MPS is the standard, accepted perfusion fluid used in clinical practice.

Mechanisms of action of HMP

Early work on hypothermic machine perfusion focused on its functional benefits without full understanding of the mechanisms of action (50). However, such mechanisms are now better understood (79, 80).

Considering flow dynamics, HMP acts to reverse the vasospasm caused by hypothermia. Prior to initiating HMP there is an absence of flow in capillary beds with stasis of initial cold flush perfusion fluid. Increasing recruitment of these glomerular capillary beds with subsequent amelioration of vasospasm is likely to be the underlying mechanism by which intra-renal resistance decreases and flow increases (80). However, the presence of flow alone is not the only method by which flow dynamics change during HMP; the low potassium content of UW-MPS avoids the vasoconstriction seen in SCS solutions such as UW (81).

Figure 6 shows a typical graph of changes to flow and resistance parameters over the duration of a period of HMP. The majority of these changes to perfusion parameters occurs in the first hour of HMP.

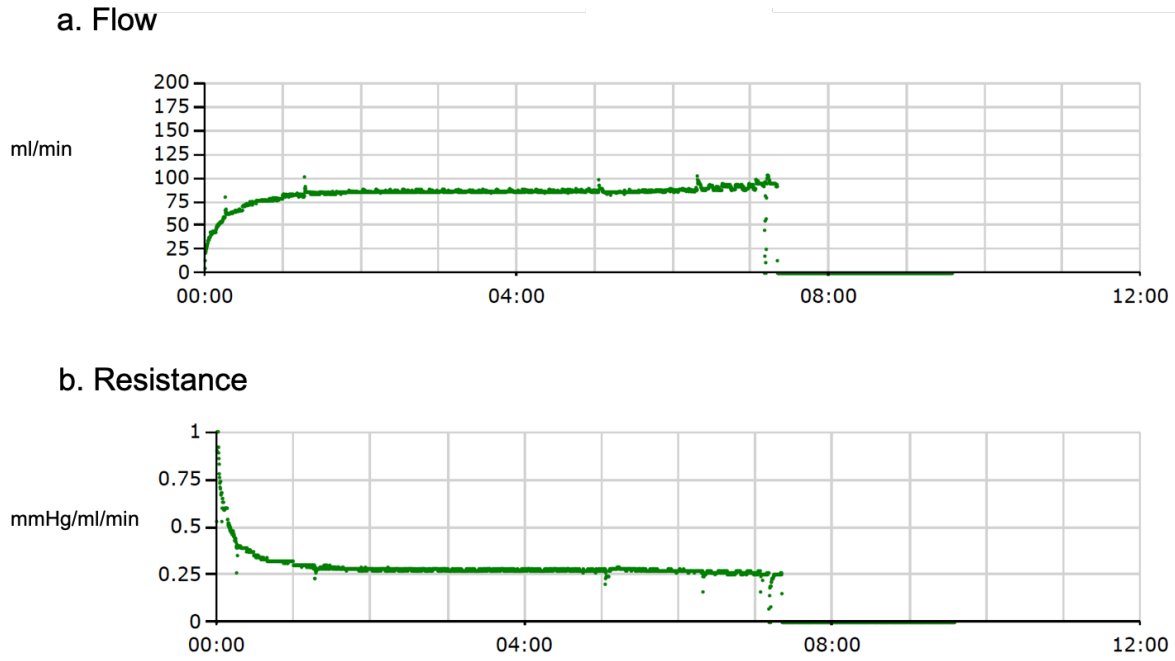

Figure 6. Typical changes in flow (a) and resistance (b) parameters during HMP using the LifePort Kidney Transporter.

On a cellular level, HMP is beneficial to both vasculature and renal parenchyma. Pulsatile flow induces shear stress and has been proposed to decrease endothelial damage through upregulation of the endothelial protective gene Kruppel-like factor 2 (KLF-2) (82, 83). KLF-2 is critical for the production of vasodilators including nitric oxide and the expression of anti-thrombogenic genes whilst potentially inhibiting pro-inflammatory responses (84-86). Vasorelaxation, proposed to be due to greater endothelial nitric oxide synthase (eNOS) phosphorylation has been observed in the HMP setting (87).

Increased cortical microcirculation on re-perfusion decreases the exposure of those areas to warm ischaemia thus kidneys with an improved circulation should have a lower incidence of DGF following implantation as a result of more uniform perfusion. This is reflected in the observation that renal resistance at the end of HMP is a risk factor for development of DGF and 1-year graft survival (88).

It is not only the presence of perfusion but also the nature of the perfusion which may promote benefit (89-91). The simulated arterial waveform during pulsatile perfusion may facilitate the re-opening of capillary beds collapsed during cold storage. In doing so, low flow rates continually wash out metabolic waste products, such as lactate, and by-products of cellular damage from the kidney. Buffers within UW-MPS prevention of the accumulation of lactate serve to maintain homeostatic pH levels within the kidney (75).

Perfusion fluid is circulated via rollator pump at low sub-physiological pressures (<30mmHg), much below the range of pressures in which ultra-filtration occurs. Conventional urine production does not occur although it is likely that the collecting system receives a small amount of fluid from upstream parts of the nephron as a consequence of damage to Bowman's capsule. However, low perfusion pressures are beneficial during HMP as they result in a lower activation of Von Willebrand factor, less damage to the proximal tubule and improved cortical microcirculation resulting in better functional recovery after transplantation (92). Unlike normothermic perfusion, Urine production cannot be used to assess graft quality during HMP.

For every 10°C reduction in temperature, metabolic rates are thought to halve (93). Hence hypothermia reduces metabolism, yet it does not cease completely. The extent to which metabolic pathways remain active during HMP has not been fully described although one would suspect it is anaerobic pathways that remain active given the largely hypoxic hypothermic environment of HMP. The 10mM glucose is readily available to cells as a metabolic substrate as it passes through vascular beds during HMP with evidence of both anaerobic and aerobic metabolism such that HMP kidneys consume more oxygen and restore ATP levels compared to SCS kidneys (94). Metabolism during HMP is further discussed later in this chapter.

Opportunities for graft assessment and optimisation

A major advantage of HMP over static storage methods is the potential to assess organ viability and potentially predict post-transplant outcomes. Perfusion parameters, perfusate biomarkers and histological scoring systems have all been evaluated as markers of outcome.

Perfusate biomarkers

Aside from a plausible biological basis, properties of a good biomarker include sensitivity and specificity for a particular outcome. Identifying such a biomarker for use during HMP would provide a multitude of benefits including preparation and counselling for DGF, and information regarding patient and graft function and longevity. With the advent of technologies such as oxygenated HMP and normothermic perfusion as a means of potentially reconditioning organs, the identification of targets which would benefit from such reconditioning would be beneficial.

Substances expelled from functioning cells or products of cell damage are washed out from the kidney during HMP. Hence the circulating perfusate can be readily sampled with changes in composition reflecting both cell damage and ongoing cell metabolism. Thus, the sampling port of the LifePort® offers a non-invasive means of monitoring changes in perfusate composition.

In recent years a weak association has been demonstrated between several biomarkers sampled during HMP and post-transplantation outcome (95, 96) demonstrating potential clinical utility. However, no one marker has or can be used in isolation for such purpose reflecting a lack of specificity and sensitivity of any one detrimental biological pathway in describing organ viability.

Biomarkers of note showing promise are lactate dehydrogenase (LDH) (96), glutathione s transferase (GST) (97) and aspartate transaminase (AST) (96). Their role is further discussed in Chapter 7.

Perfusion parameters

Given that HMP recruits capillary beds and causes vasorelaxation with beneficial reperfusion patterns, it would seem logical that renal resistance (RR) should decline over the duration of HMP. Should renal resistance start and remain high, one would speculate that irreversible ischaemic damage has occurred, therefore renal resistance should correlate with post-transplant function.

Several papers have assessed the prognostic significance of renal resistance during HMP. Two studies by Jochmans et al (88) and de Vries et al (98) are commonly quoted as showing an association between renal resistance and DGF, PNF and 1-year graft survival. However statistical analyses of the study populations showed only a limited predictive value. Hence RR should not be used to discard kidneys as described by other groups (99) where conclusions drawn are subject to bias due to the discard rates of those organs with a higher renal resistance.

Cost effectiveness of HMP

Particularly in the current economic climate from a health economics perspective, demonstration of clinical benefit must be off-set against the cost of HMP. Interestingly the National Institute for Health and Care Excellence guidance published in January 2009 (69) was based on evidence preceding the full report of the Machine Preservation Trial and other research since then. The guidance states kidney preservation with the LifePort® Kidney Transporter is one option for organ preservation as a mere alternative to static

storage with UW solution. Of the 2 cost-benefit analyses cited, the UK based analysis preceded the main evidence base of HMP (38).

Following the longer-term follow-up data of the Machine Preservation Trial, an accompanying cost-benefit analysis (100) determined there were major cost benefits in addition to the gain in life-years and quality adjusted life years (QALYs). Similar conclusions were drawn from an analysis observing the outcomes of ECD kidneys in a single centre in Spain (101). Perhaps in the wake of a lack of positive finding in UK-based HMP trials, a cost-benefit analysis of HMP in the UK has not been repeated.

Outcomes of HMP vs SCS

The clinical benefits of HMP over SCS have been analysed using case-control studies, single centre observational studies, registry analyses, randomised control trials (40, 70) and meta-analyses (102, 103). Of the evidence base, a handful of well-designed RCTs provide compelling evidence for the short-term benefits of HMP with longer term benefits in some sub-populations.

The Machine Preservation Trial, often quoted as the evidence for the benefits of HMP over SCS, was performed within the European Transplant zone observing the differences in the outcomes of 336 pairs of kidneys retrieved from both DBD and DCD donors. Importantly, HMP was initiated by a perfusionist at the time of retrieval. The trial itself recruited subjects over a one year period ending in November 2006 before being reported in 2009 (70), with a further follow-up commentary published in 2012 (71).

Donor pairs of kidneys were randomised to receive HMP or SCS prior to implantation into 672 recipients. The primary endpoint of the study was delayed graft function with

secondary endpoints included patient and graft survival. The Machine Preservation Trial observed a statistically significant difference (p=0.03) in the incidence of delayed graft function in kidneys undergoing hypothermic machine perfusion (n=77, 22.9%) compared with static cold storage (n=101, 30.1%). For DBD kidneys, HMP was associated with improved graft survival at 1 year (hazard ratio of 0.52, p=0.03).

Of the 336 pairs of kidneys included in the study, DCD kidneys made up an eighth of the sample size (12.5%); machine perfusion was associated with lower rates of DGF for DCD kidneys but it was not associated with improved 3-year graft survival. The study was not without criticism. For example, kidneys with multiple arteries, often rendering HMP difficult, are known to be associated with inferior graft outcomes (104). Organs with such anatomy were allocated to the SCS arm in the Machine Preservation Trial which may have contributed to the observed differences.

An analysis of the outcomes from all DCD kidneys in Belgium and the Netherlands which were part of the Machine Preservation Trial showed HMP significantly reduced the rate of DGF compared to SCS (69.5% vs 53.7%) but did not improve patient or graft survival. Interestingly the study did show some functional improvement with HMP; creatinine clearance was improved 1 month post-op compared to SCS kidneys (105).

A randomised controlled trial funded by the NHSBT was conducted in DCD (Maastricht category 3) donors within the UK between August 2006 and October 2007 (40). DCD donors were selected due to higher rates of DGF. In contrast to the Eurozone study, clinicians had the choice of when to initiate HMP following organ retrieval.

Results from this UK based RCT contrasted with the Eurozone transplant study. The study was stopped after 45 pairs of kidneys as analysis showed no differences were observed

between the rate of delayed graft function in HMP kidneys compared with those in SCS (58% vs 56%). Not all HMP was commenced at the time of retrieval, although the authors did not find a difference between those kidneys which did and did not undergo HMP from source.

The lack of significant difference may be attributed to a small sample size, but may also have been in part due to the delay in initiating HMP, plausible given the aforementioned mechanisms of action of HMP. Within the study however, there was no difference in outcome between those kidneys where HMP was initiated at retrieval or at arrival in transplant centre. The contrasting evidence for the European and UK experiences is interesting, particularly in the context of differences in timing of initiation of HMP. Timing of initiation is further discussed in Chapter 4.

Results of the Machine Preservation Trial suggest that HMP is most beneficial for ECD kidneys with a lower rate of DGF (106), lower rate of PNF and improved 1-year and 3-year graft survival compared with ECD kidneys stored in static cold storage.

Two meta-analyses collating the results of the above RCTs concluded that kidneys preserved with HMP had a lower incidence of DGF yet no consistent association with 1-year graft survival was observed (102, 103).

Concluding remarks

The last decade has seen a resurgence in interest in hypothermic machine perfusion with a focus on providing an evidence base describing its utility and exploring methods of optimisation.

Nuclear Magnetic Resonance Spectroscopy

Nuclear Magnetic Resonance (NMR) Spectroscopy is used to analyse the abundance and structure of organic compounds. In this section, key concepts relating to NMR spectroscopy are discussed including spin, chemical shift, j-coupling, the NMR spectrometer and pulse sequences.

Basic NMR concepts

Spin and the Boltzmann distribution

NMR spectroscopy takes advantage of the magnetic properties of certain nuclei in order to study their physical and chemical characteristics thereby determining the structure of molecules which they contribute to (107).

Isotopes of an element share the same number of protons, defining the atomic number of that element. Differing numbers of neutrons give rise to different isotopes of an element, with the summation of nucleons giving rise to the atomic mass of that element's isotope. For example, the isotopes of carbon include ^{12}C, ^{13}C and ^{14}C. The latter isotope is radioactive whilst ^{12}C and ^{13}C are stable isotopes which are considered in this thesis.

Nuclei of these isotopes possess a quantum mechanical property known as 'spin' which determines whether they are observable by NMR spectroscopy or not. Nuclei can have zero spin, such as ^{12}C, integer spin, such as ^{14}N, and half-integer spin such as ^{1}H or ^{13}C. Spin ½ nuclei occupy one of two possible spin states. Most biologically relevant nuclei have stable (i.e. non-radioactive) spin ½ isotopes (e.g. ^{1}H, ^{13}C, ^{15}N, ^{31}P). The magnetic moment of these nuclei is a consequence of nuclear mass, charge and spin; this magnetic moment is utilised in NMR spectroscopy.

In the absence of an external magnetic field, the magnetic moment of nuclei usually does not possess an orientational preference (Figure 7a). However, when nuclei inside a sample are exposed to an external, oriented, static magnetic field (B_0), as depicted in Figure 7b, nuclei with spin ½ orientate themselves either with or against the direction of the external magnetic field.

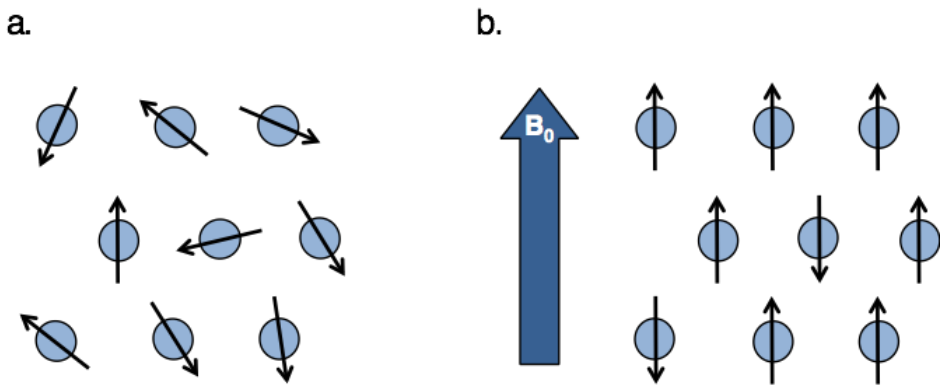

Figure 7. The orientation of the magnetic moments of nuclei in a magnetic field before and after the application of an external magnetic field (B_0)

Considering energy states, nuclei can adopt a high energy state in an anti-parallel (β) direction to the external magnetic field or a low energy state which is parallel to the external magnetic field (α) (Figure 8).

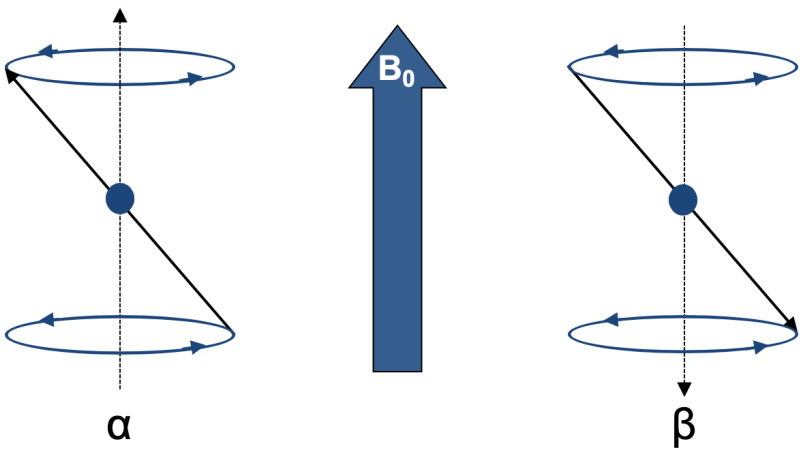

Figure 8.Parallel (α) and anti-parallel (β) spin states adopted by nuclei in B_0.

The proportion of nuclei occupying high and low energy states is described by the Boltzmann distribution (Equation 1) (107).

$$\frac{N_1}{N_2} = e^{-\Delta E/kT}$$

Equation 1. The Boltzmann distribution. N_1 and N_2 represent the number of nuclei in spin up (α) and spin down (β) configurations. ΔE is the difference in energy between the two states, k is the Boltzmann constant (1.381×10^{-23} joules/K) and T is the absolute temperature in Kelvin.

At high temperatures, almost equal numbers of nuclei occupy the high and low energy state respectively. At low temperatures, a higher proportion of nuclei occupy low energy state.

Spin is an angular momentum around the axis of the external magnetic field. The Larmor frequency is the term used to describe the frequency of precession- the frequency at which the magnetic moment precesses around the unique axis of the external magnetic field. The precession frequency (v_0) of a nucleus is proportional to the strength of the magnetic field (B_0) and the gyromagnetic ratio (γ; a constant physical property for each isotope) as described in Equation 2 (107).

$$v_0 = -\frac{\gamma}{2\pi} B_0$$

Equation 2. Calculation of the Lamor frequency/ frequency of precession (v_0) of a nucleus. B_0 represents the strength of the magnetic field. γ represents the gyromagnetic ratio.

Therefore, for a given magnetic field strength, the magnitude of the gyromagnetic ratio determines the Larmor frequency of a particular nucleus.

Chemical shift

In order to understand how ^{1}H NMR spectra differentiate molecules, it is necessary to understand two key concepts; shielding of the nucleus by the surrounding electron cloud, leading to what is known as chemical shift, and scalar coupling between different nuclei in the same molecule (also known as J-coupling) (107, 108).

Given Equation 2, it would seem that all protons in a molecule have the same resonance frequency. However, the magnetic field experienced by an individual nucleus is a combination of both the externally applied field B_0 and a small magnetic field produced by their electrons surrounding the nucleus. The net magnetic field (B_{local}) experienced by a nucleus is given by the equation below where σ denotes a shielding constant.

$$B_{local} = B_0(1 - \sigma)$$

Equation 3. Calculation of the local magnetic field (B_{local}) experienced by a nucleus where σ denotes a shielding constant and B_0 represents the external magnetic field.

A proton experiences less of the external magnetic field as a result of orbiting electrons and is therefore considered to be shielded from the effects of the external magnetic field. Electronegative groups attached to a carbon atom within a molecule draw electrons away from protons. Protons are then more exposed to the external magnetic field hence are said to be de-shielded. Thus, chemically distinct nuclei in a molecule all experience a slightly different external magnetic field strength due to differences in local chemistry.

The frequency at which a nucleus resonates is proportional to the experienced field strength. It should also be noted that differences in frequency are proportional to the strength of the external magnetic field.

$$v = \left(\frac{\gamma B_0}{2\pi}\right)(1 - \sigma)$$

Equation 4. Calculation of the Lamor frequency (v) using B_0 (the external magnetic field), σ (a shielding constant) and γ (the gyromagnetic ratio).

According to the above equation, the frequency difference between two signals in the spectrum is proportional to the strength of the external magnetic field. For example, if two signals from one molecule were 500 Hz apart on a 11.7 T magnet, they would be 900 Hz apart from each other on a 21.4 T magnet. Thus, there is a requirement for an *x* axis where corresponding signals from the same molecule resonate at the same 'frequency' independent of the strength of the external magnetic field.

The chemical shift axis is such a scale in which corresponding signals remain at the same position independent of external magnetic field strength. By referencing the absolute resonance frequency of a nucleus to the absolute resonance frequency of a reference molecule and by dividing that frequency difference by the absolute resonance frequency of the reference compound, the dependency on the external magnetic field strength is eliminated (Equation 5). The resultant chemical shift is calculated in parts per million (ppm) relative to a reference molecule.

$$\text{Chemical shift} = \frac{(\text{frequency of signal} - \text{frequency of reference}) \times 10^6}{\text{frequency of reference}}$$

Equation 5. Calculation of chemical shift.

A reference molecule must be chemically inert, such that it does not react with compounds within the sample, in addition to displaying simple, predictable signals which can be easily attributed on NMR spectra. The molecule 4,4-dimethyl-4-silapentane-1-sulfonic acid (DSS) shown in Figure 9 is commonly utilised as a reference molecule. The presence of

d^6-DSS results in a high intensity proton signal which defines the origin of the chemical shift axis.

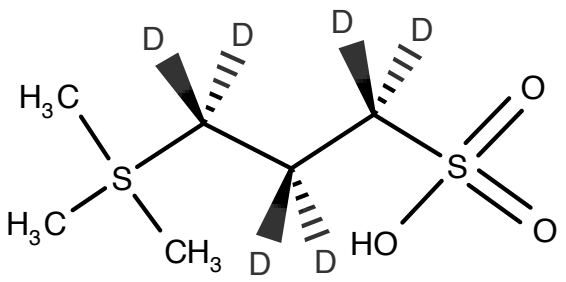

Figure 9. d^6-DSS (4,4-dimethyl-4-silapentane-1-sulfonic acid).

Figure 10 shows the consequences of shielding on chemical shift.

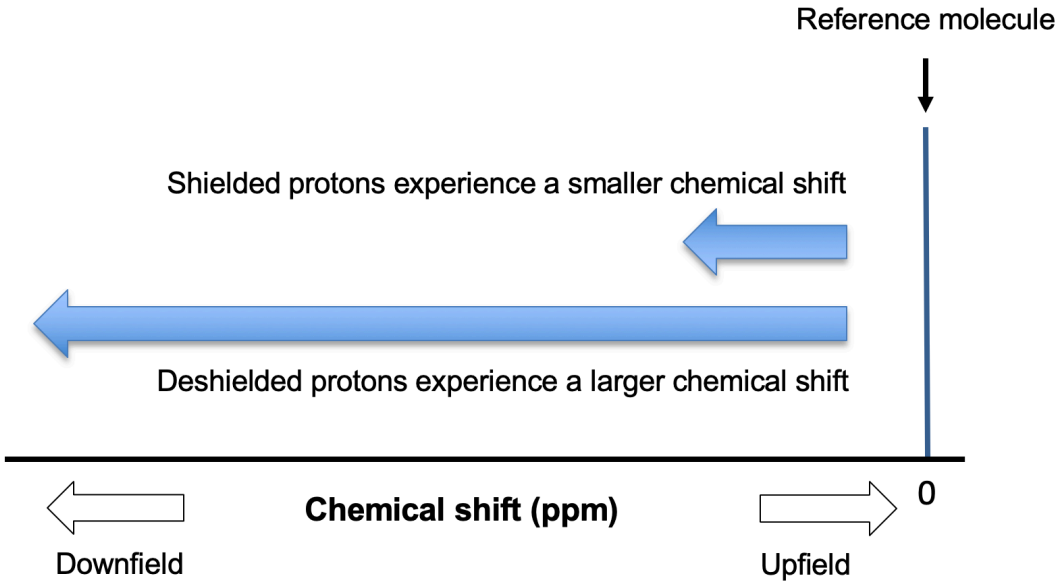

Figure 10. The effect of shielding on chemical shift.

The presence of the same electronegative group on a neighbouring carbon has a lesser effect on the magnetic field experienced by that proton as it is further away, thus the chemical shift experienced is less. Figure 11 shows the resultant chemical shift experienced by a proton according to the proximity and nature of electronegative groups

within the molecule. If more than one electronegative group acts to draw electrons away from a proton, the effect is cumulative.

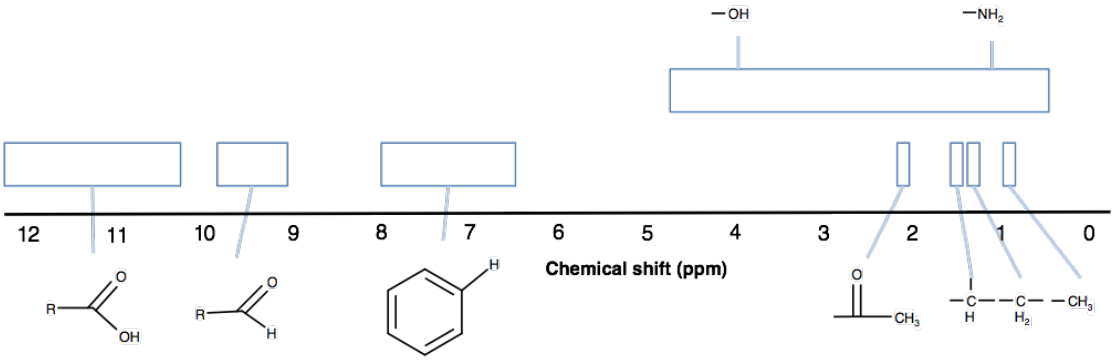

Figure 11. The effect of neighbouring electronegative groups on observed chemical shift. Blue boxes denote the position at which signals for protons appear on the chemical shift axis according to the respective proximity of the specified neighbouring electronegative groups

J-Coupling

Two adjacent nuclei in a magnetic field which both possess the property of spin will interact. The interaction, or coupling, recognises the change in magnetic field a nucleus experiences due the spin state of a nearby nucleus. Two types of coupling exist: J-coupling (or scalar coupling) and dipolar coupling (or magnetic dipole-dipole interaction), although only J-coupling will be explained here as dipolar coupling is not relevant to the work presented in this thesis (107, 108).

J-coupling is mediated via the electrons of chemical bonds, not by the spatial distance between the interacting nuclei. NMR active nuclei, in this case protons, exert the biggest influence when they are three chemical bonds or less away. Most couplings observed in 1D-^{1}H NMR spectra are either vicinal (i.e. protons attached to neighbouring carbon atoms or three chemical bonds apart from each other) or geminal (i.e. protons attached to the same carbon atom or two chemical bonds apart from each other) in the absence of ^{13}C labelling.

A neighbouring proton increases or decreases the net magnetisation experienced by a group dependant on whether this neighbouring proton is in the α or β configuration. As a single neighbouring proton can exist in either α or β state, but approximately 10^{16} molecules contribute to the same signal in the spectrum where the protons are almost equally distributed between α and β state, the signal of a group is split into two peaks due to the effect of that neighbouring proton with equal areas under each peak (1:1). The splitting of the signal for a group with two equivalent neighbouring protons is determined by the four combinations of spin states ($\alpha\alpha$, $\alpha\beta$, $\beta\alpha$ and $\beta\beta$) of those two protons which results in three unique combinations. The areas under the three resultant peaks therefore exist in the ratio 1:2:1. Continuing the same theme, the signal of a group with three

equivalent neighbouring protons is split into four peaks with areas under each peak in the ratio 1:3:3:1.

A signal with *n* number of equivalent neighbouring protons is split into *(n+1)* peaks with intensities according a Pascal triangle (Figure 12). Complex splitting patterns are encountered where neighbouring protons are non-equivalent. The distance between peaks in a signal which has been split is determined by the J-coupling constant, measured in Hz, as J-coupling is independent of the external magnetic field strength. The J-coupling constant is a measure of the interaction between a pair of non-zero net spin nuclei.

Regarding J-coupling nomenclature, the number of bonds between the two nuclei are usually indicated as leading suffix, e.g. $^{3}J_{HH}$ for a ^{1}H-^{1}H coupling three chemical bonds apart. Signal multiplets in 1D-^{1}H NMR spectra are usually dominated by $^{2}J_{HH}$ and $^{3}J_{HH}$, in the absence of ^{13}C enrichment, as the coupling constants are typically in the range of 4-15Hz. If ^{13}C nuclei are present in the sample, the $^{1}J_{CH}$ coupling will usually be the largest coupling with typical values between 120 and 165Hz.

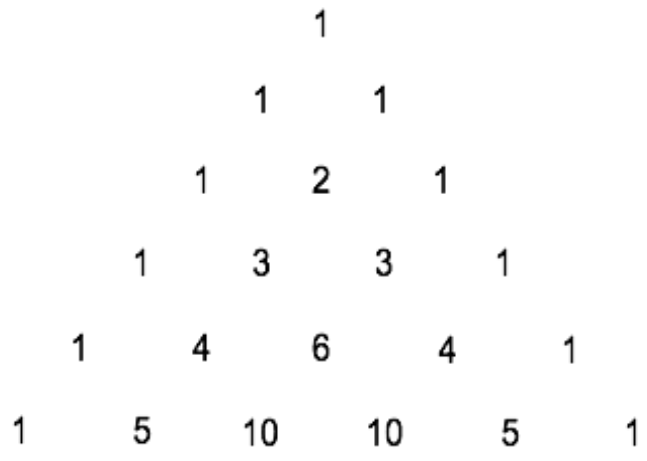

Figure 12. Pascal's triangle

Basic NMR concepts applied to 1D spectra of lactate

Chemical shift, splitting patterns and area under each signal are characterised by the chemical environment of NMR active nuclei. Therefore, NMR spectra of unknown compounds can be utilised to derive structural information about the molecule under investigation. Let us apply the aforementioned concepts to the 1D-^{1}H NMR spectra acquired of lactate which is annotated in Figure 13. The proton attached to the second of three carbons is de-shielded due to the adjacent hydroxyl group therefore experiences a larger chemical shift. The signal of C(2) seen at 4.10 ppm is split into four resonance lines (quartet) due to the combination of spin states of the three protons in the adjacent methyl group. The signal at 1.32 for the methyl group, or C(3), is split into two peaks (doublet) due to the two possible spin states of the adjacent proton attached to C(2). Signals from the oxygen bound protons are usually not observed as they are in fast exchange with the solvent, the resonance of which will be suppressed.

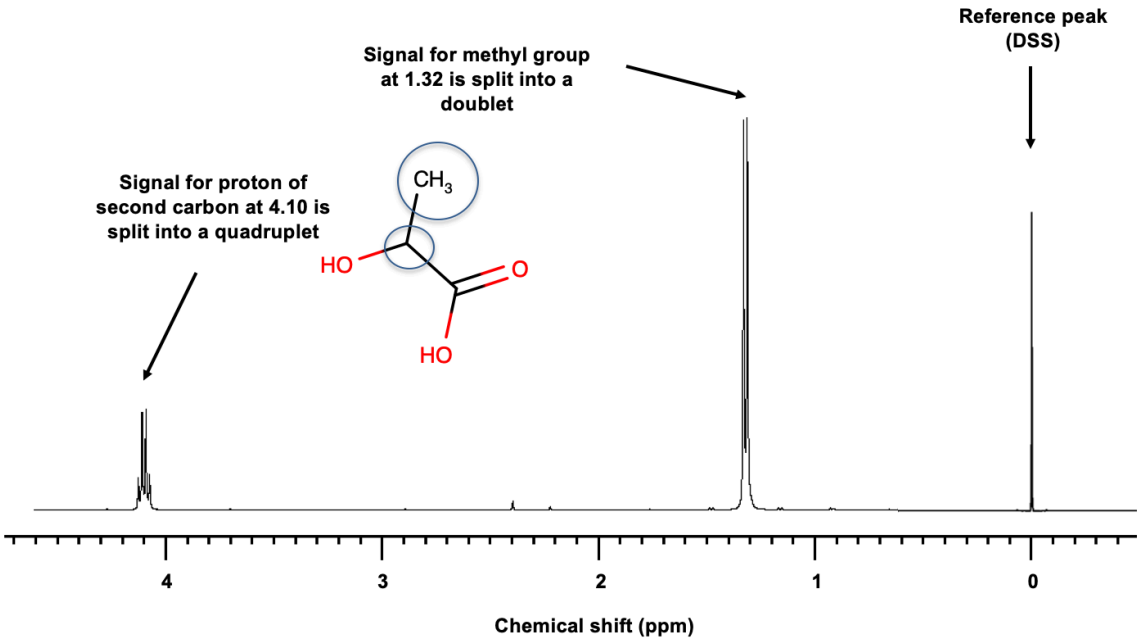

Figure 13. Annotated 1D ^{1}H NMR spectrum for ^{12}C lactate (unlabelled) where DSS is used as a reference molecule

The NMR Spectrometer

The Henry Wellcome Building at the University of Birmingham houses several NMR spectrometers varying in magnetic field strength and probe type. An NMR spectrometer is constructed from three components: The NMR magnet, the probe and the spectrometer console (107).

NMR Magnet

The homogenous magnetic field is produced by a large superconducting electromagnet. In order to reach the very large magnetic field strengths required for NMR, the magnet coil needs to be cooled down to temperatures below 6K, which is usually achieved by placing the magnet coil into a bath of liquid helium (T = 4.2K). At these temperatures the coil material becomes superconducting and hence electrical resistance of the coil is reduced to zero. Therefore, the current in the coil continues to flow in a closed system without need for further electrical power after the initial charge.

However, the field generated by such a large magnet is not homogenous enough and as a result several smaller coils known as shim coils surround the sample in order to generate the field homogeneity required. The combination of the larger magnetic field and these smaller shim coils, when calibrated, results in a homogenous magnetic field (field disturbances < $1{:}6*10^{8}$) corresponding to a linewidth less than 1Hz.

Probe

The probe is the part of the spectrometer closest to the sample. The probe in itself consists of several parts. The most important parts of a probe are the transmitter and receiver coils. The transmitter coil emits radiofrequency pulses and thus excites desired nuclei within the

sample, whereas the receiver coil, usually the same as of the transmitter coils, detects radiofrequency emitted by the sample. In order to maximise the signal-to-noise ratio in the resulting NMR spectrum, the receiver coil is positioned as close to the sample as possible.

Calibration of the probe involves tuning, the process in which the circuit resonates at the Larmor frequency, and matching, the process by which the impedance of the probe is adjusted to match that of the transmitter. The probes used in this thesis also contained a pre-amplifier cooled down to 25K to minimise spectral noise originating from electronic noise in the console. On Bruker spectrometers, this type of probe is known as a CryoProbe™.

Spectrometer Console

Following application of a pulse sequence, nuclei return to equilibrium and in doing so, release absorbed energy thereby re-orientating themselves in B_0, returning to the Boltzmann distribution regarding occupancy of alpha and beta states. It is during this time where the radiofrequency signals generated by the change in nuclei orientation are recorded, as a consequence of change in transverse magnetisation. In the acquisition phase of the pulse sequence, transient oscillations in the receiver probe are the basis of an analogue signal known as free induction decay (FID).

The spectrometer console contains all the electronic components to generate radiofrequencies, receiving the signals from the probe and digitising the analogue signal. The generated FID is further amplified and sent to the acquisition computer for data processing. The FID is converted from the time domain to the frequency domain via Fourier Transformation.

The console also contains microcontroller and real-time computers which allow the execution of pulse sequences and therefore the performance of various NMR experiments. In the following section we will discuss different pulse sequences used during NMR experiments in this thesis.

Pulse sequences

In order to understand the types of pulse sequence used in this thesis it is necessary to discuss a few key concepts relating to NMR, namely the vector model and the rotating frame concept (109, 110).

The vector model, chemical shift and quadrature detection

In simple terms, NMR spectrometers first orientate nuclei in the direction of a strong magnetic field prior to the transient application of a smaller oscillating magnetic field in the form of a radiofrequency (RF) pulse. The net magnetisation can be described as a vector in terms of the x, y and z-axes.

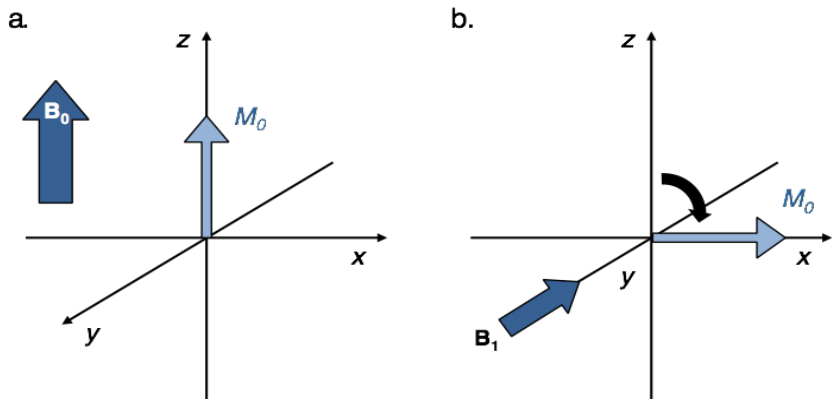

Figure 14. The effect of application of a 90-degree pulse along the y-axis on nuclei in the equilibrium state where M_0 denotes the net magnetisation, B_0 shows the direction of the external magnetic field, B_1 represents a pulse which results in a magnetic field causing an element of transverse magnetisation

The vector model refers to the changes in net magnetisation experienced as a result of the application of an RF pulse. The model assumes that the net magnetisation behaves like a classical, not quantum mechanical, magnetic field vector and can therefore be described by the Bloch equations (107). Nuclei exposed to an external magnetic field B_0 nuclei precess at the Larmor frequency; conventionally the z-axis is chosen to be parallel

to the main axis of the external magnetic field (Figure 14a). In the equilibrium state, nuclei do not possess any net transverse magnetisation, which occurs along the x- or y-axis in the vector model.

The application of a radiofrequency pulse at the Larmor frequency along the y-axis changes the net magnetisation resulting in a transverse component of magnetisation seen in Figure 14b. This angle of change of the magnetisation vector is dependent on the direction, length and duration of RF pulse applied.

The concept of rotating frame is necessary to simplify the description of changes in net magnetisation during the application of RF pulses or delays within pulse sequences. This is achieved by viewing the above vector model from the top of the z-axis much like an observation deck rotating in the *xy* plane at the Larmor frequency (see Figure 15a). The effect of an RF pulse on net magnetisation is visualised relative to the Lamor frequency in one or two axes. Figure 15a shows observation from the y-axis.

Despite consideration of precession at the Larmor frequency using the rotating frame concept, net magnetization continues to rotate due to chemical shift dispersion of resonance frequencies. The transmitter frequency remains in the middle of the spectrum, an apparent frequency of zero, therefore discrimination is required between positive and negative frequencies.

The concept of quadrature detection is used to describe detection of signals along two axes in the *xy* plane in order to differentiate between positive and negative frequencies. In Figure 15a, both rotations (positive and negative frequencies) will generate identical signals. Therefore, FT will generate the same spectrum for both as shown in Figure 15b. In Figure 15c where observation is along the x axis, both magnetization vectors will

generate the same signal again but as they start on opposite sides, FT will lead to a spectrum as displayed in Figure 15d. Summation of both spectra leads to frequency discrimination as the negative frequency signals cancel each other out as shown in Figure 15e.

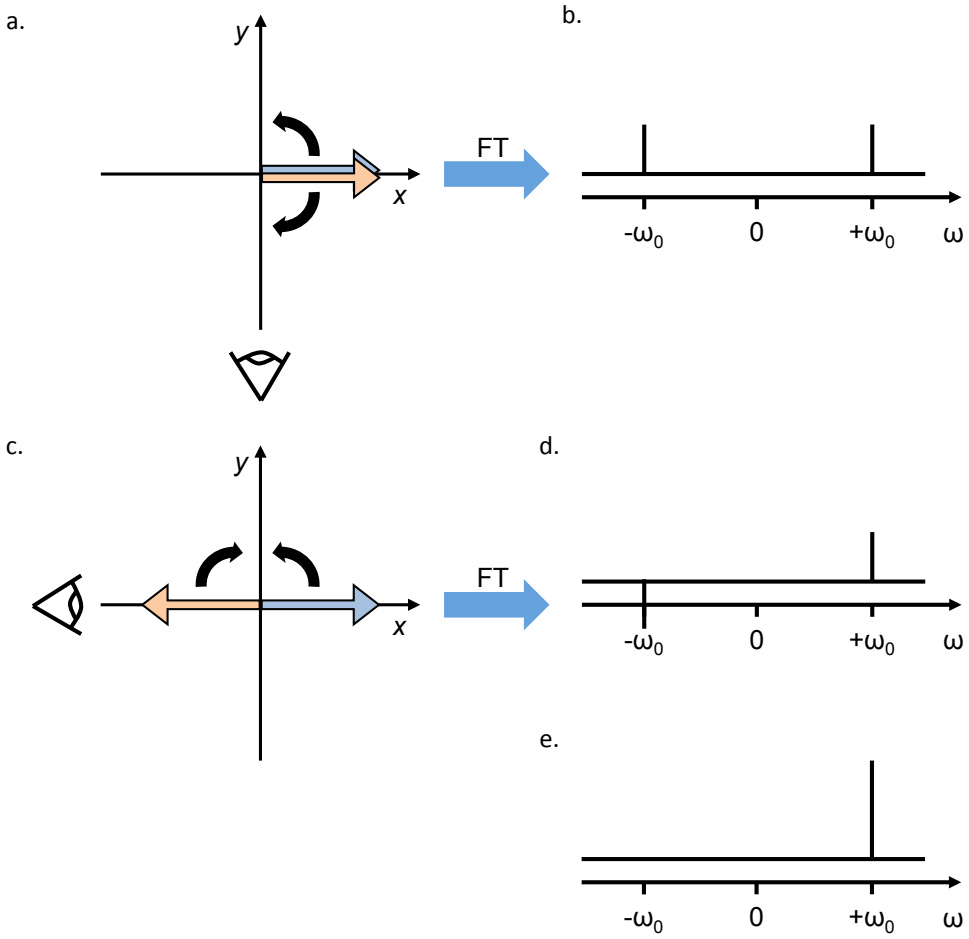

Figure 15. Pictoral representation of quadrature detection showing the effects of observation along x and y axes resulting in output spectra (b) and (d) following fourier transformation, prior to frequency discrimination. This is achieved as negative frequencies are eliminated following summation of (b) and (d) as shown in panel (e)

J-coupling occurs in addition to chemical shift. The transmitter frequency remains centred on the chemical shift in question (i.e. the centre of the multiplet generated by the coupled spin system). Initially after a 90-degree pulse, net magnetization vectors can be considered in the rotating frame shown in Figure 16, similar to Figure 15. Hence two signals are generated displayed on a spectrum separated by the J coupling constant.

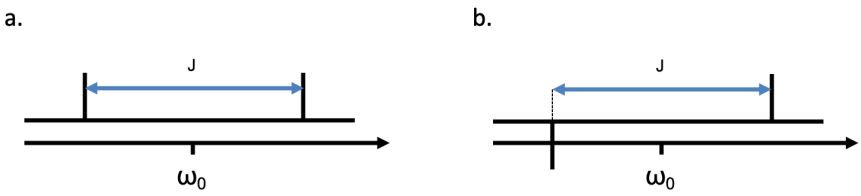

Figure 16. Representation of J-coupling showing in-phase (b) and anti-phase (d) magnetisation. J represents the J-coupling constant. The multiplet generated is centred around the chemical shift in question (ω_0)

Initially, after spin excitation through a RF pulse, magnetic moments from both spins with neighbouring spins in alpha or beta state, point in the same direction. However, because of their difference in rotation frequency, if the spins are allowed to develop their J-coupling, at some point magnetisation from spins next to neighbouring spins in alpha state will point in the opposite direction compared to the magnetisation originating from spins next to neighbouring spins in beta state. The former state is known as in-phase magnetisation, while the latter represents anti-phase magnetisation. Because the two coupled spins are in a coherent state when they are in anti-phase state, this state can be used to transfer magnetisation in pulse sequences such as the $^{1}H,^{13}C$-HSQC pulse sequence. Figure 16a represents in-phase magnetisation whilst Figure 16b represents anti-phase magnetisation which can be used to transfer magnetisation in pulse sequences such as HSQC.

Characteristics of pulses

The characteristics of a pulse include length, strength, frequency, shape and axis (109, 110). Pulse notation thus describes the effect of the applied magnetic field strength (γB_1 [Hz]), time the pulse is applied for (μs -ms) and the axis in which the pulse is applied at the frequency (ω). The most commonly used pulse is a 90-degree pulse ($\pi/2$) which results in transferring magnetisation from the *z* axis into the *xy* plane or *vice versa*. A 180-degree pulse (π) acts to invert the populations of the spin system.

A hard pulse (a pulse with a very large B_1 field strength), usually square in shape, acts to indiscriminately excite a large bandwidth of frequencies using a high-power pulse applied for a short amount of time. A soft pulse (a pulse with a much smaller B_1 field strength) acts to excite only a small bandwidth of frequencies, as narrow as a single peak, classically using lower power pulses are applied for a longer duration to achieve the same rotation angle. Adiabatic pulses, a type of shaped pulse, are able to excite a much larger bandwidth than hard pulses.

Decoupling

Decoupling simplifies an NMR spectrum as signal splitting due to J-coupling is not observed. This is of particular importance in spectra where signals from ^{1}H nuclei are split due to ^{13}C-^{1}H coupling. Decoupling is of particular use in heteronuclear single-quantum coherence (HSQC) spectra which selectively observe protons bound to ^{13}C atoms. Without decoupling, in HSQC spectra, every signal would be observed twice leading to crowded spectra. Decoupling removes signal splitting, aiding interpretation of spectra.

1D pulse sequences

1D-^{1}H NMR spectroscopy is the most commonly used high resolution experiment due to its simplicity, speed and sensitivity. Chemical shift is used to define the presence of different functional groups whilst integration of proton signals provides information on the number of protons within each signal. Due to overlap of signals there is frequently uncertainty relating to the identity of molecules and concentrations of those molecules within the sample.

The simplest 1D-^{1}H NMR experiment comprises of a preparation period and a detection period. The preparation period consists of a relaxation period prior to application of a

pulse. This is followed by the acquisition period in which FID occurs as the magnetisation of the nucleus returns to equilibrium. In reality, several transients are acquired of a sample in order to enhance the signal to noise ratio. While true signals accumulate proportionally to the number of transients, noise signals only accumulate proportionally to the square root of the number of transients. Therefore, the overall signal to noise ratio in a NMR spectrum increases with the square root of the number of transients (e.g. the signal to noise ratio will double if the number of transients is quadrupled).

The pulse sequence starts with a recycling delay followed by a 90 degree pulse ($\pi/2$) prior to acquisition time (see Figure 17). In practice, 2.2 seconds is a typical value for the time it takes to acquire the FID. Typical relaxation delays are 4-5 seconds, so that the total time it takes to acquire one transient (also known as the repetition time) is about 7 seconds.

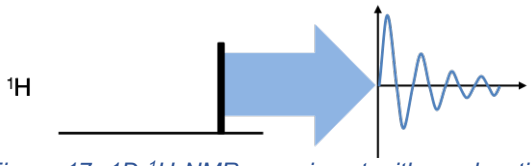

Figure 17. 1D ^{1}H NMR experiment with a relaxation period prior to a 90 degree pulse depicted by a black rectangle. Blue arrow depicts transfer of magnetization subsequent to acquisition of an FID.

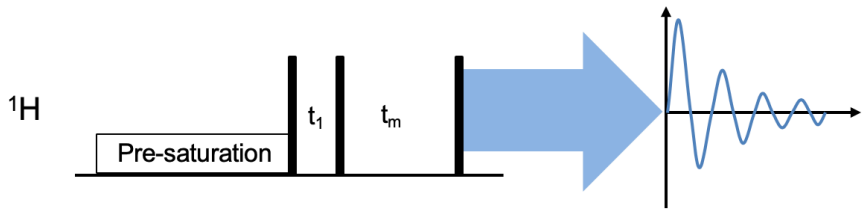

Figure 18. The NOESY pulse sequence incorporates a period of pre-saturation prior to three 90 degree pulses.

The high concentration of protons within water (approximately 110 mol/L) relative to that of any metabolite within the sample (typically 50 μM – 5 mM) warrants the signal from the solvent protons to be suppressed. Several methods for solvent suppression exist, the simplest being irradiation of the sample with a weak RF pulse for an extended period at

the frequency of the solvent resonance, known as pre-saturation. The 1D-^{1}H NMR experiments in this thesis were acquired with a slightly modified pulse sequence known as NOESY pre-saturation which results in an improved saturation of the water resonance over a simple 1D pre-saturation pulse sequence.

In the NOESY pulse sequence (Figure 18), pre-saturation is followed by a sequence of three 90 degree pulses, collectively known as a 90 degree composite pulse which leads to more even excitation across the entire spectrum than a single 90 degree pulse and enhances water suppression. It should be noted that while this pulse sequence can be used to transfer magnetisation between different protons in the same molecule, this requires the mixing time (t_m in the pulse sequence shown above) to be on the order of 450ms for small molecules. If the pulse sequence is used for enhanced water suppression, the mixing time is reduced to 10ms, so that magnetisation transfer via the nuclear Overhauser enhancement (NOE) is negligible.

A 1D spectrum targeting ^{13}C nuclei would suffer from a low signal to noise ratio due to the low abundance and low gyromagnetic ratio of this nucleus.

2D pulse sequences

2D NMR serves to give extra information that cannot be displayed on a single 1D spectrum by introducing an independent second frequency axis. A series of 1D spectra is acquired with a systematic variation of one parameter, usually a time delay during the pulse sequence. The introduction of a second dimension helps with signal overlap by increasing the signal dispersion. This aids signal assignment reducing ambiguity when assigning such signals.

Types of 2D NMR experiments include correlation experiments and Overhauser effect experiments. Correlation experiments rely on J-coupling between nuclei connected by chemical bonds. The two sub-types of correlation experiments are termed either homonuclear when the two nuclei used to create the two different spectral dimensions are the same, such as ^{1}H-^{1}H, or heteronuclear when the two nuclei are different, such as ^{1}H-^{13}C.

2D NMR experiments consist of a sequence of pulses with variation of one parameter. In addition to the preparation and acquisition periods which make up 1D pulse sequences, additional steps include an evolution time (t_1) and potentially a mixing period prior to or after the evolution period. As the duration of the evolution time t_1 is systematically varied to create an indirect time axis, this resulting in two independent time axes which can be Fourier transformed independently to form a 2D spectrum.

2D-^{1}H,^{13}C HSQC NMR experiment is an example of an inverse NMR experiment, an experiment which studies insensitive nuclei via magnetisation transfer from a high-sensitivity nucleus, usually ^{1}H. As previously mentioned, ^{13}C nuclei have a lower gyromagnetic ratio compared to protons, which have a gyromagnetic ratio approximately four times higher than ^{13}C nuclei. The 2D-^{1}H,^{13}C HSQC NMR experiment therefore overcomes the poor sensitivity of the 1D-^{13}C NMR spectrum which is vital for NMR experiments conducted as part of this thesis, as metabolite concentrations are usually too low to allow the acquisition of a 1D-^{13}C NMR experiment in a reasonable time frame.

HSQC is an example of an inverse NMR experiment, an experiment which studies insensitive nuclei from a high-sensitivity nucleus, usually ^{1}H. As previously mentioned, ^{13}C nuclei have a lower gyromagnetic ratio compared to protons, which have a gyromagnetic ratio approximately four times higher. There is therefore a need to design NMR

experiments to overcome the poor signals generated from ^{13}C nuclei when observed in isolation (1D-^{13}C NMR).

The 2D-^{1}H,^{13}C HSQC NMR pulse sequence utilises the INEPT (Insensitive Nuclei Enhanced by Polarization Transfer) pulse sequence element to transfer ^{1}H magnetisation to ^{13}C nuclei (shown in Figure 19) before the magnetisation which has undergone a period of evolution, is transferred back to the ^{1}H nucleus for observation (108). Thin lines represent $\pi/2$ pulses whilst thicker lines represent π pulses.

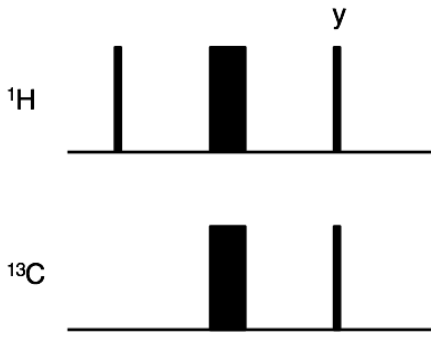

Figure 19. The INEPT pulse sequence during which magnetisation is transferred from ^{1}H to ^{13}C nuclei.

The FID of such ^{1}H nuclei in this scenario are classically acquired with ^{13}C decoupling such that ^{1}H,^{13}C J-coupling is not active during the FID acquisition in the direct time domain.

Figure 20 depicts the HSQC pulse sequence with RF pulses targeting ^{1}H and ^{13}C nuclei and a blue arrow depicting magnetisation transfer. Evolution of J-coupling occurs during t_1. Transfer of magnetisation occurs when nuclei are anti-phase.

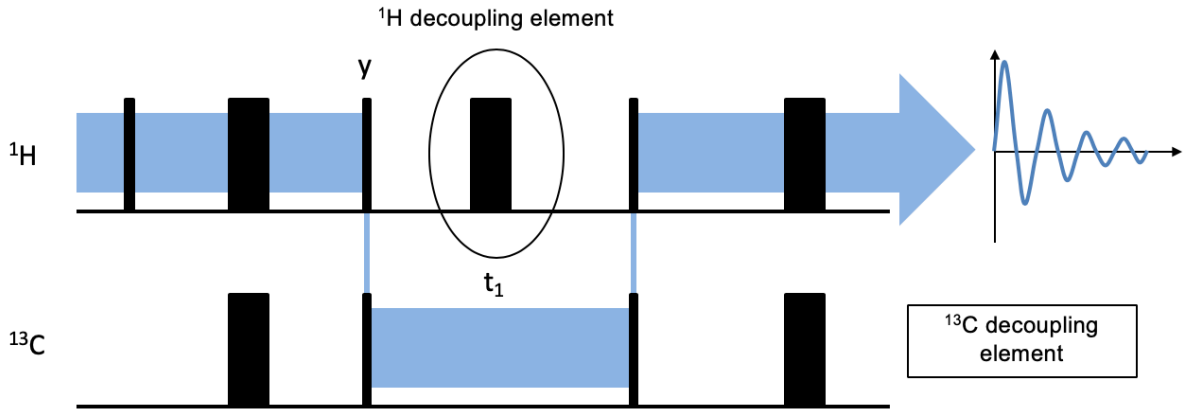

Figure 20. $^{1}H,^{13}C$ HSQC pulse sequence with ^{1}H and ^{13}C decoupling elements highlighted. The blue arrow depicts transfer or magnetisation from ^{1}H to ^{13}C nuclei before transfer back to ^{1}H nuclei.

The spectrum produced is a result of plotting spectral frequency due to variations in the t_1 domain against the spectra acquired from the FID, similar to 1D experiments. The output spectra for 2D HSQC is a 3-dimensional plot with chemical shift for the two nuclei of interest (^{1}H and ^{13}C) displayed on the two axes. Analysis of 2D HSQC spectra is discussed in Chapter 2.

Acquisition and Fourier transformation

In the acquisition phase of a pulse sequence, the raw output signal is the summation of multiple signals, the amplitude of which decreases with time with a half-life decay pattern (107). This raw output observed analogue signal produced during an NMR experiment is known as free induction decay (FID). Two types of relaxation occur, both showing exponential decay.

Transverse relaxation or T_2 relaxation, is responsible for interaction of spins with other nuclei. The signal decay of an FID is dominated by this T_2 relaxation which results in loss of transverse magnetisation and therefore loss of signal intensity towards the end of the FID.

Longitudinal (spin-lattice) relaxation, known as T1, is responsible to restore the Boltzmann distribution in order for a subsequent transient acquisition in the case of 1D spectra, or increment acquisition if 2D spectra are being acquired.

Before processing of this signal occurs, the analogue signal is converted to a digital signal by analogue-digital convertors. This is achieved by sampling the signal at regular points along the analogue signal prior to conversion to a data point in the form of a binary value. The sampling rate used is determined by the maximum frequency (f_{max}) which can be represented correctly. The below equation is used to calculate this maximum frequency (f_{max}), known as the Nyquist frequency, using the interval between data points (Δt).

$$f_{max} = \frac{1}{2\Delta t}$$

Equation 6. Calculation of the Nyquist frequency (f_{max}) where Δt represents the interval between data points.

The same equation is rearranged to calculate the sampling interval, or dwell time, from the Nyquist frequency.

$$\Delta = \frac{1}{2f_{max}}$$

Equation 7. Calculation of the sampling interval (Δ) using the Nyquist frequency (f_{max}).

An analogue signal is thus converted to a good quality digital signal which accurately represents the original signal. Subsequently, Fourier transformation permits decomposition of a complex signal, composed of a number of exponentially decaying sinusoidal functions, its constituent frequencies. The Fourier transformation is required to convert a raw output signal, of amplitude (y-axis) and time (x-axis), into a plot of frequency

(x-axis) against amplitude (y-axis). Peaks seen on NMR spectra commonly have a Lorentzian shape which can be expressed in terms of peak height, spectral width at half height and frequency at the centre of each peak.

A signal with a pattern not showing much exponential decay, resulting in a long FID, leads to a spectral peak of narrow width. A signal showing fast exponential decay, resulting in a short FID, leads to a wide peak in the NMR spectrum with a smaller signal height to noise ratio as a result. If the analogue FID signal contains detected frequencies higher than f_{max}, these frequencies will be aliased inside the spectra at different frequencies following digitisation and Fourier transform.

Modern spectrometers overcome this by oversampling the FID and applying a digital filter to remove any signal contribution from outside the spectra. It should be noted that this process, known as oversampling, is only possible for the direct dimension.

Conclusion

NMR is a sensitive modality which can be used to identify a profile of metabolites containing NMR active nuclei with spin 1/2; commonly ^{1}H and ^{13}C nuclei. In a latter section we will explore the utility of NMR in the detection of molecules containing ^{13}C atoms within the field of tracer-based metabolism.

Ischaemia Reperfusion Injury and the Kidney

The ongoing ischaemic injury prior to implantation, in addition to the collective damage inflicted on the kidney due to a second 'hit' following reperfusion, is known collectively as Ischaemia Reperfusion Injury (IRI). All transplanted kidneys experience IRI to varying degrees. Major insults occur during procurement and storage of organs as a result of both warm and cold ischaemia despite hypothermic conditions with IRI continuing following re-perfusion. The pathological changes which occur determine clinical outcome following transplantation.

In this section, anatomy and physiology of the kidney is reviewed, prior to exploring key metabolic pathways which are active in normal physiological conditions. The consequences of ischaemia during the transplantation process are discussed with the consequential pathological effects and clinical consequences of IRI.

The Kidney

Renal Anatomy

The kidneys are paired organs lying in the retroperitoneum either side of the vertebral column with arterial blood flow originating directly from the abdominal aorta via renal arteries (111). Despite accounting for less than one percent of body mass the kidneys receive roughly 25 percent of cardiac output, roughly 1.2L/min. Venous blood flow reaches the vena cava via a main renal vein whilst urine leaves the kidney via the renal pelvis forming the ureter shortly afterwards. In addition to the divisions and tributaries of these structures, lateral bisection reveals an outer cortex in addition to inner medullary pyramids shown in Figure 21.

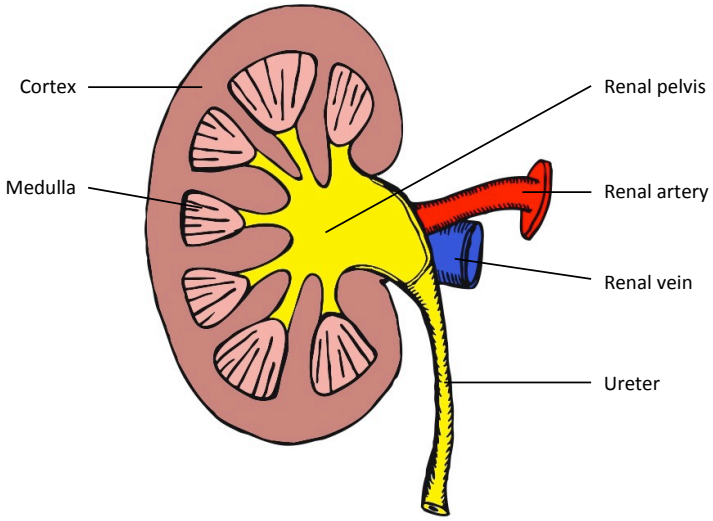

Figure 21. Schematic diagram of a laterally bisected left kidney with a patch of aorta still attached to renal artery.

A main renal artery divides sequentially into progressively smaller arteries with the smallest afferent arterioles supplying the nephron, the functional unit of the kidney. Each kidney contains roughly 1.2 million nephrons. A nephron consists of a hollow tube in which filtered fluid enters via ultrafiltration within the glomerulus and changes composition constantly throughout the length of the nephron prior to entering the collecting system. Each part of the nephron shown in Figure 22 plays a role in electrolyte and water homeostasis.

Renal Physiology

Primarily, the kidneys are key regulatory organs responsible for electrolyte and water homeostasis. In addition, the kidney has 3 key endocrine functions, namely secretion of renin, calcitriol and erythropoietin. It is also responsible for the excretion of some substances including metabolic waste products and some toxins (74).

Electrolyte homeostasis involves several active and passive processes in different regions of the nephron. Along with being structurally and functionally heterogenous, these regions of the nephron also differ with regards to metabolism with pathway activity reflecting the

regional disparity in oxygen availability. In terms of renal parenchymal oxygenation, the cortex experiences the highest oxygen levels with progressive reduction in the outer medulla and the lowest levels in the papillae (112).

Cells in the proximal convoluted tubule (PCT) are the most metabolically active, accounting for roughly two thirds of the volume of the renal cortex. Given the greater abundance of oxygen in the renal cortex, compared with the renal medulla, it is unsurprising that cortical cells are more dependent on aerobic metabolism and are consequently more sensitive to ischaemia. A high metabolic rate is required to meet the energy demands of PCT cells. This is largely due to their many resorptive mechanisms which are coupled to transport of sodium ions which occurs via a Na^+/K^+ ATPase pump on the basal membrane in tandem with a Na^+/H^+ cotransporter on the luminal side of epithelial cells.

Proximal tubule cells, along with tubular cells in the thick ascending limb of the loop of Henlé and distal tubule, have an abundance of mitochondria in order to meet high energy requirements. It is estimated that 90 percent of the oxygen consumption of a cell is mitochondrial with 80 percent of this linked to ATP generation via oxidative phosphorylation (113).

In contrast, the inner medulla has a lower energy requirement. Medullary blood flow is relatively lower (114, 115) due to shunting of blood flow in the cortex resulting in permanently hypoxic environment in which reliance is on anaerobic means of ATP synthesis and are therefore less influenced by hypoxia (112).

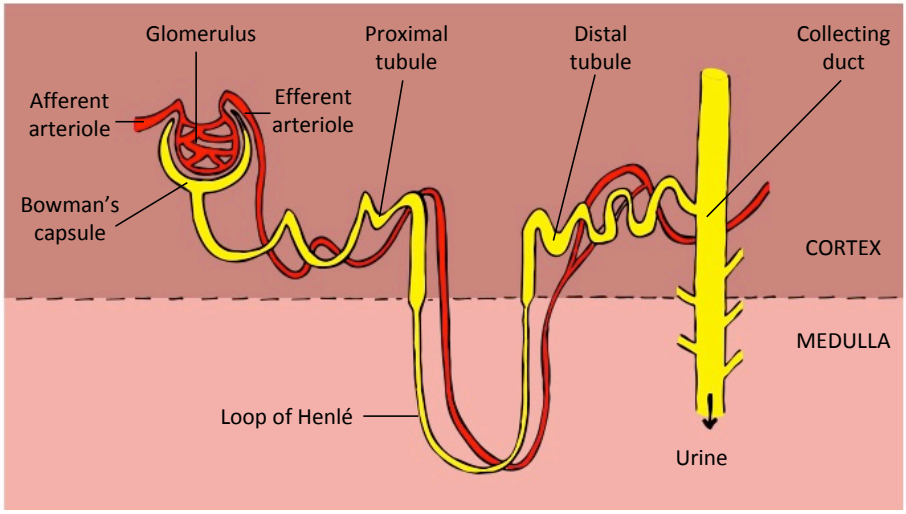

Figure 22. Schematic diagram showing the components of the nephron and their position with relation to cortex and medulla.

Metabolic Pathways

Energy stores such as glycogen are low within the kidney, in contrast to the liver. The kidney utilises substrates for metabolism within the bloodstream including glucose, lactate, and free fatty acids. In the following section aerobic and anaerobic metabolic pathways will be described in more detail (116, 117).

In addition to variation in energy requirements and oxygen delivery to different regions of the kidney in normal physiological conditions, metabolic pathway activity is affected at different stages of the transplantation process due to conditions of hypothermia and hypoxia. In this section key metabolic pathways are explored prior to introducing the concept of ischaemia reperfusion injury.

Glucose is metabolised within cells to produce adenosine triphosphate (ATP), the cell's 'energy currency' from adenosine diphosphate (ADP), CO_2 and water. The conversion of ADP to ATP occurs during 2 processes; substrate-level phosphorylation and oxidative phosphorylation. Three metabolic pathways are mainly responsible for energy generation

from carbohydrates within the cell (117); glycolysis, the Tricarboxylic acid (TCA) cycle and the electron transport chain.

Glycolysis and the fate of pyruvate

Glycolysis is the main metabolic pathway using glucose (Figure 23) as a substrate to generate ATP. Over a series of ten reactions catalysed by enzymes, glucose, a 6-carbon molecule, is converted to 2 pyruvate molecules, each consisting of a 3-carbon atom backbone. Glycolysis is a primitive pathway, releasing free energy in the form of adenosine triphosphate (ATP) and reduced nicotinamide adenine dinucleotide (NADH).

Pyruvate molecules can either undergo transamination, forming alanine, or are reduced to form lactate under anaerobic conditions. Both alanine and lactate concentrations are thus markers of glycolytic pathway activity. Lactate concentrations are commonly used in the clinical environment as a marker of anaerobic metabolism in a range of clinical conditions, all the result of inadequate end-organ perfusion such as septic shock and hypovolaemic shock.

In aerobic conditions, pyruvate undergoes decarboxylation via the enzyme pyruvate dehydrogenase to form acetyl co-enzyme A (acetylCoA), resulting in energy production via NADH, or alternatively undergoes carboxylation via the enzyme pyruvate carboxylase to form oxaloacetate, filling in additional intermediates in the tri-carboxylic acid cycle for biomass production (Figure 24).

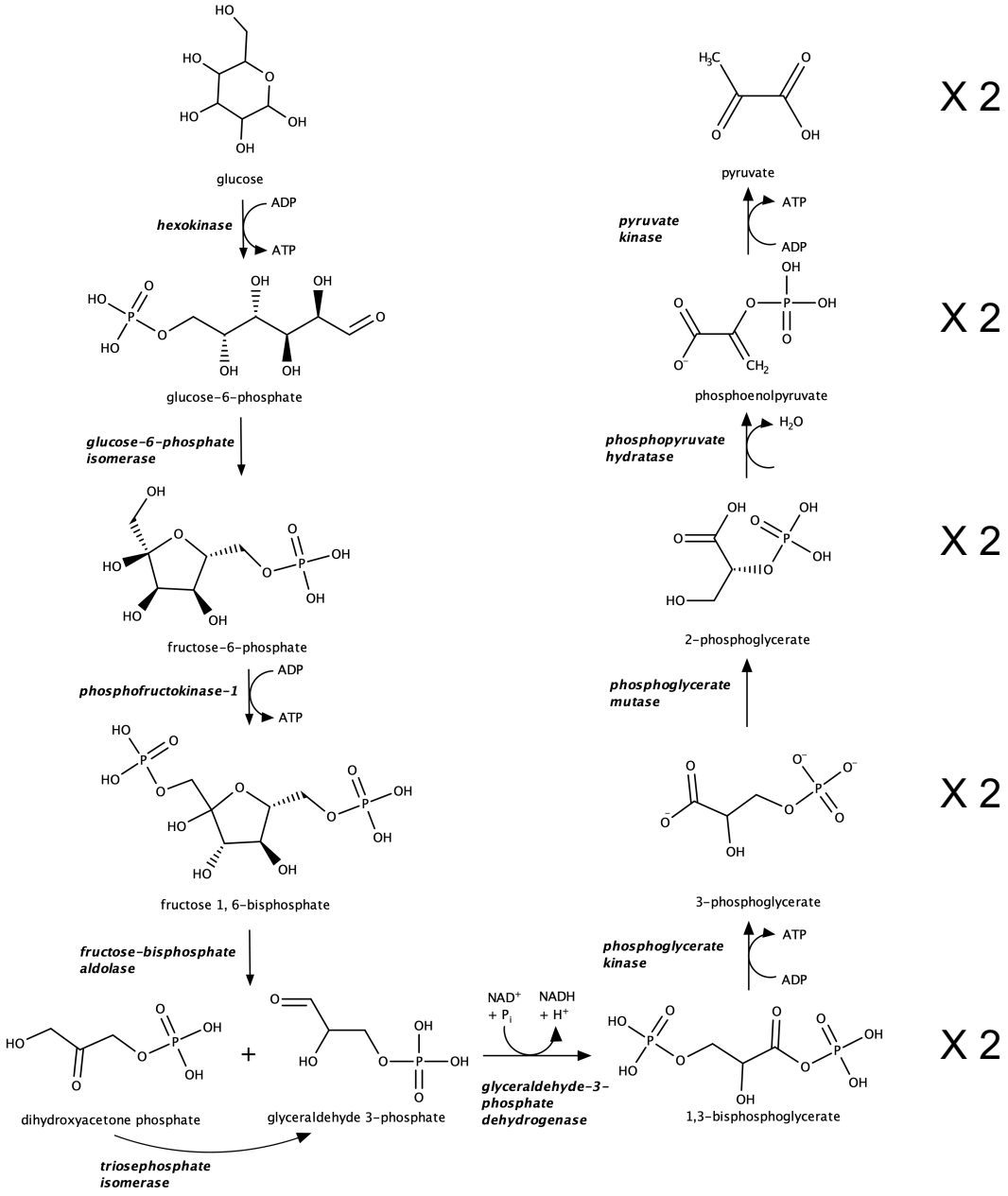

Figure 23. Glycolysis pathway

Tri-carboxylic acid (TCA) cycle

Relative to the TCA cycle, glycolysis is responsible for only a small amount of ATP production. The TCA cycle, also referred to as the Krebs cycle or the citric acid cycle, is a cyclical metabolic pathway. The cycle takes place in the mitochondrial matrix under the control of 8 enzymes. Though glycolysis yields a net of 2 ATP molecules per molecule of

glucose, approximately 32 ATP can be generated using the TCA cycle and its accompanying electron transport chain (117). Whilst it is not directly dependant on oxygen, it is linked to oxygen consumption via NADH/$FADH_2$ and the electron transport chain.

Pyruvate dehydrogenase, is considered the gatekeeper of the TCA cycle as it regulates the incoming flux of glycolytic products, converting pyruvate into acetyl-CoA. The 2-carbon acetyl group from this molecule is transferred to the 4-carbon molecule oxaloacetate forming citrate, a 6-carbon molecule (Figure 24). In subsequent reactions in the TCA cycle, citrate loses 2 carboxyl groups as carbon dioxide, giving rise to 5-carbon (alpha-ketoglutarate) then 4-carbon molecules (succinate, fumarate, malate, oxaloacetate).

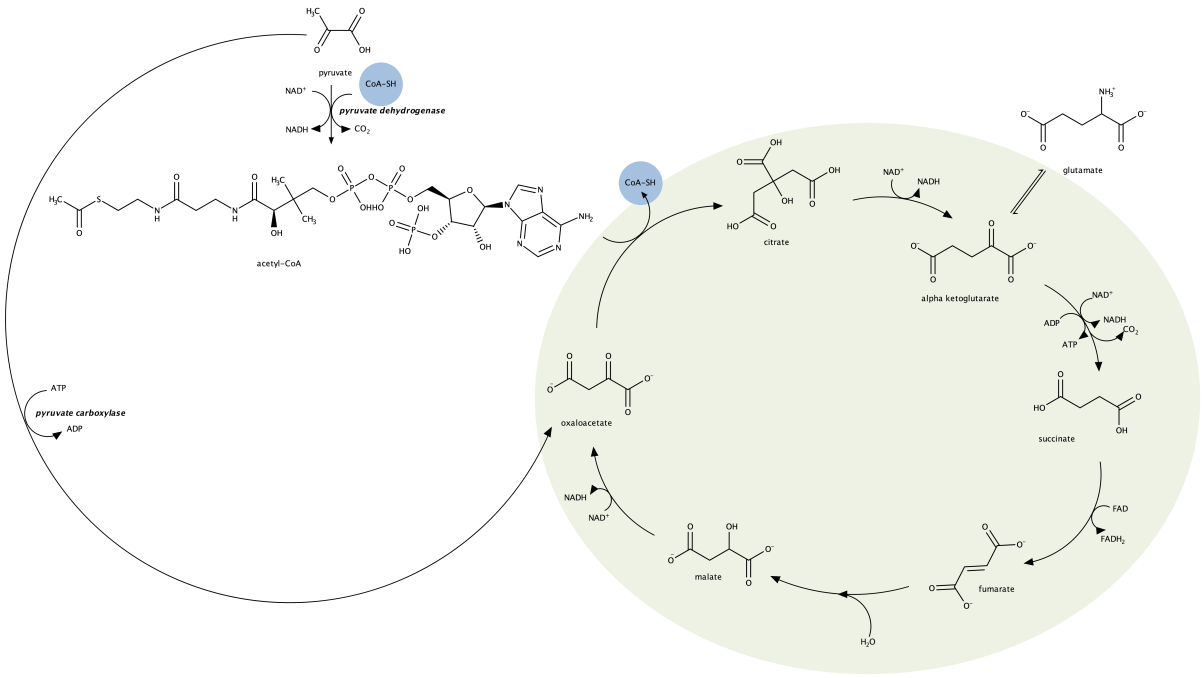

Figure 24. The TCA cycle metabolites and entry points of pyruvate into the cycle. The TCA cycle is shown in green.

Pyruvate can also enter the TCA cycle as oxaloacetate via carboxylation, but this tends to happen when the energy requirement of cells increases acutely, such as during exercise, in order to provide enough oxaloacetate to react with acetyl-CoA (118). During the TCA

cycle, acetyl-CoA is oxidised to produce NADPH and $FADH_2$ for energy generation via the electron transport chain.

The 2 carbon atoms entering the TCA cycle as acetyl-CoA as part of the pyruvate dehydrogenase are not the same 2 carbons lost from citrate when it forms alpha-ketoglutarate and subsequently succinate. Instead, these carbons are incorporated into the newly formed backbone of the succinate molecule.

The electron transport chain

The electron transport chain, sited in the inner mitochondrial membrane, is a series of reactions whereby electrons are sequentially transferred between electron donors and acceptors. The transfer of electrons pumps protons into the inter-membrane space, generating an electrochemical gradient. At the end of the chain, electrons are passed to oxygen, the most electronegative acceptor in the chain. Energy generated in the presence of oxygen via the phosphorylation of ADP to form ATP; the process is termed oxidative phosphorylation.

During oxidative phosphorylation, the reduced forms of hydrogen carriers NADH and $FADH_2$ are oxidised to NAD^+ and FAD. Oxidative phosphorylation is an oxygen dependent process and generates much higher levels of ATP in contrast to glycolysis.

The pentose phosphate pathway

Whilst the majority of glucose entering cells is utilised for glycolysis, breakdown products of glucose can also be used to facilitate pentose phosphate pathway (PPP) activity. The principal function of this pathway is the production of pentose sugars such as ribose, a

key component of ribonucleic acid (RNA) and deoxyribonucleic acid (DNA) nucleotides. There are 2 parts to the cycle, an oxidative and a non-oxidative phase.

During the oxidative phase, glucose-6-phosphate, the second intermediate of glycolysis, is oxidised to form ribose-5-phosphate, a 5-carbon sugar. During this phase, 2 nicotinamide adenine dinucleotide phosphate ($NADP^+$) molecules accept electrons to form 2 molecules of the molecule's reduced form (NADPH). These NADPH molecules are required in multiple reductive reactions throughout the cell including fatty acid biosynthesis, cholesterol biosynthesis and nucleotide biosynthesis.

The non-oxidative phase sees the interconversion of phosphorylated sugars to 6-carbon intermediates of the glycolytic pathway and 5-carbon sugars used in the synthesis of nucleotides.

Beta-oxidation of fatty acids

Energy release from fatty acids occurs via beta-oxidation in the mitochondria. This catabolic process releases acetyl-CoA, which supplies the TCA cycle, in addition to electron carriers NADH and $FADH_2$. NADH and $FADH_2$ generate ATP via the electron transport chain.

Ischaemia Reperfusion Injury

Ischaemia reperfusion injury (IRI) describes cellular damage after reperfusion of previously viable ischemic tissues (119). Such injury is thought to be a key non-immunological cause of delayed graft function as it is responsible for the development of post-ischaemic acute tubular necrosis (120). IRI occurs in 2 phases, the first ischaemic phase due to interruption of blood flow with changes invoked setting the scene for further damage to be inflicted during the second reperfusion phase. Both phases are characterised by disruption of regulatory functions at a cellular level. In this section, the major deleterious processes central to IRI will be discussed, including reduction in ATP stores, accumulation of intracellular calcium ions, propagation of reactive oxygen species and subsequent mitochondrial dysfunction.

Reduction of ATP stores

Cessation of blood supply promptly results in whole organ ischaemia due to exhaustion of oxygen supply by aerobic tissue. During ischaemia, the lack of oxygen supresses oxidative phosphorylation, decreasing ATP synthesis. Cellular ATP stores are thus quickly depleted with consequences for energy dependant processes within the cell and a resultant switch from aerobic to anaerobic metabolism. Following the switch, ATP is produced almost exclusively by glycolytic pathway activity with a consequent build-up of lactate resulting in a decrease in intracellular pH. However, this switch ultimately fails to meet the high energy demands of aerobic tissue due to the lower yield of ATP per glucose molecule. Once ATP stores have been exhausted, phosphorylation of fructose-6-phosphate cannot occur thus glycolytic pathway activity also stops, preventing excessive acidosis.

Energy dependant processes responsible for electrolyte homeostasis, such as the crucial membrane bound Na^+/K^+ ATPase, fail following depletion of ATP stores. The effect of this is a net accumulation of intracellular Na^+ ions with a consequent rise in Cl^- ion concentration. The accumulation of intracellular Na+ ions results in cellular oedema due to hydrostatic effects. Furthermore, the dephosphorylation of ATP to adenosine and 3 particles of inorganic phosphate is a contributor to the hyperosmolarity of the intracellular compartment which further attracts water via diffusion, aquaporin and the glucose transporter (121).

Oedema disrupts organelles including lysosomes, mitochondria and the endoplasmic reticulum. The latter is responsible for an initial rise in intracellular Ca^{2+} which is particularly detrimental. Destabilisation of lysosomal membranes leads to release of lysosomal enzymes causing damage to cell structure (122) whilst mitochondrial oedema results in disruption of oxidative phosphorylation.

Intracellular calcium excess

Several adverse events are a result of the disruption to intracellular calcium homeostasis during IRI. The increase in intra-cellular Ca^{2+} ions occurs due to several mechanisms. Early accumulation of intracellular Ca^{2+} is thought to be due to redistribution of stores from the endoplasmic reticulum (123). Following longer periods of ischaemia, intracellular Ca^{2+} ions are no longer actively pumped out of cells by the ATP dependant Na^+/Ca^{2+} antiporter with possible reversal of flow leading to Ca^{2+} accumulation in the cytoplasm. Reperfusion is responsible for a further increase in intra-cellular calcium concentration.

The increase in cytosolic Ca^{2+} activates calcium dependent enzymes such as proteases and phospholipases which directly cause damage to cellular components, initiating steps

towards apoptosis on reperfusion. Proteases such as calpains and caspases, have numerous targets including the cytoskeleton, proteins within plasma membranes, lysosomes, mitochondria and the nucleus whilst Phospholipase A2 cleaves phospholipids (121).

Reactive Oxygen Species

Oxidative damage is inflicted by ROS, a term which incorporates free radicals and non-radical species. Oxidative damage commences during ischaemia due to intracellular ROS formation (124), although only a small amount of ROS are produced during this initial ischaemic phase. The electron transport chain of mitochondria is the main source of intra-cellular ROS but several other sources are implicated in the production of ROS. Membrane and cytosolic oxidases, such as xanthine oxidases and NADPH oxidases, are upregulated during ischaemic insult although they may remain inactive due to low intracellular pH prior to reactivation when pH is normalised at reperfusion.

Re-oxygenation on reperfusion is responsible for significant ROS production as the kidney lies vulnerable with such upregulated enzymes lying inactive. Chemokines are responsible for attracting neutrophils, macrophages and eosinophils which also release ROS, contributing to this second ‘wave’ of damage as part of reperfusion injury.

The presence of unpaired electrons within a molecule confers a high degree of reactivity. Such molecules are known as free radicals. Non-radical species do not contain unpaired electrons. At high concentrations, ROS are detrimental to cell structures inflicting widespread damage to lipids, proteins and nucleic acids (125). It should be mentioned that at low concentrations ROS are beneficial, acting as cell signalling molecules for

pathways which act to promote cell proliferation, differentiation and migration thereby promoting tissue remodelling and angiogenesis (126).

The superoxide anion, a free radical species, is considered the “primary” ROS but does not itself react with proteins or nucleic acids (127). Superoxide undergoes a dismutation reaction, catalysed by the enzyme superoxide dismutase, producing hydrogen peroxide and oxygen. Hydrogen peroxide is removed by 2 enzymes, catalase and glutathione peroxidase, both of which work in conjunction with superoxide dismutase. Catalase, located in peroxisomes, promotes the conversion of hydrogen peroxide to water and molecular oxygen. Glutathione peroxidase decomposes hydrogen peroxide forming water, whilst oxidising glutathione.

The enzymes superoxide dismutase, catalase and glutathione peroxidase are the cell’s most effective enzymatic defence against low levels of ROS, limiting ROS accumulation. Non-enzymatic anti-oxidants include thiol anti-oxidants such as glutathione.

The Fenton reaction describes the conversion of hydrogen peroxide to the highly reactive hydroxyl free radical during conditions of oxidative stress. For this reaction to occur, the superoxide radical reacts with iron containing molecules to release free intracellular iron which then reacts with hydrogen peroxide to form the hydroxyl free radical (128). The hydroxyl free radical is highly reactive and has a short half-life within the cell, reacting with substrate close to its site of production.

Mitochondrial dysfunction

Mitochondria are both a major source of ROS via the disrupted electron transport chain and are also a major target of ROS. The mitochondrial permeability transposition pore (mPTP) is a non-selective pore within the inner mitochondrial membrane which is formed

during certain pathological conditions. High levels of mitochondrial Ca^{2+} are responsible for opening of the mPTP which allows molecules <1,500 Daltons to pass through (121).

Calcium and reactive oxygen species (ROS) are the most important triggers for opening of the mPTP (129); its opening results in mitochondrial swelling and release of caspase dependant co-factors into the cytosol (130). During reperfusion these caspase dependant co-factors activate executioner caspase enzymes which are responsible for cell death via energy dependant processes such as apoptosis.

Microvascular dysfunction and the contribution of the immune system

The detrimental sequelae of ischaemic insults are not limited to renal parenchyma. Vascular endothelium experiences a multitude of changes which are more evident on reperfusion. Endothelial cells swell via the mechanisms described above. In addition, loss of glycocalyx and breakdown of the actin cytoskeleton are observed (131)leading to interstitial fluid aggregation.

Ischaemia promotes expression of pro-inflammatory gene products such as leucocyte adhesion molecules and cytokines. In addition, ischaemia promotes increased levels of vasoconstrictor substances such as platelet derived growth factor-B, endothelins and thromboxane A_2 (132) and a decreased production of vasodilatory substances such as nitric oxide. These mechanisms create unfavourable conditions for reperfusion (119). Complement activation also results in the formation of several pro-inflammatory mediators (133). The ensuing proinflammatory state is more evident on reperfusion.

Increased expression of adhesion molecules recruits both leucocytes and neutrophils into tissues. At reperfusion, leucocytes enter the interstitial compartment following a sequence of events that include leucocyte activation, chemotaxis, leucocyte-endothelial cell

adhesion and transmigration (134, 135). Further damage occurs at this stage as a result of the release of toxic ROS, proteases and elastases by leucocytes whilst neutrophils in post-ischaemic tissue also release ROS, cytokines and proteases.

In combination, endothelial cell swelling, leucocyte-endothelial cell adhesion, interstitial fluid accumulation and decreased endothelial cell mediated vasorelaxation result in mechanical obstruction to blood flow resulting in a well described ‘no-reflow’ phenomenon (119).

The effects of hypothermia

Hypothermia is well known to reduce metabolic activity with an accompanying decrease in oxygen consumption forming the basis of organ preservation. However, not all effects of such decrease in temperature are beneficial (136); the use of hypothermia is a trade-off between beneficial and deleterious effects (137).

The difference between hypothermia inflicted in the clinical setting, and the physiology of hibernating animals demonstrate during hypothermic conditions, is the control of suppression of metabolism. The desired effect of hypothermia in the clinical setting, for example during organ preservation, cardiac-pulmonary bypass and neurosurgical procedures, is a suppression in metabolism. In contrast, in hibernating mammals, a regulated metabolic depression is observed in which ATP supply and demand is balanced (138). Regulated metabolic depression is not limited to cold-adapted mammals and has infact been observed in primates such as fat-tailed dwarf lemurs in which body temperature can decrease as low as 5°C to match ambient surroundings during hibernation (139).

Hypothermic injury is largely attributed to loss of cell ion homeostasis, in particular sodium homeostasis. This occurs as a result of differential temperature effects on ion channels compared to ATP driven pumps such as the Na^+/K^+ ATPase pump. Reduced efflux of Na^+ from cells is observed due to decrease in Na^+/K^+ pump activity (140) in addition to passive influx of Na^+ via ion channels (141). Both mechanisms of increasing Na^+ ions result in dissipation of ion gradients, cell swelling and inhibition of ATP generation (142). In addition, ROS are also thought to contribute to damage inflicted due to hypothermia (143).

Several processes also increase cytosolic Ca^{2+} during hypothermia including efflux of Ca^{2+} in exchange for Na^+, membrane depolarisation leading to opening of voltage gated Ca^{2+} channels and loss of Ca^{2+} from the sarcoplasmic reticulum (140). As a result, increased phospholipase activity leads to cell membrane hydrolysis which results in further increases in cell membrane permeability and ultimately cell death (140).

Manifestation of ischaemia reperfusion injury in cadaveric kidneys

The mechanisms of damage resulting in DGF in cadaveric donors differs between donor sub-types. DBD and DCD donor organs are susceptible to different physiological insults. Brainstem death results in inflammatory immunological signals such as upregulation of cell adhesion molecules leading to leucocyte and neutrophil localisation to donor organ (136, 144, 145). The attraction of such immune cells amplify damage during the reperfusion phase of IRI (146).

In contrast, the period of warm ischaemia which DCD organs are subject to results in pathological processes central to depletion of ATP stores, such as cell swelling and oedema as a result of failure of the Na^+/K^+ pump. Perivascular oedema decreases flow

during reperfusion, leading to a further period of warm ischaemia. This observed microvascular ‘no-reflow’ phenomenon contributes to reperfusion injury (147).

The pathological changes seen on biopsy of cadaveric kidneys with DGF are known as acute tubular injury or acute tubular necrosis (148) with the observed spectrum of histological changes seen reflecting the timing and nature of IRI. Changes in metabolism during ischaemic and hypothermic insults are detrimental to regulatory functions within the cell, damaging kidneys during the preservation period but also setting the scene for further damage at reperfusion.

Metabolomics

Metabolomic studies aim to comprehensively and quantitatively analyse the wide array of metabolites present in biological samples (149). Metabolomics is the endpoint of the -omics cascade occupying a niche which separates itself from genomics, the study of the genome, and proteomics, the study of proteins produced by an organism, tissue or cell. Whilst the genome is a static entity, the proteome and metabolome undergo dynamic changes; both proteomics and metabolomics complement genomics as phenotypic molecular markers revealing the effects of environmental changes on biological systems (150). Metabolomics in particular measures the short-term chemical response of cells and tissues to a biological event, thereby linking protein and gene expression (151).

Metabolomic studies can be divided into untargeted studies, which aim to comprehensively analyse all measurable analytes in a sample, and targeted studies, which aim to measure defined groups of chemically characterized and biochemically annotated ‘labelled’ metabolites (152).

Investigative techniques

NMR spectroscopy and mass spectrometry are the two most successful and widely used analytical techniques in the field of metabolomics. Mass spectrometry measures the mass to charge ratio of ions within a sample. Molecules are ionized then continually fragmented with the mass to charge ratio measured for each ion. Their relative abundance within the sample is measured with the potential to calculate absolute concentrations. Gas chromatography and liquid chromatography are two techniques by which molecules can be separated prior to mass spectrometry. One limitation inherent to mass spectrometry is the extent to which samples undergo ionization. Not all compounds are visible using mass

spectrometry as not all samples readily undergo ionization and due to the differing ionisation of different metabolites.

NMR spectroscopy takes advantage of the magnetic properties of nuclei with the property of spin in order to study their physical and chemical characteristics thereby determining the structure of molecules which they contribute to. Quantification of metabolites in a sample is permitted by 1D ^{1}H NMR spectroscopy, although the accuracy of such quantification depends on the overlap of spectral pattern of such a metabolite.

Compared with mass spectrometry, NMR is able to analyse samples with a high throughput, requiring minimal sample preparation, simple methods of quantifying metabolites and non-destructive acquisition of data (153-155). NMR also allows more accurate description of a metabolite as it is able to determine chemical structure and also distinguish between metabolites with identical masses. However, NMR is less sensitive than mass spectrometry.

The majority of metabolomic studies use either analytical technique in isolation however the distinct limitations described apply to such a unilateral approach. Several approaches to combining the two techniques have been described with respect to both ‘conventional’ metabolomics and incorporation of a metabolic tracer (156) in an attempt to overcome the limitations of each technique in isolation.

Metabolic isotope tracers

Cellular metabolism involves a complex network of pathways resulting in metabolite production from different substrates, or perhaps even the same substrate from different pathways. Purely observational non-interventional analytical techniques, such as proton

NMR and mass spectrometry, do not allow differentiation of such pathways. A metabolic isotope tracer permits such observations. Techniques such as NMR spectroscopy and mass spectrometry follow the fate of a metabolic tracer molecule, thereby providing information regarding the metabolism of the molecule of interest (157). Molecules used as metabolic tracer must be biologically and functionally identical to the naturally occurring molecule of interest known as the tracee (157).

Metabolic tracers can be either stable or radioactive isotopes. A stable isotope tracer can be defined as a molecule with one or more isotopes with a different mass than the most abundantly occurring mass incorporated somewhere in the molecule (157).

For the purpose of this thesis, we will consider incorporation of ^{13}C into a glucose molecule. With respect to carbon, ^{12}C is the most frequently observed isotope containing 6 protons and 6 neutrons within its nucleus. The isotope ^{13}C is a non-radioactive and therefore stable isotope of carbon containing 6 protons and 7 neutrons in its nucleus, accounting for 1.07% of all carbon. The third isotope ^{14}C is found within the atmosphere, containing 8 neutrons within its nucleus and is therefore unstable resulting in radioactive decay.

Figure 25 shows standard ^{12}C glucose and [U-^{13}C] glucose, a synthetically produced glucose molecule in which each of the six ^{12}C atoms within the glucose molecule has been substituted for a ^{13}C atom.

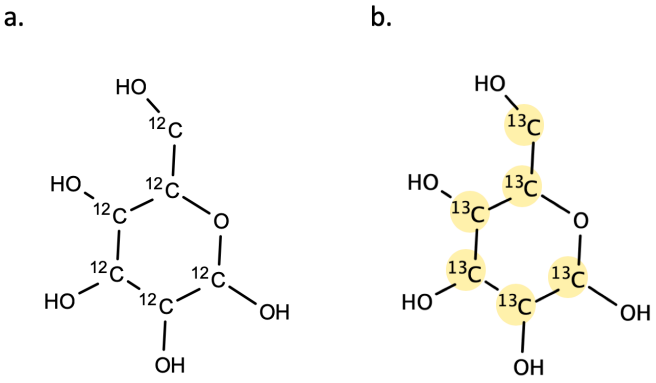

Figure 25. Standard ^{12}C glucose (a) and [U-^{13}C] glucose (b).

With regards to glycolytic pathway activity, universally ^{13}C labelled glucose as the substrate for glycolysis produces universally ^{13}C labelled pyruvate which undergoes conversion to universally ^{13}C alanine and universally ^{13}C labelled lactate as shown in Figure 26.

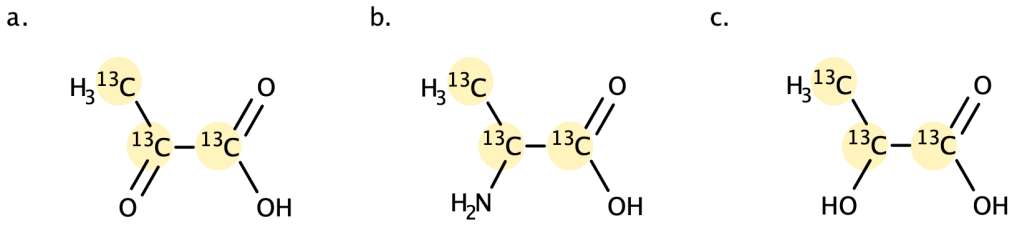

Figure 26. [U-^{13}C] pyruvate (a), [U-^{13}C] alanine (b) and [U-^{13}C] lactate (c).

Different labelling patterns occur in metabolites within, and as a product of, the TCA cycle depending on whether universally labelled ^{13}C pyruvate enters via the pyruvate dehydrogenase or less commonly, the pyruvate carboxylase pathway. The TCA cycle does not transfer carbon atoms to hydrogen carriers, thus no ^{13}C labelled compounds are seen as a result of electron transport chain activity.

As discussed, 2D ^{1}H,^{13}C HSQC NMR experiments exploit the spin properties of ^{1}H and the ^{13}C isotope such that [U-^{13}C glucose] and some of its associated metabolites are identifiable on the output spectra. In addition, the difference in mass between ^{12}C and ^{13}C

nuclei results in differentiation between isotopes using mass spectrometry. The two approaches can be combined by first simulating ^{13}C multiplets in NMR spectra and utilizing mass increments to obtain long range information prior to combining this information to derive isotopomer distributions for metabolites of interest (158). This combined use of both 2D $^{1}H,^{13}C$ HSQC NMR and mass spectrometry aids isotopomer distribution determination.

Metabolomic studies in renal transplantation

Metabolomic studies have a key role in describing metabolic mechanisms in addition to helping identify biomarkers of disease (159) with several reported studies specific to renal transplantation (160-167).

Studies to date have aimed to demonstrate several roles for metabolomics in the field of renal transplantation including the ability to localise kidney damage, assess organs at risk of rejection and assess the extent of damage to kidneys as a result of IRI (160). Each of these studies have focused on discovering a biomarker, or biomarkers, of either function or representation of an insult inflicted during the transplantation process. The properties of an ideal biomarker include ease of measurement with samples taken in a non-invasive manner, reliable measurement with a rapid turn-around time, sensitivity for early detection and risk stratification at low cost (161). Both NMR and mass spectrometry fulfil several of these characteristics and can thus be used to identify potential biomarkers.

Studies have observed significant differences in the urinary metabolome of kidneys with immediate and delayed graft function with three studies suggesting trimethylamine-N-oxide, a marker of medullary injury, is a prognostic marker of functional outcome post-transplantation (162-164). One study examining the urine metabolome described the prognostic value of the sum of lactate/fumarate and branched chain amino

acids/pyroglutamate which adequately predict prolonged duration of DGF with AUC 0.85 (165). Furthermore, with respect to immunological causes of DGF, the urinary metabolome may be predictive of types of cellular rejection in both adult (166) and paediatric recipients (167). Given the kidneys alone produce urine, it would seem logical that metabolites detected in the urine reflect metabolic processes occurring in transplanted organs although concentrations of such metabolites in the urine may be confounded by the existing urine output of native kidneys.

To a lesser extent, metabolomics studies have also investigated changes in the serum in animal (162) studies post-transplantation in an attempt to predict outcomes including DGF and rejection. However, blood and its constituents represent an average of several homeostatic processes in the body. This may be viewed as an advantage but difficulties lie in attributing changes to transplanted organs alone. Studies using serum are also subject to interference from extra-corporeal haemolysis which greatly affects analysis of samples in untargeted studies (168-170).

In addition to blood and urine metabolites, examination of whole organs preserved with HTK solution using ^{31}P NMR suggested the energy status of kidneys could be calculated using the ratio of phosphomonoesters and inorganic phosphate (171). In the study performed by Hené et al, energy status correlated with type of donor kidney and incidence of acute tubular necrosis.

Metabolomics studies involving *ex vivo* kidneys during the organ preservation period

Metabolomic studies in transplantation have investigated the changing composition of urine, blood and the organ itself both pre and post-implantation. As demonstrated by Hené

et al (171), the organ preservation period between retrieval and implantation of an organ allows a period of observation during which time metabolomics studies can be performed.

During hypothermic machine perfusion, single kidneys are isolated and remain in a temperature regulated environment in which perfusion fluid circulates. In this closed system, the kidney alone effects a change in the constituents of the circulating fluid. It would therefore seem logical that identification of a biomarker in perfusion fluid adds value to HMP as a tool for identifying damage and therefore predicting function post-transplantation.

Indeed several studies and meta-analyses have discussed the use of proteomic biomarkers in such a context. These are discussed further in Chapter 7. Studies by our unit and others (172, 173) have described the evolving role of metabolomics in identification of a biomarker.

Using a purely 1D ^{1}H NMR approach, Guy et al. (173) aimed to describe the metabolic profile of human kidneys awaiting transplantation by analysing changes in circulating perfusate. In this study the perfusate of 26 cadaveric kidneys was analysed with perfusate concentrations of glucose, inosine and leucine identified as potential indicators of graft function post-transplantation. However, concentrations of glucose determined by ^{1}H 1D-NMR did not correlate with those measured by blood glucometer.

Bon et al (172) showed how changing metabolite levels in circulating perfusate correlated with functional outcome in a porcine DCD auto-transplantation model. An increase in several metabolites including lactate, choline and amino acids including valine, glycine and glutamate increased with time. Total glutathione concentrations decreased during the

duration of perfusion. The NMR sample processing turnaround period of 2 hours showed the potential application of NMR analysis of HMP perfusate samples to the clinical setting.

Previous research has demonstrated the validity of the pig model as similar metabolic profiles of pig kidneys and human kidneys were observed during hypothermic machine perfusion using a 1D-NMR approach (174). Discussion of the pig model with relevance to renal transplantation is discussed further in Chapter 5.

Using the porcine DCD model described in depth in Chapter 2, six porcine kidneys were perfused with fluid enriched with [U-^{13}C] glucose for 24 hours. Kidneys were subject to 24 hours of perfusion during which time sequential perfusate samples were taken with cortex samples taken at the end of the perfusion period (175).

Analysis of tissue and perfusate samples identified metabolites including [U-^{13}C] lactate and [U-^{13}C] alanine in all end point cortex samples representing *de novo* anaerobic activity. Of note, several samples of renal cortex revealed the presence of [4,5-^{13}C] glutamate, representing *de novo* TCA cycle activity.

Conclusion

Metabolomics studies possess the ability to detect in excess of a thousand metabolites. Yet given this ability, and the observation that most metabolomics studies are conducted on small samples sizes of less than 100 (176), the risk of false positives is high. Thus, any significant relationships in untargeted studies should be approached with a degree of skepticism, including the identification of individual metabolites as biomarkers.

In the context of organ preservation, metabolomic studies displays changes within transplanted organs which occur quickly in relation to ever changing environmental stimuli such as ischaemia and hypothermia. The use of a metabolic tracer enables direct interrogation of metabolic pathways of choice, accurately attributing changes in metabolite levels to these particular pathways. In doing so the risk of identifying false positive relationships is reduced. When used *ex vivo* in hypothermic machine perfusion, both targeted and untargeted studies demonstrate a changing metabolome with the potential to identify a panel of biomarkers of injury.

Chapter 2 : Methods

In this chapter the process of acquiring, preparing and initiating hypothermic machine perfusion for porcine and human kidneys is described. Metabolomic analytical techniques including NMR and mass spectrometry methods are described along with methods for histological analysis and biochemical assays. The porcine model is appraised in Chapter 8.

Porcine model of Donation after Circulatory Death

Porcine kidneys were procured from 22 to 26 week-old male English White pigs weighing between 80 and 85 kg from a local abattoir (F.A. Gill, Wolverhampton, UK) in a model previously used by our group (174) designed to simulate a Maastricht category III DCD donor (22).

Pigs were hung from their hind legs following electrical stunning to permit exsanguination via transected jugular veins. Sternopubic laparotomy and bilateral nephrectomy followed 14-15 minutes later following a series of hair removal procedures with this time period between exsanguination and nephrectomy considered the warm ischaemic time. En-bloc nephrectomy was performed by abattoir staff with requests that maximal lengths of vasculature and ureter be preserved prior to transfer of organs to a sterile bench set up as described below.

To permit fair comparison, pairs of kidneys were only included if both kidneys were supplied by a single artery at the point of origin from the abdominal aorta. However, no organs were discarded on this basis. No animals were killed solely for experimental purposes; all were due for human consumption, therefore no ethical approval was required.

A sterile set up was used on site at the abattoir with reusable surgical equipment washed and autoclaved prior to usage. Disposable equipment was discarded via appropriate means. Figure 27 shows the sterile set up used on site at the abattoir.

Figure 27. Abbatoir set-up for assessment and flush of porcine kidneys showing a 1L bag of Soltran (A) attached to giving standard giving set (B) attached to a 14G cannula resting in sterile metal bowl filled with crushed ice (C).Syringe containing 5,000iU heparin (D) prepared next to two 8mm T-connectors (E), straight clips (F), 3/0 Vicryl ties (H), tissue scissors (I) and two pairs of non-toothed forceps (J) on a sterile blue drape (K).

On receipt of a pair of porcine kidneys, each kidney was quickly checked for anatomical damage to cortex and for adequate length of vasculature prior to identification, placement of a surgical clip and cannulation of main renal artery with 14G cannula.

Kidneys were flushed with 500ml Soltran® (Baxter, UK) kept at 2-4°C at a pressure of 120-150mmHg in order to removed blood from renal vasculature, thereby preventing thrombosis prior to initiation of HMP, and to promote rapid cooling of organs. Soltran® (Baxter, UK) fluid bags were placed on a drip stand as shown in Figure 27. In some sets of experiments flush solution was supplemented with an additional 0.93 g [U-^{13}C] labelled glucose (5 mM) at 4°C and 5000 iU heparin. Kidneys were flushed via the renal artery with

a large bore cannula held in place by hand. During flush kidneys were observed for changes in flow rate of flush solution, indicated by drip rate in flow chamber, and change in colour of renal cortex and flow of effluent flush solution from renal vein. In all cases by the end of initial flush, effluent was noted to be clear. Following flush, excess perinephric fat was removed from the kidney with major vessels and ureter identified prior to placement in cold storage.

For the purpose of transport both kidneys were placed in a sterile autoclave bag containing 500ml Soltran® (Baxter, UK) and 20ml PenStrep (ThermoScientific Fisher, UK). Air was expelled from this bag prior to closure with autoclave tape. The bag was surrounded by crushed ice in a polystyrene box for transport back to the laboratory. Kidneys were commonly kept in such static cold storage for 2 hours prior to initiation of HMP in order to simulate transport of organs to transplantation centres.

Preparation of human cadaveric kidneys in the clinical setting

Human cadaveric organs were received in static cold storage conditions (Figure 3). Sterile equipment was set up as show in Figure 28 prior to opening of the three Aldon bags which kidneys are commonly stored in during transfer.

Following removal from static cold storage, arterial and venous anatomy was identified and dissected free from surrounding peri-hilar tissue, tying non-essential arterial and venous branches securely to ensure haemostasis on reperfusion. The aortic patch was divided to leave a wide circumference of aorta around the renal artery ostium which permitted attachment of a RingSeal connector as described below. Main renal vein and inferior vena cava, when present, were not divided to allow transplanting surgeon to decide about reconstructing venous anatomy prior to transplantation. The ureter was

dissected free from surrounding tissue whilst ensuring immediate peri-ureteric tissue remained intact to minimise ureteric ischaemic insult. Excess perinephric tissue was removed so as to expose the renal cortex with attention not to incise capsule. Anatomical variants and pathology such as renal cysts and tumours were identified. Main renal artery and main renal vein were checked for leakage with a non-traumatic Tibbs cannula attached to a 20ml syringe filled with Ringer's lactate.

Following this, the kidney was prepared for attachment to the hypothermic machine perfusion circuit.

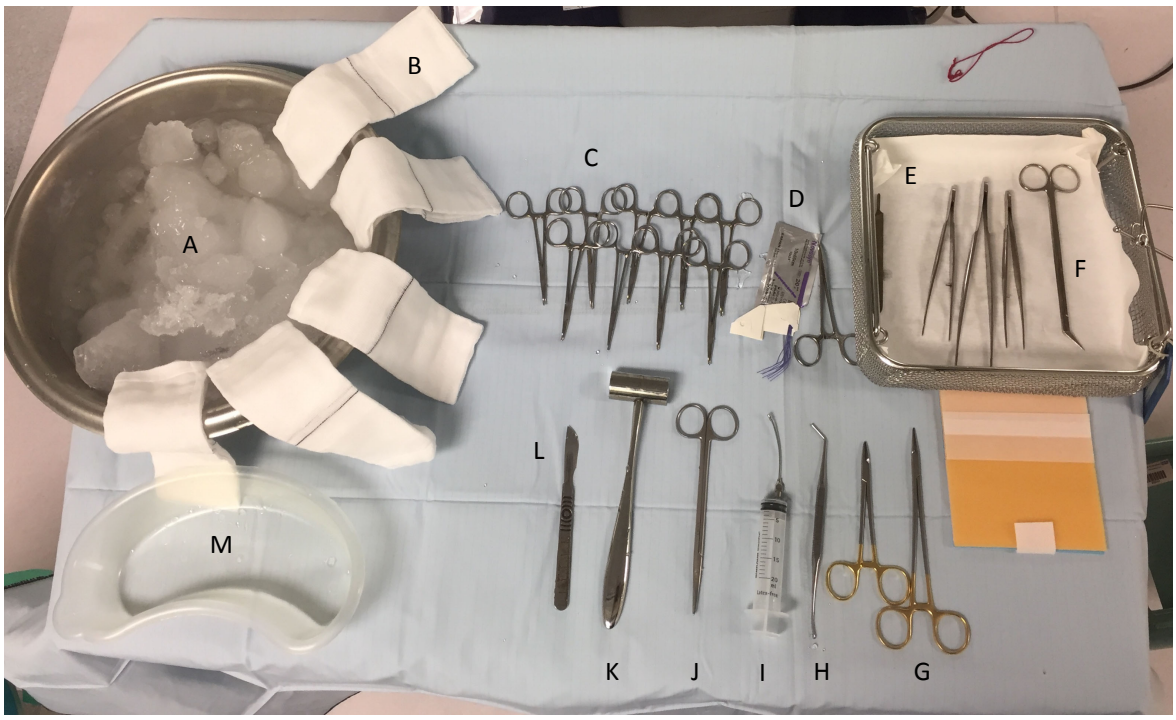

Figure 28. Theatre backbench set-up for preparation of human cadaveric kidneys. On a sterile operating theatre trolley, crushed ice in chilled fluid (3L frozen, 3L chilled Ringer's lactate solution) (A) were placed in a metal bowl accompanied by equipment for preparation of grafts including small swabs (B), straight clips (C), 3/0 Vicryl ties (D), non-toothed and fine toothed forceps (E), Potts scissors (F), needle holders (G) next to a sharps discarder pad, in addition to Watson Cheyne probe (H), 20ml syringe with Tibbs cannula attached, tissue scissors (J), mallet for smashing ice (K), scalpel handle with 22 blade attached (L) and kidney dish (M).

Figure 29 shows a cadaveric kidney retrieved en-bloc complete with aortic patch. Main renal artery ostium is positioned to the left of the patch. Note atherosclerotic disease of patch. Perinephric fat surrounds the cortex which is visible in places.

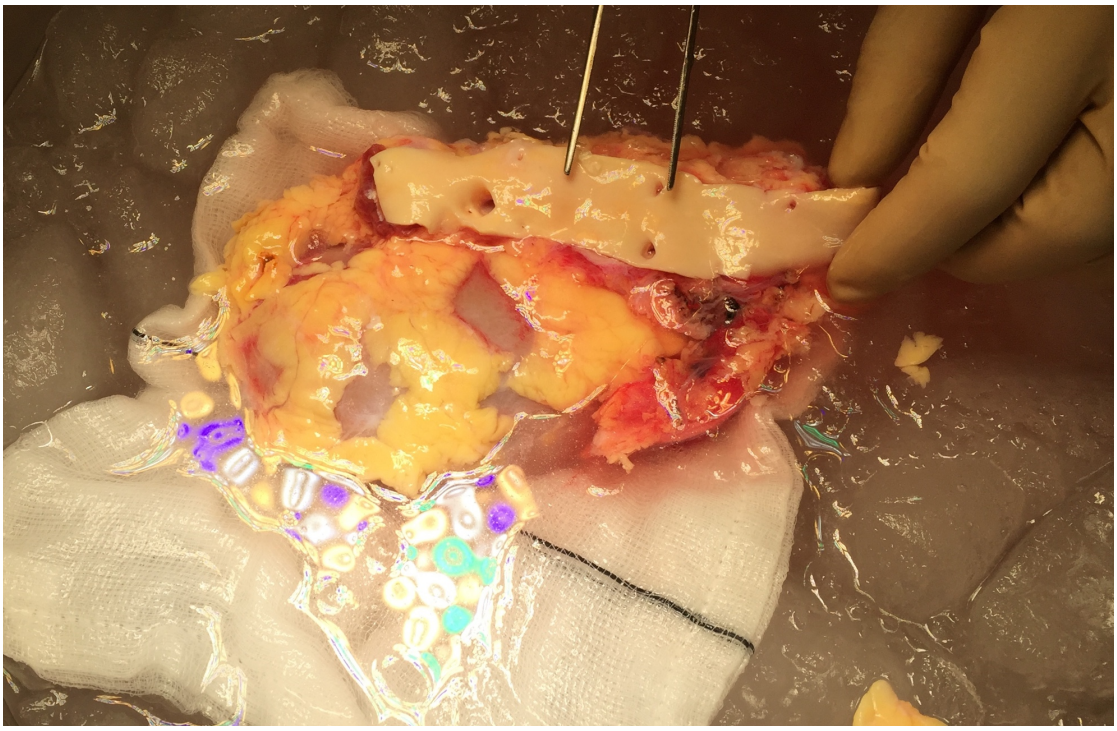

Figure 29. Cadaveric kidney following removal from static cold storage conditions.

Hypothermic Machine Perfusion

LifePort® Kidney Transporter

A LifePort® Kidney Transporter (Organ Recovery Systems, Chicago, USA) was used to provide hypothermic machine perfusion with key design features as described in Chapter 1. One of two versions of the LifePort® Kidney Transporter were used for experiments in this thesis. Experiments performed in the clinical setting were performed on either version 1.1 (Figure 30) or version 1.0 (Figure 31). All laboratory experiments were performed on the original version 1.0. Function and mechanism of action was identical between both versions.

Figure 31 shows version 1.0 in use in the laboratory setting perfusing a porcine kidney connected via a 5mm T-connector. Note this circuit includes a membrane oxygenator used for experiments in Chapter 6. Figure 30 shows a human kidney perfused on version 1.1 in the clinical setting via a RingSeal connector.

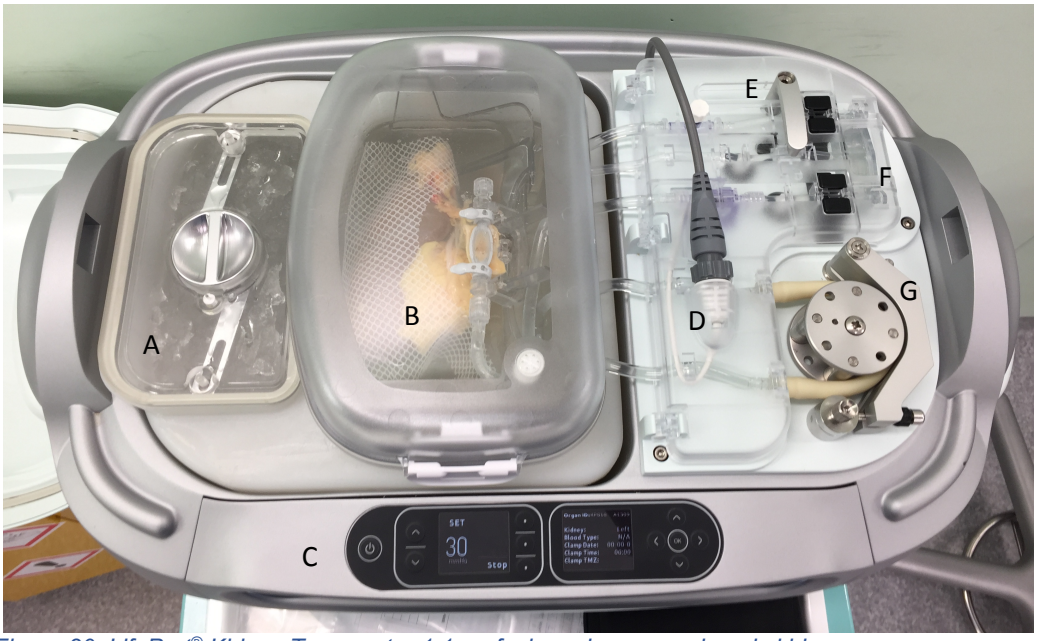

Figure 30. LifePort® Kidney Transporter 1.1 perfusing a human cadaveric kidney.

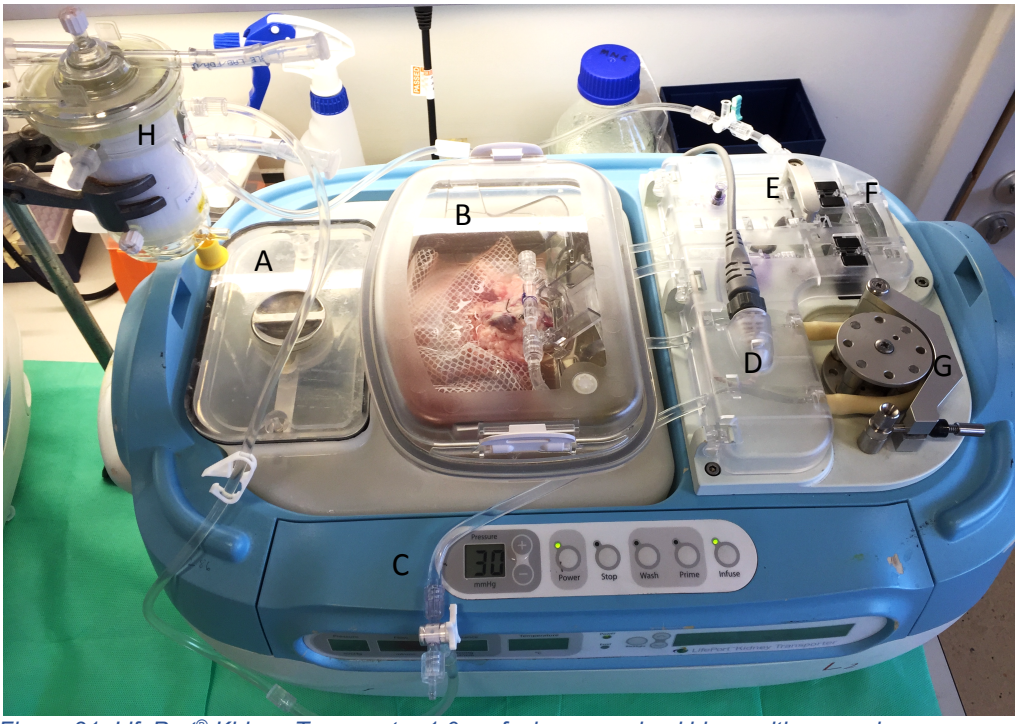

Figure 31. LifePort® Kidney Transporter 1.0 perfusing a porcine kidney with a membrane oxygenator incorporated into the perfusion circuit.

Preparation of renal artery prior to initiation of HMP

Pulsatile perfusion via the renal artery during machine perfusion requires the renal artery to be cannulated. Aside from an occlusive seal, the connection should also be non-traumatic to the intima of the artery to avoid pre-disposition to thrombosis post-operatively.

As per manufacturer instructions this is achieved via a RingSeal connector or a T-connector. A RingSeal connector requires a single main renal artery with an appropriate circumference of aortic patch in order to allow 2 overlapping plastic rings to seal the circumference of the patch. One ring covered in a rubber seal provides a view of the ostium via a transparent window whilst the exterior side of the artery/patch passes through the second ring as shown in Figure 32. This does not damage the intima of the renal artery or the aortic patch but does require a single renal artery and an appropriate circumference of patch to permit application of the RingSeal connector.

To attach the RingSeal connector, the edge of aortic patch was grasped gently and brought through lower ring. The overlying ring with viewing window was lowered into place ensuring a circumference of patch lay between upper and lower ring resulting in a water-tight seal. Two rubber ties were then used to secure the Ringseal in place. Flushing with a 20ml syringe with distal end of the connector open was used to check for an intact seal and also expel air from the viewing chamber. If the seal was not intact, the above steps were repeated. The distal end cap was then replaced with the viewing chamber full of fluid.

To attach the T-connector, a surgical clip was attached to the cut edge of the renal artery. An appropriate sized connector, either 3mm/ 5mm/ 7mm T-connector, was lowered into the lumen. The connector was secured with a 2/0 or 3/0 Vicryl tie (Ethicon, UK) lying in the fixation groove. Additional securing sutures were placed as required. As with the RingSeal connector, the connector was then flushed with 20ml syringe prior to placement of distal cap.

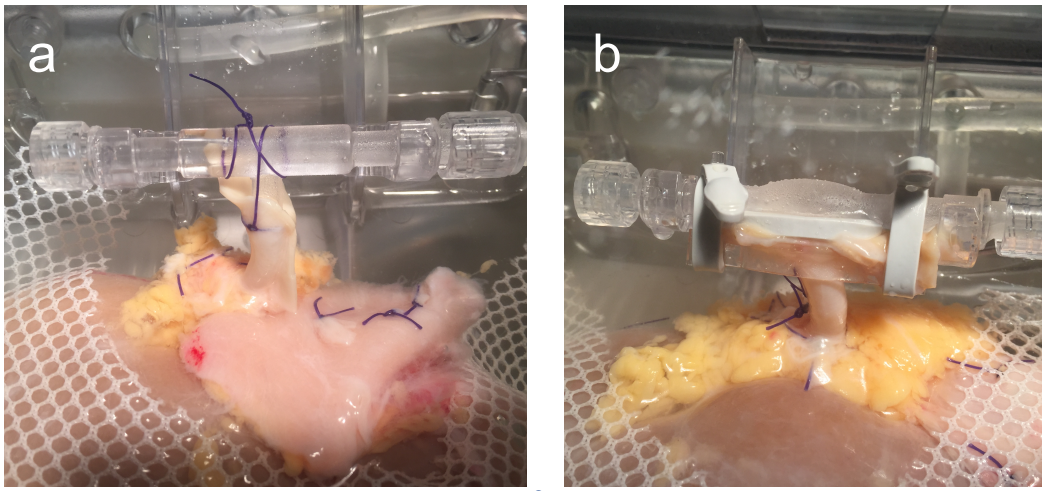

Figure 32. Attachment of the kidney to the LifePort® inflow limb using a T-connector (a) and RingSeal connector (b).

Figure 33 shows a prepared cadaveric kidney prior to insertion into the pre-prepared LifePort® cassette.

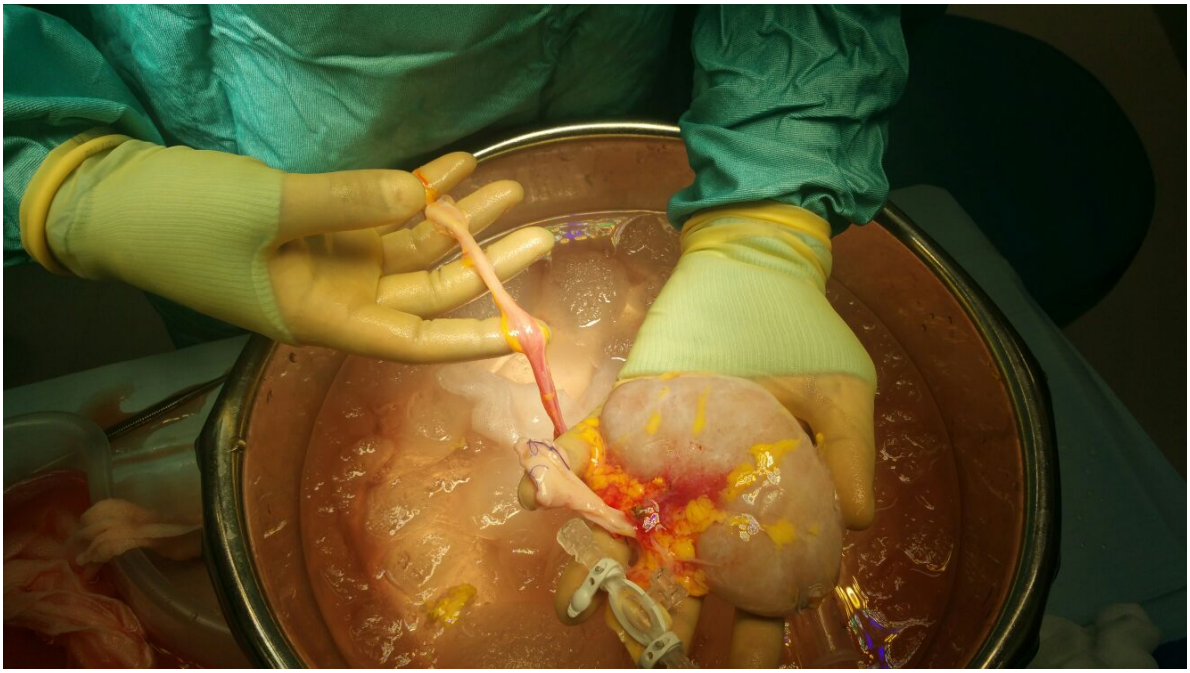

Figure 33. Cadaveric kidney prepared for hypothermic machine perfusion.

Set up of HMP

Kidneys were preserved using the LifePort® Kidney Transporter version 1.0 or 1.1 (Organ Recovery Systems, Chicago, USA). The following steps were performed as per manufacturer's instructions to prepare the cartridge prior to insertion of the kidney and attachment of T-connector/ RingSeal connector to perfusion tubing.

The ice reservoir was loaded with non-sterile crushed ice and agitated to ensure as much ice as possible filled the reservoir. The reservoir was then filled with tap water until enough ice had melted to permit further filling of crushed ice at which point ice was filled again. This latter step was repeated until ice/water level reached the brim of the reservoir at which point the reservoir lid was secured in place.

A disposable cassette was filled with 1 litre of UW-MPS on the sterile back-bench preparation table before replacing the internal and external cassette lids. The cassette pre-filled with UW MPS was placed into the ice reservoir of the LifePort®. The hinges of

the cartridge were secured in place with gentle pressure prior to placing rubber tubing over peristaltic mechanism. Rubber tubing of the peristaltic pump mechanism was secured in place with hinged lever. The cartridge lock was rotated into place prior to attachment of pressure/temperature sensing cable.

The 'flush' function was initiated for a pre-determined time, usually 5 minutes, allowing perfusion fluid to circulate through the tubing of the cassette. After placing sterile drape over LifePort® cassette, the outer lid and inner lid were removed and placed on backbench preparation table.

Following cessation of the 'flush' function by pressing 'stop', the pre-prepared kidney was placed on supporting platform of the LifePort® cassette covered by netting. Attention was paid to placing the artery and associated connector in the supporting jig so as not to place the renal artery under tension in order to avoid traction injury. This was always a vertical orientation which permitted direct visualization of the ostium via the transparent viewing chamber on Ringseal connector. Where possible, the kidney was placed with renal vein anteriorly to permit view of effluent.

The inflow limb of the perfusion circuit was connected to the T-connector/ Ringseal. The distal end cap was kept loose. At this point an assistant should press 'prime' in order to fill the inflow limb of the perfusion circuit, expelling any air via the distal end of the connector. Once all air is removed the cap should be tightened after pressing 'stop'. The 'start' button was then pressed to initiate perfusion.

Following initiation of perfusion, flow parameters were observed, the perfusion circuit checked for leaks and the kidney examined for leakage around T-connector/ RingSeal connector. Once satisfied, inner and outer lids were replaced. The sterile drape was then

removed. The outer insulating covering lid of the LifePort® machine was placed on the LifePort® when sampling was not in progress.

Perfusion pressure for all kidneys should be set at 30mmHg as a default, the pressure used in the initial Machine Preservation Trial (70) forming the evidence base for the use of HMP. Perfusion fluid used in all experiments was an identical composition to UW-MPS as originally described by Belzer (75) with formulation as described in Chapter 1. The solution is supplied by 2 manufacturers with product names Kidney Perfusion Solution (KPS-1®, Organ Recovery Systems limited) and Belzer Machine Perfusion Solution (Belzer MPS®, Bridge to Life Europe limited). The formulation is identical regardless of supplier.

Figure 34. Custom made Kidney Perfusion Solution containing U-^{13}C glucose.

In some experiments the 10mM glucose in a standard 1L bag of perfusion fluid was supplemented with an additional 0.93g U-^{13}C glucose resulting in a concentration of 15mM. In Chapter 7 human cadaveric kidneys were perfused with a specially made batch of clinical grade KPS-1 in which all glucose was U-^{13}C labelled supplied in bottles as shown in Figure 34.

Sampling of perfusate from the LifePort®

Timing and volume of perfusate sampled from the LifePort® varied according to experiment protocol. However, the aseptic technique for sampling remained the same. Before sampling, perfusion parameters and temperature were noted. Such data was noted prior to sampling as disturbance of flow in the perfusion tubing resulted in the LifePort® machine recalibrating flow and resistance parameters.

Wearing sterile gloves, the cap was removed from the sampling port. Following this a fresh sterile 5ml syringe was inserted firmly into the sampling port creating a water-tight seal and kept vertical. The desired volume of fluid was aspirated into the syringe prior to removal from the sampling port.

Fluid was then expelled into 2ml cryovials then placed in -20°C freezer storage prior to transfer to -80°C freezer storage until sample analysis. In Chapter 7 where experiments were performed in the clinical setting, cryovials were placed directly in dry ice prior to freezer storage at -80°C.

Where perfusion fluid was sampled to be run in a Point of Care blood gas analyser, 1ml was retrieved in a blood gas syringe. Samples were run in a calibrated Point of Care analysis machine (Cobas® b221, Roche Diagnostics Limited) to provide pH, pO_2, pCO_2, lactate and glucose readings level in real time. At no point was any perfusion fluid returned to the perfusion circuit or reservoir.

End-point tissue sampling

At the end of the perfusion period, kidneys were removed from the LifePort® and quickly taken to a work station where they were laterally bisected to maximise medullary

exposure. Following this, sections of cortex and medulla no larger than 1cm^3 were dissected out and placed in 50ml Falcon tubes then flash frozen in liquid nitrogen prior to storage at -80°C. Figure 35 shows a laterally bisected porcine kidney with dotted lines indicating where tissue would be sampled for cortex and medulla samples.

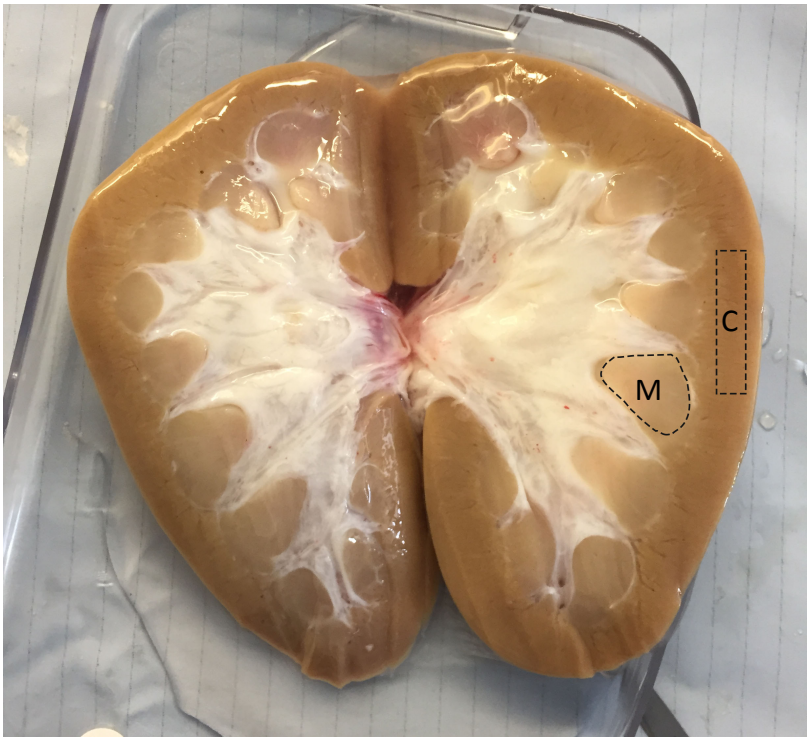

Figure 35. Laterally bisected porcine kidney following hypothermic machine perfusion with examples of areas of renal cortex (C) and medulla (M) highlighted from which tissue was sampled.

NMR and MS sample preparation

Preparation of perfusate samples

Perfusate samples were either extracted for analysis or run 'neat'. When samples were extracted, perfusate samples for 1D ^{1}H NMR, 2D ^{1}H,^{13}C HSQC NMR and GC-MS analysis were taken from the upper layer of a biphasic solution containing polar metabolites, formed from a vigorously mixed solution of equal amounts of neat perfusate, methanol (-80°C) and chloroform (-20°C). Polar extracts were dried at 35°C in a vacuum drier.

When analysed 'neat,' perfusates were thawed and vortexed before 430µl was added to an Eppendorf in addition to 230µl NMR buffer. Contents were mixed by vortexing for ten minutes before being sonicated for ten minutes to break up any microparticles.

Preparation of end-point tissue samples

Cortex and medulla samples were cryo-homogenised manually using a Cryo-cup grinder (Biospec Products, Bartlesville, OK, USA). From this, 0.5g was suspended in 5.1ml methanol (-80°C) and homogenised in 7ml Tissue homogenizing CK28 tubes (Bertin Technologies, Montigny-le-Bretonneux, France) using a Precellys® 24 Dual homogeniser (Bertin Technologies, Montigny-le-Bretonneux, France) at low speeds in short intervals (5000 RPM for 8x10 s) to prevent samples from heating. Following this, 5.1ml Chloroform (-20°C) and 4.65ml de-ionised water were then added and the resultant solution mixed vigorously. From the upper polar layer of the sample, 1.5ml was aspirated and dried at 35°C overnight in a vacuum drier.

Re-suspension of extracted tissue samples

The composition of standard NMR Buffer solution is as follows: 100 mM phosphate buffer, containing 0.5 mM DSS, 2mM Imidazole and 10% D_2O. In the case of extracted samples, dried polar residue was resuspended in 600µl of standard NMR buffer.

Neat perfusate samples were prepared using a four-fold concentrated NMR buffer solution with the following composition: 400 mM phosphate buffer containing 2 mM DSS and 8 mM imidazole. 150µl of four-fold buffer was mixed with 390µl of each fluid sample and 60µl of D_2O to reach a final D_2O concentration of 10%.

For all neat samples and resuspended polar extracts, 600µl of sample was added to a 5mm NMR tube and then hand-centrifuged to remove air bubbles before being wiped with methanol using a lint free cloth. Sample cassettes were then loaded into the Bruker 600MHz spectrometer auto-sampler where they were kept at 4°C until NMR experiments were performed.

NMR

NMR data was acquired using a 600 MHz Bruker Avance III NMR spectrometer at the Henry Welcome Building for Biomolecular NMR Spectroscopy, University of Birmingham. One-dimensional proton NMR spectroscopy (1D-^{1}H NMR) and two-dimensional proton-carbon Heteronuclear Single Quantum Coherence spectroscopy (2D-^{1}H,^{13}C HSQC) were used with a 5mm inverse Cryoprobe.

1D ^{1}H NMR acquisition protocols

Acquisition time per sample was 15 minutes. Sample temperature was set to 300 K. Water resonance was suppressed using NOESY-presat. The spectral width was set to 7288.6 Hz (12 ppm). For 1D-^{1}H spectra, 32768 data points were acquired using a 4 second relaxation delay and 128 transients. Automated tuning, matching and shimming to a DSS line width of <1Hz was performed prior to acquisition of each spectrum.

1D ^{1}H NMR analysis

Following acquisition, 1D-^{1}H Spectra were read into MetaboLab, a MATLAB based NMR software (177) where manual phase correction and spline baseline correction were performed before data export into Chenomx NMR Suite 8.3 (Chenomx INC, Edmonton, AB, Canada) where spectra were once again visualised with the area under each peak corresponding to the concentration of each metabolite. Where multiple peaks at different chemical shift positions related to a particular metabolite, metabolite concentration was determined via peak fitting at the same chemical shift position for each metabolite.

One function of Chenomx software is automated peak assignment for a pre-selected group of metabolites, also allowing for signal shift. Following automatic peak assignment, the allocation of each metabolite was checked/ re-allocated in each spectrum where allocation was deemed to be incorrect. All samples were effectively blinded from point of NMR experimentation when they were assigned a sample number until after spectral analysis.

To ensure reproducibility and consistency of analysis, the same peak annotation was performed at one area of chemical shift for all experiments. A reference table for metabolites was created with corresponding areas of chemical shift where peak annotation was performed (Table 3).

For metabolites where more than one peak appears in the same chemical shift area, Chenomx software shows peak assignment for each metabolite in addition to a summation spectral line for all metabolites which have been assigned. The reported concentrations were adjusted to account for dilution by NMR buffer.

Table 3. Position of spectral peaks used for metabolite quantification

Metabolite	NMR Chemical Shift Reference (ppm)	Metabolite	NMR Chemical Shift Reference (ppm)
3-Hydroxybutyrate	1.204	Hippurate	7.82
3-Methylxanthine	8.02	Hypoxanthine	8.20
Acetate	1.91	Inosine	6.055
Adenine	8.11	Isoleucine	0.997
Alanine	1.46	Isopropranolol	1.162
Citrate	2.67	Lactate	1.40
Ethanol	1.17	Leucine	0.948
Formate	8.44	Malonate	3.11
Fumarate	6.51	Mannitol	3.840
Gluconate	4.12	N-Phenylacetylglycine	7.412
Glucose	3.524	Ribose	2.21
Glutamate	2.341	Tyrosine	6.877
Glutathione	2.97	Uracil	7.52
Glycine	3.54	Valine	1.029

2D -^{1}H,^{13}C HSQC acquisition protocols

For 2D-^{1}H,^{13}C HSQC experiments, spectral widths were set to either 7,288.6 Hz (^{1}H, 12 ppm) or 24,155 Hz (^{13}C, 160 ppm). 512 complex data points were acquired for the ^{1}H dimension of 2D-^{1}H, ^{13}C-HSQC NMR spectra. 30% of 2048 complex data points (614 complex data points) were acquired for the ^{13}C dimension. The spectra were zero-filled to 1024 (^{1}H) times 16384 (^{13}C) real data points prior to multiplet simulation analysis.

Acquired spectra were reconstructed with compressed sensing using the MDDNMR and NMRpipe software (178-180) prior to analysis using MetaboLab, which uses pyGamma software for multiplet simulations (181).

2D -^{1}H,^{13}C HSQC analysis

Chemical shift was first calibrated using the methyl group of lactate as per its assignment in the human metabolome database (182) resulting in a 2D spectrum display shown in Figure 36 where ^{1}H chemical shift is shown on the x-axis and ^{13}C chemical shift is shown in the *y*-axis.

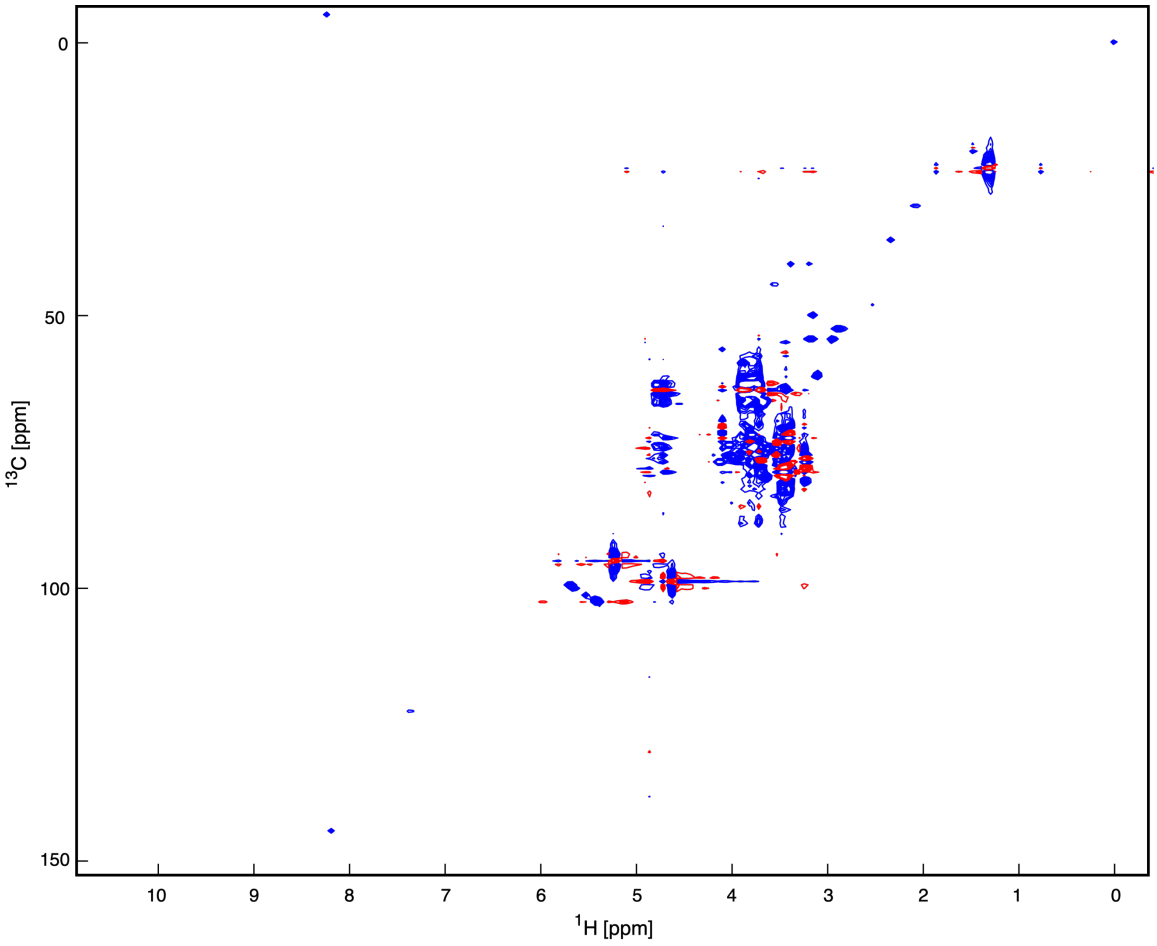

Figure 36. 2D ^{1}H-^{13}C HSQC spectrum of perfusate sample using KPS-1 supplemented with universally labelled glucose. Axes denote chemical shift of ^{13}C nuclei (y-axis) and ^{1}H nuclei (x-axis).

Spectral peaks were manually allocated to the nuclei of carbon atoms with an attached proton within metabolites from the metabolite library available in Metabolab (Figure 37). Simulated spectral patterns reflecting combinations of different isotopomer distributions

were then matched to observed splitting patterns of each carbon nucleus (Figure 38, Figure 39).

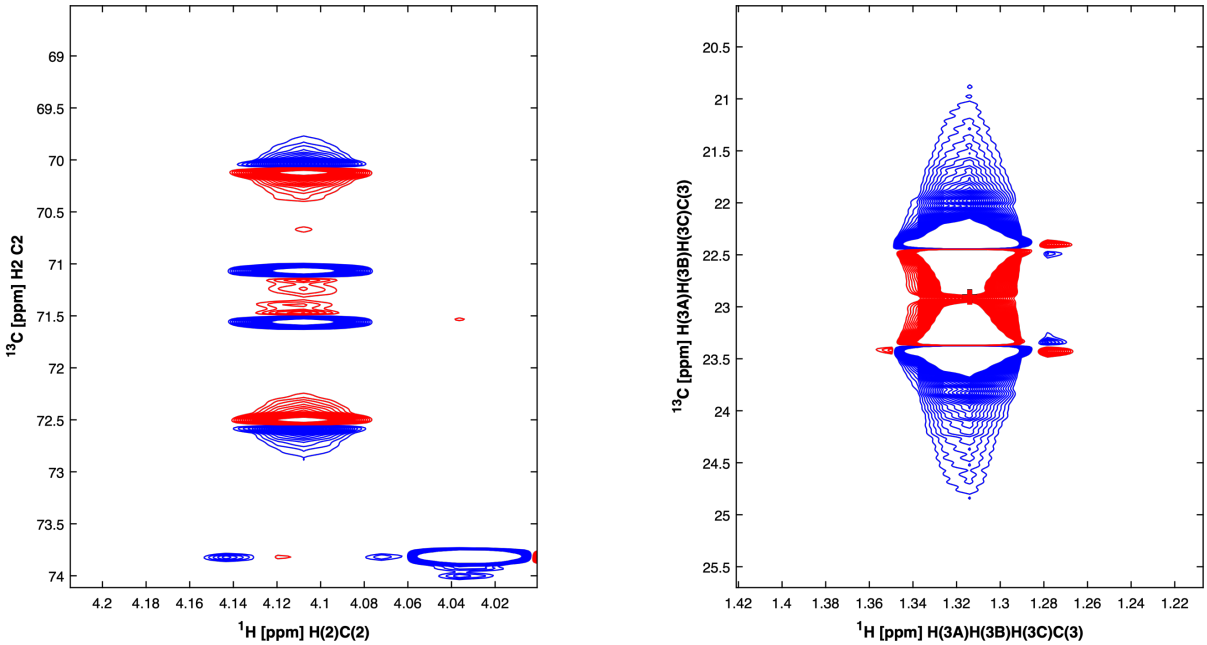

Figure 37. Spectral peaks attributed to C(2) and C(3) of lactate

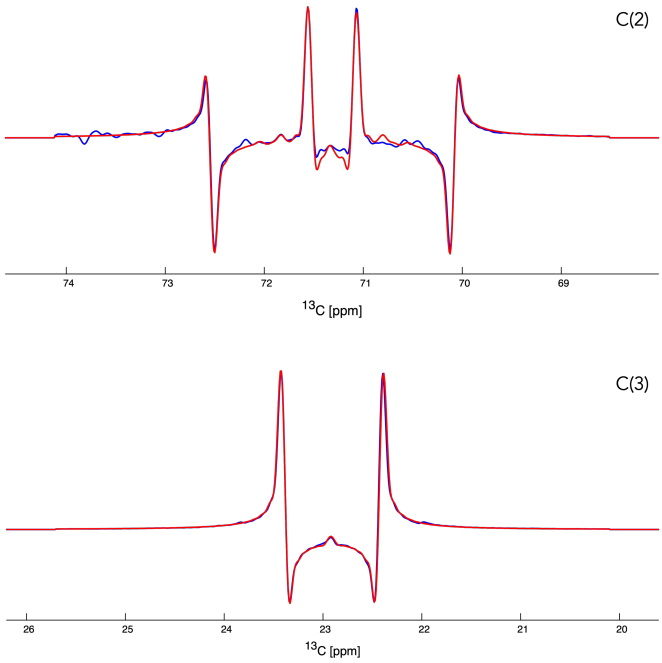

Figure 38. Splitting of C(2) and C(3) of lactate.

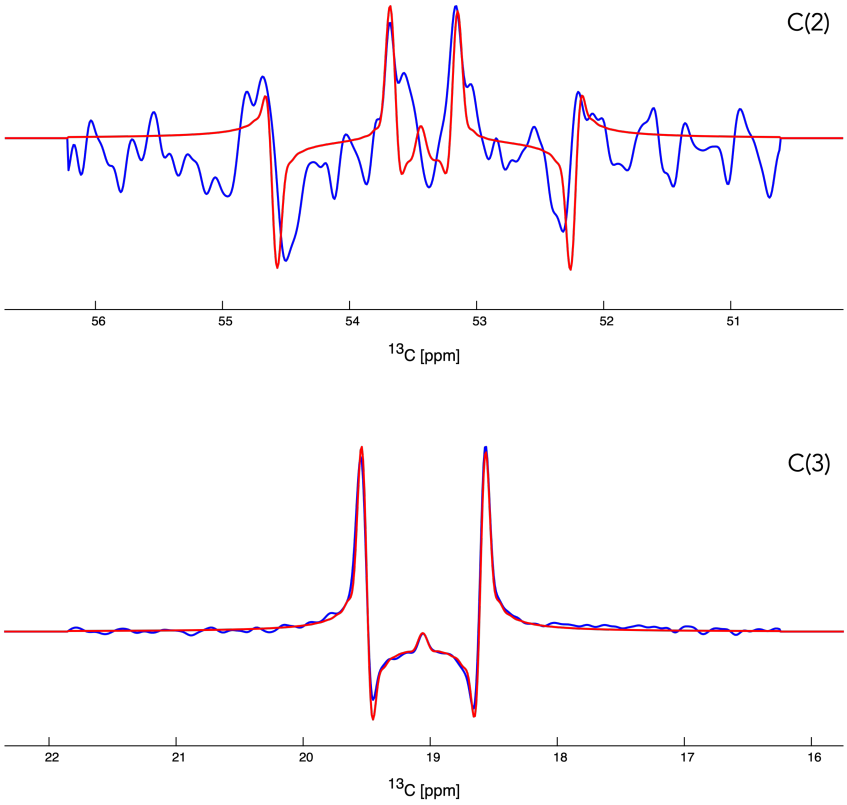

Figure 39. Splitting of C(2) and C(3) of alanine.

Where mass spectrometry was also used to analyse samples, MetaboLab was used to integrate data from 2D $^{1}H,^{13}C$ HSQC NMR and GCMS using a model free approach (158) to derive isotopomer distributions for key metabolites of interest.

Firstly, a set of isotopomers to be fitted was proposed including an estimation of how much isotopomer was present. Following this, Metabolab software back-calculated multiplet percentages as well as MID percentages. The software then compared the back-calculated percentages with experimental data. A simplex fitting algorithm was then used to determine the optimum percentages of proposed isotopomers to fit the experimental data. After fitting, any major discrepancy between simulated and experimental data required the selection of alternative or additional isotopomer distributions.

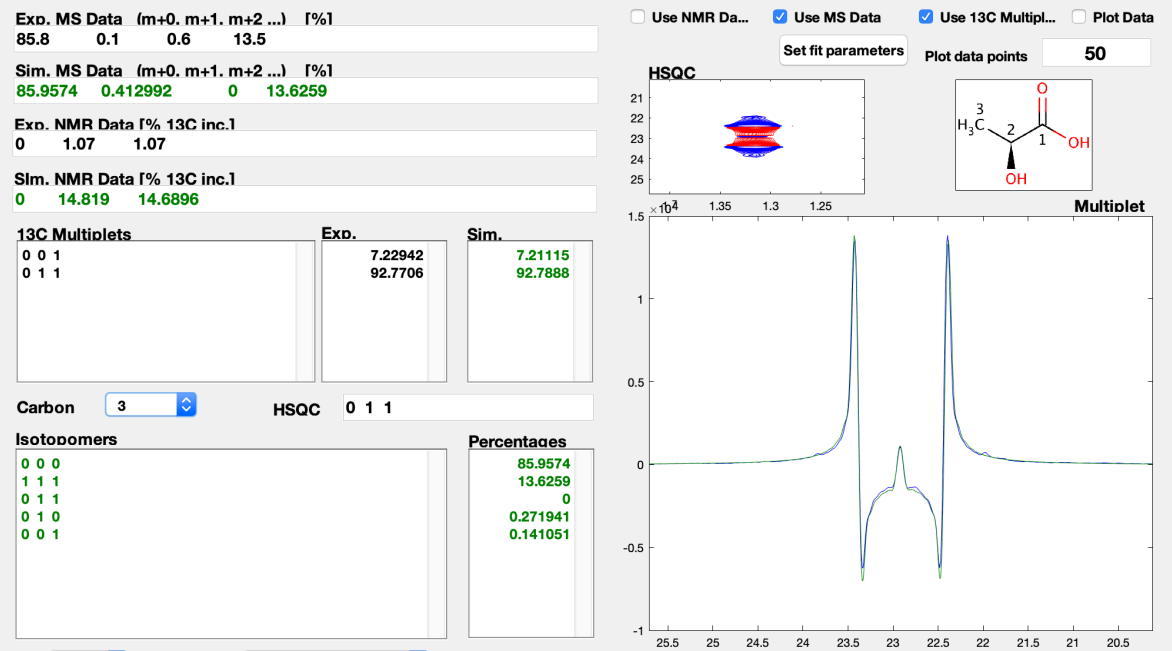

Figure 40. Calculation of isotopomer combinations of lactate using imputed 2D NMR and MS data on Metabolab software.

Gas Chromatography-Mass Spectrometry

Mass spectrometry samples were analysed by Alpesh Thakker in the metabolic tracer analysis core (MTAC) facility in the Institute of Metabolism and Systems Research. GC-MS was performed on a standard volume of sample described for each set of experiments.

Sample derivatisation

In order to derivatize proteinogenic amino acids, organic acids and glycolytic intermediates for GC-MS analysis, the dried extract was incubated at 95°C for 60 minutes in open tubes in order to remove any residual moisture in the samples. The dried polar extract was dissolved in 40µl 2% methoxyamine HCL in pyridine (Sigma-Aldrich, Dorset,UK) followed by incubation for 60 minutes at 60°C. Subsequently, 60µl N-tertbutyldimethylsilyl-N-methyltrifluoroacetamide (MTBSTFA) with 1% (w/v) tertbutyldimethyl-chlorosilane (TBDMSCI) (Sigma-Aldrich, Dorset, UK) derivatization reagent was added. The sample was then again incubated for 60 minutes at 60 °C in a

well-sealed tube which prevented evaporation. Samples then underwent centrifugation at 13,000 rpm for 5 minutes. The clear supernatant was transferred to a chromatography vial with a glass insert (ThermoFisher, Scientific, Chromacol, Hertfordshire, UK) and proceeded immediately to GC-MS analysis.

Analysis of derivatised samples

GC-MS was performed using an Agilent 7890B Series GC/MSD gas chromatograph with a polydimethylsiloxane GC column coupled, with a mass spectrometer (Agilent Technologies UK Limited, Stockport, UK). Prior to sample analysis the GC-MS was tuned to a full width at half maximum (FWHM) peak width of 0.60 atomic mass units (a.m.u) in the mass range of 50 to 650 mass to charge ratio (m/z) using PFTBA tuning solution. A total of 1µl of each sample was injected into the GC-MS in split mode 1:10 with helium carrier gas at a rate of 1.0 ml/min. The inlet liner containing glass wool was set to a temperature of 270°C. Oven temperature was set at 100°C for 1 minute before ramping to 280°C at a rate of 5°C/min. Temperature was further ramped to 320°C at a rate of 10 °C min/min held at 320°C for 5 minutes. Compound detection was carried out in full scan mode in the mass range 50 to 650 m/z, with 2-4 scans/sec, a source temperature of 250°C, a transfer line temperature of 280°C and a solvent delay time of 6.5 minutes. The injector needle was cleaned with acetonitrile three times before measurement commencement and three times following every measurement thereafter.

Raw GC-MS data was converted to common data format (CDF) using the acquisition software. For determination of the mass isotopomer distributions (MIDs), spectra were corrected for natural isotope abundance. Data processing from raw spectra to MID correction and determination was performed using MetaboliteDetector software (183).

Calculation of the concentration of labelled metabolites

The area of chemical shift at which peak annotation was performed in 1D spectra corresponded to the chemical environment of a proton, group or neighbouring protons. This chemical environment is influenced by the presence of a neighbouring ^{13}C atom. Hence when quantifying the concentration of lactate using 1D ^{1}H NMR, the quantification is based on the ^{1}H signal neighbouring a ^{12}C atom in the position of carbon 2 in the lactate molecule.

Combined analysis using 2D NMR and GCMS data using Metabolab details isotopomer distributions, enabling a calculation to be performed to determine the proportion of isotopomers of lactate, for example, with an unlabelled ^{12}C atom at the position of the second carbon in the lactate molecule. Using this information and the concentration of lactate determined using ^{1}H signal adjacent to ^{12}C atom at the carbon 2 position, the concentration of U-^{13}C lactate can be determined by scaling concentrations according to the isotopomer distribution. Similar calculations were performed to determine the absolute concentration of U-^{13}C alanine.

Histology

Light Microscopy

Wedges of renal cortex and medulla from 3 pairs of HMP/O_2 and HMP/Air kidneys and renal arteries were fixed in formalin and processed to a paraffin block. Following this, 4µm sections of renal cortex and medulla were stained with Haematoxylin and Eosin (H&E) and Periodic Acid Schiff (PAS) whilst renal artery sections underwent staining with H&E alone.

Photomicrographs of 10 random glomeruli (40x magnification), 10 random areas containing predominantly tubules (5 subcapsular and 5 mid-cortex at 20x magnification) and 5 transverse sections of intra-parenchymal arteries (20x magnification) were assessed. Image J 1.05i software (National Institute of Health, USA) was used for morphometric assessment.

Images were assessed for evidence of injury using glomerular shrinkage, interstitial oedema and perivascular oedema as indicators of damage. To calculate glomerular shrinkage, the percent glomerular area occupied by glomerular tuft was determined for each glomerulus. The mean distance between 25 random tubules for each photomicrograph was used as a surrogate marker of interstitial oedema. The proportion (%) of vessel area to adventitia was calculated to determine the extent of perivascular oedema; lower percentages indicated more perivascular oedema.

The injury of extra-parenchymal renal arteries were semi-quantitatively graded: endothelial denudation: 0 nil, 1 minimal, 2, moderate, 3 extensive; Intimal oedema: 0 nil, 1 focal, 2 moderate to extensive; medial oedema and vacuolation of smooth muscle cells: 0 normal, 1 minimal, 2 moderate to extensive.

Electron Microscopy

Standard protocols of the Electron Microscopy Laboratory, University Hospitals Birmingham, Birmingham, UK were followed. For electron microscopy (EM), biopsies (2mm x 2mm x 5mm) of renal cortex were fixed in 2.5% glutaraldehyde in 0.1 M phosphate buffer, pH 7.4 then postfixed in osmium tetroxide and en-bloc stained with uranyl acetate before being processed by standard techniques to an epon araldite block. Thick sections

were stained with toluidine blue and ultrathin sections stained with lead citrate and examined by a Joel JEM1200-EX 11 electron microscope.

Random photomicrographs were taken of glomeruli, tubules and arteries/arterioles at 6800x to include mesangial areas and glomerular capillary loops. Of the total mitochondria present, the percent of glomeruli of normal morphology, condensed and containing flocculent densities were determined for each kidney. Both the pathologist and technician who acquired and analysed images with light and electron microscopy were blinded to the kidney allocation groups.

Histological analysis was performed by Desley Neil, Consultant Pathologist.

Biochemical Assays

Glutathione assay

Samples were prepared by adding 0.2g powdered renal cortex to 5ml ice cold cell lysis buffer (0.1 % Triton X-100 in PO_4-EDTA assay buffer) prior to mixing via vortex. PO_4-EDTA assay buffer consisted of 5 mM EDTA, 100 mM NaH_2PO_4, adjusted to pH 8.0. At this point 200 μL was removed for protein estimation, performed using the Bradford assay.

In a new tube, 900 μl of the sample was added to 100 μL ice-cold 50% trichloroacetic acid (TCA). Protein-free supernatants containing reduced glutathione (GSH) were prepared by centrifugation of the samples at 20,000 rpm for 20 minutes at 4°C. Of the supernatant, 10 μL was used as the sample in the GSH assay.

The GSH assay, first described by Hissin and Hilf (184), was used to calculate GSH concentrations. Samples prepared as above were transferred to a 96 well plate with prior addition of 180 μL PO_4-EDTA assay buffer to each well. A standard curve was constructed (0.1-1.2 μg GSH) using a freshly made GSH stock solution (0.1 mg/ml in ice-cold assay buffer), which was added to wells containing 180μL of PO_4-EDTA assay buffer and 10μl 5% TCA.

Following addition of 10 μl *o*-phthalaldehyde solution (1 mg/ml in 100% methanol), samples were mixed thoroughly via agitation. Fluorescence was measured using a microplate reader (Infinite 200 Pro, Tecan) at an excitation wavelength of 355 nm and an emission wavelength of 420 nm. Total GSH (nmol) was determined from the standard curve and normalised to protein mass.

ThioBarbituric Acid Reducing Substances (TBARS) assay

Samples were prepared by adding 0.1g powdered renal cortex to 1ml KCl buffer (1.15% KCl and 1% DMSO) prior to mixing via vortex. At this point 200μL was removed for protein estimation, performed using the Bradford assay.

In a new tube, 200 μL of the sample was added to 200μL 8.1 % (w/v) sodium dodecyl sulphate, 1.5ml 20% (v/v) acetic acid (pH 3.5), 900μl thiobarbituric acid (TBA) solution, and 1.2ml distilled water. TBA was prepared as a 25mg/ml solution in 0.2M NaOH and the final TBA solution was prepared by mixing TBA, trichloroacetic acid and 12M HCl at a 6:5:1 ratio. The sample was heated at 95°C for 45 minutes, allowed to cool in a room temperature water bath, and centrifuged at 2000 g for 10 minutes. 250μl of each samples was transferred into triplicate wells in a 96-well plate. A standard curve was constructed for malondialdehyde (MDA) (0.5-5mM) using an MDA standard solution (500mM). Varying volumes of the MDA standard were added to wells containing 250μL of the TBA solution described above. The absorbance was measured at 532nm using a microplate reader (CLARIOstar, BMG Labtech) and total MDA (nmol) was determined from the standard curve and normalised to protein mass.

TBA and GSH were purchased from Sigma-Aldrich, UK. TCA and BSA were purchased from Fisher Scientific, UK. OPT was purchased from MP Biomedicals, UK. The MDA standard solution was purchased from Cayman Chemical, supplied by Cambridge Bioscience, UK.

Glutathione S Transferase Pi assay

A glutathione s transferase pi (GST Pi) enzyme-linked immunosorbent assay (ELISA) was performed as per manufacturer's instructions (Oxford Biomedical Research, UK). Following thawing of perfusate samples, 100μL of perfusate sample was added to a corresponding well on the 96 well microplate provided prior to incubation at room temperature for 1 hour. A standard curve was prepared for GST Pi (0-10ng/mL) using a GST Pi standard solution (10ng/mL) prior to the same incubation period.

The contents of each well was then washed. This involved the contents of the microplate being shaken out prior to washing of each well three times with 300μL wash buffer. The microplate was then tapped on a lint free towel to ensure no solution remained in the well. The microplate was then incubated at room temperature for 1 hour following addition of 100μL of detection antibody prior to repeating the wash step as described. The microplate was then incubated again at room temperature for 30 minutes following addition of 100μL HRP conjugate to each well. The wash step was then repeated.

After addition of 100μL TMB substrate (stabilised TMB reagent), colour was allowed to develop in the plates. The reaction was stopped with the addition of 25μL 3N sulphuric acid to each well. The base of each microplate was wiped with a lint free cloth prior to insertion into the plate reader. Plates were read at 450nm in a microplate reader. The change in standard concentration was plotted against the concentration of GST Pi, in order to determine final concentrations of GST Pi in each perfusate sample, with a standard curve plotted using linear regression and a line of best fit intersecting the origin of *x* and *y* axes.

Neutrophil Gelatinase-Associated Lipocalin assay

Human Lipocalin-2/ neutrophil gelatinase-associated lipocalin (NGAL) ELISA was performed as per manufacturer instructions (R&D Systems, UK). A standard curve was prepared for NGAL (0-10ng/mL) using the calibrated diluent RD5-24 supplied (100ng/ml).

To begin with, 100μL of assay diluent RD1-52 was added to each well of the 96 well microplate provided. Either 50μL standard or 50μL sample was then added to each well. Wells were covered with adhesive tape prior to incubation for 2 hours at 2-8°C in a laboratory fridge. Each well was then aspirated and washed with wash buffer solution 400μL using a squirt bottle. This wash step was performed 4 times. Following the 4^{th} wash, any remaining liquid was removed by decanting then blotting against a lint free towel.

Following addition of 200μL cold Human Lipocalin-2 conjugate to each well the plate was covered with adhesive strips and incubated for 2-8°C in a laboratory fridge for 2 hours. The plate was washed 4 times as described above. Following addition of 200μL of substrate solution to each well, the plate was then incubated at room temperature for 30 minutes protected from light.

A total of 50μL of stop solution was then added to each well following observation of colour change from yellow to blue. The base of each microplate was wiped with a lint free cloth prior to insertion into the plate reader. Plates were read at 450nm in a microplate reader. The change in standard concentration was plotted against the concentration of NGAL, in order to determine its final concentration in each perfusate sample, with a standard curve plotted using linear regression and a line of best fit intersecting the origin of x and y axes.

Lactate Dehydrogenase assay

Lactate dehydrogenase assay was performed according to manufacturer's instructions (Sigma-Aldrich, St. Louis, USA). A standard curve was prepared by adding 0, 2, 4, 6, 8 and 10μL of 1.25mM NADH generating 0 to 12.5nmol. 25μL of perfusate samples was added to each well of a 96 well plate in addition to 25μL of assay buffer. The contents of each plate was mixed via horizontal shaking for 1 minute.

The base of each microplate was wiped with a lint free cloth prior to insertion into the plate reader. After 2 minutes, plates were read at 450nm in a microplate reader. The plate was then incubated in the dark at 37°C for 5 minutes prior to a second absorbance reading taken at 450nm.

Further absorbance readings were taken at 450nm until the most active sample was near the end of the linear range of the standard curve. To analyse results, the absorbance reading from the blank 0nmol NADH reference sample was subtracted from the final absorbance reading from each sample for plates read at each time point. The change in absorbance measurement between initial and end point plates was calculated for each sample and for standard concentrations. The change in standard concentration was plotted against the concentration of NADH, in order to determine final concentrations of NADH in each perfusate sample, with a standard curve plotted using linear regression and a line of best fit intersecting the origin of x and y axes.

Chapter 3 : Developments in NMR spectroscopy techniques: ^{13}C spectral filters and J-Coupling based splitting enhancement

In this Chapter, two advances in NMR methodology are described with their utility demonstrated for analysing perfusate and tissue samples following HMP. The techniques were written up and submitted in the form of a manuscript which was published in Wellcome Open Research in September 2018 (185).

The techniques were developed in conjunction with my supervisor Christian Ludwig. I wrote and refined the manuscript in addition to performing porcine kidney experiments to demonstrate the utility of ^{13}C spectral filters and J-Coupling based splitting enhancement in 2D-NMR spectra. The manuscript follows a short commentary.

Introduction

Advances in NMR methodology including modification and development of pulse sequences are key to improving sensitivity of such experiments with shorter sample run time. The combination of NMR and mass spectrometry data is useful to determine isotopomer distribution when both techniques are combined in a model-free approach (158). However, such methodology does not readily aid quantification of labelled metabolites as 2D $^{1}H,^{13}C$ HSQC pulse sequences also require 1D ^{1}H NMR pulse sequences to allow metabolite quantification. The time taken to analyse one sample using such pulse sequences is around 4 hours.

For the purposes of identifying labelled metabolites which are a product of universally labelled glucose, the ideal pulse sequence would be permit quantification of labelled metabolites in a short time enabling multiple samples to be run in a short period. Bon et al suggested simple 1D ^{1}H NMR pulse sequences may be useful to analyse perfusate samples during HMP in the clinical setting (172).

In this Chapter, quantitative spectral filters were developed and used to analyse the perfusate of kidneys undergoing HMP. In addition, the attached publication describes J-Coupling based splitting enhancement in 2D-NMR spectra. This technique was applied to extracted renal cortex samples acquired from a kidney which underwent oxygenated HMP as part of experiments described in Chapter 7.

Quantitative spectral filters

It is not possible to determine whether the singlet component in the multiplet is present due to natural abundance or label incorporation over and above natural abundance. As a

consequence, the quantitative multiplet analysis needs additional information to scale the multiplet percentages. Such information could be mass isotopomer distribution data. In the absence of such data, the additional information can either be created by preparing paired samples (labelled/ unlabeled), albeit at the risk of incorporating biological noise into the data, or by the use of quantitative spectral filters, which allow the determination of absolute per carbon percentages of ^{13}C incorporation. Quantitative spectral filters therefore provide a quick test for ^{13}C incorporation with the limitations that 1D spectra are subject to signal overlap restricting the extent to which signals can be assigned accurately.

Enhancement of J-coupling based splitting

The manuscript describes pulse sequences which enhance J-coupling based splitting with the main advantage being a reduction in the number of increments which need to be acquired as a result of the pulse sequence reducing NMR data acquisition times.

This was used routinely for NMR experiments conducted during this thesis with a resultant four-fold decrease in acquisition times. When used in conjunction with non-uniform sampling, this permitted a further four-fold decrease in acquisition time meaning increments which were previously acquired in 16 hours were acquired within an hour.

Manuscript

Smith TB*, **Patel K***, Munford H, Peet A, Tennant DA, Jeeves M, Ludwig C. High-Speed Tracer Analysis of Metabolism (HS-TrAM). Wellcome Open Research. 2018; 3:5

(*denotes equal contribution)

METHOD ARTICLE

REVISED High-Speed Tracer Analysis of Metabolism (HS-TrAM) [version 2; referees: 4 approved]

Thomas Brendan Smith[1*], Kamlesh Patel[1*], Haydn Munford[1], Andrew Peet[2,3], Daniel A. Tennant [1], Mark Jeeves [2*], Christian Ludwig [1*]

[1]Institute of Metabolism and Systems Research, University of Birmingham, West Midlands, UK
[2]Institute of Cancer and Genomic Sciences, University of Birmingham, West Midlands, UK
[3]Birmingham Children's Hospital NHS Foundation Trust, West Midlands, UK

[*] Equal contributors

v2 **First published:** 12 Jan 2018, **3**:5 (doi: 10.12688/wellcomeopenres.13387.1)
Latest published: 22 Aug 2018, **3**:5 (doi: 10.12688/wellcomeopenres.13387.2)

Abstract

Tracing the fate of stable isotopically-enriched nutrients is a sophisticated method of describing and quantifying the activity of metabolic pathways. Nuclear Magnetic Resonance (NMR) spectroscopy offers high resolution data in terms of resolving metabolic pathway utilisation. Despite this, NMR spectroscopy is under-utilised due to length of time required to collect the data, quantification requiring multiple samples and complicated analysis. Here we present two techniques, quantitative spectral filters and enhancement of the splitting of ^{13}C signals due to homonuclear $^{13}C,^{13}C$ or heteronuclear $^{13}C,^{15}N$ J-coupling in $^{1}H,^{13}C$-HSQC NMR spectra. Together, these allow the rapid collection of NMR spectroscopy data in a quantitative manner on a single sample. The reduced duration of HSQC spectra data acquisition opens up the possibility of real-time tracing of metabolism including the study of metabolic pathways *in vivo*. We show how these techniques can be used to trace the fate of labelled nutrients in a whole organ model of kidney preservation prior to transplantation using a porcine kidney as a model organ. In addition, we show how the use of multiple nutrients, differentially labelled with ^{13}C and ^{15}N, can be used to provide additional information with which to profile metabolic pathways.

Keywords

NMR, stable-isotope tracing, 13C, 15N, splitting enhancement, metabolism, tracer

Open Peer Review

Referee Status: ✓ ✓ ✓ ✓

	Invited Referees 1	2	3	4
REVISED **version 2** published 22 Aug 2018	✓ report	✓ report		✓ report
version 1 published 12 Jan 2018	? report	? report	✓ report	? report

1 **Sebastien Serres**, University of Nottingham, UK

2 **Paul C. Driscoll**, Francis Crick Institute, UK

3 **Julian L. Griffin**, University of Cambridge, UK

4 **Hector C. Keun**, Imperial College London, UK

Discuss this article

Comments (0)

Corresponding authors: Mark Jeeves (M.Jeeves@bham.ac.uk), Christian Ludwig (C.Ludwig@bham.ac.uk)

Author roles: Smith TB: Data Curation, Formal Analysis, Investigation, Methodology, Validation, Writing – Original Draft Preparation, Writing – Review & Editing; **Patel K**: Data Curation, Formal Analysis, Investigation, Methodology, Validation, Writing – Original Draft Preparation, Writing – Review & Editing; **Munford H**: Data Curation, Investigation, Methodology, Writing – Original Draft Preparation, Writing – Review & Editing; **Peet A**: Funding Acquisition, Resources, Supervision, Writing – Original Draft Preparation, Writing – Review & Editing; **Tennant DA**: Funding Acquisition, Resources, Supervision, Writing – Original Draft Preparation, Writing – Review & Editing; **Jeeves M**: Data Curation, Formal Analysis, Investigation, Methodology, Supervision, Validation, Writing – Original Draft Preparation, Writing – Review & Editing; **Ludwig C**: Conceptualization, Data Curation, Formal Analysis, Funding Acquisition, Investigation, Methodology, Project Administration, Resources, Software, Supervision, Validation, Visualization, Writing – Original Draft Preparation, Writing – Review & Editing

Competing interests: No competing interests were disclosed.

Grant information: This work was supported by the Wellcome Trust [099185] and through an Institutional Strategic Support Award given to the University of Birmingham; the National Institute for Health Research [13-0053]; Help Harry Help Others [HelpCU09]; UHB Charitable Funds [17-3-846] and the metabolic tracer analysis core (MTAC) at the University of Birmingham.
The funders had no role in study design, data collection and analysis, decision to publish, or preparation of the manuscript.

How to cite this article: Smith TB, Patel K, Munford H *et al.* **High-Speed Tracer Analysis of Metabolism (HS-TrAM) [version 2; referees: 4 approved]** Wellcome Open Research 2018, **3**:5 (doi: 10.12688/wellcomeopenres.13387.2)

First published: 12 Jan 2018, **3**:5 (doi: 10.12688/wellcomeopenres.13387.1)

REVISED **Amendments from Version 1**

This version addresses all major and most minor criticisms of the reviewers. We simplified the biological models and concentrated mostly on renal metabolism, by adding new experimental data. We also removed 900 MHz data and are now using NMR data acquired at 600 MHz only. We redesigned most figures to exclude spectral overlays to improve clarity and added line shape simulations. We also added a new figure, which is now Figure 5, so that the previous Figure 5 and Figure 6 are now Figure 6 and Figure 7, respectively.

See referee reports

Introduction

Investigations of metabolism in health and disease increasingly rely on tracing the use of stable isotope-enriched nutrients through the cell's metabolic pathways. The most widely utilised technology platform to analyse the resulting complex patterns of labelling in multiple cellular metabolites is mass spectrometry (MS), due to its high sensitivity, short run times and a resulting low-cost operation[1–12]. Conversely, NMR spectroscopy is relatively under-utilised, despite being able to provide higher resolution information on the conversion of synthetically produced stable isotopes of nutrients are incorporated into cellular metabolites[12–19]. This is because NMR spectroscopy has historically suffered from low sensitivity, long acquisition times and the need for complex analytical tools.

NMR spectroscopy is, however, ideally suited to answering some of the more pressing questions about metabolic control in health and disease. We currently have limited knowledge about the compartmentalisation of metabolic pathways in metabolically-active organelles, such as mitochondria, and therefore whether the same metabolite is selectively utilised for distinct purposes in different compartments[20]. Given the recent drive to target metabolism in various diseases, understanding the control of metabolism by different tissues is critical to the ability to select specific therapies which target the desired pathways within appropriate cellular compartments. While sample analysis by high-resolution NMR spectroscopy is performed *ex vivo* or *in vitro*, the data obtained provide information on metabolic pathways *in vivo*.

Stable isotope-enriched metabolic precursors, such as glucose or glutamine, are employed as metabolic tracers. These synthetically produced nutrients are enriched in isotopes with a low natural abundance, such as ^{13}C or ^{15}N. Despite the fact that metabolites can arise from multiple sources, the contribution of the different metabolic pathways to the synthesis of this metabolite can be determined through the analysis of the ^{13}C and/or ^{15}N distribution within the metabolite (Figure 1). The couplings

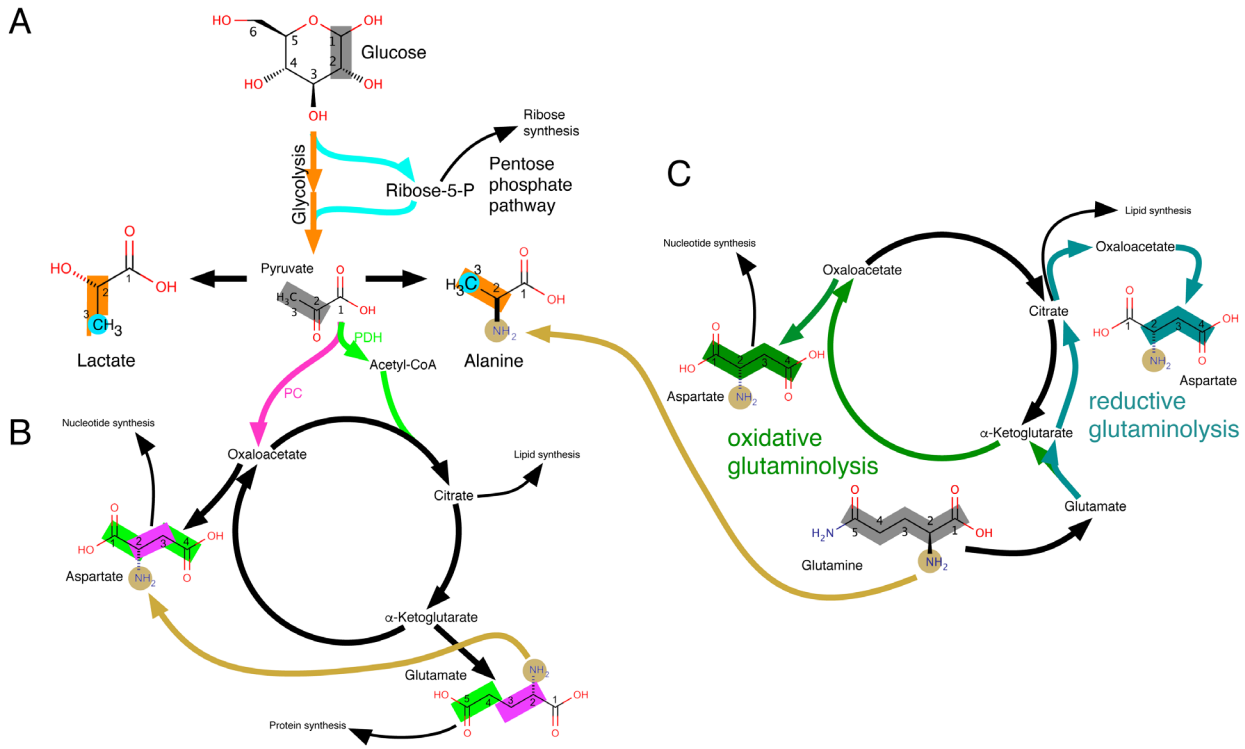

Figure 1. Tracing of metabolic pathways. The labelling patterns arising from [1,2-^{13}C] glucose (**A** & **B**) as well as from [U-^{13}C,^{15}N] glutamine (**C** for ^{13}C labelling and **A**–**C** for ^{15}N labelling) are shown. Metabolism of [1,2-^{13}C] glucose leads to distinctive labelling patterns in lactate and alanine ([2,3-^{13}C] lactate/alanine when using glycolysis and [3-^{13}C] lactate/alanine when using the pentose phosphate shunt, PPP) (Panel **A**). Similarly, glutamate and aspartate express different labelling patterns from [1,2-^{13}C] glucose, depending whether they were synthesised via pyruvate dehydrogenase (PDH; resulting in [4,5-^{13}C] glutamate) or via the pyruvate carboxylase (PC; resulting in [2,3-^{13}C] aspartate) route (Panel **B**). Metabolisation of labelled glutamine can reveal other anaplerotic pathway activities such as reductive carboxylation (Panel **C**).

are visualised in the indirect dimension of an HSQC spectrum allowing the determination of the percentage incorporation of isotopic label into adjacent nuclei. While MS data does not need a reference sample to distinguish between labelled and unlabelled metabolites, it is not always possible to derive the exact distribution of labelled nuclei within a molecule. In contrast, NMR spectroscopy data can resolve label distribution at the atomic level, enabling a clearer picture of the label distribution in metabolites.

Our recently published combined NMR spectroscopy and MS approach (CANMS) harnesses the strengths of both modalities to produce highly-resolved metabolism information in the form of metabolite isotopomers[19]. The detailed interpretation of MS isotopologue data, when using MS data in isolation, requires use of a pre-defined metabolic model. In contrast, the integrated analysis of NMR spectroscopy and MS data makes fewer assumptions about the metabolic network, providing a more accurate insight into relative pathway contributions than is possible with current established methods or the independent analysis of MS or NMR spectroscopy data alone. For example, proton-less carbon atoms do not give rise to a signal in 2D-HSQC NMR spectra, although incomplete information on those carbons is available via splitting of adjacent carbon nucleus signals. The combination of NMR spectroscopy and MS analysis fills this gap as the MS data provides information on the amount of single carbon labelling into those carbon nuclei via "m+x" isotopologues. [1,2-^{13}C] glucose is the optimal tracer to assess metabolic flux through glycolysis vs pentose phosphate pathway (PPP) shunting back into glycolysis. While the glycolytically derived isotopomer of lactate is [2,3-^{13}C] lactate, the PPP derived isotopomers can be [3-^{13}C], [1-^{13}C] or [1,3-^{13}C] lactate. Although the first isotopomer can be assessed with NMR spectroscopy data, the other two isotopomers include labelling in C(1), which HSQC NMR spectroscopy is "blind" to. In these cases, MS data adds new information to the NMR spectroscopy data by contributing the isotopologues NMR spectroscopy is not able to detect, while NMR spectroscopy adds to the MS data by differentiating between [1,3-^{13}C] and [2,3-^{13}C] lactate.

A major drawback of utilising ^{13}C-^{13}C scalar coupling information to derive isotopomer distributions is the time required to acquire spectra. For example, around four hours are required for the acquisition of a 2D-HSQC NMR spectrum with high-resolution in the ^{13}C dimension, even when using fast, state-of-the-art non-uniform sampling (NUS) techniques.

Here we describe two developments, quantitative spectral filters and signal splitting enhancement, to facilitate and speed-up the acquisition of NMR spectra for tracer-based analysis of metabolism. Such techniques permit high throughput metabolic pathway profiling, increasing access, affordability and sensitivity when using NMR spectroscopy as an investigative modality. Additionally, these developments facilitate fast detection of ^{15}N labelling, especially when combined with ^{13}C tracing, thus providing extra information allowing more accurate metabolic pathway profiling.

Methods and results

Quantitative spectral filters for ^{13}C tracer observation: 1D Spectral filters

Experimental setup. A porcine kidney was procured from a slaughterhouse (FA Gill, Wolverhampton) following approximately 14 minutes warm ischaemic time (WIT) as per previous experimental methodology[18]. No animal was killed solely for experimental purposes; all were due for human consumption, therefore no ethical approval was required. After 2 hours cold ischaemic time, kidneys were subject to 18 hours of hypothermic machine perfusion. The perfusate sample was collected after 6 hrs of perfusion and prepared for NMR analysis.

1D NMR spectra were acquired using a Bruker Avance III 600 MHz NMR spectrometer equipped with a 5mm z-PFG TCI Cryoprobe. 128 transients were acquired for each spectrum with a 5 s interscan relaxation delay. A total of 32768 data points with a spectral width of 12 ppm was acquired for each FID using an adiabatic bi-level decoupling scheme to suppress ^{1}H, ^{13}C J-coupling during acquisition[21]. While decoupling for this long (2.25 s) was possible because of the cryogenic probe and may potentially work with a room temperature probe, care must be taken as there will be significant sample heating. The sample heating can be significantly reduced, with only very minor reduction in resolution, by acquiring for only 1.125 s. In order to estimate whether a specific spectrometer with a cryoprobe can tolerate the power dissipation originating from the decoupling sequence specific attention should be paid to the cryogas heater current, which should never fall below its system specific lower limit.

The spectra were processed within the MetaboLab software package (version 2018.07182055)[22]. A 0.5 Hz line broadening was applied with zero-filling of the data up to 131072 real data points prior to Fourier transformation. The resulting spectra were referenced using DSS and manually phase corrected. Subsequently the spectral baseline was corrected using MetaboLab's spline baseline correction before the spectra were exported to Bruker format for metabolites to be quantified in the Chenomx software package (version 8.2, http://www.chenomx.com).

NMR methodology. Despite their relative simplicity and limited resolution, 1D-NMR spectra are highly sensitive tools with which to identify and quantify metabolites. Spectral filters enable the acquisition of spectra which filter out certain signals, thereby reducing ambiguity in 1D spectra associated with attributing peaks to nuclei within metabolites. For example, one can acquire 1D ^{1}H NMR spectra of protons bound to ^{13}C only, simplifying signal assignment and analysis of the acquired spectra. The simplest approach to collect such spectra would be to acquire the first increment of a 2D-^{1}H, ^{13}C-HSQC spectrum. However, signal intensities are not directly comparable with those in standard 1D-^{1}H NMR spectra. It is therefore not possible to directly derive ^{13}C percentages based on a comparison of those spectra with standard proton 1D spectra unless only a small subset of molecules is labelled with ^{13}C and one accompanying spectrum is scaled so that

the majority of signals within the two spectra are of same intensity[23]. Spectral filters such as BIRD, TANGO and POCE[24–28] originated in protein NMR spectroscopy to filter out certain parts of the magnetisation and therefore quantitative data cannot be gained from resultant output spectra. Quantitative comparisons between unfiltered and filtered spectra are usually unnecessary, except for tracer-based analysis. Here we present a novel spectral filter which enables quantitative analysis of resultant spectra from single samples, enriched with ^{13}C tracer.

Panels A-1 and B-1 in Figure 2 show the pulse sequences implementing the quantitative spectral filter. While the central

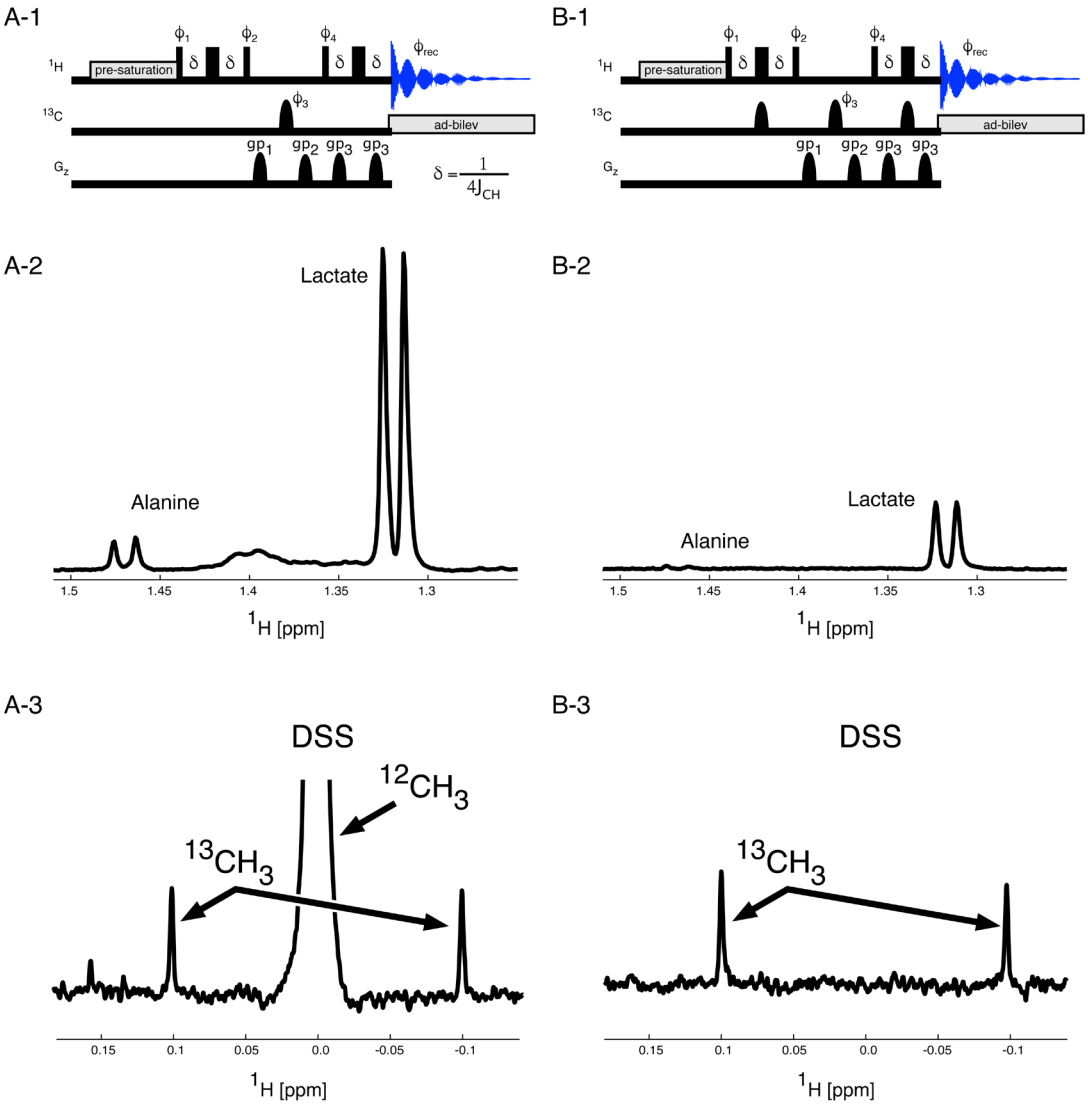

Figure 2. Spectral Filters in 1D spectroscopy. To determine percentage ^{13}C incorporation two spectra are acquired per sample. One spectrum (**A**) contains ^{1}H signals originating from all protons (all ^{1}H spectrum), while the second spectrum (**B**) only contains signals from protons attached to a ^{13}C nucleus. The central ^{13}C π–pulse with phase ϕ_3 is executed every second transient in both experiments. The proton magnetisation in the all ^{1}H pulse sequence is the same for ^{12}C and for ^{13}C bound protons and as a consequence, all ^{1}H magnetisation is longitudinal during the interval between ^{1}H pulses with the phases ϕ_2 and ϕ_4. Because of the additional ^{13}C π–pulses in the ^{13}C bound ^{1}H pulse sequence, the magnetisation for the two different kinds of protons develops differently. Here only the ^{13}C bound ^{1}H magnetisation is longitudinal in the interval between the ^{1}H pulses with the phases ϕ_2 and ϕ_4. Therefore, the ^{12}C bound ^{1}H magnetisation can be destroyed using the two pulse field gradients labelled gp_1 and gp_2. A recovery delay of 200 µs was used after each gradient. The central ^{13}C π–pulse with phase ϕ_4 improves magnetisation selection as it is accompanied by phase changes of the ^{1}H pulses and the receiver. All ^{13}C π-pulses are adiabatic Chirp pulses with γB_{1max} = 10 kHz. ^{1}H,^{13}C J-coupling is suppressed during acquisition using adiabatic bilevel decoupling (ad-bilev)[21]. The pulse phases are: ϕ_1 = x, x, -x, -x; ϕ_2 = x, x, -x, -x for the all ^{1}H spectrum (**A-1**) and y, y, y, y for the ^{13}C bound ^{1}H spectrum (**B-1**), ϕ_3 = x, y, -x, -y, ϕ_4 = x, -x, -x, x, y, -y, -y, y for the all ^{1}H spectrum (**A-1**) and y, -y, -y, y, -x, x, x, -x for the ^{13}C bound ^{1}H spectrum (**B-1**). Panels **A-2** and **B-2** show the peaks from Alanine and Lactate methyl protons in the all ^{1}H spectrum (**A-2**) and the ^{13}C bound ^{1}H spectrum (**B-2**). The scaling of the two spectra is identical allowing easy determination of the percentage incorporation of ^{13}C metabolites. Panels **A-3** and **B-3** demonstrate the complete removal of the ^{12}C bound proton signal from the ^{13}C edited spectrum (**B-3**) leaving only the natural abundance ^{13}C signals to be observed.

^{13}C π-pulse (phase ϕ_3) is used only in odd numbered transients and replaced with a delay of the same length during even numbered transients, the two other ^{13}C π-pulses are only used in the ^{12}C filtering experiment (B-1), where ^{1}H magnetisation to ^{12}C neighbours is filtered out, so that only ^{13}C bound ^{1}H magnetisation contributes to the signal intensities in the 1D spectrum. The phase cycle ϕ_1 changes as well between the 2 experiments, as indicated in the figure legend.

Panels A-2 and B-2 in Figure 2 depict two sample spectra from a perfusate sample where a cadaveric porcine kidney was perfused with modified University of Wisconsin machine perfusion solution (UW MPS) during a period of hypothermic machine perfusion. The standard unlabelled glucose constituent (10 mM) within classical UW MPS was replaced with 10 mM universally labelled glucose, for use as a metabolic tracer during the 18 hour perfusion.

While filters such as BIRD utilise relaxation to minimise the unwanted part of the magnetisation, methods such as TANGO or POCE generate magnetisation where ^{12}C bound ^{1}H atoms possess either the same or the opposite phase compared to the magnetisation of ^{13}C bound ^{1}H atoms, generating two different spectra. By subtraction of these two spectra, the magnetisation of ^{13}C bound ^{1}H atoms can then be calculated. In case of low ^{13}C incorporation, as with any difference technique, subtracting two very large signals in presence of a small signal can lead to substantial artefacts. The quantitative spectral filter works slightly differently compared to TANGO and POCE as the pulse sequence depicted in Figure 2, panel B-1 makes use of two gradient pulses (gp_1 and gp_2) to destroy unwanted magnetisation. As an example, panels A-3 and B3 in Figure 2 show a variant of the pulse sequences where the adiabatic bilevel decoupling (ad-bilev)[21] has been omitted, so that the ^{12}C and the ^{13}C bound ^{1}H signals appear separated in the spectrum. The $^{12}CH_3$ signal in A-3 has been truncated to be able to visualise the ^{13}C satellites, which appear with 0.5% of the peak height of the $^{12}CH_3$ signal. As can be seen in panel B-3, the $^{12}CH_3$ signal is completely suppressed without leaving an artefact, so that even signals from naturally occurring ^{13}C alone are easily detectable in a ^{13}C decoupled spectrum.

The quantitative spectral filter is invariant with respect to differential ^{1}H relaxation rates or signal multiplicities. As with any J-coupling based filtering approach, the ^{12}C filtered spectrum will be scaled with a factor that is proportional to $\sin(2\pi\delta J_{CH})^2$, where δ is the delay during the first and last spin echo. δ is usually set to $¼J_{CH}$ with J_{CH} = 145 Hz. Assuming a minimum J_{CH} of 120 Hz and a maximum J_{CH} of 165 Hz, results in a maximum downscaling of 7.2%.

J-Coupling based splitting enhancement in 2D-NMR spectra

Experimental setup. Slaughterhouse porcine kidneys (WIT-15 minutes) were cannulated and flushed with chilled Soltran solution (Baxter) as performed in clinical practice. Kidneys were placed in static cold storage en route to our laboratory, where they were immediately perfused with modified KPS-1 using the Lifeport Kidney Transporter 1.0 (Organ Recovery Systems), which has been modified to include a paediatric oxygenator. Oxygen was supplied at a flow rate of 0.7 L/min for the duration of the 24 hours perfusion period.

At the end of the perfusion period, the kidney was removed from the perfusion circuit and laterally bisected. Sections of cortex and medulla were isolated and snap frozen in liquid nitrogen. These tissues were powdered, also under liquid nitrogen, and 0.5 g was placed in 7 ml homogenisation tube (Precellys, CK28), containing 5.1 ml of HPLC grade methanol (−80°C) to quench metabolism. These were homogenised using the Precellys 24 dual homogeniser (8x 5000 rpm for 15 s). The samples were mixed with 4.65 ml deionised water and 5.1 ml HPLC grade chloroform and vigorously agitated. Biphasic separation of polar and non-polar solvents was performed by centrifugation (1300 g, 15 minutes, 4°C), after which 4.5 ml of the polar layer was aspirated and dried overnight at 35°C.

The dried extracts were resuspended in 60 µl NMR buffer (0.1 M phosphate buffer, 0.5 mM 4,4-dimethyl-4-silapentane-1-sulfonic acid, 2 mM imidazole and 10% D_2O). These suspensions were sonicated to dissolve micro particles and then 35 µl of this solution was added to 1.7 mm NMR tubes.

^{1}H,^{13}C-HSQC spectra were acquired using a Bruker Avance III 600 MHz NMR spectrometer equipped with a 1.7 mm z-PFG TCI Cryoprobe. The HSQC spectra were acquired using 2 transients per increment with echo/anti-echo gradient coherence selection and an additional pre-saturation for suppressing the water resonance during the 1.5 s interscan relaxation delay. The ^{1}H dimension was acquired with a spectral width of 13 ppm using 512 complex data points. The ^{13}C dimension was acquired with a spectral width of 160 ppm using 25% (2048) of 8192 data points using a non-uniform sampling scheme. The non-uniformly sampled spectra were reconstructed via the compressed sensing algorithm within the MDDNMR (version 2.5)[29] and processed using NMRPipe (version 9.2)[30]. All spectra were processed without baseline correction to avoid complications in the multiplet analysis procedure.

NMR methodology. The relatively long acquisition times of 2D-HSQC spectra are necessary to generate the spectral resolution required to resolve complex multiplet patterns[19]. Here we present a technique to manipulate the appearance of NMR multiplets in the indirect dimension of 2D-HSQC spectra. The ability to expand the splitting caused by J-coupling has previously been reported[31,32]. Here we apply this technique in order to negate the requirement for the collection of large number of increments in the ^{13}C dimension, which, together with methods such as non-uniform sampling[29,33] and variation of the repetition time[34] significantly reduces the time required to acquire 2D-HSQC spectra with sufficient resolution. It also means that at increasingly higher magnetic fields, the advantages of extra sensitivity and increased ^{1}H chemical shift resolution are not negated by the increased ^{13}C increments needed in in order to resolve J-couplings. Enhancement of the splitting due to J-coupling can be achieved by incrementing the spin echo delay after the period where chemical shift of ^{13}C evolves in parallel with the chemical shift evolution (Figure 3). This spin

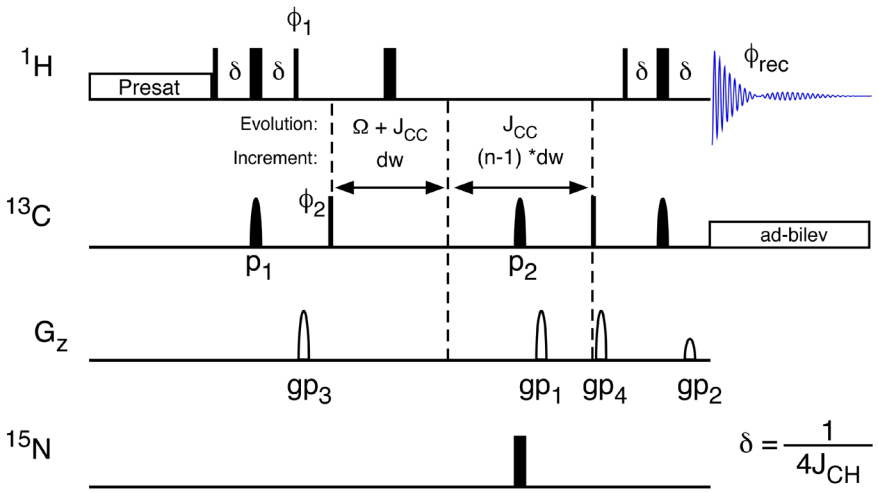

Figure 3. Splitting Enhanced HSQC Spectroscopy. The splitting enhancement due to J-coupling is achieved using an additional spin echo subsequent to the ^{13}C evolution period. The delays in the spin-echo for the J-coupling enhancement are multiples of the dwell time (dw). While the chemical shift evolves with dw, which is determined by setting the spectral width of the spectrum, splittings are enhanced depending on the increment of the ^{13}C gradient selection spin-echo. The HSQC spectrum is acquired using echo/anti-echo for quadrature detection to allow for efficient removal of artefacts in only two scans per increment. Optionally, the ^{13}C,^{15}N-couplings can be scaled by the introduction of the ^{15}N π-pulse simultaneously with the ^{13}C π-pulse (labelled p2). ^{1}H,^{13}C J-coupling is suppressed during acquisition using adiabatic bilevel decoupling (ad-bilev)[21]. The pulse phases are: ϕ_1 = y; ϕ_2 = x, -x; ϕ_{rec} = x, -x.

echo refocuses the ^{13}C chemical shift and the ^{1}H-^{13}C coupling, but allows the ^{13}C-^{13}C coupling to evolve further. The delays in the spin echo are proportional to those in the $\Omega+J_{CC}$ evolution period with the amount of extra coupling achieved being defined by the stretch of the J_{CC} increment compared to the $\Omega+J_{CC}$ increment. Thus, the ^{13}C-^{13}C J-couplings can be expanded as required (Figure 4). The ability to scale the signal splittings to varying extents means that the experiment can be tuned to the requirements of the sample and which metabolites are present, and of interest. Figure 4 demonstrates the effect of J-coupling splitting enhancement on 2D HSQC spectra, displaying C(6) of ^{13}C enriched glucose. The ^{13}C trace through the left-most signal (Figure 4D), demonstrates clearly that while the singlet in the middle of the multiplet does not change, the splitting due to the $^{1}J_{CC}$ coupling increases and in fact splits into multiple signals as the splittings of previously unresolved long-range couplings are amplified so that they are large enough to become resolved in the spectrum. These splittings can easily be simulated (Figure 4E), thereby providing additional information with which to model metabolic pathways.

Large expansion of J-coupling also allows for rapid collection of data, as the resolution required to resolve them becomes diminished (Figure 5). However, this should be tempered by the need to avoid unnecessary overlap of signals. To date, the authors have acquired 2D spectra with up to eight fold enhanced ^{13}C J-couplings, combined with shortening the acquisition by using variable pulse sequence repetition times[34], leading to an overall decrease in acquisition time by a factor larger than 10 (Figure 5). Panels A to D show the spectral region of the methyl groups of lactate and alanine. Panel E shows a cross section, as marked in the 2D spectra, from alanine, whereas panel F shows the corresponding simulations of those multiplets. The acquisition times for the different spectra were 233, 110, 51 and 24 minutes (Table 1). Whilst the lines in the spectrum become broader due to the shorter acquisition times, this is negated by the increase in splittings, allowing the analysis of the multiplets with similar precision. Shorter acquisition times may be achieved by including spectral folding in the acquisition protocol or by incorporating new fast acquisition schemes such as ASAP- or ALSOFAST-HSQC[35].

^{15}N tracing

Experimental setup. *2D ^{14}N spectral filter* - Sample preparation is described elsewhere[16]. 2D ^{1}H ^{13}C-HSQC NMR spectra with and without ^{14}N filtering were acquired using a Bruker Avance III 600 MHz NMR spectrometer equipped with a 1.7 mm z-PFG TCI Cryoprobe. The HSQC spectra were acquired using 2 transients per increment with echo/anti-echo gradient coherence selection and an additional pre-saturation during the 1.5 s interscan relaxation delay to suppress the water resonance. The ^{1}H dimension was acquired with a spectral width of 13 ppm using 512 complex data points. The ^{13}C dimension was acquired with a spectral width of 160 ppm using 2048 data points. The spectra were processed with quadratic cosine window functions and without baseline correction to avoid complications in the multiplet analysis procedure.

^{13}C, ^{15}N J-coupling splitting enhancement. The human Renal Proximal tubule cell line (RPTEC/TERT1, supplied by Evercyte GmBH, Austria) was used to investigate the metabolic fates of both carbon from glucose, and carbon and nitrogen from glutamine. Cells were expanded as described elsewhere[36], with population doubling level (PDL) routinely tracked using in-house software (PDL calculator, EcoCyto). Cells with PDL between 43 and 45 were collated and seeded at a density of $4\times10^4/cm^2$ in 75 cm^2 flasks containing 240 µl/cm^2 flux media (Zenbio, cat DMEMf12-NGG002), supplemented as above with the addition of 17.5 mM [1,2-^{13}C] D-Glucose (sigma 453188) and 2 mM [U-^{13}C,U-^{15}N] L-Glutamine (sigma, 607983). Cell

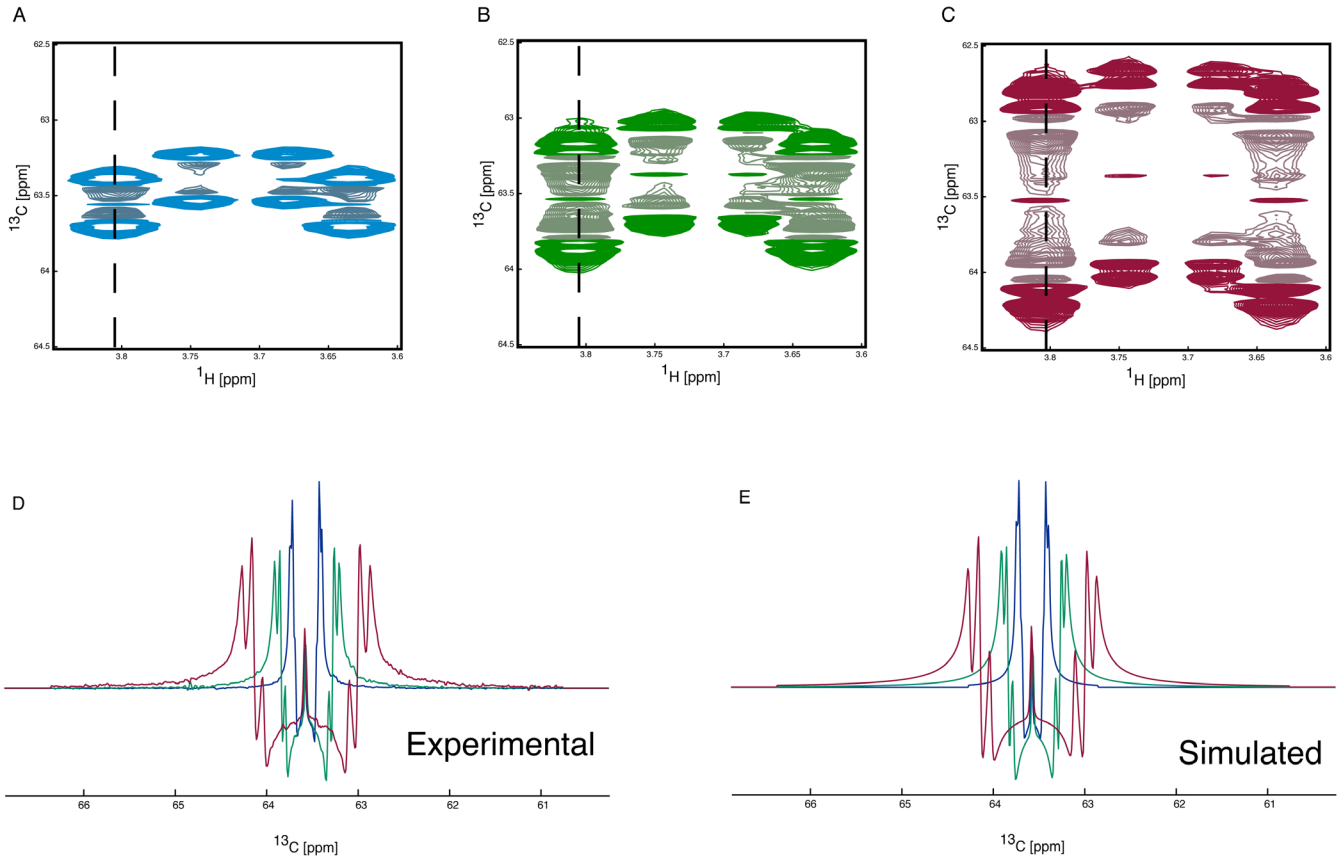

Figure 4. J-coupling splitting enhancement HSQC spectroscopy. ^{1}H,^{13}C HSQC spectra showing the C(6) of glucose are shown (**A**, **B** and **C**). The spectrum with no J-coupling splitting enhancement is shown in blue (**A**), with an enhancement of two in green (**B**) and with an enhancement of four in red (**C**). The ^{13}C trace of the HSQC spectra (**D**), taken from the ^{1}H frequency as depicted by the dashed line, clearly shows the increase in observed splitting. The J-coupling splitting enhancement is achieved using an additional spin echo subsequent to the ^{13}C evolution period. The delays to achieve the scaling of the splittings are multiples of dw such the use of a delay of 3*dw will result in a J-coupling splitting enhancement of 4 (one from the t_1 evolution and three from the J-coupling splitting enhancement spin echo). The observed splitting can be simulated (**E**) giving the following incorporation percentages. From the no J-coupling splitting enhancement spectrum 6.8% / 41.2% / 52 % for [6-^{13}C] / [5,6-^{13}C] / [U-^{13}C], from the two-fold J-coupling splitting enhancement 6.3% / 41.4% / 52.3 % for [6-^{13}C] / [5,6-^{13}C] / [U-^{13}C] and from the four-fold J-coupling splitting enhancement 5.9% / 41.6% / 52.5 % for [6-^{13}C] / [5,6-^{13}C] / [U-^{13}C].

culture was continued for 48 hours to allow isotopic labelling, after which cells were washed with ice-cold saline solution (0.9%) and collected by scraping into 2 ml pre-chilled methanol (-20°C), 2 ml water (4°C) and 2 ml chloroform (-20°C). The solution was vigorously mixed for 10 minutes, after which lysates were centrifuged at 15,000 *g* for 15 min at 4°C. 1 ml of the sample was aspirated for NMR analysis. Samples were dried using a Savant (SPD1010) speedvac concentrator and then resuspended in 60 µL of 100 mM sodium phosphate buffer, containing 0.5 mM DSS, 2 mM Imidazole in D_2O, pH 7.0. The samples were vortexed and subsequently sonicated for 10 min and then centrifuged at 15000 *g* for 30 seconds to collate the fluid. Finally 35 µl of the samples were transferred to 1.7 mm NMR tubes.

2D-^{1}H,^{13}C-HSQC and 2D-^{1}H,^{15}N-HSQC NMR spectra were acquired using a Bruker Avance III 600 MHz NMR spectrometer equipped with a 1.7 mm z-PFG TCI Cryoprobe. The HSQC spectra were acquired using 2 transients per increment with echo/anti-echo gradient coherence selection with an additional pre-saturation to suppress the water resonance during the 1.5 s interscan relaxation delay. The ^{1}H dimension of the ^{1}H,^{13}C-HSQC spectra was acquired with a spectral width of 12 ppm using 512 complex data points. The ^{13}C dimension was acquired with a spectral width of 160 ppm using 25% (2048) of 8192 data points using a non-uniform sampling scheme. The ^{1}H dimension of the ^{1}H,^{15}N-HSQC spectra was acquired with a spectral width of 12 ppm using 1024 complex data points. The ^{15}N dimension was acquired with a spectral width of 40 ppm using 256 data. All non-uniformly sampled spectra were reconstructed via the compressed sensing algorithm within MDDNMR (version 2.5)[29] and processed using NMRpipe (version 9.2)[30]. All spectra were processed without baseline correction to avoid complications in the multiplet analysis procedure especially with regards to the negative peaks caused by the echo/anti-echo coherence selection with gradients.

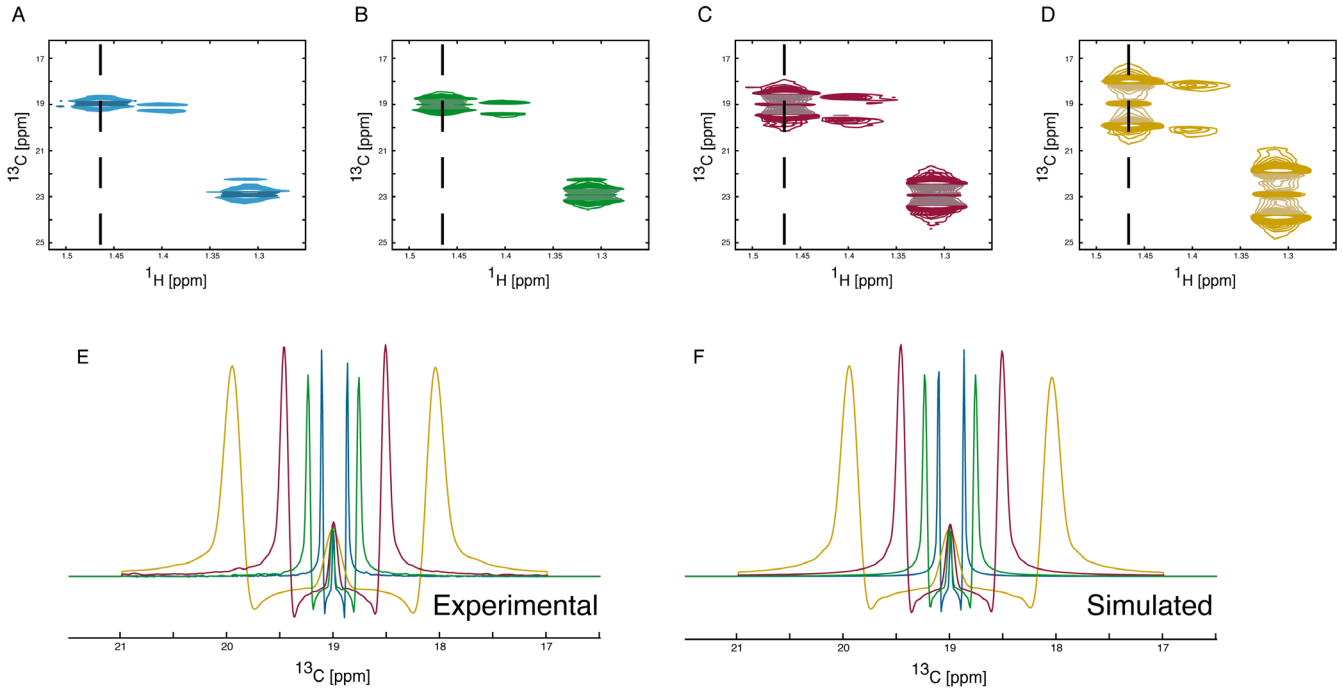

Figure 5. Simulation of J-coupling splitting enhanced spectra. ^{1}H,^{13}C HSQC spectra showing the C(3) of alanine are shown (**A**, **B**, **C** and **D**). The enhancement of J-coupling in the ^{1}H,^{13}C-HSQC spectra leads to increased separation of coupled peaks and allows the collection of data with reduced numbers of increments in the ^{13}C dimension resulting in shorter acquisition times. The number of points collected in the ^{13}C dimension can be reduced to match the increase in J-coupling enhancement as the loss of resolution will be counteracted by the increase in separation of the coupled peaks. Spectra with no enhancement (**A**), two-fold enhancement (**B**), four-fold enhancement (**C**) and eight-fold enhancement (**D**) were collected. The overlay of the differently enhanced spectra clearly shows the effect of the enhancement (**E**). The enhancement can be tailored to meet the need in order to maximise separation without significantly increasing signal overlap whilst achieving the maximum reduction in acquisition time possible. The splitting enhancement can easily be included in the simulation parameters (**F**) resulting in no adverse effects on the simulated spectra. The simulation gives the following incorporation percentages. From the no J-coupling splitting enhancement spectrum 12.1% / 87.9% for [3-^{13}C] / [2,3-^{13}C], from the two-fold J-coupling splitting enhancement 12.0% / 88.0% for [3-^{13}C] / [2,3-^{13}C], from the four-fold J-coupling splitting enhancement 12.0% / 88.0% for [3-^{13}C] / [2,3-^{13}C] and from the eight-fold J-coupling splitting enhancement 12.1% / 87.9% for [3-^{13}C] / [2,3-^{13}C].

Table 1. Comparison of spectroscopic techniques. The acquisition time and signal to noise ratios of various experiments used in this study. A good signal to noise ratio can be achieved using the spectral filtering allowing rapid measurement of quantitative spectra. The signal to noise benefit of the HSQC over the 1D ^{13}C acquisition is clearly seen. The effect of increasing the J-coupling splitting enhancement whilst simultaneously reducing the number of increments on the acquisition time of ^{1}H,^{13}C-HSQC spectra is also shown.

Experiment	Acquisition time [mins]	Signal to noise ratio (CH_3 of lactate)	Transients	TD	SW [ppm]	Splitting enhancement
^{1}H 1D (all ^{1}H)	2	327.31	8	16384	12	1
^{1}H 1D (^{13}C bound ^{1}H)	2	66.13	8	16384	12	1
^{1}H,^{13}C-HSQC	233	823.86	2	1024/8192	12/160	1
^{1}H,^{13}C-HSQC	110	770.98	2	1024/4096	12/160	2
^{1}H,^{13}C-HSQC	51	426.41	2	1024/2048	12/160	4
^{1}H,^{13}C-HSQC	24	283.38	2	1024/1024	12/160	8
^{13}C 1D (30° excitation)	1414	59.95	16384	65538	239	1

All NMR spectra in this article were processed within the MetaboLab software package (version 2018. 07182055; http://metabolab.uk)[22].

NMR methodology. Both aforementioned methods can be used to detect ^{15}N labelling in metabolites, which alongside ^{13}C isotope incorporation can provide additional much-needed information

on the overlapping activity of multiple metabolic pathways. 2D spectroscopic filters are an extension of the 1D concept and as such can be used to simplify increasingly complex 2D spectra by selectively observing a subset of metabolites in which nuclei of interest have been incorporated. For example, the analysis of the ^{13}C nuclei that are adjacent to ^{15}N nuclei using 2D spectra permits a simplified unequivocal description of the nature in which two metabolic pathways converge.

Similar to the 1D method, the acquisition of two spectra is required in order to enable a quantitative analysis of the amount of ^{15}N labelling in the presence of ^{13}C labelling within the metabolite. If spectral simplification is the goal, a single spectrum is sufficient[16]. The pulse sequence (Figure 6) is a gradient selected $^{1}H,^{13}C$-HSQC spectrum with the spectral filter added once the ^{1}H magnetisation has been transferred to the ^{13}C nucleus. The spectrum collected with the ^{14}N spectral filter (Panel C-2,

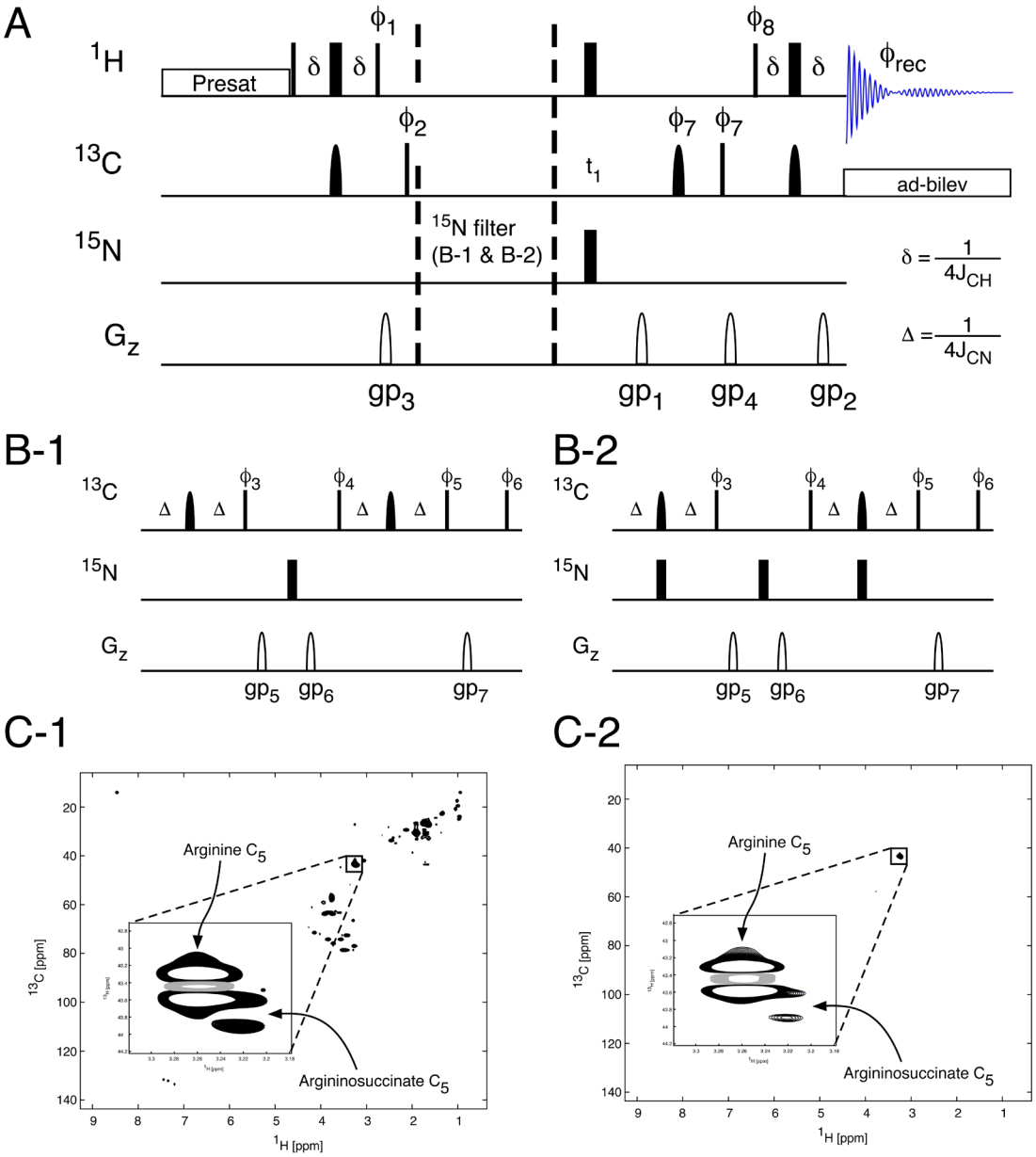

Figure 6. Filtered HSQC spectroscopy. The application of a ^{15}N filtering block in the $^{1}H,^{13}C$-HSQC pulse sequence (**A**) allows the observation of $^{1}H,^{13}C$ groups directly coupled to ^{15}N nuclei. In the sequence in panel **B-1** no filtering will be observed and the resulting spectrum (**C-1**) will contain all ^{1}H, ^{13}C groups adjacent to either ^{14}N or ^{15}N nuclei. The use of a ^{15}N filter (**B-2**) will result in only those ^{1}H, ^{13}C groups adjacent to a ^{15}N nuclei being observed in the resulting ^{1}H, ^{13}C HSQC spectrum (**C2**). $^{1}H,^{13}C$ J-coupling is suppressed during acquisition using adiabatic bilevel decoupling (ad-bilev)[21]. The pulse phases are: ϕ_1 = y; ϕ_2 = x, -x; ϕ_3 = x for the no filter sequence (panel **B-1**) and y for the ^{15}N filtered sequence (panel **B-2**); ϕ_4 = y, –y for the no filter sequence and y, y for the ^{15}N filtered sequence; ϕ_5 = y, -y for the no filter sequence x, -x for the ^{15}N filtered sequence; ϕ_6 = x, x, -x, -x; ϕ_7 = x, x, x, x, -x, -x, -x, -x; ϕ_8 = x, x, x, x, y, y, y, y; ϕ_{rec} = x, -x, -x, x, y, -y, -y, y.

Figure 6) contains only two visible NMR signals, corresponding to arginine and arginosuccinate, clearly showing how the filter can simplify complex spectra for easier analysis.

While 2D spectral filters serve a purpose, their quantitative usage is limited by the variability of the $^{1}J_{CN}$ constant. J-coupling splitting enhancement on the other hand can be easily extended to include ^{13}C-^{15}N J- coupling splitting enhancement. Indeed, the addition of a single ^{15}N π–pulse simultaneous with the central ^{13}C π–pulse (Figure 3) is sufficient to enhance the apparent ^{13}C-^{15}N J-coupling splitting in ^{1}H,^{13}C-HSQC spectra, an example of which is given in Figure 7. The 2D signals for the J_{CN} splitting scaled spectrum are shown in panel A. Panels B and C show traces of the ^{13}C multiplets for carbon atoms 2 and 3 of alanine. While the J_{CC} splittings are enhanced by a factor of 4 in both spectra, the apparent J_{CN} splittings are unchanged in the spectrum in panel B, whereas they are enhanced by a factor of 4 in the spectra in panel C. Because the $^{2}J_{CN}$ coupling between C(3) and N is negligible, both traces for C(3) overlap perfectly. C(2) on the other hand experiences a $^{1}J_{CN}$ coupling,

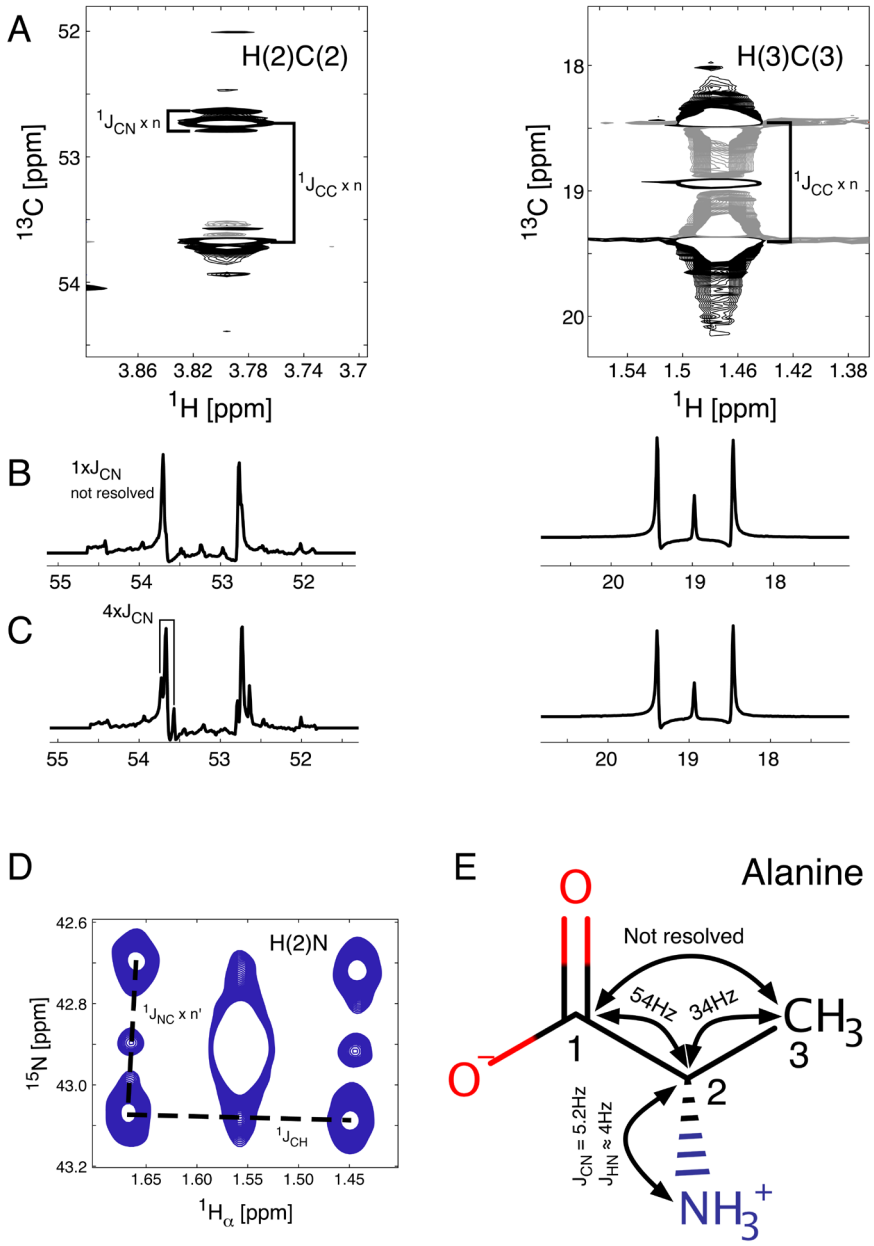

Figure 7. Splitting due to ^{15}N and ^{13}C incorporation. Regions of the ^{1}H,^{13}C-HSQC spectrum containing signals from alanine (panels **A** & **B**). The ^{13}C traces of the alanine signals are shown with either no J_{CN}-coupling splitting enhancement (**B**) or four-fold J_{CN}-coupling splitting enhancement (**C**). The signals are split by either $^{1}J_{CC}$ or $^{1}J_{CN}$ coupling contributions. The long range ^{1}H,^{15}N-HSQC spectrum (**D**) is composed of unlabelled alanine (central peak) and ^{13}C/^{15}N labelled alanine (6 outer signals, 4 split by $^{2}J_{HC}$ and $^{1}J_{NC}$ couplings and 2 only split by $^{1}J_{HC}$ (values for the coupling constants are shown in panel **E**)).

which is too small to be resolved when the J_{CN} splitting is not enhanced and is only detectable in panel C.

J_{CN} coupling, as any J-coupling, works in two directions, therefore a similar approach can be followed from the opposite direction. While amine groups of small molecules are notoriously difficult to observe due to chemical exchange of amine protons with solvent molecules, a long-range HSQC spectrum can be acquired. In such a spectrum proton magnetisation is transferred from H_{α} (the proton bound to C(2)) via the $^{2}J_{HN}$ coupling. The splitting due to the J_{NC} coupling then can be enhanced to show the appearance of ^{13}C labelling in molecules which contain ^{15}N next to those labelled carbon nuclei. As in this case, where the ^{13}C nucleus is also bound to the proton determining the chemical shift on the horizontal axis, that same proton signal will be split by the $^{1}J_{CH}$ coupling constant. The result in this case is therefore a signal split into 7 2D components (Figure 7, panel D), demonstrating that alanine was either recycled from unlabelled alanine which was incorporated into proteins, synthesised *de-novo* from [U-^{13}C] glucose and ^{15}N labelled glutamate which originated from [U-^{13}C, U-^{15}N] glutamine that was added to the growth medium in addition to the [U-^{13}C] glucose or just synthesised *de novo* from [U-^{13}C] glucose with an unlabelled amino group transferred to form alanine. In conjunction with MS data, this complementarity between the 2D-^{1}H,^{13}C- and the 2D- ^{1}H,^{15}N-HSQC spectra enables a model-free metabolism analysis using multiple nutrients as tracer sources in a single sample.

Discussion

Changes in metabolism are increasingly being recognised as central to the pathogenesis of a number of different diseases. Although metabolomic studies have helped determine aspects of disease phenotype, tracing the changing use of specific metabolic pathways using stable isotope-enriched nutrients provides higher resolution information on altered metabolic pathway activity that may lead to the identification of specific novel therapeutic targets. Over the last few years, development of magnet and probe technology, including innovative ultra-sensitive microprobes, has enabled the study of systems that were not previously amenable to NMR spectroscopy. Parallel advancement in the methods used to acquire and analyse data from samples will increase the amount of information we can gain from such samples.

In this paper, we describe how spectral filters and J-splitting enhancement can be used in tracer-based metabolism studies. These techniques overcome some of the major hurdles in the use of NMR spectroscopy. A challenge in the analysis of NMR HSQC spectroscopy data has been the need for an additional "unlabelled" sample in order to determine absolute per carbon ^{13}C incorporation percentages. However, samples cannot be assumed to be biologically identical, thus making analyses problematic due to the inability to determine accurate ^{13}C isotope incorporation values. Systems that demonstrate greater inter-sample variation, such as *in vivo* tracer studies, are even more prone to these analytical issues. The use of spectral filters negates the requirement for two samples and instead a single sample can be used to determine absolute percentage ^{13}C incorporation and thus allow the scaling of multiplets.

The 2D HSQC spectrum is a powerful tool in the study of metabolism as it takes advantage of the increased sensitivity of the ^{1}H nucleus over ^{13}C and using the splitting due to J-coupling in the ^{13}C dimension allows the indirect visualisation of the ^{13}C incorporation into quaternary carbons. However, long acquisitions times, even when using the latest NUS techniques, limits the number of samples that can be acquired. Reducing the experimental time makes the use of HSQC spectra a much more attractive method in the study of tracer-based metabolism. The use of echo/anti-echo for quadrature detection ensures efficient elimination of unwanted artefacts, whilst using only two scans per increment in the indirect dimension. The changes observed in line shape due to the quadrature detection are predictable and can be easily incorporated into line fitting analysis. As described elsewhere[19], the simulation procedure assumes weak coupling between the different carbon nuclei. The simulation is implemented as a spin echo before the acquisition of a ^{13}C-FID to allow the evolution of ^{13}C,^{13}C spin coupling prior to the first increment.

The ability to scale the visualised splittings due to J-coupling allows HSQC spectra to be acquired in time equivalent to that of a 1D ^{1}H spectrum, but the HSQC spectrum contains significantly more information. The reduced time required to acquire HSQC spectra means that it is feasible to apply 2D methods to *in vivo* tracer-based metabolism studies, as well as allowing the use of greater sensitivity of higher field spectrometers while avoiding longer experiment times (Table 1). Expansion of the splitting due to J-coupling can also bring out smaller long-range couplings that were not apparent in a normal HSQC spectrum. Thus, the scaling of splittings can either be used to decrease acquisition imes by allowing data collection at lower resolution or to bring out smaller couplings not previously visible. These small couplings include the $^{1}J_{CN}$ couplings that are found in many metabolites after the addition of metabolites labelled ^{15}N in conjugation with ^{13}C. This increases the information available and allows more in-depth analysis of complex metabolic pathways. In the example shown (Figure 6), the cells used for this experiment were deficient in the expression of fumarate hydratase[16] and therefore contained high fumarate levels. One hypothesis was that argininosuccinate is synthesised from fumarate and arginine to minimise intracellular fumarate. In order to ascertain the signal assignment, we used [U-^{13}C, U-^{15}N] arginine and were able to show that ^{15}N labelled argininosuccinate was being produced in the cells containing the knock out, but not in wild-type cells[16]. This shows the utility of using multiple labelled nutrients to answer fundamental questions in metabolism.

In summary, the spectroscopic tools presented here open up new avenues for tracer-based metabolism studies. Scaling of signal splittings due to J-coupling leads to faster data collection of samples supplemented with nutrients enriched in stable isotopes, such as ^{13}C and ^{15}N. This enables profiling of metabolic pathways and can also be used to enhance sensitivity beyond current technical developments whilst maintaining reasonable data acquisition times. Ultimately, the use of 1D spectral filters

as well as the fast acquisition of HSQC spectra leads to the possibility of tracing metabolism in real-time. In addition, simultaneous tracing with multiple nutrients will lead to unprecedented insight into the interplay of converging and intersecting metabolic pathways, both *in vitro* and *in vivo*[37].

Data availability

All experimental data for this article is available at: http://doi.org/10.17605/OSF.IO/EQHN3[38].

Experimental NMR datasets for HS-TrAM: ^{12}C filtered (subdirectory 2) ^{1}H spectrum, both of which are ^{13}C decoupled during acquisition. Subdirectories 3 and 4 contain an unfiltered (3) and a ^{12}C filtered (4) spectrum, both without ^{13}C decoupling during acquisition. Subdirectories 5 and 6 contain POCE spectra, either with ^{12}C- and ^{13}C-bound ^{1}H with same phase (subdirectory 5), or with opposite phase (subdirectory 6), both without ^{13}C decoupling during acquisition. Subdirectory 7 contains a 30 degree excitation 1D ^{13}C spectrum, acquired using a TXO Cryoprobe. The file jEnhanced_13C_HSQC.zip contains the ^{1}H, ^{13}C-HSQC spectra with different J-coupling splitting enhancements.

The file 13C_HSQC_14N_filter_and_15N_HSQC.zip contains an unfiltered (subdirectory 1) and a ^{14}N filtered (subdirectory 2) ^{1}H,^{13}C-HSQC spectrum. The file jEnhanced_13C_15N_HSQC.zip contains the following spectra: 4 x ^{13}C,^{13}C splitting enhancement ^{1}H,^{13}C-HSQC in subdirectory 1, 4 x ^{13}C,^{13}C splitting enhancement and 4 x ^{13}C,^{15}N splitting enhancement ^{1}H,^{13}C-HSQC in subdirectory 2 and 4 x ^{13}C,^{15}N splitting enhancement ^{1}H,^{15}N-HSQC in subdirectory 3.

Grant information

This work was supported by the Wellcome Trust [099185] and through an Institutional Strategic Support Award given to the University of Birmingham; the National Institute for Health Research [13-0053]; Help Harry Help Others [HelpCU09]; UHB Charitable Funds [17-3-846] and the metabolic tracer analysis core (MTAC) at the University of Birmingham.

The funders had no role in study design, data collection and analysis, decision to publish, or preparation of the manuscript.

Acknowledgements

We thank HWB-NMR at the University of Birmingham for providing open access to their Wellcome Trust-funded spectrometers. Organ Recovery Systems donated perfusion equipment.

References

1. Frezza C, Zheng L, Folger O, *et al.*: **Haem oxygenase is synthetically lethal with the tumour suppressor fumarate hydratase.** *Nature.* 2011; **477**(7363): 225–228.
PubMed Abstract | Publisher Full Text
2. Walther JL, Metallo CM, Zhang J, *et al.*: **Optimization of ^{13}C isotopic tracers for metabolic flux analysis in mammalian cells.** *Metab Eng.* 2012; **14**(2): 162–171.
PubMed Abstract | Publisher Full Text | Free Full Text
3. Hiller K, Metallo CM: **Profiling metabolic networks to study cancer metabolism.** *Curr Opin Biotechnol.* 2013; **24**(1): 60–68.
PubMed Abstract | Publisher Full Text
4. Gravel SP, Andrzejewski S, Avizonis D, *et al.*: **Stable isotope tracer analysis in isolated mitochondria from mammalian systems.** *Metabolites.* 2014; **4**(2): 166–183.
PubMed Abstract | Publisher Full Text | Free Full Text
5. Huang X, Chen YJ, Cho K, *et al.*: **X^{13}CMS: global tracking of isotopic labels in untargeted metabolomics.** *Anal Chem.* 2014; **86**(3): 1632–1639.
PubMed Abstract | Publisher Full Text | Free Full Text
6. Chouchani ET, Pell VR, Gaude E, *et al.*: **Ischaemic accumulation of succinate controls reperfusion injury through mitochondrial ROS.** *Nature.* 2014; **515**(7527): 431–435.
PubMed Abstract | Publisher Full Text | Free Full Text
7. Buescher JM, Antoniewicz MR, Boros LG, *et al.*: **A roadmap for interpreting ^{13}C metabolite labeling patterns from cells.** *Curr Opin Biotechnol.* 2015; **34**: 189–201.
PubMed Abstract | Publisher Full Text | Free Full Text
8. Mackay GM, Zheng L, van den Broek NJ, *et al.*: **Analysis of Cell Metabolism Using LC-MS and Isotope Tracers.** *Methods Enzymol.* Elsevier, 2015; **561**: 171–196.
PubMed Abstract | Publisher Full Text
9. Jiang L, Shestov AA, Swain P, *et al.*: **Reductive carboxylation supports redox homeostasis during anchorage-independent growth.** *Nature.* 2016; **532**(7598): 255–258.
PubMed Abstract | Publisher Full Text | Free Full Text
10. Quek LE, Liu M, Joshi S, *et al.*: **Fast exchange fluxes around the pyruvate node: a leaky cell model to explain the gain and loss of unlabelled and labelled metabolites in a tracer experiment.** *Cancer Metab.* 2016; **4**: 13.
PubMed Abstract | Publisher Full Text | Free Full Text
11. Zhang H, Badur MG, Divakaruni AS, *et al.*: **Distinct Metabolic States Can Support Self-Renewal and Lipogenesis in Human Pluripotent Stem Cells under Different Culture Conditions.** *Cell Rep.* 2016; **16**(6): 1536–1547.
PubMed Abstract | Publisher Full Text | Free Full Text
12. Sauer U: **Metabolic networks in motion: ^{13}C-based flux analysis.** *Mol Syst Biol.* 2006; **2**(1): 62.
PubMed Abstract | Publisher Full Text | Free Full Text
13. Lane AN, Fan TW, Higashi RM: **Isotopomer-based metabolomic analysis by NMR and mass spectrometry.** *Methods Cell Biol.* 2008; **84**: 541–588.
PubMed Abstract | Publisher Full Text
14. Lane AN, Fan TW, Bousamra M 2nd, *et al.*: **Stable isotope-resolved metabolomics (SIRM) in cancer research with clinical application to nonsmall cell lung cancer.** *OMICS.* 2011; **15**(3): 173–182.
PubMed Abstract | Publisher Full Text | Free Full Text
15. Yang Y, Lane AN, Ricketts CJ, *et al.*: **Metabolic reprogramming for producing energy and reducing power in fumarate hydratase null cells from hereditary leiomyomatosis renal cell carcinoma.** *PLoS One.* 2013; **8**(8): e72179.
PubMed Abstract | Publisher Full Text | Free Full Text
16. Adam J, Yang M, Bauerschmidt C, *et al.*: **A role for cytosolic fumarate hydratase in urea cycle metabolism and renal neoplasia.** *Cell Rep.* 2013; **3**(5): 1440–1448.
PubMed Abstract | Publisher Full Text | Free Full Text
17. Lussey-Lepoutre C, Hollinshead KE, Ludwig C, *et al.*: **Loss of succinate dehydrogenase activity results in dependency on pyruvate carboxylation for cellular anabolism.** *Nat Commun.* 2015; **6**: 8784.
PubMed Abstract | Publisher Full Text | Free Full Text
18. Nath J, Smith T, Hollis A, *et al.*: **^{13}C glucose labelling studies using 2D NMR are a useful tool for determining ex vivo whole organ metabolism during hypothermic machine perfusion of kidneys.** *Transpl Res.* 2016; **5**: 7.
PubMed Abstract | Publisher Full Text | Free Full Text
19. Chong M, Jayaraman A, Marin S, *et al.*: **Combined Analysis of NMR and MS Spectra (CANMS).** *Angew Chem Int Ed Engl.* 2017; **56**(15): 4140–4144.
PubMed Abstract | Publisher Full Text
20. Banke NH, Lewandowski ED: **Impaired cytosolic NADH shuttling and elevated UCP3 contribute to inefficient citric acid cycle flux support of postischemic cardiac work in diabetic hearts.** *J Mol Cell Cardiol.* 2015; **79**: 13–20.
PubMed Abstract | Publisher Full Text | Free Full Text

21. Kupce Ê, Freeman R, Wider G, *et al.*: **Suppression of Cycling Sidebands Using Bi-level Adiabatic Decoupling.** *J Magn Reson A.* 1996; **122**: 81–84.
Reference Source

22. Ludwig C, Günther UL: **MetaboLab--advanced NMR data processing and analysis for metabolomics.** *BMC Bioinformatics.* 2011; **12**: 366.
PubMed Abstract | Publisher Full Text | Free Full Text

23. Howe PW, Ament Z, Knowles K, *et al.*: **Combined use of filtered and edited ^{1}H NMR spectroscopy to detect ^{13}C-enriched compounds in complex mixtures.** *NMR Biomed.* 2012; **25**(11): 1217–1223.
PubMed Abstract | Publisher Full Text

24. Garbow JR, Weitekamp DP, Pines A: **Bilinear rotation decoupling of homonuclear scalar interactions.** *Chem Phys Lett.* 1982; **93**(5): 504–509.
Publisher Full Text

25. Wimperis S, Freeman R: **An excitation sequence which discriminates between direct and long-range CH coupling.** *J Magn Reson 1969.* 1984; **58**(2): 348–353.
Publisher Full Text

26. Uhrin D, Liptaj T, Kover KE: **Modified BIRD Pulses and Design of Heteronuclear Pulse Sequences.** *J Magn Reson A.* 1993; **101**(1): 41–46.
Publisher Full Text

27. Briand J, Sørensen OW: **Simultaneous and independent rotations with arbitrary flip angles and phases for I, ISalpha, and ISbeta spin systems.** *J Magn Reson.* 1998; **135**(1): 44–49.
PubMed Abstract | Publisher Full Text

28. Henry PG, Marjanska M, Walls JD, *et al.*: **Proton-observed carbon-edited NMR spectroscopy in strongly coupled second-order spin systems.** *Magn Reson Med.* 2006; **55**(2): 250–257.
PubMed Abstract | Publisher Full Text

29. Kazimierczuk K, Orekhov VY: **Accelerated NMR spectroscopy by using compressed sensing.** *Angew Chem Int Ed.* 2011; **50**(24): 5556–5559.
PubMed Abstract | Publisher Full Text

30. Delaglio F, Grzesiek S, Vuister GW, *et al.*: **NMRPipe: a multidimensional spectral processing system based on UNIX pipes.** *J Biomol NMR.* 1995; **6**(3): 277–93.
PubMed Abstract | Publisher Full Text

31. Willker W, Flögel U, Leibfritz D, *et al.*: **Ultra-high-resolved HSQC spectra of multiple- ^{13}C-labeled biofluids.** *J Magn Reson.* 1997; **125**(1): 216–219.
PubMed Abstract | Publisher Full Text

32. Furihata K, Tashiro M: **BASHD-J-resolved-HMBC, an efficient method for measuring proton-proton and heteronuclear long-range coupling constants.** *Magn Reson Chem.* 2014; **52**(1–2): 27–31.
PubMed Abstract | Publisher Full Text

33. Kazimierczuk K, Zawadzka A, Koźmiński W: **Optimization of random time domain sampling in multidimensional NMR.** *J Magn Reson.* 2008; **192**(1): 123–30.
PubMed Abstract | Publisher Full Text

34. Macura S: **Accelerated multidimensional NMR data acquisition by varying the pulse sequence repetition time.** *J Am Chem Soc.* 2009; **131**(28): 9606–9607.
PubMed Abstract | Publisher Full Text

35. Schulze-Sünninghausen D, Becker J, Koos MRM, *et al.*: **Improvements, extensions, and practical aspects of rapid ASAP-HSQC and ALSOFAST-HSQC pulse sequences for studying small molecules at natural abundance.** *J Magn Reson.* 2017; **281**: 151–161.
PubMed Abstract | Publisher Full Text

36. Aschauer L, Gruber LN, Pfaller W, *et al.*: **Delineation of the key aspects in the regulation of epithelial monolayer formation.** *Mol Cell Biol.* 2013; **33**(13): 2535–2550.
PubMed Abstract | Publisher Full Text | Free Full Text

37. Nilsson R, Jain M: **Simultaneous tracing of carbon and nitrogen isotopes in human cells.** *Mol Biosyst.* 2016; **12**(6): 1929–1937.
PubMed Abstract | Publisher Full Text | Free Full Text

38. Ludwig C: **HS-TrAM.** 2017.
http://www.doi.org/10.17605/OSF.IO/EQHN3

Chapter 4 : Outcomes of cadaveric kidneys undergoing hypothermic machine perfusion: Analysis of registry data

In this chapter, National Health Service Blood and Transfusion service registry data were analysed to assess the outcomes of cadaveric kidneys undergoing hypothermic machine perfusion compared to those stored in static cold storage alone.

Data for DCD kidneys formed the basis of a study which was presented by myself as an oral presentation at the European Society of Transplantation Congress in Barcelona in September 2017 with accompanying abstract published in the journal Transplantation International (Appendix A).

Data regarding DBD kidneys is discussed in this chapter in addition to a further commentary which appears alongside the main manuscript which reports data for DCD kidneys.

I designed the study and was responsible for requesting data from NHSBT, initial data analysis and subsequent analysis, data interpretation and write-up of manuscript. I wrote the manuscript which was published in the American Journal of Transplantation in 2018 (186) with accompanying supplementary tables.

Introduction

Prior to commencing experimental research aiming to better understand and optimise hypothermic machine perfusion, a review of the evidence base for HMP revealed a lack of understanding of current practice in the UK. The current recommendations for the usage of HMP were a result of a technology appraisal conducted by the National Institute of Health and Care Excellence in 2009 (69) which pre-dated the main research widely quoted as the evidence for and against the use of HMP; namely the Machine Preservation Trial conducted by Moers et al. (70, 71, 187) and the results of a multi-centre randomised controlled trial in the UK conducted by Watson et al. (40).

The Machine Preservation Trial (70), which forms the majority of the evidence base for HMP, is the largest RCT describing short and long-term benefits of HMP for DBD cadaveric kidneys, including ECD kidneys (106) with an extended dataset from the same trial showing benefits for DCD kidneys (105). This extended dataset including only DCD kidneys reported a significant reduction in DGF rates for machine perfused kidneys but no longer-term benefits to graft survival.

In contrast, Watson et al (40) reported no difference in outcomes between DCD kidneys stored using HMP and those stored purely in static cold storage in a five centre UK based study. The contrasting results from the two studies is interesting and the reasons for the differences in reported outcomes are speculative. A likely contributing factor is that the two studies varied in methodology; differences included choice of standardised immunosuppression regimes, storage fluid for static storage conditions and most notably the timing of initiation of HMP. In the Machine Preservation Trial, HMP was initiated at retrieval centre by a dedicated perfusionist in contrast with Watson et al's RCT in which implanting surgeons were allowed to decide on the timing of initiation of HMP (40).

For DBD kidneys in the UK, the evidence is more contentious. No randomised controlled trials have assessed the benefits of HMP for such kidneys where HMP was not initiated from source.

The aim of conducting this analysis of national registry data was to determine whether HMP confers any short or long-term benefits for DBD and DCD cadaveric kidneys in the UK. This is important given the lack of a logistical framework in which HMP can be initiated at source; for the majority of cadaveric organs, HMP would have been initiated following arrival to implanting centre. Secondary aims were to determine the usage of HMP for different deceased donor organ sub-types.

Methods

As described in the manuscript, demographic and clinical data for all renal transplants occurring in the United Kingdom are submitted by transplant centers to the UK Transplant Registry held by the NHSBT.

Data were requested for all adult patients receiving a single-organ cadaveric renal transplant between January 2007 and December 2015 to allow sufficient follow-up to determine long-term functional outcome data. Kidneys which underwent normothermic perfusion, blood group and HLA antibody incompatible transplants were excluded. Creatinine was only recorded for those patients who were being followed up, and who remained dialysis independent at the time of follow up.

Preliminary statistical analysis divided cadaveric organs into DBD and DCD sub-types. Survival outcomes were assessed using Kaplan-Meier curves, with Cox regression used to generate hazard ratios (HRs) and p-values. Patient survival was only considered from a patients first transplant. Rates of DGF were compared between the groups using Fisher's exact test, whilst creatinine levels were reported as medians and interquartile ranges (IQRs), with comparisons performed using Mann-Whitney tests. Further statistical methods are described for DCD kidneys in the accompanying manuscript. Graft survival rates were death censored.

All analyses were performed using IBM SPSS 22 (IBM Corp. Armonk, NY), with $p<0.05$ deemed to be indicative of statistical significance throughout. Cases with missing data were excluded from analyses using a pairwise approach.

Results

There were 11,302 renal transplants eligible for inclusion in the study. Of these, 6,773 kidneys (59.9%) were from DBD donors with the remaining 4,529 (40.0%) from DCD donors.

Outcomes following transplantation of DBD donor kidneys

Of 6,773 DBD donor renal transplants, 6,721 (99.2%) underwent preservation using static cold storage alone with less than one percent undergoing hypothermic machine perfusion (n=52, 0.8%). Comparisons between outcomes by preservation modality are reported in Table 4. The rates of DGF were not found to differ significantly between the groups, with this occurring in 22.8% of SCS organs, compared to 28.3% of those preserved with HMP (p=0.380). Neither patient nor graft survival were found to differ significantly between the groups, with hazard ratios for HMP vs. SCS of 1.73 (95% CI: 0.89 – 3.33, p=0.100, Figure 41) and 0.81 (95% CI: 0.36 – 1.80, p=0.601, Figure 42), respectively. Creatinine levels at follow up were also similar in the SCS and HMP groups, with medians of 130μmol/L vs. 140μmol/L (p=0.166), 131μmol/L vs. 129μmol/L (p=0.912) and 130μmol/L vs. 150μmol/L (p=0.301) at 1, 3 and 5 years, respectively.

The small number of DBD kidneys undergoing HMP precluded multivariate analysis as the incidence of DGF was also similar in SCS and HMP groups.

Table 4. Univariable analysis of patient outcomes by preservation modality for DBD kidneys. DGF: Data reported as N (%), with p-value from Fisher's exact test. Survival: Data reported as Kaplan-Meier estimated rates at five years, with p-value from a log-rank test based on all available follow up. Creatinine: Data reported as median (IQR), with p-value from a Mann-Whitney test. Bold p-values are significant at p<0.05.

	N	SCS	HMP	p-Value
DGF	6166	1398/6120 (22.8%)	13/46 (28.3%)	0.380
5 year Graft Survival	6768	85.6%	87.3%	0.601
5 year Patient Survival	5551	88.1%	81.3%	0.100
12 month Creatinine (μmol/L)	5834	130 (104 – 167)	140 (115 – 179)	0.166
36 month Creatinine (μmol/L)	4018	131 (104 – 172)	129 (104 – 164)	0.912
60 month Creatinine (μmol/L)	2527	130 (103 – 170)	150 (112 – 202)	0.301

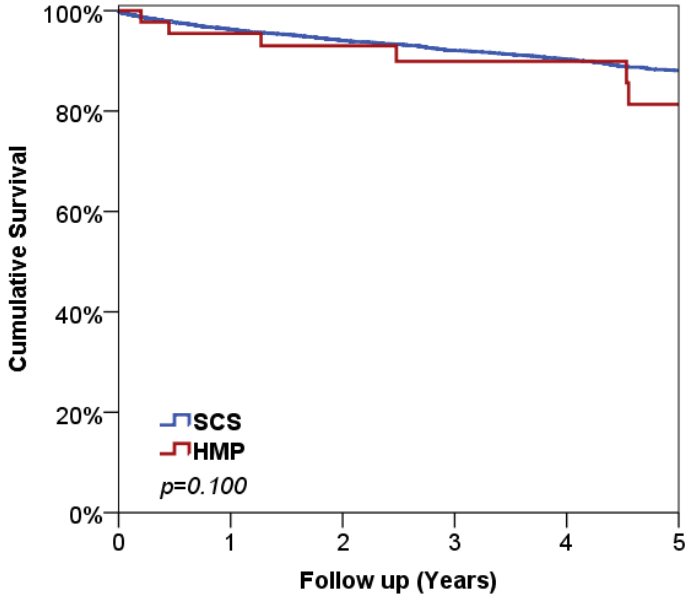

Figure 41. Kaplan Meier curve of patient survival by preservation modality.

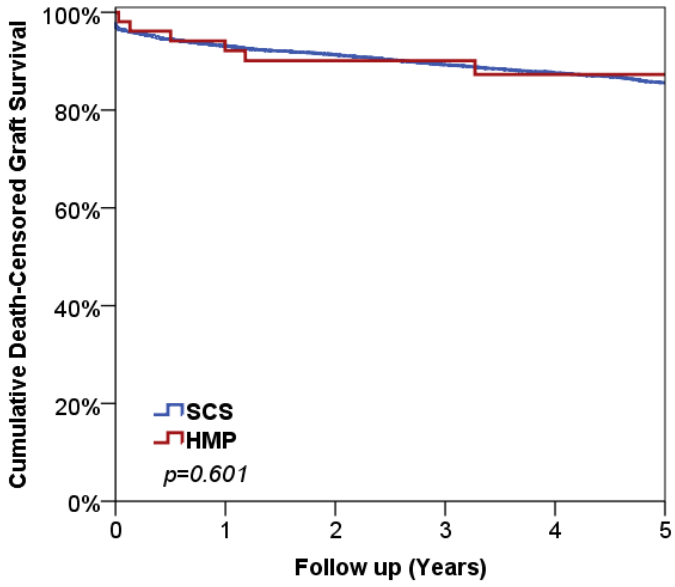

Figure 42. Kaplan Meier curve of death-censored graft survival by preservation modality.

Outcomes following transplantation of DCD donor kidneys

In contrast to DBD organs, HMP was used in 19.1% (n=864) of the 4,529 DCD kidneys transplanted over the study period. Key findings for DCD kidneys included a significantly lower incidence of delayed graft function for organs preserved with HMP than for organs preserved with SCS (34.2% vs 42.0%, p<0.001), despite a slightly longer cold ischemic time (median: 14.8 vs 14.1 hours, p<0.001).

Multivariable analysis found the effect of preservation modality to remain significant, with HMP organs having a significantly lower rate of DGF (odds ratio 0.65, 95% confidence interval 0.53-0.80, p<0.001) and significantly shorter times to DGF resolution (average 6.1 vs 7.4 days, p=0.003) than SCS organs. Both patient (p=0.313) and graft (p=0.263) survival rates were similar in the two preservation groups. HMP was associated with a marginal functional benefit in 1-year creatinine values, with serum creatinine values of 120μmol/L (HMP) vs 124μmol/L (SCS) (p=0.044). Serum creatinine values were converted for manuscript purposes to reflect the country of publication of the journal.

HMP utilisation was found to decline over the study period, from being used in 25.6% of the transplants in 2007-2010, to 14.4% of transplants in 2014-2015 (p<0.001). HMP was most commonly used in organs that were perfused with the recipients' blood during the daytime (08:00 - 16:59, p<0.001), and cases where HMP was used had significantly longer CIT than SCS organs (median 14.8 vs. 14.1 hours, p<0.001). Full results for DCD kidneys are reported in the attached manuscript which follows this commentary.

Discussion

Differences in utilisation of HMP for DBD and DCD kidneys

The utilisation of HMP almost exclusively for DCD kidneys in the UK is surprising given that the most convincing evidence to support HMP, the Machine Preservation Trial, showed the most benefit in DBD with a reduction in DGF rates (26.5% in the cold storage group vs 20.8% HMP group) and significant improvement in 1 and 3 year graft survival (70, 71).

It is well known that the incidence of DGF in DCD kidneys is higher than that of DBD kidneys (188). An extended dataset of solely DCD kidneys as an extension of the Machine Preservation Trial reported by Jochmans et al (105) described a decrease in the incidence of DGF from 69.5% to 53.7%. Hence a potential reason for the disparity in utilization of HMP for DBD and DCD kidneys may be the notable difference in absolute risk reduction in DGF for DCD kidneys compared with DBD kidneys (15.8% vs 5.7%) in these studies (70, 105). However, such findings were reported during the inclusion period for this study. One might suggest HMP is only used as a tool for reducing the incidence of DGF, explaining its preferential use for DCD kidneys.

Outcomes of DCD kidneys undergoing HMP

As discussed in the manuscript, key findings were a reduction in the incidence of DGF for kidneys which underwent HMP with a reduction in the duration of DGF for those kidneys preserved using HMP compared with those stored in static conditions alone. These findings were in contrast with the randomised controlled trial conducted by Watson et al (40) which included DCD kidneys included in this study. The study found no difference in short-term outcome, contrasting with findings by Jochmans et al (105) who observed a

reduction in the incidence of DGF from 69.5% to 53.7% for kidneys preserved in static conditions compared to HMP in an extension of the Machine Preservation Trial reflecting a larger absolute risk reduction compared to DCD kidneys in our cohort (42.0% static cold storage vs 34.2% kidneys preserved using HMP). One reason for this may be timing of initiation of HMP as all machine perfusion was initiated at source in contrast with kidneys in the UK. A clinical trial is underway in the UK in which HMP is initiated in DCD organs at source in order to address the effect of timing of initiation (189).

DGF as an outcome measure

The overall incidence of DGF in DCD kidneys was lower than that reported in trials by Jochmans et al (105) and Watson et al (40). However, DGF as an outcome measure indicates, but does not directly measure graft functional post transplantation. The now widely accepted definition of DGF is subject to criticism, with the contentious issue being the threshold for the use of dialysis between centres (36). Earlier transplantation research used alternative definitions of DGF (190) including variations in the dialysis-based definition of DGF (191, 192), a creatinine clearance-based definition of DGF (193-195) or a combination of both (196, 197).

DGF includes patients who underwent dialysis for any reason, perhaps over-estimating the number of patients with non-functioning grafts. Importantly in our observational study, in addition to afore mentioned RCTs by Moers et al (70) and Watson et al (40), clinicians would not have been blinded to the use of HMP which may have influenced decision making regarding dialysis in the post-operative period. If clinicians view kidneys preserved with HMP as less likely to experience DGF, the threshold for dialysis may be higher resulting in a lower incidence of DGF compared with those organs in which the incidence of DGF is likely to be high, such as those organs stored in static conditions alone.

The lack of consistency in the definition of DGF and the variation in clinical practice with respect to dialysing patients limits the extent to which results from different studies can be compared. For this reason, time to resolution of DGF was also included as an outcome measure to determine whether there were any further short-term benefits of HMP.

Study design

Although considered a lower level of evidence compared to well-designed randomised control trials (198, 199), one major criticism of cohort studies is the vulnerability of subjects to the influence of confounding factors with randomised controlled trials designed to isolate single interventions. Most randomised controlled trials assessing the benefits of HMP involve a relatively small number of transplants and are therefore may also be unable to control for multiple confounding factors. Hence one strength of a cohort study is the ability to control for multiple confounding factors due to a large sample size.

Similar to other registry analyses (200), it would be false to assume any differences in outcomes are due to preservation modality alone. In a single centre study, Guy et al previously described explored a role of HMP in prolonging cold ischaemic time from a median 13 to 28 hours, reducing the incidence of DGF in kidneys preserved using HMP from 47 to 27%, without impacting on graft survival (72). This may have been the case with some DCD kidneys in our cohort as median CIT was increased and reperfusion time more likely to be in the daytime for kidneys preserved using HMP. However, such practice is unlikely to be widespread as the increase in CIT was less than one hour. Kidneys with multiple renal arteries, associated with inferior graft outcomes (104), may not have been preserved using HMP as such anatomy renders HMP difficult. In addition, kidneys placed on HMP may be have been discarded depending on perfusion parameters when using such parameters as an assessment of graft quality, thereby resulting in a better overall

outcome for kidneys stored with HMP. The difference in DGF rates may therefore in part be due to graft assessment not due to the treatment effect of HMP.

Limitations

Cohort studies are subject to several disadvantages. First of all, as with any registry analysis, accuracy of data may be questioned. Several desired data fields were not fully populated in addition to a lack of some relevant data fields discussed within the manuscript and in this discussion.

Duration and timing of initiation of HMP

The primary aim of the study was to determine whether there were any benefits of HMP usage within the confines of current practice. One major limitation was the lack of data regarding initiation and cessation of HMP. Data regarding the mean duration and timing of initiation of HMP are not routinely collected in the United Kingdom. In kidneys preserved using HMP it is likely that those organs with a longer overall cold ischaemic time were preserved with HMP for longer. However, given this lack of data, our study does not describe a dose-response type relationship whereby the optimal timing of initiation and duration of HMP to promote the most clinical benefit is described.

The duration and timing of initiation of HMP are likely to determine the extent to which HMP results in functional benefit for each individual kidney (81). Such functional benefits likely result from the several mechanisms of action of HMP discussed in Chapter 1 which act concurrently following its initiation.

It is well known that renal vascular resistance falls during HMP with one study indicating a renal resistance at the end point of the HMP period was predictive of the development

of DGF and 1-year graft failure (88) and renal resistance at 4 hours approached statistical significance for the development of DGF.

Concerning the duration of HMP, between 1 and 4 hours of HMP following a period of cold storage both improved renal resistance on reperfusion and resultant functional outcome in a porcine model (82) suggesting benefit even with such short durations of HMP. Yet such improvements in functional outcome with short durations of HMP contrasts with the results of a porcine study by Hosgood et al comparing 18 hours of cold storage, 18 hours of HMP and 4 hours of HMP following 14 hours of cold storage (201). In this study no functional benefit was seen with 4 hours of HMP after cold storage suggesting a deleterious effect in delaying the initiation of HMP with a period of static cold storage. It could be argued that the initial static cold storage period may continually damage organs resulting in ischaemia reperfusion injury which cannot be reversed by a short period of HMP. A retrospective analysis by Matos et al was performed in a centre where DBD kidneys are received after 22 hours static cold storage (202). In this study, a further increase in CIT with a mean HMP duration 11 hours resulted in a reduction in the incidence of DGF with a reduction in duration of DGF for those kidneys without immediate graft function compared with those implanted soon after arrival at the implanting centre. Such outcomes indicate HMP has a role to play in organ reconditioning even after a significant period of static cold storage.

In the Machine Preservation Trial and associated studies which showed benefits for DBD (70, 71), DCD (105) and ECD kidneys (106), HMP was initiated at source resulting in a high proportion of the median CIT being accounted for by dynamic perfusion compared with static storage. Subsequent sub-group analysis of the Machine Preservation Trial data described the striking reduction in the incidence of DGF for those machine perfused kidneys with less than 10 hours cold ischaemic time compared with those in static storage

(187). Similarly, a registry analysis in the USA observed a significant reduction in the incidence of DGF for all kidneys irrespective of cold ischaemic time, including those with a cold ischaemic time less than 6 hours (200). Interestingly in this large registry analysis, there was no such reduction in the incidence of DGF for DCD and ECD kidneys preserved with HMP for less than 6 hours suggesting such higher risk kidneys require a longer duration of HMP to translate into clinical benefit.

Final comments

This observational study demonstrates that HMP is used almost exclusively for DCD kidneys in the UK, acting to reduce the incidence and duration of DGF with the suggestion of a small functional benefit at 1 year. This study aids decision making regarding initiation of HMP in DCD kidneys in centres where organs are received following a period of SCS although findings do not clearly define the most beneficial timing of initiation or duration of HMP.

Several influencing factors such as pre-HMP exposure to static storage conditions and the subtype of cadaveric kidney in question influence the minimum duration of HMP which promotes functional benefit following transplantation. In Chapter 5, metabolism during HMP is compared with SCS kidneys in order to explain how metabolism contributes to the development of ischaemia reperfusion injury which is known to influence post-transplantation graft function.

Manuscript

Patel K, Nath J, Hodson J, Inston N, Ready A. Outcomes of donation after circulatory death kidneys undergoing hypothermic machine perfusion following static cold storage: A UK population-based cohort study. American Journal of Transplantation. 2018;18:1408–1414

Received: 4 August 2017 | Revised: 24 October 2017 | Accepted: 8 November 2017

DOI: 10.1111/ajt.14587

ORIGINAL ARTICLE

AJT

Outcomes of donation after circulatory death kidneys undergoing hypothermic machine perfusion following static cold storage: A UK population-based cohort study

Kamlesh Patel[1,2] | Jay Nath[1,2] | James Hodson[3] | Nicholas Inston[1] | Andrew Ready[1]

[1]Department of Renal Surgery, University Hospital Birmingham NHS Foundation Trust, Birmingham, UK

[2]Institute of Metabolism and Systems Research, School of Medical and Dental Science, University of Birmingham, Birmingham, UK

[3]Institute of Translational Medicine, University Hospitals Birmingham NHS Foundation Trust, Birmingham, UK

Correspondence
Kamlesh Patel
Email: kamleshpatel@doctors.org.uk

Evidence is currently lacking regarding the outcomes of kidneys undergoing hypothermic machine perfusion (HMP) in patients in the United Kingdom. Using the National Health Service Blood and Transplant database, the authors compared outcomes for recipients of single-organ donation after circulatory death (DCD) kidneys preserved with HMP with those preserved using only static cold storage (SCS). Between 2007 and 2015, HMP was used in 19.1% (864/4,529) of kidneys. Rates of delayed graft function (DGF) were significantly lower in organs preserved with HMP than for organs preserved with SCS (34.2% vs 42.0%, $P < .001$), despite a slightly longer cold ischemic time (median: 14.8 vs 14.1 hours, $P < .001$). Multivariable analysis found the effect of preservation modality to remain significant, with HMP organs having a significantly lower rate of DGF (odds ratio 0.65, 95% confidence interval 0.53-0.80, $P < .001$) and significantly shorter times to DGF resolution (average: 6.1 vs 7.4 days, $P = .003$) than SCS organs. The patient ($P = .313$) and graft ($P = .263$) survival rates were similar in the 2 preservation groups. HMP was associated with a marginal functional benefit in 1-year creatinine values ($P = .044$), with adjusted averages of 1.36 mg/dL (HMP) versus 1.40 mg/dL (SCS). This study supports the use of HMP and aids decision-making over its instigation, which may improve short-term patient outcomes.

KEYWORDS
clinical research/practice, kidney transplantation/nephrology, organ perfusion and preservation, organ procurement and allocation, registry/registry analysis

1 | INTRODUCTION

Hypothermic machine perfusion (HMP) has been shown to reduce the incidence of delayed graft function (DGF) after transplantation of deceased donor kidneys from brainstem death (DBD) and circulatory death (DCD) donors.[1-5] DCD kidneys are now widely used, accounting for just under half of deceased donor kidneys transplanted in the United Kingdom.[6] While longer-term outcomes for such kidneys are equivalent to those from DBD kidneys,[7,8] the risk of developing DGF is increased.

Given the reduction in DGF rates demonstrated by multiple studies for HMP kidneys,[9] DCD organs would seemingly have most to gain from a period of HMP. Yet, surprisingly, the evidence for HMP of DCD kidneys is less unilateral than that for DBD kidneys,[1,2] with 1 UK-based randomized trial stopped prematurely after interim analysis found no difference in DGF rates between HMP and SCS-preserved organs.[10]

In the United Kingdom, HMP using the LifePort Kidney Transporter (Organ Recovery Systems, Itasca, IL) is permitted by the National Institute of Health and Care Excellence[11] and has been used in clinical practice for over a decade, albeit with varying rates of uptake in individual units. Such variation between centers may relate to the logistical challenges associated with the initiation of HMP but may also be due to a lack of evidence detailing the outcomes of kidneys undergoing

Abbreviations: CIT, cold ischemia time; DBD, donation after brainstem death; DCD, donation after circulatory death; DGF, delayed graft function; HMP, hypothermic machine perfusion; NHSBT, National Health Service Blood and Transplant; SCS, static cold storage.

HMP in the United Kingdom, particularly where the opportunity to commence HMP at the time of donation rarely exists. Hence, clinicians are required to decide whether HMP should be commenced only after the kidney has arrived at their units in SCS conditions.

Against this background, the aim of this study was to review current practices and outcomes for DCD kidneys in an attempt to strengthen future decision-making regarding commencing HMP when DCD kidneys arrive at the recipient unit.

2 | METHODS

2.1 | Study population

Demographic and clinical data for all renal transplants occurring in the United Kingdom are submitted by transplant centers to the UK Transplant Registry held by National Health Service Blood and Transplant (NHSBT) service. Reviewing the resulting database, all adult patients receiving a single-organ DCD donor kidney transplant between January 2007 and December 2015, where the preservation modality was hypothermic (SCS or HMP), were included in the study. Creatinine was only recorded for those patients still alive and being followed up at the time.

2.2 | Outcome measures

Primary outcome measures were rates of DGF and graft survival (death censored). DGF was defined as the need for dialysis in the first week after renal transplantation. Secondary outcome measures were time to resolution of DGF; serum creatinine values at 1, 3, and 5 years; and patient survival.

2.3 | Statistical methods

Initially, univariable analyses were performed to compare a range of factors and outcomes between the HMP and SCS groups. Ordinal and non-normally distributed variables were compared between groups by using Mann-Whitney tests, while nominal variables were compared by using the Fisher exact test where there were 2 categories and χ^2 tests otherwise. Patient and graft survival rates were compared by using Kaplan-Meier curves with log-rank tests. Patient survival was considered only for patients receiving their first graft. Creatinine levels and the time to resolution of DGF both followed skewed distributions and so were $\log_{10}$-transformed before analysis. The resulting values were compared between groups by using independent-samples *t*-tests and summarized by using geometric means and 95% confidence intervals (CIs).

Multivariable analyses were then performed to assess the differences between the HMP and SCS groups, after accounting for the effects of potentially confounding factors. This analysis was based on binary logistic regression models for dichotomous outcomes, general linear models of $\log_{10}$-transformed data for continuous outcomes, and Cox regression for the survival outcomes. Before the analysis, the goodness of fit of each continuous factor was assessed, either using Hosmer-Lemeshow tests or by examination of the standardized or Martingale residuals, as applicable. Where poor model fit was detected, continuous variables were divided into categories and treated as categorical in the analysis.

For each of these analyses, a backward stepwise approach was used to select independent predictors of outcome. Factors with substantial quantities of missing data that were not selected for inclusion in the final model were excluded, and the analysis was repeated to maximize the included sample size. Where the preservation method (HMP vs SCS) was not included in the final model due to nonsignificance, factors in the model were entered into a new model alongside the preservation method. For the analysis of creatinine levels and the time to resolution of DGF, adjusted averages were calculated for HMP and SCS groups by using values predicted when the same "average" patient had been in either preservation group. Adjusted averages were generated by multiplying coefficients for continuous variables by the mean of the cohort, and the coefficients for categorical variables were multiplied by the proportion of the cohort in each category.

A secondary analysis was performed for DGF to assess how the effect of preservation method varied according to duration of cold ischemia time (CIT). Initially, a binary logistic regression model was produced with the preservation method, CIT, and an interaction term as factors. Multivariable subgroup analyses were then performed for the SCS and HMP groups separately, as detailed previously.

All analyses were performed by using IBM SPSS 22 (IBM Corp., Armonk, NY), with $P < .05$ deemed to be indicative of statistical significance throughout. Cases with missing data were excluded on an analysis-by-analysis basis.

3 | RESULTS

3.1 | Demographics

Data were available for a total of 4529 transplantations across 23 centers (median 180 transplantations per center, range 30-503 transplantations). Overall, HMP was used in 864 (19.1%) cases, but usage rates varied by center, ranging from the 5 centers that did not use HMP in any transplantations during the period to 1 center that used HMP in 64.4% (197/306) of cases.

Comparisons for a range of factors between SCS and HMP kidneys are reported in Tables 1 and 2. Data for baseline factors were generally well populated (greater than 95%), with the exception of recipient hepatitis C virus infection, dialysis at transplantation, and donor terminal creatinine, which were recorded in only 77%, 88%, and 90% of cases, respectively. Organs preserved with HMP were from donors with a significantly higher body mass index than those in the SCS group (median 26.4 vs 26.1 kg/m^2, $P = .006$) and were less likely to be from donors with hypertension (24.2% vs 28.1%, $P = .028$). In addition, HMP use was found to differ by both donor and recipient ethnicity (both $P < .001$) and dialysis modality at time of transplantation ($P = .008$). HMP kidneys had a longer CIT (median 14.8 vs 14.1 hours, $P < .001$), and reperfusion more commonly took place during the daytime ($P < .001$). HMP use was also found to be in decline during the study

TABLE 1 Donor and recipient factors by use of hypothermic machine perfusion (HMP) vs static cold storage (SCS)

	No.	SCS cohort	HMP cohort	*P*-value
Donor				
Age, y (IQR)	4529	54 (43-63)	54 (41-63)	.656
Sex, n (%)				.939
Female	1817	1469 (40.1)	348 (40.3)	
Male	2712	2196 (59.9)	516 (59.7)	
Ethnicity, n (%)				**<.001**
White	4386	3534 (96.4)	852 (98.6)	
Asian	76	75 (2.0)	1 (0.1)	
Black	24	22 (0.6)	2 (0.2)	
Mixed/other	43	34 (0.9)	9 (1.0)	
Body mass index, kg/m^2 (IQR)	4404	26.1 (23.1-29.4)	26.4 (23.5-30.1)	**.006**
Blood group, n (%)				.173
A	1838	1475 (40.2)	363 (42.0)	
AB	115	97 (2.6)	18 (2.1)	
B	459	387 (10.6)	72 (8.3)	
O	2117	1706 (46.5)	411 (47.6)	
Cytomegalovirus status, n (%)				.590
Negative	2175	1758 (49.2)	417 (50.2)	
Positive	2231	1818 (50.8)	413 (49.8)	
Hypertension, n (%)				**.028**
No	3130	2528 (71.9)	602 (75.8)	
Yes	1178	986 (28.1)	192 (24.2)	
Terminal creatinine mg/dL (IQR)	4090	0.77 (0.60-1.04)	0.75 (0.62-0.97)	.952
Recipient				
Age, y (IQR)	4529	55 (46-63)	56 (47-64)	.070
Sex, n (%)				.659
Female	1507	1225 (33.5)	282 (32.6)	
Male	3017	2435 (66.5)	582 (67.4)	
Ethnicity, n (%)				**<.001**
White	3531	2788 (76.3)	743 (86.5)	
Asian	630	548 (15.0)	82 (9.5)	
Black	290	267 (7.3)	23 (2.7)	
Mixed/other	61	50 (1.4)	11 (1.3)	
Blood group, n (%)				.185
A	1799	1443 (39.4)	356 (41.2)	
AB	180	150 (4.1)	30 (3.5)	
B	555	466 (12.7)	89 (10.3)	
O	1995	1606 (43.8)	389 (45.0)	
Cytomegalovirus, n (%)				.059
Negative	1991	1580 (45.4)	411 (49.0)	
Positive	2328	1901 (54.6)	427 (51.0)	
Hepatitis C virus, n (%)				.305
Negative	3449	2753 (99.4)	696 (99.0)	
Positive	24	17 (0.6)	7 (1.0)	
Diabetes, n (%)				.949
No	4096	3315 (90.5)	781 (90.4)	
Yes	433	350 (9.5)	83 (9.6)	
Dialysis at transplantation, n (%)				**.008**
Not on dialysis	20	11 (0.3)	9 (1.2)	
Hemodialysis	2831	2274 (71.0)	557 (72.5)	
Peritoneal dialysis	1119	916 (28.6)	203 (26.4)	
Graft number, n (%)				.557[a]
1	4164	3374 (92.1)	790 (91.4)	
2	327	259 (7.1)	68 (7.9)	
>2	38	32 (0.9)	6 (0.7)	
Waiting time, d (IQR)	4527	756 (365-1203)	728 (356-1156)	.202

Data are reported as n (%), with *P*-values from Fisher exact/χ^2 tests or as median (IQR), with *P*-values from Mann-Whitney tests, unless stated otherwise. Bold *P*-values are significant at $P < .05$.

[a]Ordinal factors were compared between the groups by using Mann-Whitney tests.

period, from being used in 25.6% of the transplantations in 2007-2010 to 14.4% of transplantations in 2014-2015 ($P < .001$) (Table 2).

Patient outcomes were then compared between the HMP and SCS groups. The results of these analyses are summarized in Table 3, while the full multivariable models are reported in Tables S1-S5.

3.2 | Delayed graft function

DGF status was recorded in 4126 (91.1%) of transplantations. Overall rates of DGF were significantly lower for HMP kidneys compared with SCS kidneys (34.2% vs 42.0%, $P < .001$), with an odds ratio (OR) of 0.72 (95% CI 0.61-0.85, $P < .001$), translating into a number needed to treat of 12.9 (95% CI 8.7-25.6). For those patients where DGF occurred, the time to resolution was significantly shorter in HMP kidneys ($P = .004$), at a mean of 6.2 days (95% CI 5.4-7.0 days) compared with 7.4 days (7.0-7.8) in the SCS group.

After adjustment for confounding factors (Tables S1 and S2), multivariable analysis found the effect of preservation modality to remain significant, with HMP organs having a significantly lower rate of DGF (OR 0.65, 95% CI 0.53-0.80, $P < .001$) and significantly shorter times to DGF resolution (17.7% shorter, 95% CI 6.2%-27.8%, adjusted average: 6.1 vs 7.4 days, $P = .003$) than SCS organs.

3.3 | Patient and graft survival

There was no evidence of a significant association between preservation modality (HMP or SCS) and either patient survival ($P = .813$)

TABLE 2 Transplant and mismatch factors by hypothermic machine perfusion (HMP) vs static cold storage (SCS)

	No.	SCS cohort	HMP cohort	*P*-value
Year of transplantation, n (%)				**<.001**[b]
2007-2009	1051	782 (21.3)	269 (31.1)	
2010-2011	918	745 (20.3)	173 (20.0)	
2012-2013	1285	1046 (28.5)	239 (27.7)	
2014-2015	1275	1092 (29.8)	183 (21.3)	
Time of day recipient's blood perfused, n (%)				**<.001**
0:00-7:59	924	776 (21.3)	148 (17.2)	
8:00-16:59	2059	1613 (44.4)	446 (51.7)	
17:00-23:59	1514	1246 (34.3)	268 (31.1)	
CIT, h (IQR)	4470	14.1 (11.1-17.2)	14.8 (11.4-18.8)	**<.001**
Chronic renal failure at transplantation, n (%)				.100[b]
0	3240	2646 (72.2)	594 (68.8)	
1-20	374	285 (7.8)	89 (10.3)	
21-80	694	555 (15.1)	139 (16.2)	
81-100	221	179 (4.9)	42 (4.9)	
Human Leukocyte Antigen incompatible transplantation, n (%)				.205
No	4504	3642 (99.4)	862 (99.8)	
Yes	25	23 (0.6)	2 (0.2)	
HLA mismatch level, n (%)				.217[a]
1	140	109 (3.0)	31 (3.6)	
2	1084	874 (23.8)	210 (24.3)	
3	2667	2153 (58.7)	514 (59.8)	
4	638	529 (14.4)	109 (12.6)	

Data are reported as n (%), with *P*-values from Fisher exact/χ^2 tests or as median (IQR), with *P*-values from Mann-Whitney tests, unless stated otherwise. Bold *P*-values are significant at $P < .05$.
[a]Ordinal factors were compared between the groups by using Mann-Whitney tests.
[b]The ungrouped values were compared by using Mann-Whitney tests.

or graft survival (death censored) ($P = .452$, Figure 1) on univariable analysis. These relationships remained nonsignificant after adjustment for confounding factors on multivariable analysis, with $P = .313$ and $P = .263$, respectively (Table S3-S4).

3.4 | Creatinine

Creatinine levels at follow-up were available at 12, 36, and 60 months in 87%, 59%, and 35% of the cohort, respectively. On univariable analysis, there was a tendency for creatinine levels to be lower in the HMP group compared to the SCS group, at 12 months (geometric mean: 1.36 vs 1.40 mg/dL, $P = .055$), 36 months (1.35 vs 1.40 mg/dL, $P = .072$), and 60 months (1.35 vs 1.40 mg/dL, $P = .133$), although none of these comparisons reached statistical significance. However, after accounting for confounding factors in a multivariable analysis (Table S5), a significant difference in 12-month creatinine levels was detected ($P = .044$), with levels found to be 2.8% lower in organs preserved using HMP compared with the use of SCS (95% CI 0.1%-5.3%). Evaluating the model at the midpoints of the factors accounted for produced adjusted average 12-month creatinine levels of 1.36 and 1.40 mg/dL for HMP and SCS kidneys, respectively.

3.5 | Association between DGF and HMP by CIT

A set of analyses were then performed to assess whether the previously observed association between HMP and reduced rates of DGF varied with CIT. In a binary logistic regression model with CIT, the preservation modality and an interaction term as factors, the interaction was close to reaching statistical significance ($P = .087$). For this reason, separate multivariable analyses of DGF were produced for the HMP and SCS subgroups, to further assess the impact of CIT (Table S6). This found a tendency for the rate of DGF to increase with CIT in the SCS group (OR per 10 hours: 1.08, 95% CI 0.91-1.28, $P = .366$) but to decrease with CIT where HMP was used (OR per 10 hours: 0.76, 95% CI 0.52-1.10, $P = .142$), although neither of these effects reached statistical significance. This relationship is depicted in Figure 2.

TABLE 3 Univariable and multivariable analyses of outcomes by hypothermic machine perfusion (HMP) vs static cold storage (SCS)

	Univariable		Multivariable	
	Statistic (95% CI)	*P*-value	Statistic (95% CI)	*P*-value
DGF	0.72 (0.61 to 0.85)	**<.001**	0.65 (0.53 to 0.80)	**<.001**
Time to DGF resolution	−16.3% (−26.6% to −4.6%)	**.008**	−17.7% (−27.8% to −6.2%)	**.003**
Graft survival	0.92 (0.75 to 1.14)	.453	0.88 (0.70 to 1.10)	.263
Patient survival	0.97 (0.78 to 1.21)	.813	0.87 (0.67 to 1.14)	.313
Creatinine (12 Months)	−2.8% (−5.6% to +0.0%)	.055	−2.8% (−5.3% to −0.1%)	**.041**

DGF, delayed graft function. Statistics are quoted for HMP vs SCS. Bold *P*-values are significant at $P < .05$.

DGF: Results are reported as odds ratios from binary logistic regression models. The full multivariable analysis is reproduced in Table S1.

Time to DGF resolution: Results are reported as percentage differences between groups from general linear models of $\log_{10}$-transformed data. The full multivariable analysis is reproduced in Table S2.

Survival: Results are reported as hazard ratios from Cox regression models. Analysis of patient survival only includes those patients receiving their first graft. The full multivariable analyses are reproduced in Tables S3 and S4.

Creatinine: Results are reported as percentage differences between groups from general linear models of $\log_{10}$-transformed data. The full multivariable analysis is reproduced in Table S5.

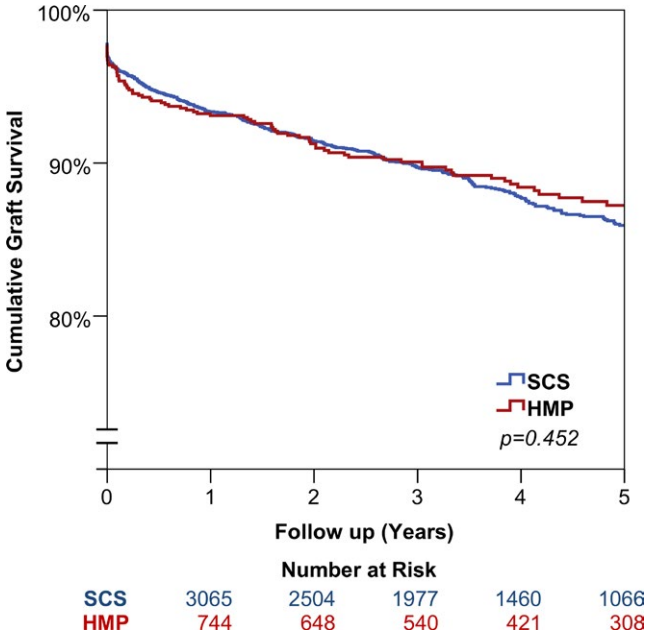

FIGURE 1 Kaplan-Meier curve of graft survival by preservation modality

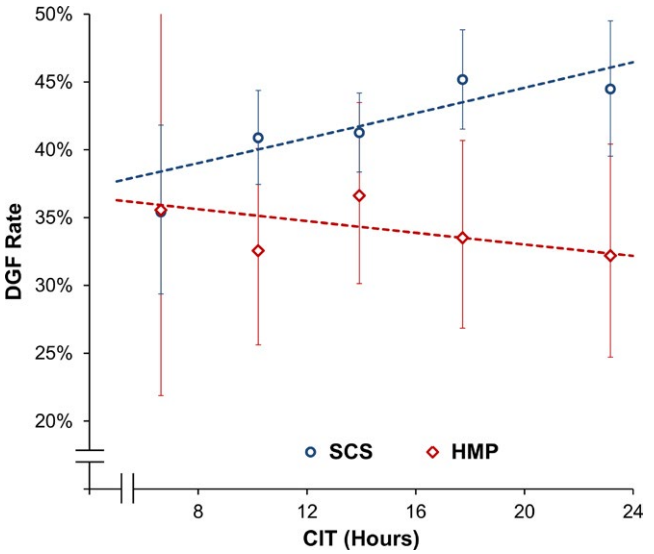

FIGURE 2 Associations between cold ischemia time (CIT) and delayed graft function (DGF) in the hypothermic machine perfusion (HMP) and static cold storage (SCS) cohorts. The points represent DGF rates and 95% confidence intervals within 4 hourly intervals of CIT, plotted at the midpoints of the interval. Trend lines are from univariable binary logistic regression models within the SCS and HMP subgroups, with CIT as a covariate

3.6 | Association between DGF rates and HMP use by centers

A subgroup analysis was performed to assess whether the reduction in DGF rates with HMP varied by the HMP use strategy of the transplanting center. The 23 transplant centers were divided into 3 groups: those that used HMP in less than 5%, 5% to 20%, and more than 20% of cases (Table 4). A binary logistic regression model was then produced to assess whether the effect of HMP on DGF differed between these groups. This found no significant interaction between these factors ($P = .081$), although there was a tendency for HMP to be more effective in reducing rates of DGF in centers where it was used more frequently (ie, in >20% of cases, OR 0.66, $P < .001$) than for the intermediate-use group (ie, in 5-20% of cases, OR 1.08, $P = .697$).

4 | DISCUSSION

This review of a national NHSBT data set provides real-world data on outcomes after a period of HMP as used in clinical practice in the United Kingdom. This study describes the short-term and longer-term outcomes after a period of HMP, which is important, given the discordance between previous trial methodology and clinical practice in many countries where HMP is not routinely commenced at the retrieval center.

Kidneys undergoing a period of HMP had a clear reduction in the risk of developing DGF, compared with SCS kidneys, corroborating findings from previous studies[1–3] and meta-analyses.[4,5] These findings are in contrast to the previously reported trial in the United Kingdom[10] investigating the effects of HMP in DCD kidneys and highlight the

TABLE 4 Subgroup analysis of delayed graft function (DGF) in hypothermic machine perfusion (HMP) vs static cold storage (SCS) by HMP use rate of transplanting center

			SCS		HMP			
HMP rate	Center	Transplant	No.	DGF	No.	DGF	Odds ratio (95% CI)	*P*-value
<5%	11	1351	1337	499 (37.3%)	16	4 (25.0%)	0.56 (0.18-1.75)	.317
5-20%	5	1088	972	484 (49.8%)	118	61 (51.7%)	1.08 (0.74-1.58)	.697
>20%	7	1682	1039	422 (40.6%)	644	201 (31.2%)	0.66 (0.54-0.82)	**<.001**

Odds ratios are from univariable binary logistic regression models within each subgroup, and are for HMP, relative to SCS. Bold *P*-values are significant at $P < .05$.

strengths of a population-based analysis. The absolute risk reduction in DGF in this study (7.8%) was greater than that in the previously reported machine preservation trial[1] (5.7%), where HMP was commenced at the retrieval center. Similar to previous studies,[1,12] our results demonstrate a reduction in the duration of DGF for kidneys undergoing HMP, further reaffirming the short-term benefits of HMP, even following an initial storage period in SCS conditions. Yet, while lower rates of DGF after renal transplantation may infer improved graft survival in general,[13] our data did not show the same benefit for HMP kidneys. In our cohort, as with previous studies,[2,3] no longer-term benefit was observed for kidneys undergoing a period of HMP.

There has been little evidence to inform clinicians faced with the choice of whether to subject kidneys to a period of HMP once organs arrive at the transplant center and effectively increase the CIT or to implant expediently. Multiple studies have correlated increased CIT with inferior outcomes for SCS kidneys,[14] yet the duration for which HMP can be safely used is not known. Our analysis of DGF rates by CIT clearly demonstrates that, at least in the short term and within a 24-hour window, the well-established detrimental effects of prolonged CIT for SCS kidneys is not applicable for HMP organs (Figure 2). For kidneys undergoing a period of HMP, the likelihood of developing DGF does not increase with prolonged CIT up to 24 hours.

While this study does not explicitly compare kidneys perfused overnight with those transplanted overnight, it does demonstrate that there appear to be no short-term adverse effects of increasing CIT with a period of HMP. This would appear to support the practice of overnight perfusion of DCD kidneys by using HMP as a bridging therapy, provided total CIT is projected to be less than 24 hours, as previously described in our unit.[15] Furthermore, we found that HMP kidneys had a slightly longer CIT and were more likely to transplanted during daylight hours. This finding suggests, at least in some centers, that kidneys arriving overnight underwent HMP and were transplanted the following morning. Cost analysis should therefore consider the beneficial effects of transplantation during daylight hours in addition to the advantages of reduction in DGF rates (number needed to treat = 12.9). Subgroup analyses of HMP use rates by transplant centers seem to support the regular use of HMP to achieve lower rates of DGF for those kidneys that undergo machine perfusion, although this analysis did not explore the nature of center-specific practices.

Kidneys undergoing HMP were generally higher risk than the SCS-alone group and, when such confounding factors were adjusted for, HMP kidneys demonstrated a small but significant benefit in creatinine at 1 year, for functioning grafts. While unlikely to be of any clinical significance, this may reflect some functional benefit of HMP past the immediate postoperative period, although this does not translate to longer-term creatinine improvements.

Conclusions drawn are limited by the nature of an observational study, including the absence of data regarding timing and duration of HMP, selection of organs for HMP, and discard rates. Because data regarding the mean duration and timing of initiation of HMP are not routinely collected for all transplantations in the United Kingdom, our study does not address the question of when HMP should be initiated and, further to this, does not define a possible dose-response relationship between duration of HMP and DGF rates.

The presence of multiple renal arteries has been associated with higher rates of DGF[16] and may have affected selection for HMP, given that organ anatomy changed allocation to preservation modality in the machine preservation trial.[1] Pump perfusion parameters, such as renal resistance, may be predictive of posttransplantation outcome[17] thereby leading to discard of organs deemed worse quality although, conversely, the same characteristics may provide reassurance, leading to lower discard rates than those assessed by transplant surgeon alone.[18]

This large, well-populated data set does, however, enable robust statistical analysis. As part of this review, it was surprising to find that despite the demonstrable benefits of HMP, its use in the United Kingdom declined during the study period. The reasons for this are not clear and contrast with results of an analysis of transplant registry data in the United States that describes HMP being used in two-thirds of DCD kidneys.[19] Nevertheless, the UK data may reflect a waning national interest, perhaps resulting from a lack of clear overall evidence supporting HMP use, combined with a lack of explicit guidance regarding specific situations in which HMP is beneficial.

However, in an era of transplantation where DCD kidneys account for between one-fourth and one-third of all single-organ kidney transplants in the United Kingdom, this study, using real-world data, supports the use of HMP, even after an initial period of SCS, and aids decision-making regarding its instigation. Applying HMP in these situations has the potential to improve short-term patient outcomes. Furthermore, recognizing the opportunity to perfuse kidneys overnight and increasingly perform transplantation during daylight hours in an increasingly medically complex donor and recipient

population offers potential financial, logistical, and patient safety benefits.

ACKNOWLEDGMENTS

The authors would like to thank NHSBT for supplying the data. We would like to thank all transplant centers in the United Kingdom who contributed data on which this article is based.

DISCLOSURE

The authors of this manuscript have conflicts of interest to disclose as described by the *American Journal of Transplantation*. Two authors (KP and JN) have ongoing research in part funded by Organ Recovery Systems. The other authors have no conflicts of interest to disclose.

ORCID

Kamlesh Patel http://orcid.org/0000-0003-1852-6468

REFERENCES

1. Moers C, Smits JM, Maathuis MH, et al. Machine perfusion or cold storage in deceased-donor kidney transplantation. *N Engl J Med*. 2009;360:7-19.
2. Moers C, Pirenne J, Paul A, Ploeg RJ. Machine perfusion or cold storage in deceased-donor kidney transplantation. *N Engl J Med*. 2012;366:770-771.
3. Jochmans I, Moers C, Smits JM, et al. Machine perfusion versus cold storage for the preservation of kidneys donated after cardiac death: a multicenter, randomized, controlled trial. *Ann Surg*. 2010;252(5):756-764.
4. Bathini V, McGregor T, McAlister VC, Luke PP, Sener A. Renal perfusion pump versus cold storage for donation after cardiac death kidneys: a systematic review. *J Urol*. 2013;189:2214.
5. Deng R, Gu G, Wang D, et al. Machine perfusion versus cold storage of kidneys derived from donation after cardiac death: a meta-analysis. *PLoS ONE*. 2013;8:e56368.
6. NHSBT. Annual report on kidney transplantation. Report for 2015/2016. Published July 2016. http://odt.nhs.uk/pdf/organ_specific_report_kidney_2016.pdf. Accessed November 29, 2017.
7. Summers DM, Johnson RJ, Hudson A, et al. Effect of donor age and cold storage time on outcome in recipients of kidneys donated after circulatory death in the UK: a cohort study. *Lancet*. 2013;381:703.
8. Summers DM, Johnson RJ, Allen J, et al. Analysis of factors that affect outcome after transplantation of kidneys donated after cardiac death in the UK: a cohort study. *Lancet*. 2010;376:1276.
9. O'Callaghan JM, Morgan RD, Knight SR, Morris PJ. Systematic review and meta-analysis of hypothermic machine perfusion versus static cold storage for kidney allografts on transplant outcomes. *Br J Surg*. 2013;100(8):991-1001.
10. Watson CJE, Wells AC, Roberts RJ, et al. Cold machine perfusion versus static cold storage of kidneys donated after cardiac death: a UK multi-center randomized controlled trial. *Am J Transplant*. 2010;10:1991.
11. Machine perfusion systems and cold static storage of kidneys from deceased donors. Technology Appraisal. Published January 2009. https://www.nice.org.uk/guidance/ta165/. Accessed November 29, 2017.
12. Matos ACC, Requiao Moura LR, Borrelli Jr M, et al. Impact of machine perfusion after long static cold storage on delayed graft function incidence and duration and time to hospital discharge [published online ahead of print October 3, 2017]. *Clin Transplant*. https://www.ncbi.nlm.nih.gov/pubmed/28972665
13. Yarlagadda SG, Coca SG, Formica Jr RN, et al. Association between delayed graft function and allograft and patient survival: a systematic review and meta-analysis. *Nephrol Dial Transplant*. 2009;24:1039-1047.
14. Debout A, Foucher Y, Trebern-Launay K, et al. Each additional hour of cold ischaemia time significantly increases the risk of graft failure and mortality following renal transplantation. *Kidney Int*. 2015;87:343-349.
15. Guy A, McGrogan D, Inston N, Ready A. Hypothermic machine perfusion permits extended cold ischemia times with improved early graft function. *Exp Clin Transplant*. 2015;13:130-137.
16. Zorgdrager M, Krikke C, Hofker SH, Leuvenink HG, Pol RA. Multiple renal arteries in kidney transplantation: a systematic review and meta-analysis. *Ann Transplant*. 2016;29(21):469-478.
17. Jochmans I, Moers C, Smits JM, et al. The prognostic value of renal resistance during hypothermic machine perfusion of deceased donor kidneys. *Am J Transplant*. 2011;11:2214-2220.
18. Schold JD, Kaplan B, Howard RJ, et al. Are we frozen in time? analysis of the utilization and efficacy of pulsatile perfusion in renal transplantation. *Am J Transplant*. 2005;5:1681-1688.
19. Lodhi SA, Lamb KE, Uddin I, Meier-Kriesche HU. Pulsatile pump decreases risk of delayed graft function in kidneys donated after cardiac death. *Am J Transplant*. 2012;12(10):2774-2780.

SUPPORTING INFORMATION

Additional Supporting Information may be found online in the supporting information tab for this article.

How to cite this article: Patel K, Nath J, Hodson J, Inston N, Ready A. Outcomes of donation after circulatory death kidneys undergoing hypothermic machine perfusion following static cold storage: A UK population-based cohort study. *Am J Transplant*. 2018;18:1408–1414. https://doi.org/10.1111/ajt.14587

Supplementary Tables relating to manuscript

Supplementary Table 1 – Multivariable analysis of DGF

	Odds Ratio (95% CI)	p-Value
Preservation Modality (HMP)	0.65 (0.53 - 0.80)	**<0.001**
Donor Age (per Decade)	1.17 (1.10 - 1.23)	**<0.001**
Donor Sex (Male)	1.27 (1.08 - 1.50)	**0.004**
Donor BMI (per kg/m^2)	1.03 (1.01 - 1.04)	**<0.001**
Donor Terminal Creatinine (per 0.1 mg/dL)	1.04 (1.02 - 1.06)	**<0.001**
Recipient Sex (Male)	1.22 (1.03 - 1.45)	**0.020**
Recipient Ethnicity		0.076
White	-	-
Asian	1.10 (0.88 - 1.38)	0.407
Black	1.48 (1.10 - 2.01)	0.010
Mixed/Other	0.95 (0.50 - 1.80)	0.870
Dialysis at Transplant		**<0.001**
Haemodialysis	-	-
Peritoneal Dialysis	0.40 (0.33 - 0.48)	**<0.001**
Not on Dialysis	0.18 (0.04 - 0.87)	**0.032**
Graft Number		**<0.001**
1	-	-
2	1.52 (1.12 - 2.07)	**0.008**
>2	4.02 (1.55 - 10.43)	**0.004**
HLA Mismatch Level		**0.027**
1	-	-
2	1.79 (1.06 - 3.01)	**0.029**
3	1.53 (0.92 - 2.55)	0.099
4	1.95 (1.14 - 3.34)	**0.015**
Year of Transplant		**<0.001**
2007-2009	-	-
2010-2011	0.73 (0.57 - 0.93)	**0.012**
2012-2013	0.57 (0.45 - 0.72)	**<0.001**
2014-2015	0.43 (0.33 - 0.55)	**<0.001**
Waiting Time		0.061
<18 Months	-	-
18-35 Months	0.99 (0.81 - 1.20)	0.909
36-59 Months	1.27 (1.04 - 1.56)	0.020
60+ Months	1.08 (0.76 - 1.54)	0.654

Results are from a multivariable binary logistic regression model and bold p-values are significant at p<0.05. Hazard ratios are relative to the reference category for categorical variables, or for an increase of the stated number of units for continuous variables. All factors from Tables 1a-c were originally considered for inclusion, but recipient HCV was subsequently excluded, due to the large quantity of missing data in the factor, and the fact that it was not selected for inclusion in the initial stepwise model. Waiting time was divided into categories, since a Hosmer and Lemeshow test indicated poor model fit when the factor was treated as continuous in univariable analysis. The resulting analysis was based on N=2,835.

Supplementary Table 2 – Multivariable analysis of time to resolution of DGF

	Coefficient (95% CI)	p-Value
Preservation Modality (HMP)	-17.7% (-27.8%, -6.2%)	**0.003**
Donor Age (per Decade)	4.7% (1.1%, 8.3%)	**0.009**
Donor Sex (Male)	15.7% (4.8%, 27.7%)	**0.004**
Year of Transplant		0.068
2007-2009	-	-
2010-2011	-15.9% (-26.6%, -3.5%)	0.013
2012-2013	-2.8% (-14.5%, 10.6%)	0.669
2014-2015	-8.2% (-20.3%, 5.7%)	0.234

Results are from a multivariable general linear model and bold p-values are significant at p<0.05. Due to the level of skew in the distribution, the times to resolution of DGF were log_{10}-transformed, prior to analysis. The coefficients from the resulting model were then anti-logged, and converted into percentage differences. As such, the quoted values represent the estimated percentage difference in the time to resolution relative to the reference category for categorical variables, or for an increase of the stated number of units for continuous variables. All factors from Tables 1a-c were originally considered for inclusion, but recipient HCV, dialysis at transplant and donor terminal creatinine were subsequently excluded, due to the large quantities of missing data in these factors, and the fact that they were not selected for inclusion in the initial stepwise model. The resulting analysis was based on N=1,656.

Supplementary Table 3 – Multivariable analysis of patient survival

	Hazard Ratio (95% CI)	p-Value
Preservation Modality (HMP)	0.87 (0.67 -1.14)	0.313
Donor BMI (per kg/m^2)	1.02 (1.00 - 1.04)	**0.019**
Donor Terminal Creatinine (per 0.1 mg/dL)	0.98 (0.95 -1.00)	0.093
Recipient Age (per Decade)	1.77 (1.59 -1.97)	**<0.001**
Recipient Diabetes	1.55 (1.16 -2.07)	**0.003**
Recipient Ethnicity		0.089
White		
Asian	0.67 (0.46 -0.96)	0.031
Black	0.72 (0.45 -1.15)	0.170
Mixed/Other	1.25 (0.55 -2.83)	0.588
Dialysis		**<0.001**
Haemodialysis		
Peritoneal Dialysis	0.50 (0.39 -0.66)	**<0.001**
Not on Dialysis	0.99 (0.25 -4.00)	0.989
HLAi	3.66 (1.16 -11.51)	**0.027**
HLA Mismatch Level		0.083
1		
2	1.97 (0.79 -4.90)	0.143
3	1.90 (0.78 -4.63)	0.158
4	2.53 (1.01 -6.31)	0.047
CIT (per 10 Hours)	1.33 (1.07 -1.64)	**0.009**
Time of Day Recipient's Blood Perfused		0.080
0:00 - 7:59		
8:00 - 16:59	1.40 (1.04 -1.89)	0.026
17:00 - 23:59	1.24 (0.90 -1.71)	0.179

Results are from a multivariable Cox regression model and bold p-values are significant at p<0.05. Hazard ratios are relative to the reference category for categorical variables, or for an increase of the stated number of units for continuous variables. All factors from Tables 1a-c were originally considered for inclusion, but recipient HCV was subsequently excluded, due to the large quantity of missing data and the fact that it was not selected for inclusion in the initial stepwise model. The preservation modality was not selected for inclusion by this analysis, and so was entered into a model alongside those factors that had been selected by the stepwise procedure. The final model was based on N=3,109.

Supplementary Table 4 – Multivariable analysis of graft survival

	Hazard Ratio (95% CI)	p-Value
Preservation Modality (HMP)	0.88 (0.70 - 1.10)	0.263
Donor Age (per Decade)	1.21 (1.14 - 1.29)	**<0.001**
Dialysis (Peritoneal)*	0.75 (0.61 - 0.92)	**0.006**
HLA Mismatch Level		**0.008**
1	-	-
2	1.19 (0.66 - 2.15)	0.552
3	1.68 (0.96 - 2.96)	0.071
4	1.35 (0.74 - 2.49)	0.327
CRF at Transplant (per 10 units)	1.06 (1.02 - 1.09)	**<0.001**
CIT (per 10 hours)	1.44 (1.21 - 1.71)	**<0.001**
Time of Day Recipient's Blood Perfused		0.292
0:00 - 7:59	-	-
8:00 - 16:59	1.08 (0.84 - 1.37)	0.563
17:00 - 23:59	1.21 (0.94 - 1.55)	0.145

*Results are from a multivariable Cox regression model and bold p-values are significant at p<0.05. Hazard ratios are relative to the reference category for categorical variables, or for an increase of the stated number of units for continuous variables. All factors from Tables 1a-c were originally considered for inclusion, but recipient HCV and donor terminal creatinine were subsequently excluded, due to a large quantity of missing data in these factors, and the fact that they were not found to be significant in the initial stepwise model. The preservation modality was not selected for inclusion by this analysis, and so was entered into a model alongside those factors that had been selected by the stepwise procedure. *Patients not on dialysis (N=20) were excluded from this analysis, as there were no graft failures in this group making hazard ratios incalculable. The final model was based on N=3,883.*

Supplementary Table 5 – Multivariable analysis of 12 month creatinine

	Coefficient (95% CI)	p-Value
Preservation Modality (HMP)	-2.8% (-5.3%, -0.1%)	**0.041**
Donor Age (per Decade)	10.7% (9.7%, 11.6%)	**<0.001**
Donor Ethnicity		**0.014**
White	-	-
Asian	12.2% (3.8%, 21.3%)	**0.004**
Black	11.4% (-4.1%, 29.4%)	0.156
Mixed/Other	-2.8% (-12.2%, 7.5%)	0.577
Donor Hypertension	4.2% (1.7%, 6.9%)	**0.001**
Recipient Age (per Decade)	-3.1% (-4.1%, -2.2%)	**<0.001**
Recipient Sex (Male)	22.6% (19.9%, 25.4%)	**<0.001**
Recipient Ethnicity		**<0.001**
White	-	-
Asian	-10.3% (-13.0%, -7.5%)	**<0.001**
Black	11.9% (7.3%, 16.8%)	**<0.001**
Mixed/Other	-5.6% (-13.7%, 3.2%)	0.206
Graft Number		0.120
1	-	-
2	-4.7% (-8.9%, -0.2%)	0.042
>2	0.1% (-10.6%, 12.0%)	0.988
CRF at Transplant (per 10 units)	0.6% (0.1%, 1.1%)	**0.016**
CIT (per 10 hours)	4.2% (2.0%, 6.5%)	**<0.001**

Results are from a multivariable general linear model and bold p-values are significant at p<0.05. Due to the level of skew in the distribution, creatinine levels were log_{10}-transformed, prior to analysis. The coefficients from the resulting model were then anti-logged, and converted into percentage differences. As such, the quoted values represent the estimated percentage difference in creatinine relative to the reference category for categorical variables, or for an increase of the stated number of units for continuous variables. All factors from Tables 1a-c were originally considered for inclusion, but recipient HCV, dialysis at transplant and donor terminal creatinine were subsequently excluded, due to a large quantity of missing data in these factors, and the fact that they were not selected for inclusion in the initial stepwise model. The final model was based on N=3,700.

Supplementary Table 6 – Multivariable subgroup analysis of the association between CIT and DGF by preservation modality

	SCS		HMP	
	Odds Ratio (95% CI)	**p-Value**	**Odds Ratio (95% CI)**	**p-Value**
CIT (per 10 hours)	1.08 (0.91 - 1.28)	0.366	0.76 (0.52 - 1.10)	0.142
Donor Age (per Decade)	1.16 (1.09 - 1.23)	**<0.001**	1.23 (1.08 - 1.40)	**0.002**
Donor Sex (Male)	1.28 (1.08 - 1.51)	**0.005**	-	-
Donor BMI	1.03 (1.01 - 1.04)	**<0.001**	-	-
Donor Terminal Creatinine (per 0.1 mg/dL)	1.03 (1.02 - 1.05)	**<0.001**	1.07 (1.02 - 1.11)	**0.002**
Recipient Diabetes	1.35 (1.02 - 1.77)	**0.035**	-	-
Dialysis at Transplant		**<0.001**		**<0.001**
Haemodialysis	-	-		
Peritoneal Dialysis	0.42 (0.35 - 0.50)	**<0.001**	0.30 (0.19 - 0.47)	**<0.001**
Not on Dialysis	0.22 (0.05 - 1.11)	0.068	*NA**	*NA**
Graft Number		**0.005**	-	-
1	-	-	-	-
2	1.38 (1.00 - 1.91)	0.051	-	-
>2	3.98 (1.46 - 10.81)	**0.007**	-	-
Year of Transplant		**<0.001**		0.147
2007 – 2009	-	-		
2010 – 2011	0.74 (0.57 - 0.96)	**0.025**	0.69 (0.41 - 1.16)	0.164
2012 – 2013	0.54 (0.42 - 0.69)	**<0.001**	0.72 (0.44 - 1.16)	0.177
2014 – 2015	0.41 (0.32 - 0.52)	**<0.001**	0.51 (0.29 - 0.91)	0.022
Waiting Time		**0.022**	-	-
<18 Months	-	-	-	-
18-35 Months	1.04 (0.85 - 1.28)	0.680	-	-
36-59 Months	1.36 (1.10 - 1.67)	**0.004**	-	-
60+ Months	1.18 (0.82 - 1.71)	0.369	-	-
HLA Mismatch Level	-	-		0.233
1	-	-		
2	-	-	2.12 (0.70 - 6.40)	0.182
3	-	-	1.62 (0.55 - 4.72)	0.379
4	-	-	2.41 (0.76 - 7.62)	0.135

*Results are from multivariable binary logistic regression models produced separately for each cohort, and bold p-values are significant at p<0.05. All factors from Tables 1a-c were originally considered for inclusion, but recipient HCV was subsequently excluded, due to the large quantity of missing data and the fact that it was not selected for inclusion in either of the initial stepwise models. Factors identified as independent predictors of DGF in the resulting models were then entered into a model alongside CIT. The resulting analyses were based on N=2,593 for the SCS cohort, and N=577 for the HMP cohort. *Recipients not on dialysis were excluded from the analysis of the HMP cohort, as none of the (N=9) cases developed DGF, making odds ratios incalculable.*

Chapter 5 : Metabolic differences between kidneys preserved with hypothermic machine perfusion and those in static cold storage

This study was performed early in my research degree using ^{1}H-1D NMR and a paired porcine study design which formed the basis of later experiments.

The study was designed in conjunction with my supervisor Jay Nath. I was responsible for performing experiments, analysing data and co-writing the manuscript which follows accompanied by additional commentary and supplementary figures and tables referred to in the body of the manuscript.

Introduction

Environmental temperature has a profound effect on the rate of biological processes including metabolism. The Arrhenius equation (203) describes the effect of temperature on a reaction at lower temperatures; reaction rates are reduced by 50% for every 10°C reduction in temperature. Southard and Belzer suggest that in ex-vivo organs preserved at 4°C, only 5-8% of normal metabolic function occurs (63). At such temperatures, demand for oxygen and substrates is also reduced.

As discussed in Chapter 1, the characterising feature of HMP is the dynamic pulsatile recirculation of chilled perfusion fluid through renal vasculature. In contrast to static storage, machine perfusion permits constant delivery of substrates to renal parenchyma with washout of toxic metabolites.

To date, few studies have explored metabolism within kidneys undergoing HMP. Bon et al. (172) used ^{1}H-1D NMR to determine metabolic changes in circulating perfusate in an auto-transplantation porcine study. Functional outcome was assessed following standard HMP with a second group undergoing HMP with an experimental perfusion fluid. Concentrations of lactate, choline, valine, glycine and glutamate increased whilst the concentration of glutathione decreased. The rate of change was associated with graft function post-transplantation.

Previous studies in our group have also used ^{1}H-1D NMR to validate porcine kidneys as a metabolic model for human studies (174). The study compared changes in the perfusate concentration of metabolites in standard criteria deceased donor human and porcine kidneys. Interestingly most metabolites seemed to increase in concentration at the same rate in both species. Similarities in changing metabolite concentrations were seen

between this study and that of Bon et al. (172); the concentration of glutathione decreased over the perfusion period whilst the concentration of lactate, glycine, glutamate and valine increased significantly.

Similar methodology was used in a clinical study in which the changing composition of the circulating perfusate of 26 cadaveric kidneys undergoing HMP was analysed prior to transplantation (173). The concentration of three metabolites at two different timepoints were associated with the onset of delayed graft function following transplantation. These metabolites, inosine, leucine and gluconate also increased significantly in concentration during the perfusion period in both human and porcine suggesting ongoing metabolism during the preservation period over time with the implication that metabolism influenced function post-transplantation.

The aim of this study was to identify differences in metabolism between static and dynamic hypothermic preservation modalities to show how HMP promotes benefit. Differences in metabolism were detected by changes in metabolite accumulation in storage fluid and changes in metabolite concentration in end-point renal cortex using ^{1}H-1D NMR in an established porcine cardiac death donor model using a paired study design.

Methodology

Perfusate was sampled from HMP kidneys whilst storage fluid was sampled for those kidneys in static storage. Of note, end-point tissue samples consisted solely of renal cortex. Full experimental methodology is described in the manuscript.

The use of porcine kidneys in organ preservation studies

Organ preservation research benefits from an appropriate animal model which permits multiple replicates of the same experiment with change of one variable in order to study that variable in isolation. A cell line model may be useful to determine experimental conditions on isolated cell lines, such as the highly metabolically active proximal tubule, but such models lack relevance to the whole organ in addition to facing problems generating conditions of shear stress. A whole organ model is necessary to demonstrate the effects of therapeutic interventions on the *ex vivo* kidney. Ideally, the use of human kidneys in such a model would be preferable in terms of applicability but such discarded human kidneys are a very heterogenous group.

Cadaveric kidneys differ due to many donor variables such as age, acute physiological insult due to donor cause of death and exposure to chronic disease such as atherosclerosis. Discard of cadaveric human kidneys occurs for multiple reasons including retrieval injury, unfavourable anatomy, cold ischaemic time. Aside from being a scare and unpredictable resource, it is evident that any cadaveric human kidneys available for preservation studies are a very heterogenous group, potentially resulting in experimental bias from the outset.

Similarities between porcine and human kidneys

Development of a robust, reliable and reproducible animal model is necessary to provide a homogenous set of organs, available at request, in which the effects of modifying isolated experimental variables can be explored. In the past, canine organs have been used (204) but porcine kidneys predominate in the current landscape of organ

preservation research for several reasons. The domestic pig is widely bred for human consumption thus animals and organs are readily available.

From an anatomical perspective, porcine and human kidneys are similar. Both share a multi-lobar structure, contrasting with the unilobar structure of rodent and canine kidneys (205). In addition, intra-renal vasculature is similar between pigs and humans although extra-renal arterial supply differs. In one research study exploring the anatomical patterns of porcine kidneys, all kidneys were supplied by a single artery (205) contrasting with the higher proportions of multiple arteries seen in human kidneys (17-35%) (206). This contrast may in essence be a limitation as the prevalence of single vessel anatomy does remove multiple vessels, known to influence clinical outcome in the human setting (104), as a confounding factor in experimental groups.

In addition to genetic similarities (207), pig kidneys display similar physiology to human kidneys (208). Metabolism of pig kidneys in-vivo has been demonstrated to be comparable to human kidneys (209, 210). Using 1D-^{1}H NMR spectroscopy, previous work within our group has validated the pig model for use in the HMP environment (174).

Practical considerations

In the context of organ preservation, large pig body sizes allows surgical procedures similar to humans (i.e donor nephrectomy, re-implantation). Such size-matched organs can therefore be used in place of human kidneys in perfusion circuits designed for the clinical setting.

In the pig model used in this thesis, kidneys were removed from male English Large White pigs weighing between 80 and 85kg. This contrasts with the choice of pig breed and size used in other groups. Studies involving auto-transplantation tend to use a smaller size pig

(between 23-40 kg) (211-215) perhaps reflecting the relative ease of caring for such animals post-operatively. Pig breeds native to locality in which research is performed are commonly used; notably the Landrace pig and English Large White pig, also known as the Yorkshire pig, tend to predominate. Kidneys from larger pigs weighing 80-100kg are also used (216), but not in the case of auto-transplantation models.

The relatively young age of pigs used in preservation studies reflects the nature in which domestic breeds are intensively fed, gaining muscle mass quickly prior to slaughter. The question remains over which demographic the pigs used in transplantation studies best represent although model design would suggest young, DCD donors with a high muscle bulk

The extent to which porcine kidneys are well matched to human kidneys is referenced by continuing work exploring the use of pig kidneys in xenotransplantation to solve organ shortages (217). Porcine kidneys have demonstrated to have similar lobar and vascular anatomy, similar physiology and similar metabolism in the HMP environment compared with human kidneys. Such organs are readily available from one breed of pig within a designated weight range, resulting in a homogenous group of organs which can be used for experimental studies.

Discussion

As described in the manuscript, key findings included a greater total amount of central metabolites in kidneys preserved using HMP compared with those stored in static storage indicating HMP conditions promoted metabolic activity through delivery of metabolic substrate. Strengths of the study included a paired model in which conditions prior to the

preservation period were similar for all kidneys, contrasting with studies involving human cadaveric kidneys which are subject to an increased number of donor organ variables.

The study model used a combination of metabolite concentration in circulating perfusion fluid and metabolite concentration within the renal cortex to show convincing evidence of ongoing metabolic activity during HMP with the suggestion that metabolism also occurs during static storage conditions. Metabolite calculations were based on a model with several assumptions including uniform distribution of metabolites throughout the kidney and complete extraction of metabolites from cells.

An important consideration for subsequent studies is the use of metabolite concentration in perfusion fluid as a surrogate marker of tissue metabolic activity. Ideal characteristics include a timely and marked change in metabolite concentration which mimics such changes within renal tissue. However, such changes in perfusate metabolite concentration also occur due to processes such as cell damage or cell death. One notable consideration should be the means by which metabolites enter and leave cells.

Following intra-cellular build up and accumulation, metabolites must either be actively transported across cell membranes, or leave by passive transport such as diffusion, osmosis and facilitated diffusion. All means of passive transport rely on permeability of the cell membrane which is affected by increases and decreases in temperature. Whilst permeability increases as temperature increases, in sub-zero temperatures ice crystals form which may pierce the cell membrane causing release of intra-cellular contents.

As described in Chapter 1, hypothermia and hypoxia result in a reliance on anaerobic metabolism which results in lactate accumulation secondary to glycolytic pathway activity. Key findings confirmed suspicions that static storage conditions lead to lactate

accumulation within renal cortex without release into storage fluid. In contrast, during HMP there was a sequential rise in concentration of lactate in perfusion fluid secondary to homeostatic cellular mechanisms which coincided with lower concentrations of lactate within the renal cortex potentially reducing ischaemia reperfusion injury secondary to intracellular acidosis. This contrasts with static storage conditions, in which lactate accumulates in tissues, potentially worsening ischaemia reperfusion injury.

Yet conclusions drawn are subject to the limitations of an untargeted metabolomics study. The origin of lactate maybe the result of preceding ischaemia during the retrieval process or secondary to the two hour period of static cold storage prior to designation to static or dynamic preservation modality. Alternatively it may be secondary to *de novo* metabolism during the preservation period itself, potentially increased during HMP due to delivery of glucose in perfusion fluid.

Similar to lactate production, increased amounts of central metabolites may indicate tricarboxylic acid cycle activity although this is less likely given the largely hypoxic environment of HMP. Other origins of such metabolites are likely. For example, glutamate is more likely to increase in concentration as it is a degradation product of glutathione-s-transferase (GST) detoxification reactions, a mark of ongoing oxidative stress during HMP (218).

In addition to assumptions made when calculating total systems metabolite concentrations for both storage conditions, the method of using metabolite concentration in storage fluid for static storage conditions falsely assumed metabolites were present in the same concentration within all fluid surrounding the kidney including that of the major vasculature. This fluid is highly unlikely to represent the interstitial compartment over the course of the preservation as metabolites accumulating in tissue are not washed out of the kidney.

However, robust conclusions can still be drawn from tissue metabolite concentration alone as detailed in the manuscript.

Concluding remarks

In conclusion, experimental results demonstrate stark differences in metabolite levels in the renal cortex of kidneys preserved with HMP compared with those stored using static storage alone inferring more metabolic activity as a result of HMP. Results showing an increase in the concentration of lactate and glutamate over the perfusion period with a decrease in glutathione concentration were consistent with previous studies using ^{1}H-1D NMR to assess the composition of circulating perfusate during HMP (172, 173). Perfusate analysis reveals an increase in the concentration of alanine and lactate indicating anaerobic metabolism is active during HMP. The depletion of glutathione and increase in glutamate concentration are a likely indication of oxidative stress which the kidney is exposed to during the hypothermic, largely hypoxic conditions of HMP.

Continual supply of metabolic substrates during HMP may contribute to its clinical benefits whilst ongoing perfusion permits washout of toxic metabolites which may otherwise accumulate in tissue causing worsening tissue injury.

Manuscript

Nath J, Smith TB, **Patel K**, Ebbs SR, Hollis A, Tennant DA, Ludwig C, Ready AR. Metabolic differences between cold stored and machine perfused porcine kidneys: A 1H NMR based study. Cryobiology. 2017;74:115-20

Cryobiology 74 (2017) 115–120

Contents lists available at ScienceDirect

Cryobiology

journal homepage: www.elsevier.com/locate/ycryo

Metabolic differences between cold stored and machine perfused porcine kidneys: A ^{1}H NMR based study

Jay Nath [a, b, *], Tom B. Smith [b], Kamlesh Patel [a, b], Sam R. Ebbs [b], Alex Hollis [b], Daniel A. Tennant [b], Christian Ludwig [b, 1], Andrew R. Ready [a, 1]

[a] Department of Renal Surgery, University Hospitals Birmingham, Birmingham, UK
[b] Institute of Metabolism and Systems Research (IMSR), College of Medical and Dental Sciences, University of Birmingham, Birmingham, UK

ARTICLE INFO

Article history:
Received 11 July 2016
Received in revised form
18 October 2016
Accepted 21 November 2016
Available online 3 December 2016

Keywords:
Hypothermic machine perfusion
Kidney
Transplantation
Metabolism
NMR
Organ preservation

ABSTRACT

Hypothermic machine perfusion (HMP) and static cold storage (SCS) are the two methods used to preserve deceased donor kidneys prior to transplant. This study seeks to characterise the metabolic profile of HMP and SCS porcine kidneys in a cardiac death donor model.

Twenty kidneys were cold flushed and stored for two hours following retrieval. Paired kidneys then underwent 24 h of HMP or SCS or served as time zero controls. Metabolite quantification in both storage fluid and kidney tissue was performed using one dimensional ^{1}H NMR spectroscopy. For each metabolite, the net gain for each storage modality was determined by comparing the total amount in each closed system (i.e. total amount in storage fluid and kidney combined) compared with controls.

26 metabolites were included for analysis. Total system metabolite quantities following HMP or SCS were greater for 14 compared with controls (all $p < 0.05$). In addition to metabolic differences with control kidneys, the net metabolic gain during HMP was greater than SCS for 8 metabolites (all $p < 0.05$). These included metabolites related to central metabolism (lactate, glutamate, aspartate, fumarate and acetate).

The metabolic environments of both perfusion fluid and the kidney tissue are strikingly different between SCS and HMP systems in this animal model. The total amount of central metabolites such as lactate and glutamate observed in the HMP kidney system suggests a greater degree of *de novo* metabolic activity than in the SCS system. Maintenance of central metabolic pathways may contribute to the clinical benefits of HMP.

1. Introduction

Hypothermic Machine Perfusion (HMP) and Static Cold Storage (SCS) are the two methods of kidney preservation that are used widely in clinical practice during the time period between organ retrieval and implantation [16]. A key concept for both preservation modalities is that cellular metabolism, and therefore cellular metabolic requirements, are minimised in these hypothermic conditions and the rate of metabolism reported to be about 5–8% at temperatures below 4 °C [29] with a similar decrease in oxygen requirement [1].

The superiority of HMP over SCS is well documented [4,17,22,23,27] but the mechanisms by which this occurs are not clear. Improvement in flow dynamics, with fall in the intra-renal resistance is likely to be one factor but the additional metabolic support derived from the circulation of nutrient-containing perfusion fluid may also help preserve organ function and have a beneficial effect [7,30].

Metabolomic analyses of preservation fluid during HMP using 1D-^{1}H NMR (One-dimensional proton nuclear magnetic resonance) spectroscopy, by groups including our own, have demonstrated this to be reproducible and highly specific for metabolite identification and quantification [2,10,24]. However, surprisingly, to our knowledge there are no studies that have sought to compare the metabolomic profiles, or metabolome, of HMP and SCS kidneys.

Porcine kidneys are widely used in transplantation studies owing to their similar physiological and anatomical properties to human organs [9,11]. In addition, the metabolic profiles during

* Corresponding author.Department of Renal Surgery, University Hospitals Birmingham, Birmingham, UK.
[1] Authors contributed equally to this manuscript.

http://dx.doi.org/10.1016/j.cryobiol.2016.11.006
0011-2240/

periods of HMP for porcine and human kidneys are comparable [24], with a correlation between metabolite profiles during storage and post transplant outcome [2]. For HMP preserved human kidneys, the metabolic profile from perfusates of immediate graft function kidneys differs from those with delayed function [10] and reinforces the concept that significant metabolism occurs during HMP and that metabolism reflects functional outcome.

The aims of this study were twofold. Firstly, to determine the distribution of metabolites between the two different compartments (fluid and tissue) during the organ preservation period. Secondly, to determine the total amount of each metabolite within HMP and SCS kidneys systems after 24 h of organ storage and through comparison with control kidneys, the metabolic changes that occur.

2. Methods

2.1. Animal research

Abattoir/slaughterhouse pig kidneys (F.A. Gill, Wolverhampton, UK) were used and no animals were sacrificed solely for the purposes of this study, negating any need for ethical board approval. Experiments were performed on 22–26 week old male 'bacon weight' pigs, weighing 80–85 kg. All experiments were performed following the principles of laboratory animal care according to NIH standards. Animals were sacrificed by electrical stunning and exsanguination. Initial organ preservation was performed following organ retrieval and occurred within 14 min of death, replicating deceased cardiac death (DCD) donor conditions. Kidneys were cold flushed (4 °C) with 1 L SPS-1 (UW) solution at a pressure of 100 mm Hg. Organs were then stored at 4 °C in SPS-1 for 2 h to replicate the clinical period of organ transportation.

2.2. Experimental groups

Paired kidneys were randomly allocated to receive either HMP or SCS for 24 h. HMP kidneys were perfused with 1 L of KPS-1 using the LifePort Kidney Transporter 1.0 (Organ Recovery Systems, Chicago, IL). (Perfusion pressure 30 mm Hg). SCS Kidneys were submerged in 1 L of fresh chilled SPS-1 solution with a surrounding ice bath. Preservation fluid was sampled for each kidney at baseline and 2, 4, 8, 12, 18, and 24 h. After 24 h, organs were rapidly dissected and tissue samples (1 cm^3 sections) flash frozen and stored (−80 °C). All experiments were performed in a cold room (4 °C) to ensure consistency.

2.3. Control kidneys

To ascertain metabolism during SCS or HMP storage conditions, baseline values prior to storage conditions were needed (time 0). Large volume tissue sampling precludes effective organ perfusion and therefore 'Control kidneys' were used to establish baseline metabolite levels. These were (n = 6) flushed and cold transported in identical fashion to experimental kidneys and tissue samples obtained as described above (i.e. not subjected to 24 hr of SCS or HMP).

2.4. Sample processing and metabolite quantification

NMR samples were prepared from storage fluid by mixing 150 μL of 400 mM (pH 7.0) phosphate buffer containing 2 mM DSS (4,4-dimethyl-4-silapentane-1-sulfonic acid) and 8 mM imidazole with 390 μL of each fluid sample and 60 μL of deuterium oxide (D_2O) to reach a final phosphate buffer concentration of 100 mM and a final DSS concentration of 500 μM. After mixing, the 600 μL samples were pipetted into 5 mm NMR tubes, sonicated and centrifuged. Technical replicates of samples (×3) were prepared for each timepoint.

For cell extract studies, 500 mg of renal cortex was manually cryo-homogenised in liquid nitrogen. 5.1 ml of both methanol (−80 °C) and chloroform was added to the powdered tissue and samples diluted with 4.65 ml of dH_20 at 4 °C. Samples were centrifuged to separate into polar and non-polar layers and 1.5 ml of the upper polar layer was dispensed into a cryovial and dried. Three technical replicates were performed for each tissue sample. Dried polar residue was then dissolved in 390 μL of dH_20 and 210 μL of buffer solution as described above.

The protocol used for ^1H NMR analysis has been described previously [10,24]. Briefly, this entailed processing on a Bruker AVII 500 MHz spectrometer, acquisition of one dimensional spectra and then metabolite identification and quantification using Matlab based 'Metabolab' software [18] and Chenomx 8.1 (ChenomxInc) software respectively. Metabolites were deemed to be present if they exhibited non-ambiguous spectral patterns or their presence deemed biologically plausible and confirmed on ultra performance liquid chromatography mass spectrometry. Any metabolites that were present in different concentrations in the SCS and HMP fluid (e.g. glucose, gluconate, mannitol, adenine, adenosine etc.) were excluded from comparative analysis. Metabolite quantifications were corrected to allow for sample dilution with sample buffer. When determining concentrations of metabolites using Chenomx, the researchers were blind to the storage group. Quantification of the total amount of metabolite in the storage fluid, tissue and total system was calculated based upon the weight of the kidney at time of sample acquisition and final volume of storage fluid.

2.5. Statistical analysis

For each timepoint, three results were obtained (technical replicates) and the median value used. For comparison of SCS and HMP conditions, analysis was performed using Wilcoxon paired signed rank test (two tailed) as one kidney from each pair was subjected to each condition and normality was not consistent on prior analysis. When comparing SCS or HMP with control kidneys, Mann-Whitney u test (two tailed) was used, as these were non-paired samples. Data were reported as median concentrations and interquartile (IQ) range. All analysis was performed using GraphPad Prism version 6.00 for Mac OS X, GraphPad Software, La Jolla California USA, with $p < 0.05$ deemed to be indicative of statistical significance.

3. Results

Metabolic optimisation of cadaveric kidneys is a potential target to improve the function of kidneys for transplantation. This study seeks to establish the degree of metabolism, if any, that occurs in the two widely used methods of kidney organ storage prior to transplantation (HMP and SCS).

The total quantity of each metabolite after 24 h of either HMP or SCS was calculated using ^1H NMR methods and compared with control organs to determine the net metabolic change during each storage method.

We found evidence of metabolite production for both storage modalities with 14 metabolites present in significantly greater quantities in the HMP or SCS system compared with controls (all $p < 0.05$) (Table 1) (Fig. 1, Fig 1(Suppl)). There were significantly more metabolites with a net increase in the HMP system (13/14) compared with the SCS system (7/14) ($p = 0.033$).

Eight of the metabolites were significantly elevated in the HMP system compared with both the control and SCS systems (all $p < 0.05$), indicating a greater degree of metabolite production.

Table 1
Total amount of metabolite present in each of the storage modalities at time zero (controls) or after 24 h of preservation (SCS or HMP). Data reported as Median (Interquartile Range), unless stated otherwise. Statistical test: [Ψ] Mann-Whitney u test (two tailed) [#]Wilcoxon paired signed rank test (two tailed). *Significant at $p < 0.05$.

	Storage Modality			p-Values		
	Control System (mmol)	SCS System (mmol)	HMP System (mmol)	Control vs SCS [Ψ]	Control vs HMP [Ψ]	SCS vs HMP [#]
Glutamate	1.54 (1.12–1.84)	1.38 (1.11–1.66)	3.97 (3.69–4.71)	0.731	0.002*	0.031*
Myoinositol	1.18 (1.16–1.19)	1.29 (1.01–1.52)	2.16 (1.85–2.41)	0.731	0.002*	0.031*
Lactate	1.11 (0.976–1.23)	1.38 (1–1.75)	2.13 (1.67–2.71)	0.138	0.002*	0.031*
Hypoxanthine	0.454 (0.356–0.515)	0.710 (0.641–0.762)	1.05 (0.909–1.17)	0.001*	0.002*	0.156
Formate	0.442 (0.274–0.638)	0.643 (0.589–0.779)	0.842 (0.750–0.943)	0.101	0.004*	0.031*
Acetate	0.210 (0.206–0.212)	0.296 (0.253–0.301)	0.552 (0.494–0.654)	0.234	0.041*	0.031*
Alanine	0.302 (0.243–0.360)	0.486 (0.339–0.499)	0.501 (0.368–0.558)	0.035*	0.015*	0.313
Succinate	0.283 (0.267–0.297)	0.462 (0.312–0.52)	0.434 (0.307–0.541)	0.001*	0.015*	0.844
Inosine	0.588 (0.561–0.628)	1.08 (0.885–1.12)	0.185 (0.146–0.233)	0.001*	0.002*	0.031*
Aspartate	0.114 (0.104–0.118)	0.107 (0.0879–0.11)	0.165 (0.140–0.215)	0.234	0.041*	0.031*
Leucine	0.0476 (0.0441–0.0517)	0.0667 (0.0513–0.0820)	0.0693 (0.0495–0.0773)	0.014*	0.026*	0.688
Niacinamide	0.0196 (0.0181–0.0207)	0.0289 (0.0243–0.0319)	0.0490 (0.0420–0.0557)	0.001*	0.002*	0.031*
Tyrosine	0.0262 (0.0217–0.0302)	0.0434 (0.0339–0.0462)	0.0387 (0.0332–0.0431)	0.001*	0.013*	0.438
Fumarate	0.00412 (0.00339–0.00418)	0.00308 (0.00145–0.00348)	0.0133 (0.0077–0.0212)	0.064	0.002*	0.031*

These included lactate, glutamate, aspartate, fumarate, acetate, myo-inisitol, niacinamide and formate (Fig. 1).

Despite the additional 24 h of organ preservation, albeit in static conditions, the amount of lactate in the SCS system was comparable to controls (1.37 vs 1.11 mmol $p = 0.138$). However the amount in the HMP system (2.13 mmol) was almost twice the amount of either controls or SCS systems ($p = 0.002$ and $p = 0.031$). However, despite greater amounts overall, the amount present in the HMP tissue (0.76 mmol) was actually lower than SCS tissue (1.14 mmol) or control tissue (1.11 mmol) ($p = 0.031$ and $p = 0.002$ respectively), reflective of lower intracellular concentrations for HMP kidneys.

The distribution of metabolites between the extracellular storage fluid and tissue samples for both storage conditions are detailed in Table 2. As expected, there were greater quantities of metabolites in the circulating HMP fluid compared with the static conditions of SCS at most time-points. After 24 h, the total amount of metabolite in the perfusate for the HMP kidneys was significantly greater than the SCS group for (21/26 = 80.8%) of metabolites. Whilst concentrations rose most rapidly in the first 2 h of perfusion and therefore may be in part due a metabolite washout phenomenon, there was an increase in most metabolites over sequential timepoints as would be expected with on-going production (Fig. 2a–c).

Reduced glutathione is a constituent of both KPS-1 (used in HMP) and SPS-1 (used in SCS) fluids at equal concentrations. Whilst this remained at stable in the SCS environment, the glutathione was clearly consumed by the HMP group and after 8 h concentrations were 17.6 fold higher in the SCS fluid (1.60 mM vs. 0.091 mM, $p = 0.001$) (Fig. 2d). Despite apparent organ uptake of reduced glutathione, there was no evidence of this in the tissue samples from either group.

4. Discussion

The aim of this study was to determine any metabolic differences between the two clinically used methods of organ storage in this animal model.

Whilst the calculation of the total amount of metabolite within the system does rely on several assumptions (complete metabolite extraction from tissue and metabolite homogeneity within tissue), we felt this was imperative to draw meaningful comparison between groups and enables the calculation of net metabolite production/consumption in these two closed systems (HMP and SCS).

Although the storage fluid used in each experimental group differs (most notably absence of glucose in the SCS fluid) and therefore caution should be exercised in attributing any differences merely to the parameters of storage (i.e. HMP or SCS), this study was designed to assess metabolism during the two clinically used organ preservation techniques, not merely the storage modality in isolation.

This study clearly demonstrates the presence of major central metabolites such as lactate, glutamate, fumarate, aspartate and acetate at greater levels in the HMP system compared with both controls and SCS (Fig. 1). This strongly suggests that these metabolites are being produced during HMP. Furthermore, the accumulation of these metabolites into the circulating perfusion fluid demonstrates effective homeostatic mechanisms are active to prevent over accumulation within the local cellular environment.

The list of metabolites reported in this study is not exhaustive and is a limitation of this study. Some interesting substrates (eg glucose) were excluded as this is only present in one of the storage fluids (KPS-1). For others the 1D ^{1}H NMR spectral pattern is either ambiguous or can be hidden under more domineering peaks from other compounds.

The increased total lactate in the HMP system is likely to reflect increased glycolysis in the HMP model. Although new glycolytic activity of the glucose within the HMP fluid is one likely contributor, this is unlikely to the singular cause. This is supported by evidence that the HMP fluid glucose concentrations did not decrease during the study period and replicates findings from previous human studies [10]. However conversion of a proportion of perfusion fluid glucose into lactate through glycolytic pathways has been corroborated by work demonstrating activity of these pathways using ^{13}C labelled glucose tracers [25].

The net gain of glutamate, fumarate, aspartate and acetate during HMP is also intriguing. Whilst identification of responsible metabolic pathways is difficult to ascribe solely with ^{1}H NMR studies, one explanation could be increased oxygen dependent tricarboxylic acid (TCA) cycle activity. Although uniform upregulation of TCA intermediates would support this theory, as discussed, many are not easily identifiable using ^{1}H NMR methods [6] and are rarely found in equipoise even *in vivo* [14]. Several (^{13}C) NMR studies have reported glutamate as a valid marker of TCA activity [3,5,20].

For some metabolites, the total system amounts for HMP and SCS kidneys were comparable to the controls, suggesting that either *de novo* production does not occur during the 24 h preservation or that consumption mirrors production (Table 1 *supplementary*). However, for metabolites with similar total amounts, the compartment in which they were located varied per metabolite. Some metabolites were entirely contained within the HMP kidney

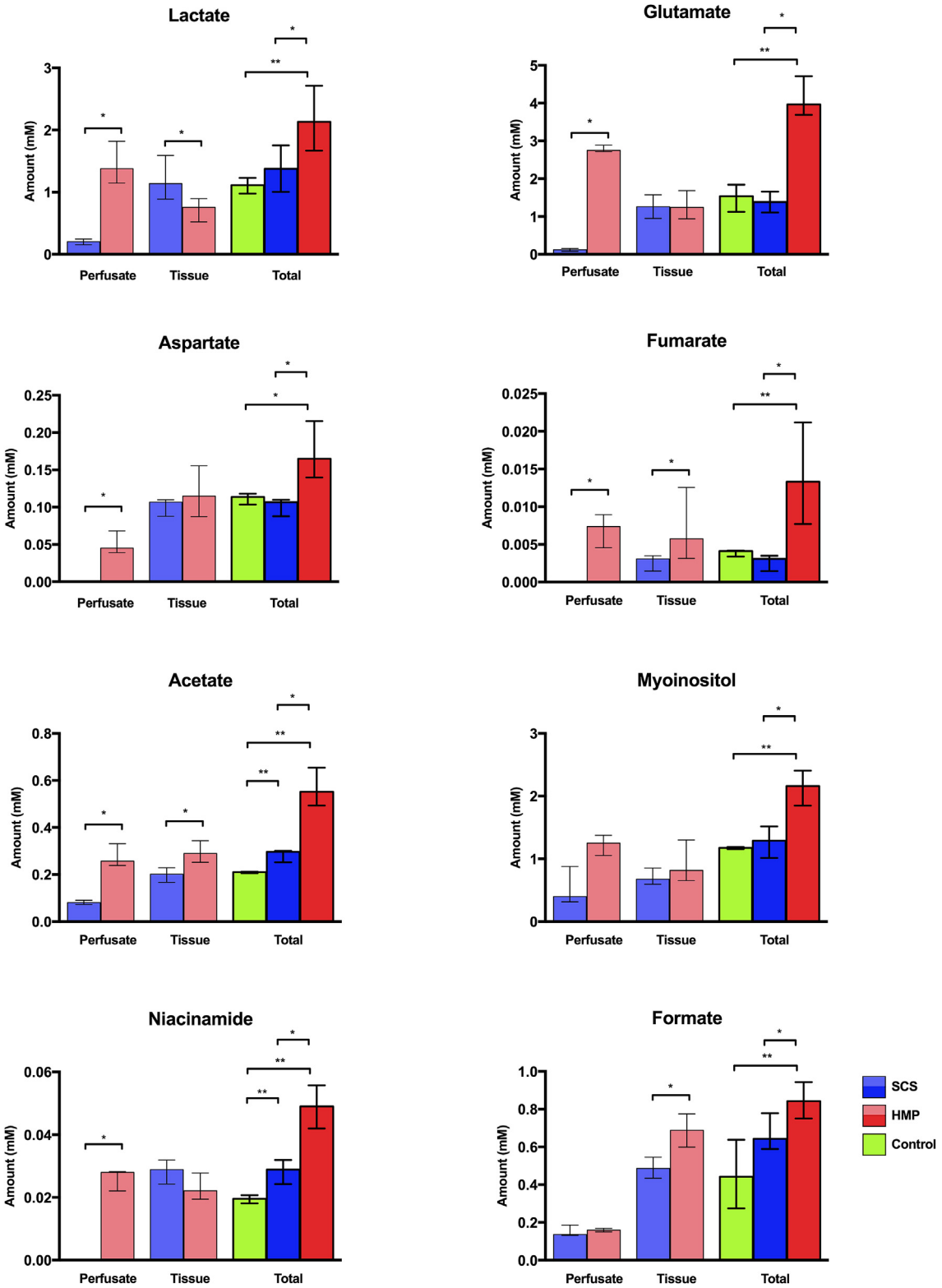

Fig. 1. Metabolites significantly elevated in the HMP system compared with both SCS and control kidneys. Metabolite levels represent total amounts (mmol) in the storage fluid, kidney tissue and entire system for porcine kidneys after 24 hr of HMP or SCS or time zero controls. Highly significant (**$p < 0.01$) and significant (*$p < 0.05$) differences between HMP system versus both controls and SCS kidneys.

tissue (e.g. ADP, AMP, NAD+) and presumably in the intracellular compartment. Other metabolites were evident in both the tissue and storage fluid but at higher concentrations in the HMP fluid. These discrepancies in metabolite location further highlight that cellular transport processes are active in this environment but that movement of metabolites into the extracellular fluid is not

Table 2
Metabolites present in tissue and storage fluid in HMP or SCS kidney systems at 24 h. Data reported as Median (Interquartile Range), unless stated otherwise. Statistical test: #Wilcoxon paired signed rank test (two tailed). *Significant at $p < 0.05$.

	Storage	Total storage fluid amount (mmol)	p-value#	Total kidney tissue amount (mmol)	p-Value#
Glutamate	SCS	0.0812 (0.125–0.155)	0.0312*	0.952 (1.26–1.58)	0.6875
	HMP	2.72 (2.75–2.89)		0.94 (1.24–1.68)	
Myoinositol	SCS	0.316 (0.399–0.879)	0.0625	0.596 (0.676–0.853)	0.5625
	HMP	1.05 (1.25–1.38)		0.653 (0.816–1.3)	
Lactate	SCS	0.153 (0.205–0.245)	0.0312*	0.89 (1.14–1.59)	0.0312*
	HMP	1.15 (1.38–1.82)		0.521 (0.755–0.895)	
Hypoxanthine	SCS	0.294 (0.328–0.404)	0.0312*	0.289 (0.407–0.424)	0.0625
	HMP	0.705 (0.781–0.867)		0.189 (0.258–0.31)	
Formate	SCS	0.132 (0.136–0.186)	0.4375	0.434 (0.486–0.545)	0.0312*
	HMP	0.151 (0.16–0.169)		0.688 (0.599–0.774)	
Acetate	SCS	0.073 (0.0808–0.0912)	0.0312*	0.167 (0.201–0.229)	0.0312*
	HMP	0.239 (0.257–0.331)		0.252 (0.289–0.344)	
Alanine	SCS	0.0465 (0.0643–0.0815)	0.0312*	0.303 (0.415–0.435)	0.0312*
	HMP	0.253 (0.306–0.358)		0.116 (0.187–0.207)	
Succinate	SCS	0.0104 (0.0155–0.0184)	0.0312*	0.298 (0.446–0.498)	0.0312*
	HMP	0.104 (0.131–0.208)		0.203 (0.294–0.347)	
Inosine	SCS	0.703 (0.852–0.961)	0.0312*	0.145 (0.182–0.201)	0.0312*
	HMP	0.0877 (0.108–0.128)		0.058 (0.0723–0.109)	
Aspartate	SCS	–	0.0312*	0.0879 (0.107–0.11)	0.3125
	HMP	0.039 (0.0452–0.0682)		0.0874 (0.115–0.155)	
Leucine	SCS	0.00442 (0.00506–0.00761)	0.0312*	0.0486 (0.0591–0.0775)	0.0312*
	HMP	0.0285 (0.038–0.0468)		0.0222 (0.0304–0.0318)	
Niacinamide	SCS	–	0.0312*	0.0243 (0.0289–0.0319)	0.0938
	HMP	0.0221 (0.028–0.0282)		0.0194 (0.0221–0.0278)	
Tyrosine	SCS	0.00336 (0.0071–0.00843)	0.0312*	0.0306 (0.0371–0.0391)	0.0312*
	HMP	0.0197 (0.0228–0.0276)		0.0112 (0.0143–0.0171)	
Fumarate	SCS	–	0.0312*	0.00145 (0.00308–0.00348)	0.0312*
	HMP	0.00456 (0.00737–0.00895)		0.00314 (0.00574–0.0126)	

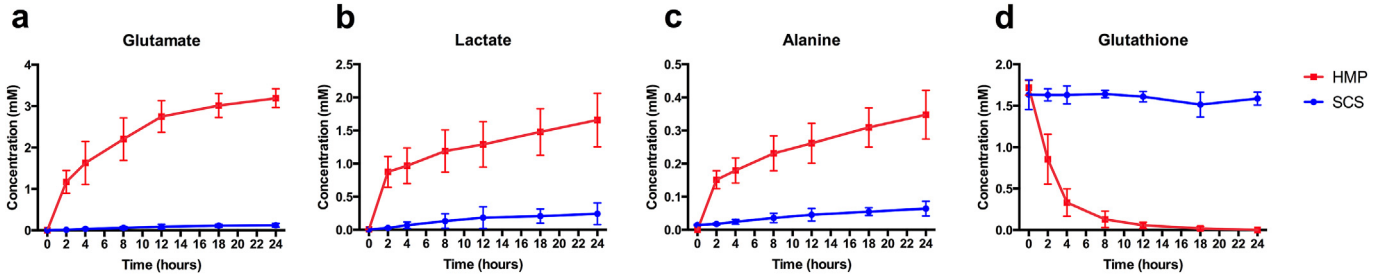

Fig. 2. Concentration of metabolites in the storage fluid of SCS and HMP kidneys over 24 h time period for four example metabolites. Values plotted as median (interquartile range).

indiscriminate.

Reduced glutathione is a constituent of the preservation fluid KPS-1 and is thought to play a role in the removal of Reactive Oxygen Species (ROS) generated during metabolism [19] In contrast to the SCS kidney, there is a rapid decrease in the concentration of glutathione in the preservation fluid of HMP stored kidneys and is about 5% of the SCS values after 8 h (Fig. 2d.). The rate of glutathione depletion observed in this study is similar to a previously reported animal model [28] and is likely to reflect cellular uptake of this protective antioxidant. Interestingly, glutathione concentration remained relatively constant in the SCS kidney group. This further reinforces the concept that HMP exerts its beneficial effects, at least in part, by providing access to the cellular components of the kidney during perfusion. Absence of reduced glutathione in tissue demonstrates that not only is this protective antioxidant readily absorbed by the kidney during perfusion but that even after a few hours it is not longer available in the reduced state.

Although the number of organs in each experimental group is small ($n = 7$), it is comparable to other porcine kidney transplant reports [8,12,15,21,26,30]. To improve validity, samples were processed in triplicate at each timepoint and over 250 NMR spectra were analysed. One strength of this study is that the kidneys stored by HMP or SCS were paired, i.e. from the same pig, thus minimising any metabolic differences arising from polymorphism in cellular mediators of porcine metabolism. Although this approach does not provide functional outcome information for the preserved organ, previous studies have demonstrated good function for otherwise healthy porcine organs stored by either SCS or HMP for similar time periods [2,8,13,15,21,26].

This study demonstrates that in a porcine model, the distribution and amounts of metabolites vary significantly with the storage method (HMP or SCS). The net gain of many central metabolites during HMP conditions further supports the notion that significant metabolism occurs during HMP and this may contribute to the beneficial role of machine perfusion.

Funding

This work was funded through grants from University Hospitals Birmingham Charities and Organ Recovery Systems.

Conflict of interest

As detailed in the funding section, the research was in-part

funded by a grant from Organ Recovery Systems, manufacturers of the LifePort Kidney Transporter used to create conditions of HMP in the laboratory. We do not have any further conflicts of interest to declare.

Acknowledgements

This work was funded through grants from University Hospitals Birmingham Charities (16-5-751) and Organ Recovery Systems.

Appendix A. Supplementary data

Supplementary data related to this article can be found at http://dx.doi.org/10.1016/j.cryobiol.2016.11.006.

References

[1] F.O. Belzer, J.H. Southard, Organ preservation and transplantation, Prog. Clin. Biol. Res. 224 (1986) 291–303.
[2] D. Bon, C. Billault, R. Thuillier, W. Hebrard, N. Boildieu, O. Celhay, J. Irani, F. Seguin, T. Hauet, Analysis of perfusates during hypothermic machine perfusion by NMR spectroscopy: a potential tool for predicting kidney graft outcome, Transplantation 97 (2014) 810–816.
[3] S.C. Burgess, E.E. Babcock, F.M. Jeffrey, A.D. Sherry, C.R. Malloy, NMR indirect detection of glutamate to measure citric acid cycle flux in the isolated perfused mouse heart, FEBS Lett. 505 (2001) 163–167.
[4] R.M. Cannon, G.N. Brock, R.N. Garrison, J.W. Smith, M.R. Marvin, G.A. Franklin, To pump or not to pump: a comparison of machine perfusion vs cold storage for deceased donor kidney transplantation, J. Am. Coll. Surg. 216 (2013) 625–633 discussion 633–4.
[5] E.M. Chance, S.H. Seeholzer, K. Kobayashi, J.R. Williamson, Mathematical analysis of isotope labeling in the citric acid cycle with applications to 13C NMR studies in perfused rat hearts, J. Biol. Chem. 258 (1983) 13785–13794.
[6] J.C. Chatham, S.J. Blackband, Nuclear magnetic resonance spectroscopy and imaging in animal research, ILAR J. 42 (2001) 189–208.
[7] B.J. Fuller, C.Y. Lee, Hypothermic perfusion preservation: the future of organ preservation revisited? Cryobiology 54 (2007) 129–145.
[8] A. Gallinat, A. Paul, P. Efferz, B. Luer, G. Kaiser, J. Wohlschlaeger, J. Treckmann, T. Minor, Hypothermic reconditioning of porcine kidney grafts by short-term preimplantation machine perfusion, Transplantation 93 (2012) 787–793.
[9] S. Giraud, F. Favreau, N. Chatauret, R. Thuillier, S. Maiga, T. Hauet, Contribution of large pig for renal ischemia-reperfusion and transplantation studies: the preclinical model, J. Biomed. Biotechnol. 2011 (2011) 532127.
[10] A.J. Guy, J. Nath, M. Cobbold, C. Ludwig, D.A. Tennant, N.G. Inston, A.R. Ready, Metabolomic analysis of perfusate during hypothermic machine perfusion of human cadaveric kidneys, Transplantation 99 (2015) 754–759.
[11] J.P. Hannon, C.A. Bossone, C.E. Wade, Normal physiological values for conscious pigs used in biomedical-research, Laboratory Animal Sci. 40 (1990) 293–298.
[12] S.A. Hosgood, M. Patel, M.L. Nicholson, The conditioning effect of ex vivo normothermic perfusion in an experimental kidney model, J. Surg. Res. 182 (2013) 153–160.
[13] I. Jochmans, E. Lerut, V. Heedfeld, T. Wylin, J. Pirenne, D. Monbaliu, Reproducible model for kidney autotransplantation in pigs, Transpl. Proc. 41 (2009) 3417–3421.
[14] H.A. Krebs, Rate control of the tricarboxylic acid cycle, Adv. Enzyme Regul. 8 (1970) 335–353.
[15] G. La Manna, D. Conte, M.L. Cappuccilli, B. Nardo, F. D'Addio, L. Puviani, G. Comai, F. Bianchi, R. Bertelli, N. Lanci, G. Donati, M.P. Scolari, A. Faenza, S. Stefoni, An in vivo autotransplant model of renal preservation: cold storage versus machine perfusion in the prevention of ischemia/reperfusion injury, Artif. Organs 33 (2009) 565–570.
[16] C.Y. Lee, M.J. Mangino, Preservation methods for kidney and liver, Organogenesis 5 (2009) 105–112.
[17] S.A. Lodhi, K.E. Lamb, I. Uddin, H.U. Meier-Kriesche, Pulsatile pump decreases risk of delayed graft function in kidneys donated after cardiac death, Am. J. Transpl. 12 (2012) 2774–2780.
[18] C. Ludwig, U.L. Gunther, MetaboLab–advanced NMR data processing and analysis for metabolomics, BMC Bioinforma. 12 (2011) 366.
[19] R.J. Mailloux, S.L. McBride, M.E. Harper, Unearthing the secrets of mitochondrial ROS and glutathione in bioenergetics, Trends Biochem. Sci. 38 (2013) 592–602.
[20] C.R. Malloy, A.D. Sherry, F.M. Jeffrey, Analysis of tricarboxylic acid cycle of the heart using 13C isotope isomers, Am. J. Physiol. 259 (1990) H987–H995.
[21] T. Minor, A. Paul, P. Efferz, J. Wohlschlaeger, U. Rauen, A. Gallinat, Kidney transplantation after oxygenated machine perfusion preservation with Custodiol-N solution, Transpl. Int. 28 (2015) 1102–1108.
[22] C. Moers, J.M. Smits, M.H. Maathuis, J. Treckmann, F. van Gelder, B.P. Napieralski, M. van Kasterop-Kutz, J.J. van der Heide, J.P. Squifflet, E. van Heurn, G.R. Kirste, A. Rahmel, H.G. Leuvenink, A. Paul, J. Pirenne, R.J. Ploeg, Machine perfusion or cold storage in deceased-donor kidney transplantation, N. Engl. J. Med. 360 (2009) 7–19.
[23] C. Moers, J. Pirenne, A. Paul, R.J. Ploeg, G. Machine Preservation, Trial Study, Machine perfusion or cold storage in deceased-donor kidney transplantation, N. Engl. J. Med. 366 (2012) 770–771.
[24] J. Nath, A. Guy, T.B. Smith, M. Cobbold, N.G. Inston, J. Hodson, D.A. Tennant, C. Ludwig, A.R. Ready, Metabolomic perfusate analysis during kidney machine perfusion: the pig provides an appropriate model for human studies, PLoS One 9 (2014) e114818.
[25] J. Nath, T. Smith, A. Hollis, S. Ebbs, S.W. Canbilen, D.A. Tennant, A.R. Ready, C. Ludwig, (13)C glucose labelling studies using 2D NMR are a useful tool for determining ex vivo whole organ metabolism during hypothermic machine perfusion of kidneys, Transpl. Res. 5 (2016) 7.
[26] M.L. Nicholson, S.A. Hosgood, M.S. Metcalfe, J.R. Waller, N.R. Brook, A comparison of renal preservation by cold storage and machine perfusion using a porcine autotransplant model, Transplantation 78 (2004) 333–337.
[27] J.M. O'Callaghan, R.D. Morgan, S.R. Knight, P.J. Morris, Systematic review and meta-analysis of hypothermic machine perfusion versus static cold storage of kidney allografts on transplant outcomes, Br. J. Surg. 100 (2013) 991–1001.
[28] K. Ormstad, T. Lastbom, S. Orrenius, Evidence for different localization of glutathione oxidase and gamma-glutamyltransferase activities during extracellular glutathione metabolism in isolated perfused rat kidney, Biochim. Biophys. Acta 700 (1982) 148–153.
[29] J.H. Southard, F.O. Belzer, Organ preservation, Annu. Rev. Med. 46 (1995) 235–247.
[30] M.J. Taylor, S.C. Baicu, Current state of hypothermic machine perfusion preservation of organs: the clinical perspective, Cryobiology 60 (2010) S20–S35.

Supplementary data

Supplementary Table 1

	Storage	Total storage fluid amount (mmol)	p-value#	Total kidney tissue amount (mmol)	p-value#
2-aminoadipate	SCS	-	0.031*	0.094 (0.063-0.112)	0.031*
	HMP	0.048 (0.037-0.062)		0.055 (0.050-0.059)	
Choline	SCS	0.039 (0.035-0.045)	0.031*	0.404 (0.329-0.423)	0.063
	HMP	0.102 (0.099-0.115)		0.267 (0.205-0.299)	
Creatinine	SCS	0.032 (0.008-0.067)	0.031*	0.564 (0.127-0.699)	0.156
	HMP	0.196 (0.038-0.386)		0.228 (0.130-0.328)	
Hippurate	SCS	0.002 (0.001-0.002)	0.031*	0.005 (0.003-0.007)	0.094
	HMP	0.006 (0.005-0.010)		0.001 (0.000-0.005)	
Isoleucine	SCS	0.004 (0.003-0.005)	0.031*	0.036 (0.032-0.041)	0.031*
	HMP	0.026 (0.023-0.027)		0.019 (0.014-0.020)	
TMNO	SCS	0.037 (0.031-0.047)	0.031*	0.152 (0.096-0.272)	0.219
	HMP	0.254 (0.165-0.266)		0.143 (0.099-0.218)	
Valine	SCS	0.006 (0.006-0.010)	0.031*	0.068 (0.057-0.083)	0.031*
	HMP	0.041 (0.038-0.053)		0.035 (0.025-0.036)	
β-Alanine	SCS	0.013 (0.010-0.021)	0.031*	0.101 (0.078-0.112)	0.031*
	HMP	0.085 (0.078-0.099)		0.038 (0.031-0.048)	
Taurine	SCS	0.196 (0.136-0.227)	0.031*	0.981 (0.929-1.056)	0.063
	HMP	0.693 (0.640-0.821)		0.505 (0.437-0.554)	
ADP	SCS	0.014 (0.013-0.015)	0.031*	0.013 (0.011-0.026)	0.438
	HMP	-		0.024 (0.019-0.031)	
AMP	SCS	0.003 (0.002-0.003)	0.031*	0.128 (0.105-0.169)	0.563
	HMP	-		0.140 (0.131-0.166)	
NAD+	SCS	-	-	0.025 (0.022-0.031)	0.094
	HMP	-		0.037 (0.033-0.049)	

S1 Table. Distribution of metabolite quantity between extracellular storage fluid and entire kidney tissue for 12 metabolites detected in comparable total amounts to controls.

Data reported as median (interquartile range), unless stated otherwise. Statistical test: #Wilcoxon paired signed rank test (two-tailed). *Significant at p<0.05.

Supplementary Figure 1

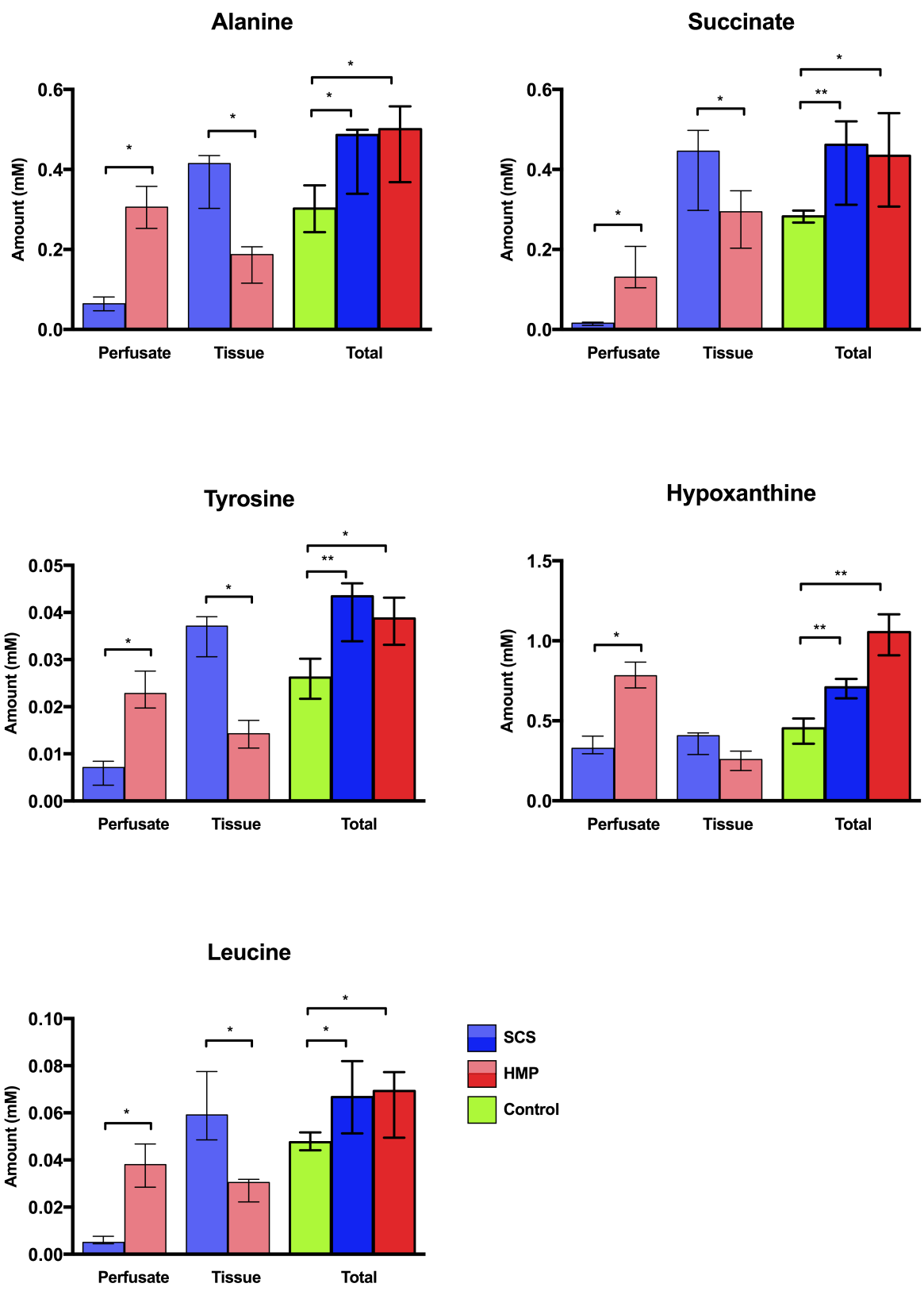

Supplementary Figure 2

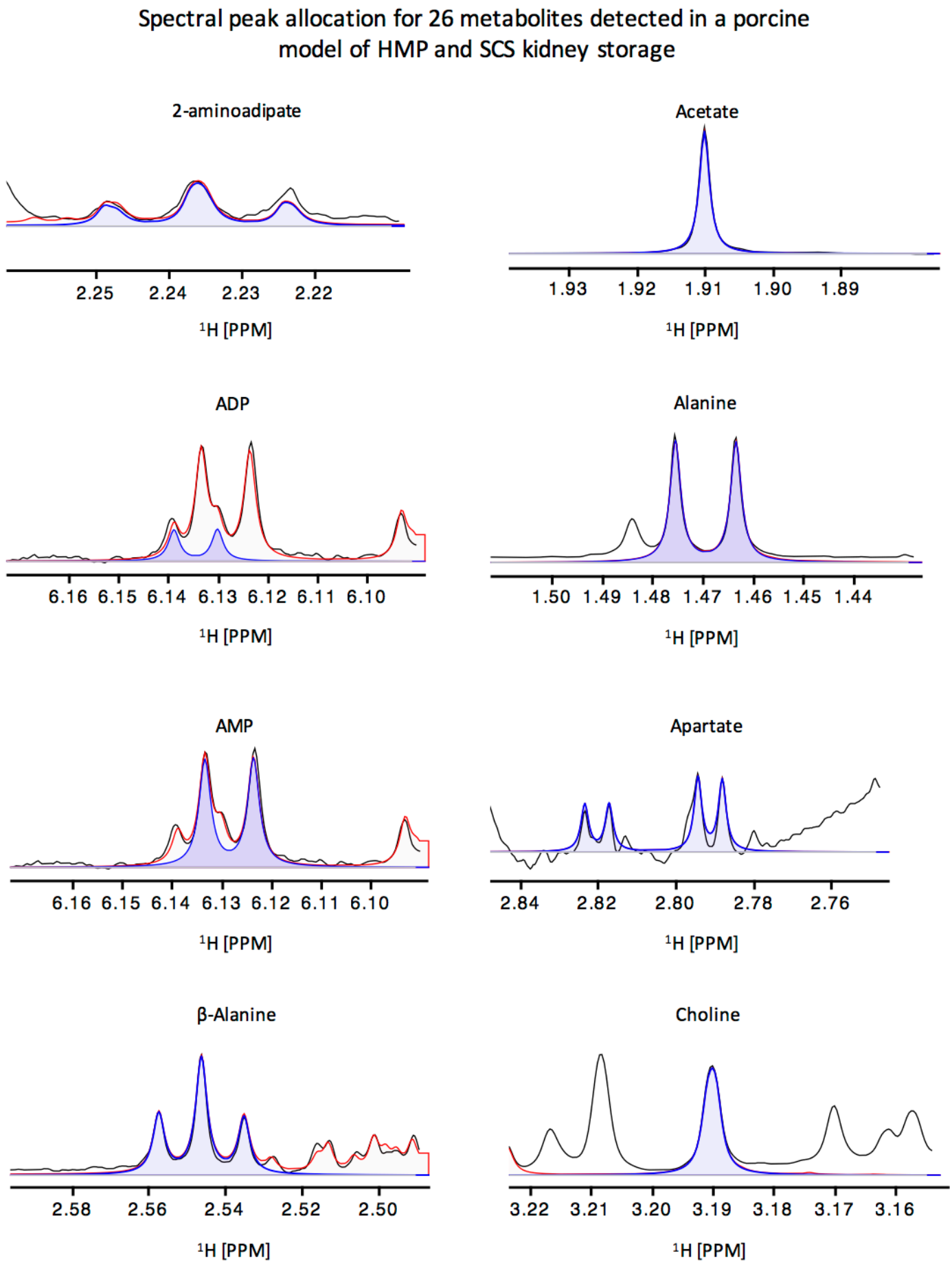

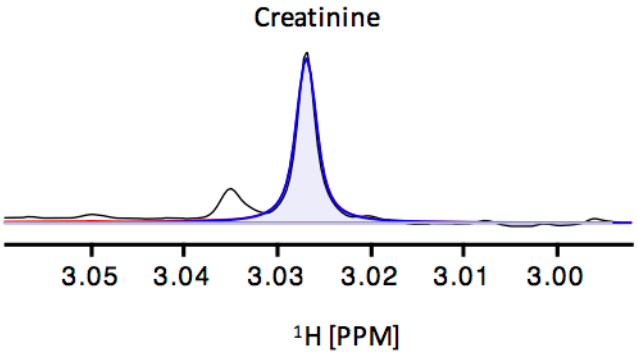
Creatinine
3.05 3.04 3.03 3.02 3.01 3.00
¹H [PPM]

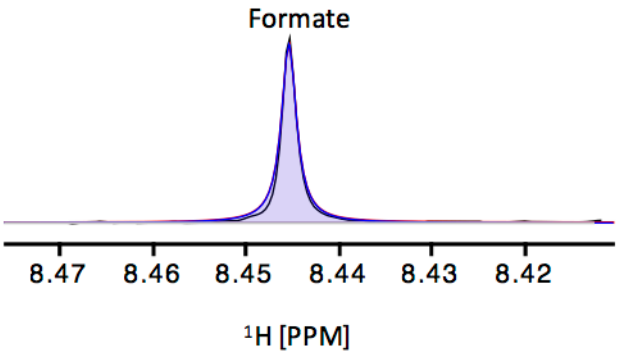
Formate
8.47 8.46 8.45 8.44 8.43 8.42
¹H [PPM]

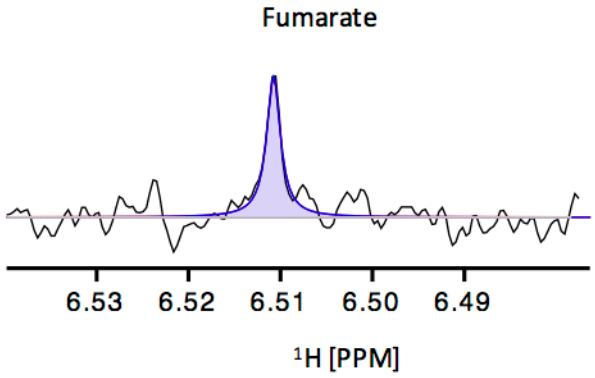
Fumarate
6.53 6.52 6.51 6.50 6.49
¹H [PPM]

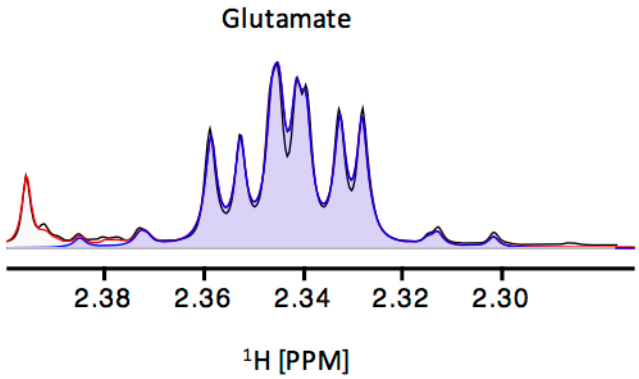
Glutamate
2.38 2.36 2.34 2.32 2.30
¹H [PPM]

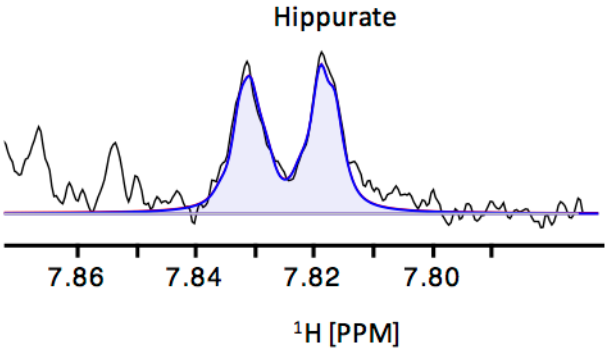
Hippurate
7.86 7.84 7.82 7.80
¹H [PPM]

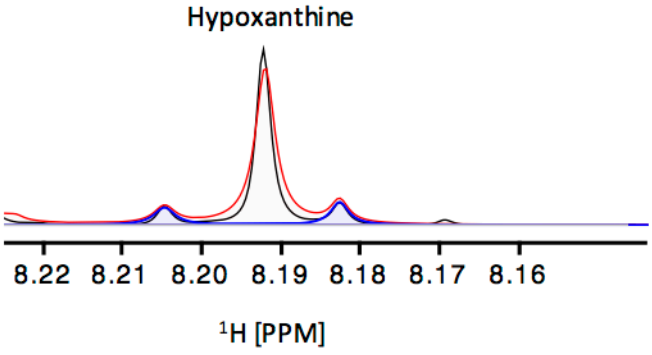
Hypoxanthine
8.22 8.21 8.20 8.19 8.18 8.17 8.16
¹H [PPM]

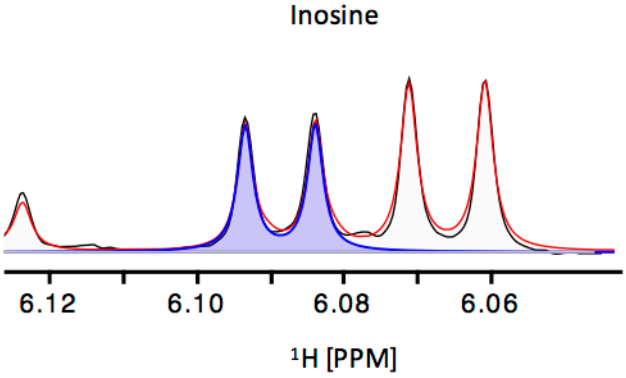
Inosine
6.12 6.10 6.08 6.06
¹H [PPM]

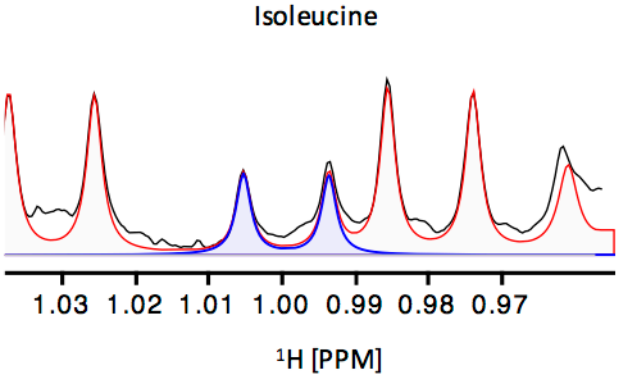
Isoleucine
1.03 1.02 1.01 1.00 0.99 0.98 0.97
¹H [PPM]

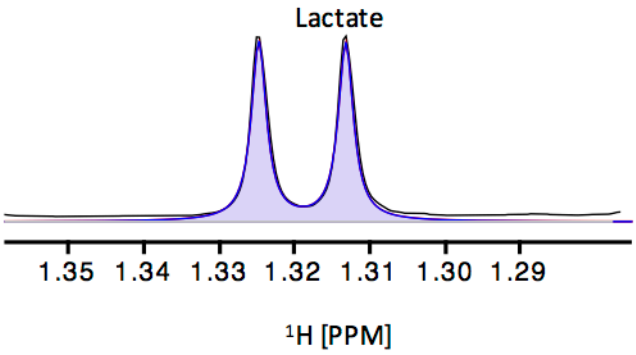
Lactate
1.35 1.34 1.33 1.32 1.31 1.30 1.29
¹H [PPM]

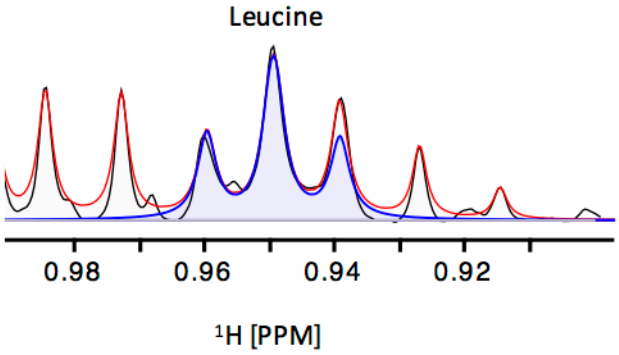
Leucine
0.98 0.96 0.94 0.92
¹H [PPM]

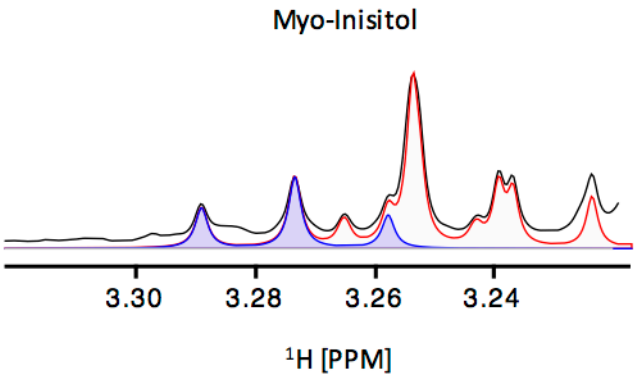
Myo-Inisitol
3.30 3.28 3.26 3.24
¹H [PPM]

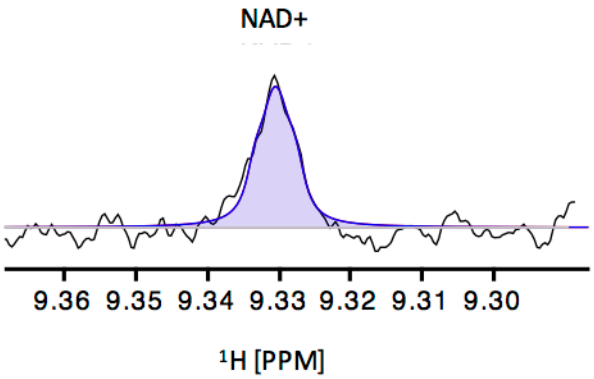
NAD+
9.36 9.35 9.34 9.33 9.32 9.31 9.30
¹H [PPM]

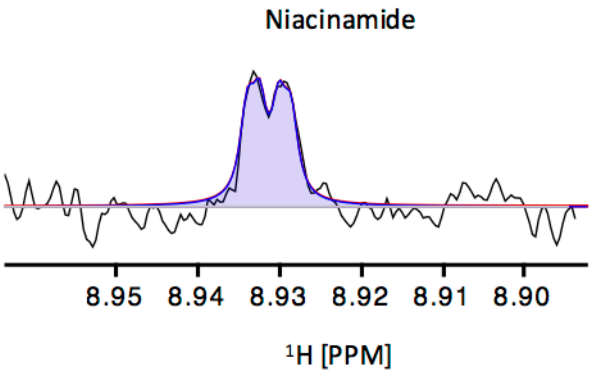
Niacinamide
8.95 8.94 8.93 8.92 8.91 8.90
¹H [PPM]

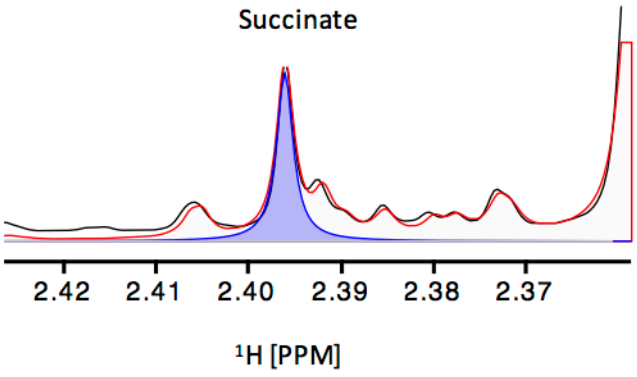
Succinate
2.42 2.41 2.40 2.39 2.38 2.37
¹H [PPM]

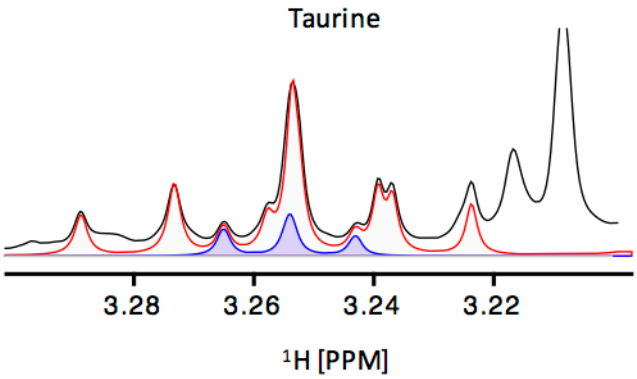
Taurine
3.28 3.26 3.24 3.22
¹H [PPM]

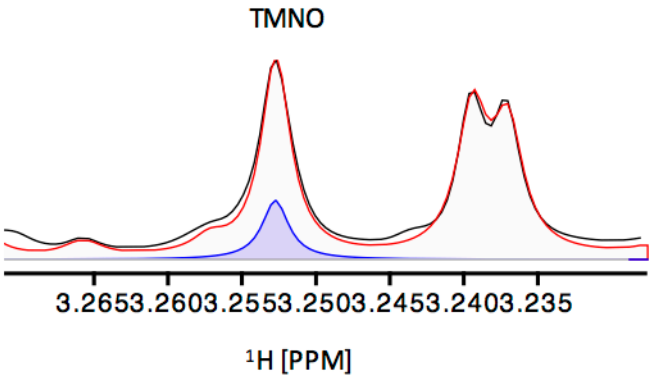
TMNO
3.2653.2603.2553.2503.2453.2403.235
¹H [PPM]

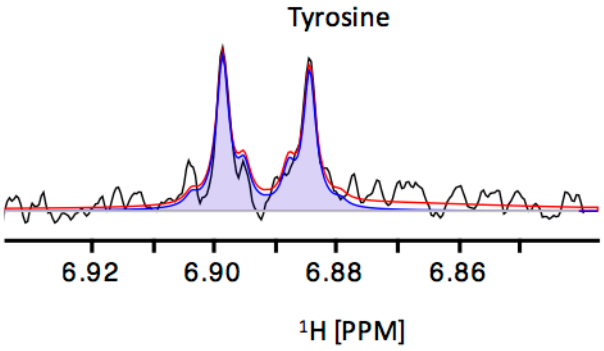
Tyrosine
6.92
6.90
6.88
6.86
¹H [PPM]

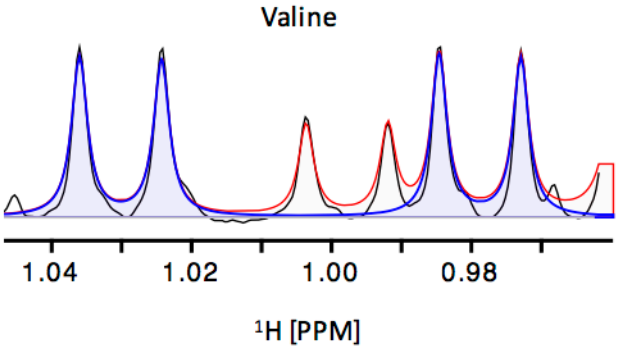
Valine
1.04
1.02
1.00
0.98
¹H [PPM]

Chapter 6 : Oxygenation of *ex vivo* kidneys undergoing Hypothermic Machine Perfusion

In this chapter a series of experiments were performed investigating the effects of oxygenation on *ex vivo* kidneys undergoing hypothermic machine perfusion. The experiments were written in the form of a manuscript with an accompanying commentary forming the remainder of the chapter.

The manuscript was published in the Tissue Regeneration and Repair special edition of the journal Transplantation in February 2019 (219). Additional methods and data are described in Supplementary Information and in Chapter 2.

I was responsible for experimental design, performing the experiments, processing and analysing tissue samples for NMR, Mass Spectrometry and immunohistochemistry in addition to writing, refining and submitting the manuscript.

Introduction

Following whole organ ischaemia inflicted during the retrieval process, ATP levels are quickly depleted as described in Chapter 1. As demonstrated in the previous chapter, hypothermic machine perfusion promotes metabolism by delivery of glucose to tissues (220). In these hypothermic conditions, in the absence of supplemental oxygen, hypothermic machine perfusion is largely anaerobic with only minimal evidence of TCA cycle activity. The was previously demonstrated by our group using modified UW-MPS supplemented with the metabolic tracer universally labelled glucose ([U-^{13}C] glucose) (175).

Several methods of oxygenation, during both normothermic and hypothermic preservation of *ex vivo* kidneys, have been described including oxygenation using a membrane oxygenator, retrograde oxygen persufflation and the use of a hyperbaric oxygen chamber (221). Whilst there is some evidence supporting the benefits of oxygenation during HMP in animal studies, there remains at present a lack of clinical evidence which use current perfusion fluids or methods of oxygenation making it difficult to compare outcomes to current practice (222).

In a DBD auto-transplant porcine model comparing a 21 hour period of either anoxic or oxygenated HMP, there was no improvement in renal function post-transplantation (223) for the oxygenated group. This contrasts with findings of a similar study again using a porcine auto-transplant model, but in this case a DCD model of transplantation (224), with a 22-hour period of oxygenated HMP. Kidneys in the oxygenated HMP arm showed lower peak serum creatinine post-operatively and faster return to baseline creatinine levels suggesting supplemental oxygen may be of benefit for DCD kidneys.

In contrast, Lindell et al observed no difference in functional outcome in a similar DCD model when perfusing canine kidneys with oxygenated and non-oxygenated HMP for 24 hours, although the type of device and running temperature differed between arms of the study (204). The study ascribed the lack of difference between oxygenated and non-oxygenated arms to the low oxygen requirements of kidneys during hypothermic storage.

Retrograde oxygen persufflation (ROP) has also been explored as a means of oxygenating kidneys during hypothermic storage (225) although it cannot be performed in conjunction with HMP due to the flow of gas. The renal vein is infused with gaseous oxygen whilst multiple pinpricks with an acupuncture needle permit escape of gases. In the most recent ROP studies, Treckmann et al (226, 227) observed superior functional outcomes with 4 hours of preservation with ROP compared to standard static cold storage and standard HMP conditions. However, no studies since have continued to explore this as a means of organ optimisation.

Studies since 1968 have investigated the benefits of preserving kidneys in hyperbaric oxygen (228, 229). Most recently one study described the effects of a short three hour preservation period on ATP levels in 5 differing conditions; static and HMP conditions using non-oxygenated conditions and oxygenation using a hyperbaric chamber, in addition to a fifth group utilising a membrane oxygenator during HMP (230). A net increase in ATP levels was observed in groups of kidneys stored using hypothermic machine perfusion oxygenated with either hyperbaric oxygen or using a membrane oxygenator despite the three hour preservation period.

Such aforementioned animal studies are limited by a small sample size and heterogenous conditions. Few studies have addressed the mechanisms by which oxygenation promotes functional benefit although one would speculate such mechanisms are due to changes in

metabolism. In this thesis so far we have discussed the metabolic products of glucose during HMP. In this series of experiments the effects of supplemental oxygen on *ex vivo* kidneys are explored using tracer-based metabolism applied to the porcine DCD model described in Chapter 2.

Methods

Preliminary work

Unlike normothermic preservation conditions, hypothermic machine perfusion does not aim to mimic physiological conditions. Given that metabolism is reduced during hypothermia, any aerobic metabolism is also likely to be minimal raising the question of how beneficial supplemental oxygen is likely to be in an HMP circuit.

Preliminary work for experiments in this chapter, reported in the results section of the manuscript, included measuring the oxygenation of arterial limb and venous effluent in a standard HMP circuit. Oxygen levels were quickly depleted in venous effluent showing an ongoing demand for oxygenation even in hypothermic conditions. A decrease in oxygen levels in the in-flow limb showed simple circulation of perfusion fluid is not adequate to oxygenate circulating perfusate.

Methods of oxygenating perfusate

In order to make the experiments relevant for the clinical setting, a means of oxygenation was selected which was sterile, non-traumatic to kidneys and could be used readily with standard UW-MPS perfusion fluid. The membrane oxygenator used in this series of experiments (Hilite 800 LT series hollow fiber oxygenator; Medos, Medizintechnik, AG) is commonly used in paediatric cardiopulmonary bypass circuits in the clinical setting with

documented use in other kidney preservation studies (82). The static priming volume of 55ml is small enough to not displace a significant proportion of the 1L perfusion fluid used whilst the unit allows a flow rate of up to 800ml/min, exceeding the maximum flow rates commonly observed during HMP (78, 231).

Unmodified UW-MPS does not include an oxygen carrier. An extra-cellular haemoglobin extract from the lugworm Arenicola Marina has been tested as an additive to preservation solutions for kidneys (232) whilst fluid containing extracted bovine haemoglobin has been successfully used to machine perfuse livers at sub-normothermic temperatures (233). For the purposes of experiments performed in this chapter, preliminary experiments suggested use of the membrane oxygenator resulted in a mean concentration of 68.7kPa.

Discussion

Despite a resurgence in interest in oxygenation during HMP, the mechanisms of action of oxygenation during HMP are perhaps suspected but not well understood. In our study, favourable changes in aerobic metabolism, higher ATP levels, improved perfusion parameters and less ultra-structural histological damage were observed in HMP/O_2 kidneys. This is in keeping with the improved functional outcomes seen with oxygenated HMP in a porcine DCD model (224) but contrasts with the equivalent outcomes seen in porcine DBD kidneys (223). DCD kidneys are subject to a warm ischaemic insult during the retrieval process resulting in fast total depletion of ATP stores contrasting with the lesser insults suffered by DBD kidneys. Thus it may be the case that oxygenation is of a greater benefit to DCD kidneys compared with DBD kidneys, accounting for the non-significant differences observed in DBD set of porcine experiments (223).

Metabolism and ATP levels

Metabolite labelling patterns observed in the cortex of HMP/O_2 kidneys indicated more TCA cycle activity with the observation of less U-^{13}C labelled glycolytic pathway end-points compared with HMP/Air kidneys. Perfusate changes showed a consistent increase in the concentration of U-^{13}C lactate and U-^{13}C alanine over time in HMP/Air kidneys indicating continual glycolytic pathway cycle activity. However, in HMP/O_2 kidneys this seemed to plateau after 8 hours. This may reflect the start of TCA cycle activity in HMP/O_2 kidneys but this is difficult to prove as no tissue samples were taken during the perfusion period itself. The small increase in TCA cycle activity indicated by higher 4,5-^{13}C glutamate levels is likely to account for the seven-fold increase in ATP levels observed in the renal cortex of HMP/O_2 vs HMP/Air kidneys.

The disparity in oxygen delivery and resultant reliance of the medulla on glycolytic pathway activity under normal physiological conditions is described in Chapter 1. One might suggest that simple aeration of perfusate is enough to meet oxygen requirements of the medulla, hence explaining why no significant differences were observed between labelled metabolites in the medulla of HMP/O_2 and HMP/Air conditions.

In this set of experiments the demonstration of aerobic respiration and higher ATP levels are used as outcome measures in the absence of a functional reperfusion or auto-transplant model. As with all organ donation, the organ preservation process is simply preparation for reperfusion with the clinically relevant measure being restoration of function of the transplanted kidney thus avoiding the need for dialysis. As discussed in Chapter 1, metabolic dysfunction is one contributor to the development of ischaemia reperfusion injury thought to cause delayed graft function.

Wijermars et al observed the effect of post-reperfusion metabolic recovery on the development of delayed graft function in transplanted human kidneys, none of which were machine perfused (234). Changes in metabolites in the arterial circulation and transplant kidney renal vein were measured following reperfusion. Grafts with delayed graft function showed continual anaerobic metabolic activity as evidenced by continuing lactate production on reperfusion, contrasting with the cessation of lactate production in kidneys with immediate graft function. Such observations reflect the necessity for restoration of aerobic metabolism in order for kidneys to function.

Observation of aerobic metabolism in HMP/O_2 kidneys shows how even under hypothermic conditions, oxygenation of perfusate stimulates aerobic metabolic processes required for immediate graft function. The observation of higher ATP levels in HMP/O_2 kidneys, also seen in other studies (230, 235, 236), is a result of such aerobic metabolism. However, on reperfusion ATP levels are likely to be fast depleted. It is likely the rate of constant production of ATP due to aerobic respiration which promotes functional graft recovery.

Further comments on flow parameters

Our findings demonstrated a non-significant improvement in perfusion parameters with higher flow rates and lower resistance observed in HMP/O_2 kidneys. These findings were consistent with other studies which observed a similar improvement of flow parameters during oxygenated HMP (223).

One benefit of HMP is the vasodilatation of renal microvasculature. This has been shown to result in improved cortical microcirculation at reperfusion (87), reducing detrimental patchy warm ischaemia. Improved flow parameters have been shown to correlate with

increased eNOS levels, central to vasorelaxation, following as little as 1 or 4 hours of non-oxygenated HMP (82). Such oxygen dependent pathways (237) are likely to be further upregulated during oxygenated HMP showing further benefits of oxygenation in addition to the metabolic benefits observed.

Mitochondrial damage

As described in the manuscript, greater mitochondrial damage was noted in non-oxygenated kidneys. As metabolic pathway activity central to aerobic metabolism occuring within mitochondria, damage to mitochondria may be the determinant of aerobic metabolic pathway activity. Conversely, mitochondrial damage may be an effect of ongoing ischaemia as a consequence of lower O_2 availability. Much current research implicates mitochondrial dysfunction as a central process in AKI (238) manifesting as DGF in transplanted kidneys.

Limitations

As with both aforementioned animal studies determining the effects of oxygenated HMP on functional outcome post-transplantation (223, 224), the experiments described are limited by a small sample size.

Experimental design did not permit acquisition of functional outcome data, limiting conclusions drawn from metabolic data. Tissue sampling prior to reperfusion may also have limited the relevance of our observation of a lack of demonstrable damage due to reperfusion injury; Given the majority of damage as a consequence of IRI occurs following reperfusion, data on tissue damage during the preservation period are of limited relevance. Further studies should investigate the extent of reperfusion injury in oxygenated kidneys which have been transplanted.

From a methodological perspective, further studies incorporating sequential tissue biopsies analysed using high resolution magic angle spectroscopy (HR-MAS) could inform decisions regarding the timing of oxygen delivery to kidneys.

Concluding remarks

This is the first study using an isotopic tracer to show the metabolic benefits of oxygenation during HMP with such changes consistent with measured ATP levels. Evidence for the clinical benefits following oxygenated HMP will be provided by two major multicentre trials currently being conducted by the COPE consortium (239).

Current UK centres use several brands of HMP device, some of which have a means of oxygenation incorporated into the circuit, such as oxygen concentrators. A superior evidence base and demonstration of cost-effectiveness is required prior to widespread usage of oxygenation during HMP although results from this set of experiments and others (212) predating the results of human clinical trials are encouraging.

Manuscript

Patel K, Smith TB, Neil D, Thakker A, Tsuchiya Y, Higgs EB, Hodges NJ, Ready AR, Nath J, Ludwig C. The effects of oxygenation on ex vivo kidneys undergoing hypothermic machine perfusion. Transplantation. 2019;103:318–327

The Effects of Oxygenation on Ex Vivo Kidneys Undergoing Hypothermic Machine Perfusion

Kamlesh Patel,[1,2] Thomas B. Smith,[1] Desley A.H. Neil, PhD, FRCPath,[3] Alpesh Thakker, PhD,[1] Yugo Tsuchiya, PhD,[3] Ellen B. Higgs,[5] Nikolas J. Hodges, PhD,[5] Andrew R. Ready, FRCS, MD,[2] Jay Nath, FRCS, PhD,[1,2] and Christian Ludwig, PhD[1]

Background. Supplemental oxygenation of the standard hypothermic machine perfusion (HMP) circuit has the potential to invoke favorable changes in metabolism, optimizing cadaveric organs before transplantation. **Methods.** Eight pairs of porcine kidneys underwent 18 hours of either oxygenated (HMP/O_2) or aerated (HMP/Air) HMP in a paired donation after circulatory death model of transplantation. Circulating perfusion fluid was supplemented with the metabolic tracer universally labeled glucose. Perfusate, end-point renal cortex, and medulla samples underwent metabolomic analysis using 1-dimension and 2-dimension nuclear magnetic resonance experiments in addition to gas chromatography-mass spectrometry. Analysis of ^{13}C-labeled metabolic products was combined with adenosine nucleotide levels and differences in tissue architecture. **Results.** Metabolomic analysis revealed significantly higher concentrations of universally labeled lactate in the cortex of HMP/Air versus HMP/O_2 kidneys (0.056 mM vs 0.026 mM, $P < 0.05$). Conversely, newly synthesized [4,5-^{13}C] glutamate concentrations were higher in the cortex of HMP/O_2 kidneys inferring relative increases in tricarboxylic acid cycle activity versus HMP/Air kidneys (0.013 mmol/L vs 0.003 mmol/L, $P < 0.05$). This was associated with greater amounts of adenoside triphosphate in the cortex HMP/O_2 versus HMP/Air kidneys (19.8 mmol/mg protein vs 2.8 mmol/mg protein, $P < 0.05$). Improved flow dynamics and favorable ultrastructural features were also observed in HMP/O_2 kidneys. There were no differences in thiobarbituric acid reactive substances and reduced glutathione levels, tissue markers of oxidative stress, between groups. **Conclusions.** The supplementation of perfusion fluid with high-concentration oxygen (95%) results in a greater degree of aerobic metabolism versus aeration (21%) in the nonphysiological environment of HMP, with reciprocal changes in adenoside triphosphate levels.

(*Transplantation* 2019;103: 314–322)

Hypothermic machine perfusion (HMP) of kidneys has been widely used as a modality of organ preservation in clinical practice for over a decade. Hypothermic machine perfusion involves the recirculation of chilled perfusion fluid at subphysiological pressures through the renal vasculature of the ex vivo kidney in the hours before transplantation.

The benefits of HMP have been reported for all subtypes of cadaveric kidneys including improved short-term outcomes[1,2] and graft survival[3,4] compared with static cold storage. The proposed mechanisms by which HMP exerts benefit include decreased vasospasm,[5] the protection of vascular endothelium,[6] the washout of toxic metabolites and supplementation of metabolism[7,8] with the potential for the metabolic profile of the ex vivo kidney to predict early graft function.[9]

Oxygenation of circulating perfusate during HMP has recently been revisited as a means of optimizing cadaveric kidneys before transplantation. Previous human and animal studies have used a variety of methodologies yielding inconsistent but promising results in terms of functional outcomes.[10] Porcine autotransplant studies have shown functional benefits when the HMP circuit is modified to include oxygenation in a

Received 28 June 2018. Revision received 20 September 2018.

Accepted 13 October 2018.

[1] *Institute of Metabolism and Systems Research, College of Medical and Dental Sciences, University of Birmingham, Birmingham, United Kingdom.*

[2] *Department of Renal Surgery, University Hospitals Birmingham, Birmingham, United Kingdom.*

[3] *Department of Histopathology, University Hospitals Birmingham, Birmingham, United Kingdom.*

[4] *Department of Structural and Molecular Biology, University College London, London, United Kingdom.*

[5] *School of Biosciences, University of Birmingham, Birmingham, United Kingdom.*

K.P., T.B.S., J.N., and C.L. contributed equally to this work.

Several authors (K.P., J.N., T.S., C.L., and A.R.) have ongoing research in part funded by Organ Recovery Systems. The other authors declare no conflicts of interest.

This work was funded through grants from University Hospitals Birmingham Charities, The Kidney Patient Association and Organ Recovery Systems.

J.N., A.R., and C.L. designed research. J.N., K.P., T.S., and C.L. performed research. K.P., T.S., J.N., C.L., A.T., D.N., Y.T., E.H., N.H., and Y.T. analyzed data. C.L. contributed new analytical tools relating to NMR spectral analyses. K.P. and T.S. wrote the article. All authors reviewed the article before submission.

Correspondence: Kamlesh Patel, Department of Renal Surgery, Queen Elizabeth Hospital Birmingham, University Hospitals Birmingham NHS Foundation Trust Mindelsohn Way, Edgbaston, Birmingham, B15 2GW, United Kingdom. (kamleshpatel@doctors.org.uk).

Supplemental digital content (SDC) is available for this article. Direct URL citations appear in the printed text, and links to the digital files are provided in the HTML text of this article on the journal's Web site (www.transplantjournal.com).

ISSN: 0041-1337/19/10302-0314

DOI: 10.1097/TP.0000000000002542

donation after circulatory death (DCD) model of transplantation,[11] but the same did not hold true for a donation after brainstem death model.[12]

KPS-1 (Organ Recovery Systems, Itasca, IL), the kidney perfusion solution commonly used in clinical practice, is a hypertonic, acellular fluid with no designated oxygen carrier. Any oxygenation of perfusion fluid is a result of passive diffusion from the air contained within the perfusion fluid reservoir. Supplemental oxygenation during HMP may be an effective way to alter metabolic pathway activity, with the presumption that oxygenation encourages aerobic metabolism and therefore replenishes cellular adenoside triphosphate (ATP) stores.[13] In addition to potential functional benefits after reperfusion, increased ATP stores prevent detrimental processes such as cellular swelling, apoptosis and necrosis.

Despite these proposed benefits of oxygenation, damage due to reactive oxygen species (ROS), responsible for many consequences of ischemia reperfusion injury (IRI) is a potential drawback.[14] Any potential metabolic benefits of organ oxygenation must, therefore, be tempered against the potentially deleterious effects of ROS injury, and it would seem rational that oxygen delivery should occur at the lowest therapeutic concentration possible to achieve such benefits. In conditions of oxidative stress leading to typical changes, such as oxidative DNA modifications[15,16] and lipid peroxidation,[17] levels of reduced glutathione (GSH) are depleted. Thiobarbituric acid reactive substances (TBARS) provide a sensitive assay for lipid peroxidation.[18]

Metabolic tracer studies using perfusion fluid supplemented with universally labeled ^{13}C glucose ([U-^{13}C] glucose) have been used to accurately demonstrate de novo metabolism within biological systems, including the ex vivo HMP kidney.[19] In conjunction with adenosine nucleotide analysis, the concentration and isotopic labeling patterns of central metabolites enable description of aerobic/anaerobic pathway activity in addition to their metabolic sequelae.

The aims of this study are to compare the metabolic consequences, changes in perfusion dynamics, damage secondary to oxidative stress, and histological changes between perfusate oxygenation with atmospheric oxygen (21%) and high concentration oxygen (95%).

MATERIALS AND METHODS

Retrieval of Organs

Experiments were performed on 8 pairs of porcine kidneys (n = 16). Porcine organs were procured from 22- to 26-week-old male English white pigs weighing 80 to 85 kg from a local abattoir (F.A. Gill, Wolverhampton, UK) in a previously described controlled model of DCD.[20]

Our model, similar to other well-reported controlled DCD models in pigs,[21] was designed to simulate a Maastricht category III donor.[22] Animals were sacrificed by electrical stunning and exsanguination before in situ warm ischemia for 15 minutes, during which time, laparotomy and bilateral nephrectomy were performed. After retrieval, all kidneys were checked for damage and suitability for the study. To permit fair comparison, pairs of kidneys were only included if both kidneys were supplied by a single artery at the point of origin from the abdominal aorta. Kidneys were initially flushed with 1 L of Soltran solution (Baxter Healthcare) at 4°C at a pressure of 120 mm Hg, supplemented with 0.93 g [U-^{13}C] labeled glucose (5 mM) at 4°C and 5000 iU heparin to remove any residual blood products and enable rapid cooling.

The purpose of adding ^{13}C-enriched glucose to the cold flush solution was to increase initial availability of glucose for generation of downstream labeled metabolic substrates later during HMP. Organs were then stored in static conditions (1 L Soltran with 1% PenStrep) for 2 hours before commencing HMP. All experiments were performed following the principles of laboratory animal care according to the National Institutes of Health standards. No animal was slaughtered solely for the purpose of experimentation.

Hypothermic Machine Perfusion

Machine perfusion was initiated using the LifePort Kidney Transporter 1.0 (Organ Recovery Systems) at a pressure of 30 mm Hg. Kidneys were perfused with 1 L KPS-1 (Organ Recovery Systems) supplemented with 0.93 g [U-^{13}C] glucose (5 mM) giving a total glucose concentration of 15 mM. Single arterial anatomy permitted cannulation with a 5 mm T-connector to attach to the LifePort.

The standard LifePort perfusion circuit was modified (Figure 1) to incorporate a pediatric membrane oxygenator (Hilite 800 LT series hollow fiber oxygenator; Medos, Medizintechnik, AG). One kidney from each pair was randomly allocated to either the oxygenated or aerated perfusion group with contralateral organ allocated to the other perfusion group. In the oxygenated perfusion group (HMP/O_2) in which 95% O_2, 5% CO_2 (Carbogen, BOC Medical) was passed through the oxygenator via a flow valve at 0.1 L/min. In the aerated perfusion fluid (HMP/Air) group, sterile filtered room air (assumed 21% oxygen) was delivered at the same rate (0.1 L/min).

During perfusion, the dissolved oxygen concentration in the fluid entering the kidney via the in-flow limb was measured using an oxygen sensor (Oxygen Microsensor NTH-PSt1; Presens GmbH, Germany) paired with a microfiber optic oxygen transmitter (Microx TX3; Presens GmbH). Before experiments, this was calibrated using the oxygen-carrying capacity of deionized water at 4°C (100%, maximum) and vigorously agitated 1% sodium sulphite solution (0%, minimum). The negative control was validated against deionized, nitrogenated water at room temperature. The mean concentration of oxygen in the inflow limb of the HMP/O_2 circuit

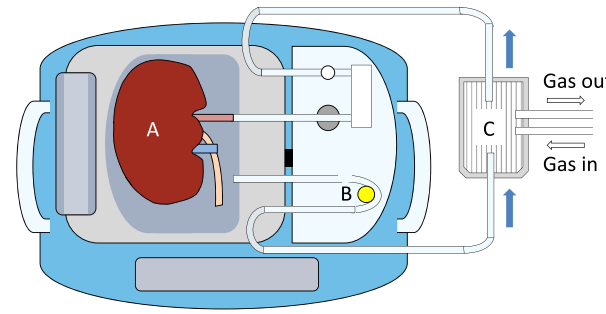

FIGURE 1. Schematic diagram of a modified LifePort circuit which includes a pediatric membrane oxygenator. Perfusate is drawn from the fluid reservoir containing the kidney (A) intro the perfusion circuit via a peristaltic pump (B) and pushed through a pediatric membrane oxygenator (C). The oxygenator allows for the gas supplied (either atmospheric air or 95% oxygen) to be dissolved in the fluid before it passes through a bubble chamber and into the kidney (A) via the cannulated renal artery.

was 68.7 kPa, whereas mean oxygen concentration in the inflow limb of the HMP/Air circuit was 21.0 kPa.

Kidneys were perfused for 18 hours. Perfusate samples (2 mL) were frozen immediately after retrieval via the sampling port of the LifePort cassette at multiple timepoints (0, 1, 6, 12, 18 hours) with perfusion parameters also reported at these times. At the end of the perfusion period, kidneys were laterally bisected with cortex and medulla samples snap frozen in liquid nitrogen before storage at −80°C for metabolic analysis. Wedges of renal cortex and medulla and pieces of renal artery were immersion fixed in 10% formalin for histology and samples of cortex (2 × 2 × 5 mm) were immersion fixed in glutaraldehyde in phosphate buffer for electron microscopy.

Sample Processing

Perfusate and tissue sample extraction was performed as previously described.[19] Perfusate samples for 1-dimension (1D) ^{1}H nuclear magnetic resonance (NMR), 2-dimension (2D) ^{1}H,^{13}C HSQC NMR, and gas chromatography–mass spectrometry (GC-MS) analysis were taken from the upper layer of a biphasic solution containing polar metabolites, and formed from a vigorously mixed solution of equal amounts of neat perfusate, high-performance liquid chromatography (HPLC) grade methanol (−80°C), and HPLC grade chloroform (−20°C). Polar extracts were dried at 35°C in a vacuum drier.

Frozen cortex and medulla samples were powdered using a Cryo-cup grinder (Biospec Products). From this, 0.5 g was suspended in methanol (−80°C) and homogenized in Precellys homogenization tubes using a Precellys 24 Dual homogenizer (Bertin Technologies, Montigny-le-Bretonneux, France) at low speeds in short intervals (5000 RPM for 8 × 10 s) to prevent samples from heating. Cholorform (−20°C) and deionized water were then added and the resultant solution mixed vigorously before sampling from the upper layer containing polar metabolites. Samples were then dried at 35°C overnight in a vacuum drier.

Nuclear Magnetic Resonance Spectroscopy

For NMR analysis, dried perfusate and tissue extracts were suspended in 100-mM phosphate buffer, containing 0.5-mM dry sealing system, 2-mM imidazole, and 10% D_2O.

Both 1D ^{1}H and 2D ^{1}H, ^{13}C heteronuclear single quantum coherence (HSQC) NMR, spectra were acquired using a 600-MHz Bruker Avance III NMR spectrometer in 5-mm NMR tubes. All 1D ^{1}H NMR spectra were processed within the MetaboLab software package version 1.0.0.1.[23] After this, 0.5 Hz line broadening was applied with zero-filling the data up to 131 072 real data points before Fourier transformation. The resulting spectra were referenced using dry sealing system and manually phase corrected. Subsequently, the spectral baseline was corrected using MetaboLab's spline baseline correction before the spectra were exported to Bruker format for metabolites to be quantified using Chenomx 8.2 (Chenomx INC, Edmonton, AB, Canada).

For 2D ^{1}H,^{13}C HSQC NMR, the ^{13}C dimension was acquired with a spectral width of 160 ppm using 25% of 8192 data points using a nonuniform sampling scheme. The nonuniformly sampled spectra were reconstructed with compressed sensing using the MDDNMR and NMRPipe software.[24-26] All spectra were processed without baseline correction to avoid complications in the multiple-analysis procedure. MetaboLab was used to combine data from 2D ^{1}H,^{13}C HSQC NMR and GC-MS using a previously described model free approach[27] to give more accurate isotopomer distributions for key metabolites of interest.

Gas Chromatography-mass Spectrometry

The dried polar extract was dissolved in 2% methoxyamine HCl in pyridine (Sigma-Aldrich, Dorset, UK) followed by incubation at 60°C and subsequently 60 μL N-tertbutyldimethylsilyl-N-methyltrifluoroacetamide with 1% (w/v) tertbutyldimethyl-chlorosilane (Sigma-Aldrich, Dorset, UK) derivatization reagent was added.

GC/MS was performed using an Agilent 7890B Series GC/MSD gas chromatograph with a polydimethylsiloxane GC column coupled, with a mass spectrometer (Agilent Technologies UK Limited, Stockport, UK).

For determination of the mass isotopomer distributions, spectra were corrected for natural isotope abundance. Data processing from raw spectra to mass isotopomer distribution correction and determination was performed using MetaboliteDetector software.[28]

HPLC: Adenosine Nucleotide Analysis

Concentrations of adenosine monophosphate (AMP), adenosine diphosphate (ADP), and ATP were determined using HLPC analysis of extracted kidney cortex and medulla samples from the oxygenated and aerated experiments. Adenine nucleotides were extracted from frozen powdered tissue with ice-cold 0.35 M perchloric acid and analyzed by ion-pair reverse phase HPLC as described elsewhere.[29]

Biochemical Assays: Markers of Oxidative Stress

The GSH assay, as originally described by Hissin and Hilf,[30] was performed on samples of renal cortex to provide an indication of oxidative stress. Quantification of cortical malonaldehyde (MDA) was performed using TBARS assay. Assay results for GSH and TBARS were normalized to protein content as per the Bradford assay.[31] Full assay protocols can be seen in the **Supplemental Materials and Methods** (**SDC,** http://links.lww.com/TP/B660).

Light Microscopy

Wedges of renal cortex and medulla from 3 pairs of HMP/O_2 and HMP/Air kidneys and renal arteries were fixed in formalin and processed to a paraffin block. After this, 4-μm sections of renal cortex and medulla were stained with hematoxylin and eosin and periodic acid Schiff, whereas renal artery sections underwent staining with hematoxylin and eosin alone.

Photomicrographs of 10 random glomeruli (40× magnification), 10 random areas containing predominantly tubules (5 subcapsular and 5 midcortex at 20× magnification) and 5 transverse sections of intraparenchymal arteries (20× magnification) were assessed. Image J 1.05i software (National Institutes of Health, Bethesda, MD) was used for morphometric assessment.

Images were assessed for evidence of injury using glomerular shrinkage, interstitial edema, and perivascular edema as indicators of damage. The extent of injury of extraparenchymal renal arteries was semiquantitatively graded. Further information on grading of injury can be seen in **Supplemental Materials and Methods** (**SDC,** http://links.lww.com/TP/B660).

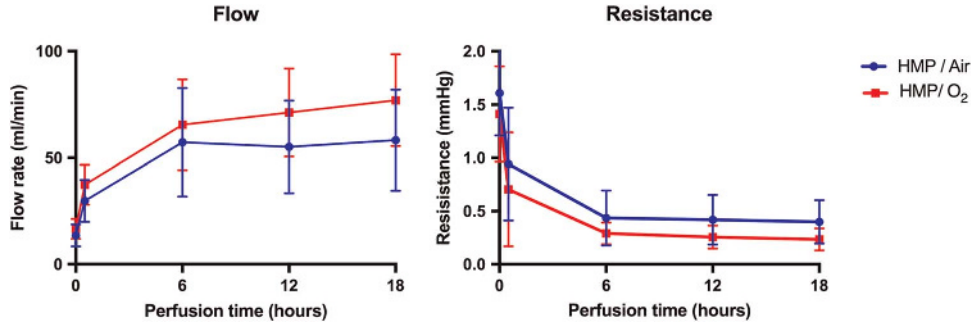

FIGURE 2. Perfusion parameters for oxygenated hypothermic machine perfusion (HMP/O_2) and aerated hypothermic machine perfusion (HMP/Air) porcine kidneys.

Electron Microscopy

Standard protocols of the Electron Microscopy Laboratory, University Hospitals Birmingham, Birmingham, UK, were followed. For electron microscopy (EM), biopsies (2 × 2 × 5 mm) of renal cortex were fixed in 2.5% glutaraldehyde in 0.1 M phosphate buffer, pH 7.4 then postfixed in osmium tetroxide and en-bloc stained with uranyl acetate before being processed by standard techniques to an epon araldite block. Thick sections were stained with toluidine blue and ultrathin sections stained with lead citrate and examined by a Joel JEM1200-EX 11 electron microscope.

Random photomicrographs were taken of glomeruli, tubules, and arteries/arterioles at 6800× to include mesangial areas and glomerular capillary loops. Of the total mitochondria present, the percentage of glomeruli of normal morphology, condensed, and containing flocculent densities were determined for each kidney. Both the pathologist and technician who acquired and analyzed images with light and electron microscopy were blinded to the kidney allocation groups.

Statistical Analysis

Statistical analysis was performed using GraphPad Prism version 6.00 for Mac OS X (GraphPad Software, La Jolla, CA). Analyses were deemed to be statistically significant when P is less than 0.05. HMP/O_2 and HMP/Air groups were compared using Mann-Whitney U test.

RESULTS

Preliminary Studies

Using previously described methodology, a porcine kidney was perfused using a standard unmodified LifePort circuit[8] which does not provide oxygenation or aeration of perfusate. After 2 hours of storage in static conditions, oxygen levels in the in-flow limb dropped by over 90% in 2 hours from an initial PaO_2 of 20.58 to 1.77 kPa, whereas the venous effluent declined from 2.15 kPa, approximately 10% of that in the in-flow limb at T0, to absolute anoxia within 80 minutes.

Perfusion Parameters

Mean resistance readings were lower, and therefore flow readings higher, for all timepoints in HMP/O_2 kidneys. However, the difference did not reach statistical significance at 6, 12, or 18 hours (P values 0.063, 0.278, 0.063, respectively) (Figure 2).

1D ^{1}H-NMR: Quantification of Metabolites Concentrations

1D ^{1}H-NMR analysis was used to determine the concentration of unlabeled metabolites within the circulating perfusate at 6, 12, and 18 hours (**Table S1, SDC,** http://links.lww.com/TP/B660). The concentrations of unlabeled metabolites in renal cortex and medulla (**Table S2, SDC,** http://links.lww.com/TP/B660) were also determined. No significant differences were observed between circulating metabolites in the perfusate of HMP/O_2 compared with HMP/Air kidneys.

2D NMR and GC-MS Analysis: Isotopomer Distributions for ^{13}C-labeled Metabolites

Using 2D NMR, isotopomer combinations were determined for the metabolites alanine, glutamate, and lactate in the perfusion fluid and tissues of both HMP/O_2 and HMP/Air kidneys, indicating de novo metabolism (Table 1). For these metabolites, 2D NMR data were combined with GC-MS data to determine isotopomer distributions in Table 1.

TABLE 1.

Isotopomer distributions for isolated labeled metabolites in the perfusate and tissue of HMP/O_2 and HMP/Air porcine kidneys

	Isotopomer		HMP/O_2, %	HMP/Air, %	P
Lactate[a]	+3	Perfusate	5.43	9.85	0.0078[b]
		Cortex	6.36	8.73	0.0078[b]
		Medulla	13.80	15.70	0.0312[b]
Alanine[a]	+3	Perfusate	4.05	8.54	0.0078[b]
		Cortex	6.07	8.09	0.0078[b]
		Medulla	6.78	8.39	0.0312[b]
Citrate	+2	Perfusate	0.00	0.00	>0.9999
		Cortex	0.48	0.33	0.6250
		Medulla	0.00	0.36	0.2500
Glutamate[a]	+2	Perfusate	1.80	0.27	0.1250
		Cortex	1.60	0.50	0.0312[b]
		Medulla	3.13	0.40	0.0312[b]
Succinate	+2	Perfusate	1.01	0.26	0.2500
		Cortex	1.46	0.41	0.0156[b]
		Medulla	2.54	0.36	0.0312[b]
Malate	+2	Perfusate	0.38	0.34	0.6250
		Cortex	1.09	0.87	0.4688
		Medulla	2.80	0.00	0.0312*

[a] Combined NMR/MS analysis used to calculate isotopomer distributions.
*$P < 0.05$.
HMP/Air, aerated hypothermic machine perfusion; HMP/O_2, oxygenated hypothermic machine perfusion.

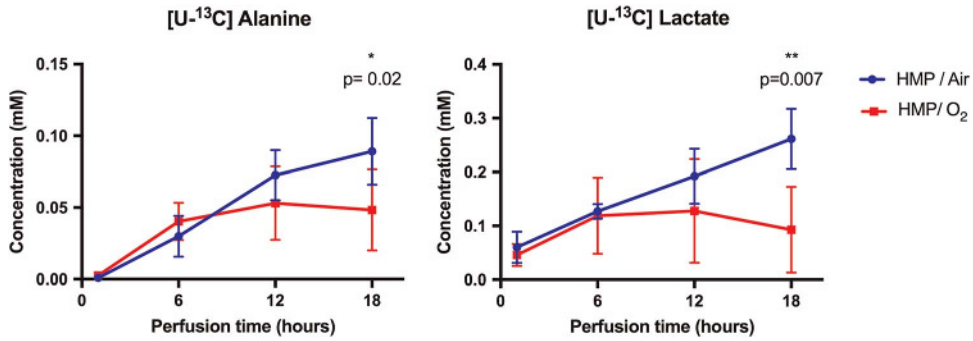

FIGURE 3. Absolute concentrations of universally labeled 13C ([U-13C]) alanine and [U-^{13}C] lactate in circulating perfusate. * $0.01 < P < 0.05$, ** $0.001 < P < 0.01$, *** $P < 0.001$.

Absolute Quantification of Labeled Metabolites

Using a combination of 1D, 2D NMR and GC-MS, concentrations of [U-^{13}C] alanine and [U-^{13}C] lactate were quantified for extracted perfusate samples at each timepoint (Figure 3). Labeled isotopomers of glutamate were absent in early perfusate samples, thus continuous data is not reported for glutamate. Absolute concentrations of [U-^{13}C] alanine, [U-^{13}C] lactate and [4,5-^{13}C] glutamate were determined for endpoint perfusate, cortex, and medulla samples (Figure 4).

Microscopy: Light Microscopy and Electron Microscopy

Glomeruli

Glomeruli were shrunken but otherwise appeared normal on light microscopy in both groups. There was significantly more shrinkage of glomeruli in the HMP/Air 52% (range, 40-70) versus HMP/O_2 67% (range, 47-83) ($P < 0.001$). There was no ultrastructural difference between the 2 groups; epithelial and endothelial cells appeared condensed with preservation of podocyte foot processes and an intact endothelial lining with retained fenestrations.

Tubules and Interstitium

Changes consistent with acute tubular injury were present up to a similar extent in both HMP/O_2 and HMP/Air kidneys on light microscopy. Ultrastructural changes include edema/separation between the basolateral infoldings, focal areas of denuded basement membranes, and moderate numbers of exfoliated epithelial cells within the lumen. The brush border was largely intact.

Abnormal mitochondrial morphology consisted of either condensed mitochondria or mitochondria containing flocculent densities, an indication of irreversible injury. Examples are

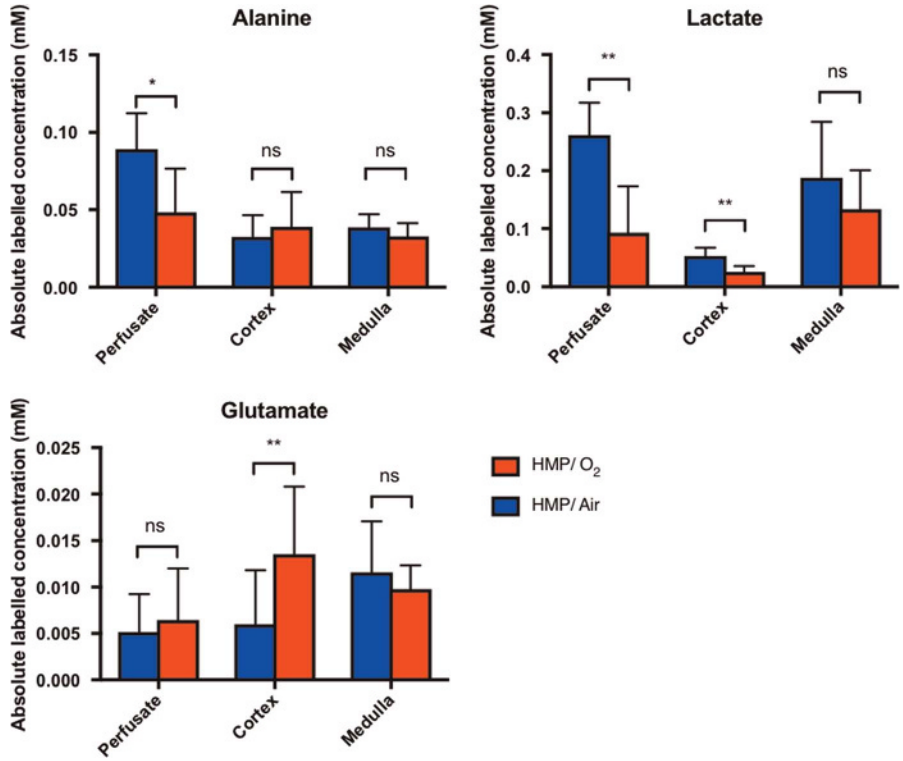

FIGURE 4. Absolute concentrations of universally labeled 13C ([U-13C]) alanine, [U-^{13}C] lactate and [4,5-^{13}C] glutamate determined using 1-dimensional ^{1}H nuclear magnetic resonance, 2-dimensional heteronuclear single quantum coherence nuclear magnetic resonance, and gas chromatorgraphy-mass spectometry data. * $0.01 < P < 0.05$, ** $0.001 < P < 0.01$, *** $P < 0.001$. HMP/O_2, oxygenated hypothermic machine perfusion; HMP/Air, aerated hypothermic machine perfusion.

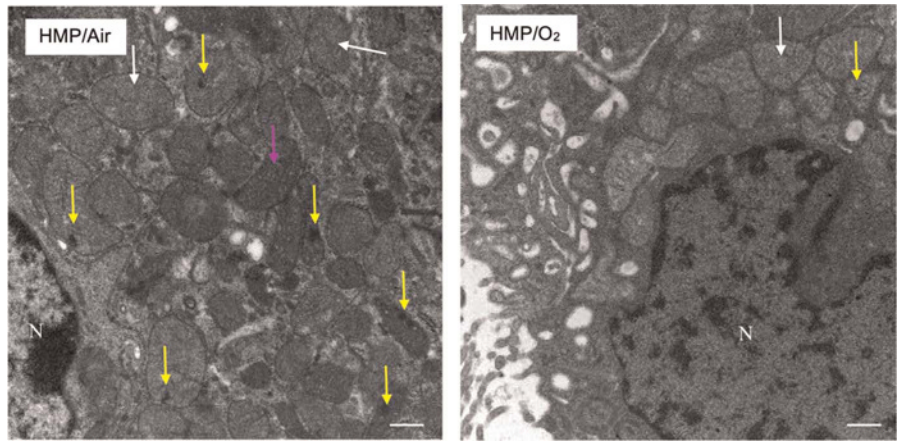

FIGURE 5. Electron micrographs of a tubular epithelial cell from A, aerated hypothermic machine perfusion (HMP/Air) and B, oxygenated hypothermic machine perfusion (HMP/O_2). The mitochondria within the HMP/Air group have a mixture of appearances: normal (white arrow), condensed (purple arrow) and contain multiple flocculent densities (yellow arrow). The mitochondria in the HMP/O_2 group are of normal appearance (white arrow) with a rare flocculent density (yellow arrow). Part of the nucleus (N) is apparent in both. Original magnification, ×18 500; bar, 500 nm.

shown in Figure 5. Swelling of mitochondria was not observed. There was evidence of increased injury in HMP/Air kidneys with 29% (24-61%) of mitochondria displaying normal morphology compared with 72% (49-78%) of HMP/O_2 kidneys (P = 0.200). The percentage of mitochondria containing flocculent densities was similar in both groups; 16% (14-23%) HMP/Air versus 20% (13-28%) HMP/O_2. Interstitial edema was similar in both groups with a median of 17 (11-34) pixels in HMP/O_2 compared with 20 (13-24) pixels in HMP/Air group (P = 0.184).

Arteries

Although endothelium was intact in intraparenchymal renal arteries and arterioles, there was at least moderate denudation of the extraparenchymal renal arteries in both groups. Patchy medial edema was seen between medial smooth muscle cells in both groups. Periarterial edema was similar in both groups with a median of 26% (13-66%) HMP/O_2 versus 34% (20-88%) HMP/Air (P = 0.211).

HPLC: Adenosine Nucleotide Analysis

Tissues samples from 4 pairs of porcine kidneys underwent analysis by HPLC. ATP levels in the cortex of HMP/O_2 kidneys were over sevenfold greater than for HMP/Air kidneys (mean, 19.8 mmol/mg protein vs 2.8 mmol/mg protein, P = 0.029). AMP levels were higher in both the cortex and medulla of HMP/O_2 versus HMP/Air kidneys although the results did not reach statistical significance, whereas ADP levels were significantly higher in the cortex of HMP/O_2 kidneys (**Table S3 SDC,** http://links.lww.com/TP/B660; Figure 6).

TBARS: MDA Quantification

Hypothermic machine perfusion/O_2 had slightly lower levels of MDA content but this was nonsignificant (7.26 ± 0.99 nmol/mg protein vs 8.07 ± 0.61 nmol/mg protein, P = 0.486).

GSH: Tissue GSH Concentrations

There was no significant difference in mean GSH concentration in the cortex of HMP/Air and HMP/O_2 groups at the end of the perfusion period (7.22 ± 0.72 nmol/mg protein vs 7.80 ± 0.96 nmol/mg protein, P = 0.200).

DISCUSSION

Supplemental oxygenation during the HMP of kidneys invokes a multitude of changes which have scope to improve outcomes after transplantation. Our results show pronounced metabolic differences between HMP/O_2 and HMP/Air kidneys in addition to significant consequences for tissue architecture, mitochondrial morphology, and cellular ATP levels.

The Role of Oxygenation in Supporting Metabolism

Cessation of blood supply during organ retrieval is the start of a period of hypoxia leading to a depletion in cellular ATP stores and a resultant switch to anaerobic metabolism,[32] reflected in the build-up of the products of glycolysis, such as lactate and alanine in both tissue and perfusate.[8] Hypothermia during this period, whether in static conditions or

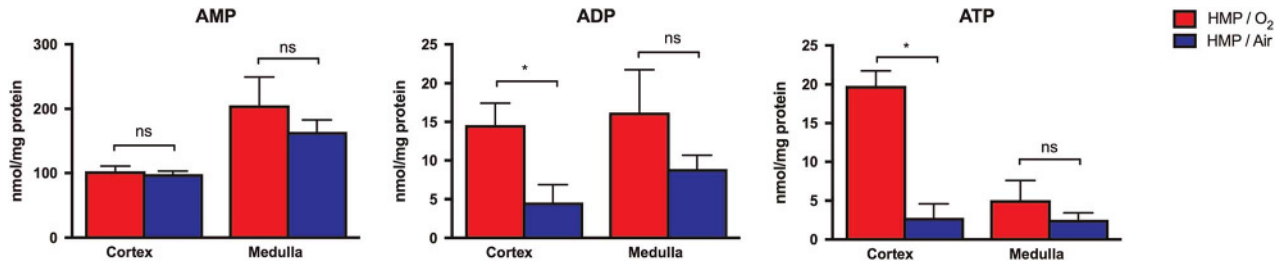

FIGURE 6. Adenoside monophosphate (AMP), adenoside diphosphate (ADP), adenoside triphophate (ATP), and overall energy levels in the cortex and medulla of oxygenated hypothermic machine perfusion (HMP/O_2) and aerated hypothermic machine perfusion (HMP/Air) kidneys. * 0.01 < P < 0.05.

HMP, leads to a reduction in metabolism[33] and consequentially, a decrease in oxygen requirement.[34]

Historically, this decrease in oxygen requirement has led to the acceptance that the hypoxic environment of a standard HMP circuit is adequate to meet the oxygen demands of ex vivo kidneys. Our results show that oxygenation promotes aerobic metabolism, as reflected in significantly higher concentrations of [4,5-^{13}C] glutamate in the cortex of HMP/O_2 kidneys versus HMP/Air kidneys. The reciprocal outcome is a decrease in de novo glycolytic activity in HMP/O_2 kidneys which is reflected in lower cortical concentrations of universally labeled alanine and lactate compared with HMP/Air kidneys.

We have previously observed small (<0.5%) proportions of [4,5-^{13}C] glutamate during standard HMP in the cortex of porcine kidneys after a 24-hour period.[19] However, the percentage of [4,5-^{13}C] glutamate observed in the cortex of both HMP/Air and HMP/O_2 conditions was higher, even with a reduced perfusion period and a lower concentration of [U-^{13}C]-labeled glucose, indicating that both conditions promote tricarboxylic acid (TCA) cycle activity compared with standard HMP.

Within the perfusate, changes in the absolute concentration of [U-^{13}C] alanine and [U-^{13}C] lactate mirrored a potential metabolic switch after several hours of HMP/O_2, resulting in a reduction in the production of glycolytic endpoints. This was in contrast to HMP/Air kidneys where a steady rate of production of [U-^{13}C] alanine and [U-^{13}C] lactate was observed.

Significantly higher proportions of labeled TCA cycle intermediates, in addition to [4,5-^{13}C] glutamate, an indication of TCA cycle activity, were observed in the cortex of HMP/O_2 kidneys compared with HMP/Air kidneys. Our results show oxygenation during HMP promotes TCA cycle activity, with ATP regeneration seen within cells as a result. In comparison, perfusate aeration seems to result in a metabolic phenotype, dependent on glycolytic pathway activity to produce ATP (Figure 7).

Other studies have also observed an increase in tissue ATP levels as a result of oxygenated HMP. In a small study using a porcine model of HMP, high levels of dissolved oxygen (100 kPa) using a membrane oxygenator increased tissue ATP resynthesis as detected by ^{13}P NMR spectroscopy.[13] Similarly, enzymatic analysis of tissue samples showed significantly higher levels of ATP after oxygenated machine perfusion compared to cold storage.[35] The relative increase in ATP levels in HMP/O_2 within the renal cortex is likely to be of benefit to graft function posttransplantation.

In contrast to the changes seen in the renal cortex, no significant changes in metabolic profile (Figure 4) or adenosine nucleotide levels (Figure 6) were observed in the medulla of HMP/O_2 and HMP/Air kidneys. This may reflect reduced perfusion of the medulla due to shunting of cortical blood flow seen in normal physiological conditions, with reduced medullary perfusion likely exaggerated in conditions of HMP, resulting in anaerobic metabolism.[36-38] Thus, the usual preponderance toward anaerobic metabolism is likely to be unaffected by oxygenated perfusion fluid if perfusion of the medulla is poor.

Changes in Perfusion Parameters

The effects of oxygenation are not limited to metabolism within the parenchyma. As a result of flow-related shear stress during nonmodified HMP, vascular endothelium may be protected by modulation of Kruppel-like factor 2 and subsequent upregulation of endothelial nitric oxide synthase signaling pathways,[39] even as a result of short durations of HMP.[6]

The observation of improved flow dynamics in HMP/O_2 kidneys did not reach statistical significance. This was likely a limitation of sample size as such improvement in renal flow dynamics has previously been observed during oxygenated HMP in other studies.[12,40] This may occur secondary to upregulation of endothelial nitric oxide synthase pathways, an oxygen-dependent process,[41] leading to increased renal artery nitric oxide–dependent vasodilation. Renal artery nitric oxide–dependent vasodilation is associated with improved early microcortical circulation after reperfusion of HMP kidneys[39] which may play a role in the prevention of

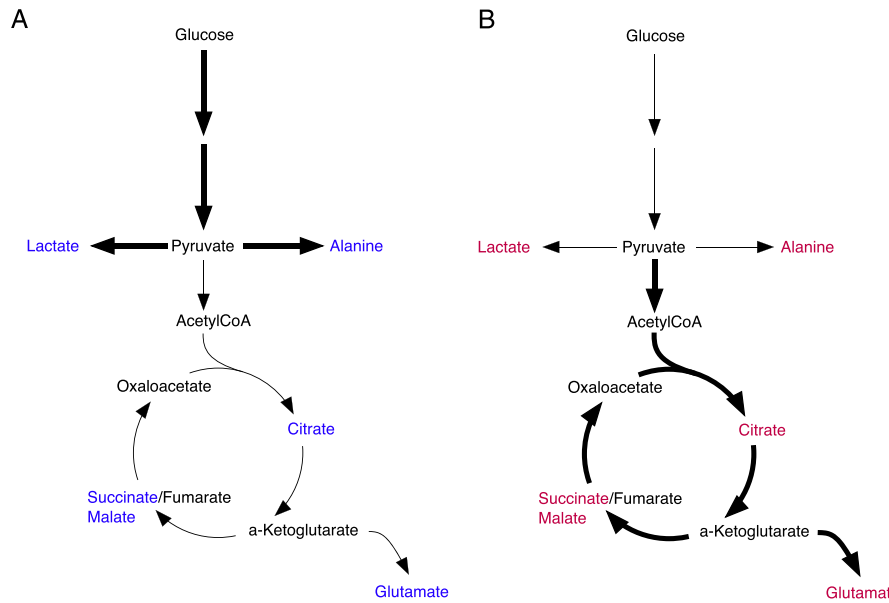

FIGURE 7. Differences in isotopic labeling patterns in the cortex of aerated hypothermic machine perfusion (HMP/Air) (blue) and oxygenated hypothermic machine perfusion (HMP/O_2) (red) kidneys. Thick black arrows indicate upregulated pathways interpreted from metabolite isotopomer combinations and metabolite concentrations indicating de novo activity.

delayed graft function. However, an alternative mechanism may be vasodilatation secondary to dissolved CO_2, a constituent of carbogen.

Given notable changes in metabolic profile between HMP/O_2 and HMP/Air kidneys in addition to a sevenfold increase in ATP levels in the renal cortex, small differences in flow are unlikely to be the sole determinant of the observed changes between the 2 groups. The localized use of the vasodilator papaverine has been explored in the setting of live donor nephrectomy with favorable clinical effect.[42] With HMP lending itself to delivery of drugs throughout the ex vivo kidney, such vasodilator administration in an unmodified HMP circuit would determine the extent to which flow effects alone promote beneficial changes in hypoxic conditions.

Structural Changes as a Result of Oxygenation

The benefits of oxygenation are reflected in the histology seen on light microscopy and electron microscopy. The increased shrinkage of glomeruli within the HMP/Air group indicates acute changes due which are likely due to lower perfusion pressures, in keeping with worse perfusion characteristics detected in this group. This diminished flow, together with the lower oxygen content of the perfusate produces relative ischemia evidenced by the increased injury to the tubules in this group with a higher percentage of morphologically abnormal mitochondria. However, the degree of change is still compatible with tubular epithelial cell recovery with well less than half the mitochondria containing flocculent densities, suggesting avoidance of irreversible cell injury.[43] Chromatin condensation of nuclei was seen in both groups and is a sign of reversible cell injury.[44] This degree of injury would suggest that, despite the cells being able to recover, the time to recovery may be increased, resulting in prolonged delayed or poor graft function.

Changes in mitochondrial architecture have been noted as a result of IRI during renal transplantation process.[45] Yet despite recent interest, no study has assessed the changes in mitochondrial morphology using EM in kidneys undergoing oxygenated HMP. Mitochondrial changes have been studied during HMP of hearts. Preserved architecture of mitochondria during oxygenated HMP of hearts has been observed with damage in those organs in static storage manifesting as mitochondrial flattening.[46]

Metabolic pathway activity central to aerobic metabolism, namely TCA activity cycle and oxidative phosphorylation, occur within mitochondria. Hence preservation of mitochondrial architecture may facilitate such aerobic metabolism contributing to higher levels of ATP in HMP/O_2 kidneys.

Harmful Effects of Oxygenation

Our results showed equivalence of damage due to ROS in both experimental conditions, suggesting that delivery of high concentrations of O_2 via perfusate during HMP is nondetrimental. However, conclusions drawn from such results may be limited due to both sample size and timing of IRI; our model does not take into account injury as a consequence of reperfusion.

Functional Outcomes

To date, 2 autotransplantation porcine studies have shown short-term functional benefits of perfusate oxygenation compared with a nonoxygenated control, both for prolonged periods (>20 hours) using DCD models.[11,47]

Potential functional benefits of the changes we have demonstrated are yet to be explored in the clinical setting. Clinical trials are currently under way investigating the use of oxygenation in HMP of kidneys in differing scenarios. The POMP trial seeks to compare outcomes of oxygenated HMP kidneys compared with static cold storage in high-risk donor organs, whereas the COMPARE trial is assessing the value of oxygenated versus nonoxygenated HMP.[48] We await the results of these trials to ascertain whether the differences we have observed translate into clinical benefit.

Limitations

While describing the metabolic profile and tissue adenine nucleotide levels of HMP/O_2 and HMP/Air kidneys, our preclinical large animal perfusion model used slaughterhouse kidneys with limitations inherent to such models.

Conclusions drawn from histology and HPLC data were limited due to sample size because not all pairs of kidneys underwent analysis. The significant differences noted between HMP/O_2 and HMP/Air kidneys should be reproduced in further research.

Oxygenation of the HMP/O_2 circuit was provided using a membrane oxygenator resulting in concentrations in the "arterial limb" of the circuit of 68.7 kPa. Arguably, such high concentrations are not required to supplement metabolism during hypothermia. Carbogen, used in the HMP/O_2 arm of the study, contains supraphysiological (5%) levels of carbon dioxide. When dissolved in the solution, it is likely to have resulted in a lower pH, changing the acid-base balance of interstitial fluid. However, KPS-1 contains pH buffers, such as HEPES which counteracts this acidity.

CONCLUSIONS

With increasing numbers of transplants from high-risk donors being performed to address organ shortage,[49] strategies to optimize donor organs have the potential to improve outcomes and increase utilization of such marginal organs. Oxygenation of circulating perfusion fluid during HMP is 1 potential method of optimization with a multitude of beneficial sequelae demonstrated by evidence of aerobic respiration using tracer-based metabolism, regeneration of ATP stores and improved perfusion characteristics with reciprocal histological changes in the absence of demonstrable damage secondary to oxidative stress.

ACKNOWLEDGMENTS

The authors would like to thank Sefa Canbilen, Samuel Ebbs, Alex Hollis, William Ries and Charlotte Turnbull for their contributions to this work.

REFERENCES

1. O'Callaghan JM, Morgan RD, Knight SR, et al. Systematic review and meta-analysis of hypothermic machine perfusion versus static cold storage of kidney allografts on transplant outcomes. *Br J Surg*. 2013;100:991–1001.
2. Patel K, Nath J, Hodson J, et al. Outcomes of donation after circulatory death kidneys undergoing hypothermic machine perfusion following static cold storage: a UK population-based cohort study. *Am J Transplant*. 2018;18:1408–1414.
3. Moers C, Smits JM, Maathuis MH, et al. Machine perfusion or cold storage in deceased-donor kidney transplantation. *N Engl J Med*. 2009;360:7–19.
4. Moers C, Pirenne J, Paul A, et al. Machine Preservation Trial Study G. Machine perfusion or cold storage in deceased-donor kidney transplantation. *N Engl J Med*. 2012;366:770–771.

5. Jochmans I, Moers C, Smits JM, et al. The prognostic value of renal resistance during hypothermic machine perfusion of deceased donor kidneys. *Am J Transplant*. 2011;11:2214–2220.
6. Gallinat A, Efferz P, Paul A, et al. One or 4 h of "in-house" reconditioning by machine perfusion after cold storage improve reperfusion parameters in porcine kidneys. *Transpl Int*. 2014;27:1214–1219.
7. Bon D, Billault C, Thuillier R, et al. Analysis of perfusates during hypothermic machine perfusion by NMR spectroscopy: a potential tool for predicting kidney graft outcome. *Transplantation*. 2014;97:810–816.
8. Nath J, Smith TB, Patel K, et al. Metabolic differences between cold stored and machine perfused porcine kidneys: A ^{1}H NMR based study. *Cryobiology*. 2017;74:115–120.
9. Guy AJ, Nath J, Cobbold M, et al. Metabolomic analysis of perfusate during hypothermic machine perfusion of human cadaveric kidneys. *Transplantation*. 2015;99:754–759.
10. O'Callaghan JM, Pall KT, Pengel LHM, et al. Supplemental oxygen during hypothermic kidney preservation: a systematic review. *Transplant Rev (Orlando)*. 2017;31:172–179.
11. Thuillier R, Allain G, Celhay O, et al. Benefits of active oxygenation during hypothermic machine perfusion of kidneys in a preclinical model of deceased after cardiac death donors. *J Surg Res*. 2013;184:1174–1181.
12. Gallinat A, Paul A, Efferz P, et al. Role of oxygenation in hypothermic machine perfusion of kidneys from heart beating donors. *Transplantation*. 2012;94:809–813.
13. Buchs JB, Lazeyras F, Ruttimann R, et al. Oxygenated hypothermic pulsatile perfusion versus cold static storage for kidneys from non heart-beating donors tested by in-line ATP resynthesis to establish a strategy of preservation. *Perfusion*. 2011;26:159–165.
14. 't Hart NA, van der Plaats A, Faber A, et al. Oxygenation during hypothermic rat liver preservation: an in vitro slice study to demonstrate beneficial or toxic oxygenation effects. *Liver Transpl*. 2005;11:1403–1411.
15. Lenton KJ, Therriault H, Fulop T, et al. Glutathione and ascorbate are negatively correlated with oxidative DNA damage in human lymphocytes. *Carcinogenesis*. 1999;20:607–613.
16. Will O, Mahler HC, Arrigo AP, et al. Influence of glutathione levels and heat-shock on the steady-state levels of oxidative DNA base modifications in mammalian cells. *Carcinogenesis*. 1999;20:333–337.
17. Sies H. Oxidative stress: from basic research to clinical application. *Am J Med*. 1991;91:31S–38S.
18. Ohkawa H, Ohishi N, Yagi K. Assay for lipid peroxides in animal tissues by thiobarbituric acid reaction. *Anal Biochem*. 1979;95:351–358.
19. Nath J, Smith T, Hollis A, et al. (13)C glucose labelling studies using 2D NMR are a useful tool for determining ex vivo whole organ metabolism during hypothermic machine perfusion of kidneys. *Transplant Res*. 2016;5:7.
20. Nath J, Guy A, Smith TB, et al. Metabolomic perfusate analysis during kidney machine perfusion: the pig provides an appropriate model for human studies. *PLoS One*. 2014;9:e114818.
21. Hosgood SA, Yates PJ, Nicholson ML. 1400W reduces ischemia reperfusion injury in an ex-vivo porcine model of the donation after circulatory death kidney donor. *World J Transplant*. 2014;4:299–305.
22. Kootstra G, Daemen JH, Oomen AP. Categories of non-heart-beating donors. *Transplant Proc*. 1995;27:2893–2894.
23. Ludwig C, Gunther UL. MetaboLab—advanced NMR data processing and analysis for metabolomics. *BMC Bioinformatics*. 2011;12:366.
24. Delaglio F, Grzesiek S, Vuister GW, et al. NMRPipe: a multidimensional spectral processing system based on UNIX pipes. *J Biomol NMR*. 1995;6:277–293.
25. Kazimierczuk K, Orekhov VY. Accelerated NMR spectroscopy by using compressed sensing. *Angew Chem Int Ed Engl*. 2011;50:5556–5559.
26. Orekhov VY, Jaravine VA. Analysis of non-uniformly sampled spectra with multi-dimensional decomposition. *Prog Nucl Magn Reson Spectrosc*. 2011;59:271–292.
27. Chong M, Jayaraman A, Marin S, et al. Combined analysis of NMR and MS spectra (CANMS). *Angew Chem Int Ed Engl*. 2017;56:4140–4144.
28. Hiller K, Hangebrauk J, Jager C, et al. MetaboliteDetector: comprehensive analysis tool for targeted and nontargeted GC/MS based metabolome analysis. *Anal Chem*. 2009;81:3429–3439.
29. Sellevold OFJynge P, Aarstad K. High performance liquid chromatography: a rapid isocratic method for determination of creatine compounds and adenine nucleotides in myocardial tissue. *J Mol Cell Cardiol*. 1986; 18:517–527.
30. Hissin PJ, Hilf R. A fluorometric method for determination of oxidized and reduced glutathione in tissues. *Anal Biochem*. 1976;74:214–226.
31. Bradford MM. A rapid and sensitive method for the quantitation of microgram quantities of protein utilizing the principle of protein-dye binding. *Anal Biochem*. 1976;72:248–254.
32. Taylor MJ, Baicu SC. Current state of hypothermic machine perfusion preservation of organs: The clinical perspective. *Cryobiology*. 2010;60: S20–S35.
33. Southard JH, Belzer FO. Organ preservation. *Annu Rev Med*. 1995;46: 235–247.
34. Belzer FO, Southard JH. Organ preservation and transplantation. *Prog Clin Biol Res*. 1986;224:291–303.
35. Minor T, Sitzia M, Dombrowski F. Kidney transplantation from non-heart-beating donors after oxygenated low-flow machine perfusion preservation with histidine-tryptophan-ketoglutarate solution. *Transpl Int*. 2005; 17:707–712.
36. Chen Y, Fry BC, Layton AT. Modeling glucose metabolism in the kidney. *Bull Math Biol*. 2016;78:1318–1336.
37. Ganguli M, Tobian L. Does the kidney autoregulate papillary plasma flow in chronic postsalt hypertension? *Am J Physiol*. 1974;226:330–333.
38. Stern MD, Bowen PD, Parma R, et al. Measurement of renal cortical and medullary blood flow by laser-Doppler spectroscopy in the rat. *Am J Physiol*. 1979;236:F80–F87.
39. Chatauret N, Coudroy R, Delpech PO, et al. Mechanistic analysis of nonoxygenated hypothermic machine perfusion's protection on warm ischemic kidney uncovers greater eNOS phosphorylation and vasodilation. *Am J Transplant*. 2014;14:2500–2514.
40. Darius T, Gianello P, Vergauwen M, et al. The effect on early renal function of various dynamic preservation strategies in a preclinical pig ischemia-reperfusion autotransplant model. *Am J Transplant*. 2018;1: DOI:10. 1111/ajt.15100.
41. Stuehr DJ. Enzymes of the L-arginine to nitric oxide pathway. *J Nutr*. 2004; 134:2748S–2751S; discussion 65S-67S.
42. Zacherl J, Bock S, Feussner H, et al. Periarterial application of papaverine during laparoscopic donor nephrectomy improves early graft function after kidney transplantation in pigs. *Surg Endosc*. 2004;18:417–420.
43. Myagkaya GL, van Veen H, James J. Quantitative analysis of mitochondrial flocculent densities in rat hepatocytes during normothermic and hypothermic ischemia in vitro. *Virchows Arch B Cell Pathol Incl Mol Pathol*. 1985;49:61–72.
44. Trump BF, Berezesky IK. Calcium-mediated cell injury and cell death. *FASEB J*. 1995;9:219–228.
45. Kosieradzki M, Rowinski W. Ischemia/reperfusion injury in kidney transplantation: mechanisms and prevention. *Transplant Proc*. 2008;40: 3279–3288.
46. Michel SG, La Muraglia GM 2nd, Madariaga ML, et al. Twelve-hour hypothermic machine perfusion for donor heart preservation leads to improved ultrastructural characteristics compared to conventional cold storage. *Ann Transplant*. 2015;20:461–468.
47. Hoyer DP, Gallinat A, Swoboda S, et al. Influence of oxygen concentration during hypothermic machine perfusion on porcine kidneys from donation after circulatory death. *Transplantation*. 2014;98:944–950.
48. Consortium C The COPE Consortium for organ preservation in Europe. Available at http://cope-eu.com/work%20programme/trials.html. Published 2018.
49. Nath J, Field M, Ebbs SR, et al. Evolution of renal transplant practice over the past decade: a U.K. center experience. *Transplant Proc*. 2015;47: 1700–1704.

Supplementary information

Supplementary methods: Light Microscopy

Grading of injury

To calculate glomerular shrinkage, the percent glomerular area occupied by glomerular tuft was determined for each glomerulus. The mean distance between 25 random tubules for each photomicrograph was used as a surrogate marker of interstitial oedema. The proportion (%) of vessel area to adventitia was calculated to determine the extent of perivascular oedema; lower percentages indicated more perivascular oedema.

The injury of extra-parenchymal renal arteries were semi-quantitatively graded: endothelial denudation: 0 nil, 1 minimal, 2, moderate, 3 extensive; Intimal oedema: 0 nil, 1 focal, 2 moderate to extensive; medial oedema and vacuolation of smooth muscle cells: 0 normal, 1 minimal, 2 moderate to extensive.

Supplementary Table 1. Concentrations of metabolites in circulating perfusion fluid in HMP/Air and HMP/O_2 kidneys at three time-points. Data reported as the mean with 95% confidence intervals. No differences were detected using Wilcoxon signed rank test.

		HMP Air	HMP O_2	
Metabolite	Timepoint (hours)	Mean concentration (mM)	Mean concentration (mM)	p-value
Acetate	6	0.6432 (0.3881- 0.8983)	0.3882 (0.1464- 0.6299)	0.1484
	12	0.4812 (0.2226- 0.7398)	0.301 (0.09802- 0.5039)	0.2969
	18	0.2892 (0.1465- 0.432)	0.2267 (0.03756- 0.4158)	0.3125
Alanine	6	0.4942 (0.311- 0.6773)	0.8764 (0.6616- 1.091)	0.0781
	12	0.7721 (0.5508- 0.9934)	1.068 (0.7442- 1.393)	0.3750
	18	0.8636 (0.5715- 1.156)	0.805 (0.2948- 1.315)	0.8438
Aspartate	6	0.09388 (0.04793- 0.1398)	0.08898 (0.02494- 0.153)	0.9453
	12	0.1129 (0.0509- 0.1748)	0.1504 (0.04669- 0.254)	0.5625
	18	0.09854 (0.05544- 0.1416)	0.232 (0.03162- 0.4324)	0.1953
Formate	6	0.6554 (0.5513- 0.7595)	0.4886 (0.4019- 0.5753)	0.0547
	12	0.6229 (0.4387- 0.8071)	0.3335 (0.2193- 0.4478)	0.1094
	18	0.5342 (0.3275- 0.7408)	0.2658 (0.1244- 0.4071)	0.0781
Fumarate	6	0.0325 (0.02372- 0.04128)	0.04 (0.02222- 0.05778)	0.3125
	12	0.03516 (0.01771- 0.0526)	0.02375 (0.0131- 0.0344)	0.2188
	18	0.02631 (0.008369- 0.04426)	0.01365 (0.001337- 0.02596)	0.1953
Glutamate	6	2.175 (1.572- 2.779)	1.798 (1.358- 2.238)	0.1484
	12	2.179 (1.2- 3.158)	1.356 (0.9- 1.812)	0.1094
	18	2.009 (1.283- 2.736)	1.038 (0.5943- 1.481)	0.0547
Glutathione	6	0.174 (0.04471- 0.3033)	0.1493 (0.07892- 0.2197)	0.9453
	12	0.08507 (0.03118- 0.139)	0.06165 (0.04287- 0.08043)	0.3750
	18	0.0499 (0.01569- 0.08411)	0.04923 (0.02442-0.07403)	>0.9999
Glycine	6	2.391 (1.021- 3.761)	2.87 (1.684- 4.057)	0.3125
	12	2.558 (0.8218- 4.294)	2.814 (1.205- 4.424)	0.8125
	18	2.579 (0.9483- 4.209)	3.027 (1.621- 4.433)	0.7422
Lactate	6	1.729 (1.531-1.927)	1.789 (1.414-2.164)	>0.9999
	12	1.926 (1.18-2.671)	1.775 (1.368-2.182)	0.5469
	18	2.29 (1.548-3.032)	1.503 (0.7044-2.302)	0.2188

Supplementary Table 2. Concentration of unlabelled metabolites in the renal cortex and medulla of HMP/O2 and HMP/Air kidneys at the end of the perfusion period. Data reported as the mean with 95% confidence intervals. *- denotes statistical significance ($p<0.05$).

		HMP Air	HMP O_2	
Metabolite		Mean concentration (mmol/L)	Mean concentration (mmol/L)	p-value
Acetate	Cortex	0.05245 (0.0432-0.0617)	0.08451 (0.0554-0.1136)	0.0391*
	Medulla	0.04685 (0.02492-0.06878)	0.05908 (0.03132-0.08684)	0.6875
Adenosine	Cortex	0.01366 (0.002765-0.02456)	0.01221 (-0.005972-0.0304)	0.2969
	Medulla	0.003717 (0.0001949-0.007238)	0.003717 (-0.0005598-0.007993)	0.8125
Alanine	Cortex	0.4041 (0.2678-0.5403)	0.7062 (0.2346-1.178)	0.2062
	Medulla	0.4391 (0.3458-0.5324)	0.4442 (0.2773-0.6111)	>0.9999
Aspartate	Cortex	0.1922 (0.115-0.2694)	0.4046 (0.2216-0.5877)	0.1094
	Medulla	0.07462 (0.02917-0.1201)	0.1536 (0.1299-0.1773)	0.0312*
Choline	Cortex	0.2869 (0.1782-0.3957)	0.1778 (0.081-0.2746)	0.0781
	Medulla	0.7114 (0.474-0.9487)	0.2215 (0.1444-0.2986)	0.0312*
Formate	Cortex	0.0833 (0.0595-0.1071)	0.09251 (0.0541-0.1309)	0.7422
	Medulla	0.1569 (0.1237-0.19)	0.1606 (0.1335-0.1877)	>0.9999
Fumarate	Cortex	0.008588 (0.006257-0.01092)	0.01221 (0.006307-0.01812)	0.1094
	Medulla	0.0054 (0.00288-0.00792)	0.003717 (0.002313-0.005121)	0.1562
Glutamate	Cortex	1.404 (0.9528-1.855)	0.8665 (0.673-1.06)	0.0391*
	Medulla	0.9594 (0.7049-1.214)	0.3343 (0.2614-0.4072)	0.0312*
Glutathione	Cortex	0.08573 (0.05128-0.1202)	0.1131 (0.07727-0.149)	0.0078*
	Medulla	0.0768 (0.03106-0.1225)	0.1293 (0.0959-0.1627)	0.1562
Glycine	Cortex	1.567 (1.22-1.913)	2.451 (1.736-3.166)	0.0781
	Medulla	1.126 (1.003-1.249)	1.087 (0.9197-1.253)	0.8438
Lactate	Cortex	0.5524 (0.4141-0.6907)	0.451 (0.2684-0.6336)	0.3828
	Medulla	1.094 (0.689-1.5)	0.8526 (0.436-1.269)	0.3125
NAD+	Cortex	0.07948 (0.06527-0.09368)	0.09638 (0.06367-0.1291)	0.2500
	Medulla	0.02218 (0.009974-0.03439)	0.0191 (0.004708-0.03349)	0.6875
NADP+	Cortex	0.004188 (0.002453-0.005922)	0.01099 (0.0009992-0.02098)	0.0391*
	Medulla	0.0005667 (-0.00089-0.002023)	0.001167 (-0.0007714-0.003105)	0.7500
Trimethylamine N-oxide	Cortex	0.2047 (0.0976-0.3119)	0.5001 (0.238-0.7621)	0.0156*

	Medulla	2.079 (1.211-2.946)	1.904 (1.283-2.524)	0.6875
Tyrosine	Cortex	0.02749 (0.02031-0.03466)	0.04108 (0.03343-0.04872)	0.0234*
	Medulla	0.02658 (0.01697-0.0362)	0.0293 (0.02292-0.03568)	0.4375
Valine	Cortex	0.03829 (0.02902-0.04755)	0.05793 (0.04086-0.07499)	0.0391*
	Medulla	0.05755 (0.04043-0.07467)	0.05982 (0.04388-0.07576)	>0.9999

Supplementary Table 3. Mean Adenine nucleotide concentrations for HMP/O_2 and HMP/Air kidneys. *-denotes significance where p<0.05

		HMP/O_2	HMP/Air	
		Concentration (nmol/mg)	Concentration (nmol/mg)	p-value
Cortex	AMP	102.7	98.3	0.485
	ADP	14.6	4.6	0.029*
	ATP	19.8	2.8	0.029*
	Total (AMP+ADP+ATP)	137.2	105.7	0.029*
Medulla	AMP	205.6	164	0.057
	ADP	16.2	8.9	0.057
	ATP	5.1	2.5	0.114
	Total (AMP+ADP+ATP)	226.9	175.5	0.057

Chapter 7 : Metabolic characterisation of machine perfused cadaveric kidneys for transplantation using ^{13}C enriched glucose

In this chapter a clinical study was performed involving human cadaveric kidneys prior to transplantation. Organs were perfused with specially formulated UW-MPS solution in which all 10mmol glucose comprised of the metabolic tracer [U-^{13}C] glucose. Whilst initially referred to as a study entitled “Metabolic characterisation of machine perfused cadaveric kidneys for transplantation using ^{13}C enriched glucose,” the study was re-branded the ^{13}CHAMPION study for easier recognition in the clinical setting (see Figure 43).

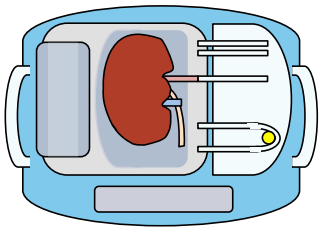

Figure 43. Champion study logo

Ethical approval for the study, along with local NHS trust Research and Development committee approval were gained by my supervisor Jay Nath prior to commencing patient recruitment. I was involved in study design and was responsible for all experimental work including local implementation of protocols, patient recruitment, preparation of all kidneys prior to perfusion, sampling, sample processing and analysis. A laboratory technician Thomas Smith assisted with performing biochemical assays. Study consumables relating to machine perfusion including customised perfusion fluid were provided by Organ Recovery Systems limited.

Introduction

Analysis of metabolites within perfusion fluid: studies to date

The 10mmol of glucose contained within each litre of UW-MPS provides a metabolic substrate to kidneys undergoing HMP. Metabolism of this glucose has been illustrated by supplementing perfusion fluid with 5mmol [U-^{13}C] glucose, a metabolic tracer, demonstrating *de novo* metabolism in porcine and discarded human kidneys (175). In this proof of concept study performed by our unit, unequivocal evidence of *de novo* anaerobic metabolism was observed as evidenced by the presence of [U-^{13}C lactate] and [U-^{13}C alanine] in perfusate and renal cortex samples. The presence of glutamate with ^{13}C enrichment in the 4 and 5 carbon positions indicated limited *de novo* aerobic activity.

Similarly in Chapter 6, the supplementation of perfusion fluid with an additional 5mmol of isotopic [U-^{13}C] glucose showed in both aerated and oxygenated porcine kidneys, anaerobic metabolism dominated in the first 8 hours of HMP as evidenced by increasing concentrations of [U-^{13}C] lactate and [U-^{13}C] alanine in circulating perfusion fluid during HMP (240). In addition, labelling patterns of glutamate indicative of aerobic metabolism were detected in both perfusion fluid and renal cortex at the study endpoint.

In these porcine experimental studies, 5mmol of [U-^{13}C] glucose was added to the UW-MPS solution containing 10mmol unlabelled ^{12}C glucose. This was performed for simplicity as there was no easy way to remove the existing glucose in a sterile manner. In both studies, supplementing perfusion fluid with additional glucose increased its osmolarity, changing the biological properties of the perfusion fluid with possibilities of such a change including increased glucose uptake into cells.

In a previously described human metabolic study of circulating perfusate, Guy et al used 1D ^{1}H NMR (173) to determine changes in metabolite concentrations in circulating perfusate, with ROC curves indicating glucose, inosine and leucine may predict the development of DGF. In this study both alanine and lactate concentrations increased over between 45 minutes and four hours. Using a porcine model, Bon et al (172) utilised 1D ^{1}H NMR to show how changes in several metabolites including lactate may be associated with graft function following auto-transplantation, with the suggestion that changes in biomarker levels were less marked in those kidneys with a better functional outcome. In both studies, the increase in concentration of metabolites in perfusion fluid cannot be attributed to *de novo* metabolism alone. Cell damage during preceding static cold storage, in addition to anaerobic metabolism during these periods likely contributes to metabolite concentrations observed in perfusion fluid as they are simply washed out of the kidney when HMP is commenced, one of the beneficial mechanisms of HMP.

Hence, ongoing metabolism, in particular *de novo* metabolism as evidenced by use of [U-^{13}C glucose] as a metabolic tracer, reflects changing conditions such as oxygenation. *De novo* metabolism during HMP may therefore be influenced by demographic variables such as donor sub-type and cold ischaemic time as a reflection of pre-HMP warm and cold ischaemic insults respectively. Description of the metabolic profile of a cadaveric kidney during HMP, as described by changes in the concentration of *de novo* metabolites, may be a useful tool in determining organ viability with the potential to predict clinical outcome.

Proteomic biomarkers in the setting of HMP

Studies continue to explore associations between perfusate proteomic biomarkers and post-transplantation outcome (95) as evidence of the potential utility of HMP to assess organ viability. Of note, Bhangoo et al performed a comprehensive systematic review in

2012 (95) identifying 3 perfusate biomarkers predictive of the development of DGF although recency, lack of good study design and the identification of only weak inconsistent correlations are the main reasons for lack of widespread use. These cytosolic proteins, lactate dehydrogenase (LDH), glutathione s transferase (GST) and aspartate transaminase (AST), leak into the interstitia and intra-vascular space through the cell membranes of ischaemically injured cells.

Lactate dehydrogenase (LDH), the enzyme which catalyses the conversion of pyruvate both to and from lactate, is a non-specific marker of cellular injury. Perfusate LDH concentrations have been found to be significantly higher in kidneys which develop DGF in several studies, with Moers et al reporting an area under the curve of 0.60 in the cohort of patients from the Machine Preservation Trial (96, 241).

Glutathione S-transferases (GST) are a family of enzymes which play a major role in detoxification, protecting cells from oxidative stress. Given the significance of urinary GST levels as a marker of renal injury in cardiac surgery (242) and other clinical settings, it is perhaps unsurprising given in the closed circuit of HMP, several studies have shown a potential role of perfusate GST as a biomarker (96). More specifically, perfusate levels of isoenzyme π-GST have been shown to be associated with delayed graft function (97).

Aspartate transaminase, an enzyme more commonly associated with the liver, is also expressed by damaged renal parenchymal cells, with one study demonstrating an AUC 0.61 (96).

More recent studies have identified further promising biomarkers including neutrophil gelatinase–associated lipocalin. The small polypeptide NGAL is expressed primarily in proliferating and regenerating tubular epithelial cells. NGAL acts to attract iron-containing

siderophores involved in cell growth and survival (243) whilst also enhancing the delivery of iron and protecting kidney tubule cells by upregulating haem oxygenase-1 (244).

As serum and urine NGAL concentrations rise in proportion to the grade of kidney injury (245) it is perhaps unsurprising that both pre-clinical (246) and clinical (247) studies have suggested that perfusate concentration of the molecule may predict graft function at 6 months. The same study by Parikh et al (247) identified liver-type fatty acid-binding protein (L-FABP) as another biomarker of graft function at 6 months.

Due to the promise of LDH, GST-Pi and NGAL as potential biomarkers of organ damage, biochemical assays for these proteomic markers were performed on perfusate samples.

Study aims

The aim of this study was to describe the *de novo* metabolism occurring in the *ex vivo* cadaveric kidney during HMP and to determine whether such metabolism correlated with functional outcomes following transplantation. A study was designed using [U-^{13}C] glucose as a metabolic tracer. Such use of a metabolic tracer in the clinical setting to describe metabolic activity during HMP is a novel, non-invasive, sensitive method of describing *de novo* metabolism in whole organs.

Secondary aims were to determine associations between demographic and transplant variables, and metabolic profile. Biochemical assays were also performed in order to determine correlation between the proteomic biomarkers LDH, GST-Pi and NGAL, and *de novo* metabolism.

Methods

Study design

Ethical approval for the study was sought from the National Research Ethics Service (NRES) Committee East Midlands – Leicester, NHS Health Research Authority (15/EM/0328) on 07/09/15 (Appendix B). The research protocol and accompanying documentation were approved by the trust's Research and Development department on 24/11/15 (Appendix C). Documentation, including a study log, recruitment log, delegation of duties, confirmation of ethical approval, University Hospitals Birmingham Research and Development department approval and copies of study documentation including data collection tools were kept securely in the study site file.

The decision to use HMP as a method of preservation was decided by the on-call consultant depending on donor-recipient issues and theatre availability. During the study period all recipients of cadaveric kidneys where donor kidney was likely to be preserved with machine perfusion were approached for inclusion in the study. All patients were consented in line with Good Clinical Practice guidance (248), asked to sign a consent form (Appendix D) and were given a patient information sheet (Appendix E). Paediatric donor kidneys and those as part of a multi-organ transplant were excluded.

Following recipient recruitment and arrival of donor organ into centre, arrangements were made for an emergency theatre to be made available for the purpose of preparing the kidney for machine perfusion. Following receipt of cadaveric organs, 'back-bench' preparation of the kidney was performed as described in Chapter 2.

Hypothermic Machine Perfusion

The kidney was fully prepared for transplantation excluding lengthening of vasculature. The LifePort® provides arterial pulsatile perfusion regulated at 30mmHg via either a RingSeal connector or a T-connector as described in Chapter 2, Figure 32. The decision was made to avoid using T-connectors unless necessary as tying a suture to secure the connector damages the artery making it more susceptible to arterial thrombosis.

All kidneys were perfused with one litre of a custom formulation of KPS-1 (Organ Recovery Systems, USA) stored at 4°C (Figure 34). In this modified KPS-1, biologically identical to industry standard UW-MPS, perfusion fluid had been formulated to include 10mmol [U-^{13}C] glucose instead of conventional ^{12}C glucose. Kidneys were perfused in either v1.0 or v1.1 LifePort® Kidney Transporters (Organ Recovery Systems (Itasca, IL, USA) used in standard clinical practice at our unit. Perfusion pressure was set at 30mmHg. This was not changed for the duration of HMP in line with normal unit practice. Temperature and perfusion parameters were recorded at each sampling timepoint.

No kidney was discarded as a result of machine perfusion parameters (flow, resistance). All patients received standard post-operative care with peri-operative and post-operative immunosuppression as per the unit's standardised protocol. Due to the unpredictable nature of theatre availability and logistics of organ transplantation, kidneys were not perfused for a predetermined time period.

Perfusate Sampling

Perfusate was sampled prior to commencing machine perfusion in addition to the following times following commencement of machine perfusion: 5 minutes, 1 hour, 4 hours then at 4 hourly intervals until machine perfusion was ceased. An additional end point sample

was taken where machine perfusion was ceased greater than half an hour following the previous perfusate sample.

At each timepoint 5ml circulating perfusion fluid was removed from the Lifeport® sampling port under aseptic conditions as described in Chapter 2. One ml of fluid was used for Point of Care (POC) analysis (Cobas® b221, Roche Diagnostics Limited) to provide pH, pO_2, pCO_2, lactate and glucose level in real time. The remaining 4ml of fluid was divided into 2 x 2ml cryovials. The cryovials were immediately placed in dry ice prior to transport to a -80°C freezer.

Determination of metabolite concentrations using NMR and Mass Spectrometry

Perfusate samples were thawed before vortexing for 30 seconds. Following this, 430μL of perfusate was removed from each 2ml cryovial in preparation for NMR processing. This involved mixing with 200μL NMR buffer with further mixing via vortexing and centrifugation prior to placing 600μL in a 5mm NMR tube. Both 1D ^{1}H NMR and 2D ^{1}H, ^{13}C HSQC NMR spectra were acquired using a 600-MHz Bruker Avance III NMR spectrometer. From each sample cryovial, 43μL was also removed for analysis by mass spectrometry.

The resulting output NMR spectra were referenced and manually phase corrected before the spectral baseline was corrected using MetaboLab's spline baseline correction (177). The spectra were then exported to Bruker format for metabolites to be quantified using Chenomx 8.2 (Chenomx INC, Edmonton, AB, Canada). Final metabolite concentrations accounted for dilution with NMR buffer during sample preparation.

The complex 1D ^{1}H NMR spectral pattern of glucose results in difficulties when determining glucose concentrations using NMR due to overlapping of spectral peaks of other metabolites at multiple positions along the chemical shift axis. Therefore glucose concentrations were determined in real time using point of care analysis.

MetaboLab was used to combine data from 2D $^{1}H,^{13}C$ HSQC NMR and GC-MS using a model free approach (158) as discussed in Chapter 1 in order to give more accurate isotopomer distributions for key metabolites of interest. The total concentrations of alanine and lactate were determined by adjusting ^{1}H NMR concentrations taking into account isotopomer distributions as determined by 2D $^{1}H,^{13}C$ HSQC NMR. More in-depth commentary and explanation of sample processing methods and analysis is described in Chapter 2.

Biochemical Assays

Once thawed and mixed via vortexing for 30 seconds, perfusate samples were removed for analysis using three biochemical assays; lactate dehydrogenase (LDH), neutrophil gelatinase-associated lipocalin (NGAL) and glutathione s transferase Pi (GST-Pi) as described in Chapter 2.

Clinical outcomes

Clinicians were not blinded to the use of HMP during the preservation period. However, this is not thought to have influenced clinical decision making. Delayed graft function was defined by the need for dialysis in the first 7 days following transplantation. Serum creatinine values were recorded at 1 week, 1 month, 6 months and 1 year post-operatively. Creatinine values were excluded from statistical analyses for patients with DGF until graft function was gained and haemodialysis subsequently stopped as a result.

Statistical analysis

Fisher's exact test and Mann-Whitney U test were used to compare groups. Unless specified, a two-tailed Spearman's rank correlation was used to determine whether there was a correlation existed for continuous data as datasets were assumed to be non-normally distributed. For continuous data, median values are reported along with range of values.

Statistical analysis was performed using GraphPad Prism version 8.00 for Mac OS X (GraphPad Software, La Jolla, CA). Analyses were deemed to be statistically significant when p-value was less than 0.05.

Results

Firstly, baseline demographics are reported for the kidneys perfused as part of this study including donor, recipient and transplant specific variables. Following this, clinical outcomes are reported for the cohort.

Changes in metabolite concentrations and flow parameters during HMP are described before possible associations are sought between such changes and clinical outcomes. Data relating to the timing of machine perfusion is also described for the cohort with a similar analysis relating to clinical outcome. Metabolite analysis according to donor subtype is then described. Biochemical assay results for the cohort follows with a search for an association between assay results and clinical outcome.

Finally, the effect of anaerobic metabolite concentrations on pH is described in addition to the composition of neat KPS-1 and accuracy of sample processing.

Baseline demographics

Between October 2016 and July 2018, 16 deceased donor kidneys were recruited for inclusion in the study and subsequently underwent perfusion with [U-^{13}C] glucose KPS-1. Following assessment after a period of HMP, one kidney was deemed unsuitable for transplantation due to anatomical reasons relating to the recipient. This kidney was transplanted at another centre following a further four-hour period of SCS. Due to this additional period of SCS and lack of consistency of clinical care between centres following transplantation, this kidney was excluded from further analysis.

One further kidney was excluded from analyses as graft failure was attributed solely to recipient factors. The patient suffered from severe haemodynamic compromise pre and

post-operatively with hypotension not responding well to vasopressor support. This caused graft hypoperfusion and subsequent renal vein thrombosis leading to graft explantation after 4 days.

Fourteen kidneys were included in the analysis. Table 5 shows baseline demographics including donor variables, recipient variables, and transplant timings including and within the total CIT. The cohort was divided by donor subtype and according to incidence of delayed graft function to determine whether donor factors differed in these groups. Differences between groups often lacked statistical significance although this was due to the small numbers involved in each group. DCD organs were retrieved from older donors compared to DBD kidneys (36.6yrs vs 33.2yrs) and were transplanted into older recipients (46.4yrs vs 33.5yrs).

Clinical outcomes

Following transplantation, recipients of four (28.6%) of the remaining 14 kidneys experienced delayed graft function which lasted between 4 and 42 days. Two of these kidneys which experienced DGF were from DCD donors, resulting in an incidence of DGF of 50% in the four DCD organs in the study. Of the 10 DBD kidneys in the study population, two recipients experienced DGF resulting in an incidence of DGF of 20% for DBD kidneys (p=0.5205).

Male gender was associated with inferior serum creatinine at 1 year but not at any other follow-up timepoint (Table 6, Table 7). No other demographic variable was associated with serum creatinine at any follow-up timepoint. Table 6 also shows serum creatinine values for sub-groups of the cohort including analysis by donor sub-type. No graft loss occurred during the one year study follow-up period for the 14 kidneys included in the analysis.

Median serum creatinine values were 168μmol/L at one week (range 89-488μmol/L, n=11), 123μmol/L at one month (range 56-233μmol/L, n=13), 122 μmol/L at six months (range 59-335μmol/L, n=14) and 129μmol/L at one year (range 75-267μmol/L, n=14).

Table 5. Description of demographic variables of study population with subgroup analysis according to development of DGF and donor sub-type. For categorical variables, data reported as N (%), with p-value from Fisher's exact test. For continuous variables, median values (range) are reported, with p-value from Mann-Whitney test. P-values significant at p<0.05.

	All **n=14**	**IGF** **n=10**	**DGF** **n=4**	**p-value**	**DBD** **n=10**	**DCD** **n=4**	**p-value**
Donor demographics							
Male	50.0% (n=7)	40.0% (n=4)	75% (n=3)	0.5594	40% (n=4)	75% (n=3)	0.5594
Age (yrs)	33.2 (18.1-73.3)	32.6 (18.1-65.5)	37.0 (26.7-73.3)	0.5395	33.2 (18.1 - 65.5)	36.6 (21.5 - 73.3)	0.8392
DCD donor	28.6% (n=4)	20.0% (n=2)	50% (n=2)	0.5205	n/a	n/a	n/a
Caucasian	100% (n=14)	100% (n=10)	100% (n=4)	>0.9999	100% (n=10)	100% (n=4)	>0.9999
Traumatic brain injury	21.4% (n=3)	30% (n=3)	0% (n=0)	0.5055	30.0% (n=3)	0% (n=0)	0.5055
History of hypertension	21.4% (n=3)	10% (n=1)	50% (n=2)	0.1758	20% (n=2)	25% (n=1)	>0.9999
History of diabetes	0% (n=0)	0% (n=0)	0% (n=0)	>0.9999	0% (n=0)	0% (n=0)	>0.9999
BMI (kg/m^2)	23.7 (17.1-43.0)	24.9 (17.1-43.0)	23.5 (20.2-23.8)	0.5395	22.66 (17.1 - 28.1)	28.0 (23.3 - 43)	0.1419
Recipient demographics							
Male	71.4% (n=10)	60.0% (n=6)	100% (n=4)	0.2507	70% (n=7)	75% (n=3)	>0.9999
Age (yrs)	37.6 (17.6-62.6)	31.3 (17.6-56.4)	42.7 (37.6-62.6)	0.1059	33.5 (17.6 - 56.4)	46.4 (31.4 - 62.6)	0.1419
BMI (kg/m^2)	29.7 (18.2-33.8)	29.7 (18.2-33.8)	25.8 (19.7-33.8)	0.8392	29.5 (18.2 - 33.8)	30.4 (21.9 - 33.8)	0.4535
Caucasian	57.1% (n=8)	80.0% (n=8)	0% (n=0)	**0.015***	60.0% (n=6)	50% (n=2)	>0.9999
History of hypertension	42.9% (n=6)	30.0% (n=3)	75.0% (n=3)	0.2448	30.0% (n=3)	75% (n=3)	0.2448
History of diabetes	21.4 (n=3)	20.0% (n=2)	25.0% (n=1)	>0.9999	20.0% (n=2)	25.0% (n=1)	>0.9999
CMV positive	42.9% (n=6)	30% (n=3)	75% (n=3)	0.2448	30.0% (n=3)	75% (n=3)	0.2448
Transplant demographics							
Total CIT (hrs)	20.4 (14.7-24.4)	20.4 (15.2-23.3)	18.4 (14.7- 24.4)	0.8392	19.6 (14.7 - 24.4)	21.5 (15.3 - 23.3)	0.3736
Duration of HMP (hrs)	8.7 (5.6-13.6)	9.4 (5.6-13.6)	8.6 (7.5-10.4)	0.5395	8.08 (5.58 - 13.6)	10.8 (7.92 - 11.8)	0.2398
HMP as % of total CIT	48.5 (34.3-65.5)	46.0 (34.3-65.5)	49.8 (37.9-51.7)	0.9451	42.9 (34.3 - 65.5)	50.1 (48.4 - 54.7)	0.3736
Outcome							
Incidence of DGF	28.6% (n=4)	n/a	n/a	**n/a**	20.0% (n=2)	50% (n=2)	0.5205

Table 6. Correlation between categorical demographic variables and serum creatinine. P-values calculated using Mann-Whitney test. P-values significant at p<0.05.

	1 week creatinine (µmol/L)			1 month creatinine (µmol/L)			6 month creatinine (µmol/L)			12 month creatinine (µmol/L)		
	Yes Median (range)	No Median (range)	p-value	Yes Median (range)	No Median (range)	p-value	Yes Median (range)	No Median (range)	p-value	Yes Median (range)	No Median (range)	p-value
Donor demographics												
Male	142 (89-488)	227 (94-425)	0.7879	112 (56-220)	130 (84-233)	0.1807	110 (59-335)	136 (100-155)	0.5583	131 (75-267)	127 (86-145)	0.8293
DCD donor	313 (137-488)	168 (89-425)	0.4364	120 (56-233)	127 (103-220)	0.6042	122 (59-335)	123 (86-150)	0.9211	129 (75-267)	122 (102-150)	0.8112
Traumatic brain injury	296 (168-315)	126 (89-488)	0.3758	114 (56-220)	181 (120-233)	0.1608	110 (59-335)	129 (115-155)	0.4368	112 (75-267)	131 (127-145)	0.5275
History of hypertension	137 (89-488)	297 (168-425)	0.4364	114 (56-233)	126 (120-220)	0.4685	110 (59-335)	142 (129-150)	0.2775	112 (75-267)	145 (131-150)	0.1209
Recipient demographics												
Male	227 (106-488)	116 (89-315)	0.2303	123 (82-233)	107 (56-181)	0.6042	136 (86-335)	108 (59-136)	0.1768	133 (100-267)	94 (75-127)	**0.0200***
Caucasian	198 (89-488)	106 (94-425)	0.6303	127 (56-233)	104 (84-220)	0.7242	122 (59-155)	125 (86-335)	0.977	129 (75-145)	129 (86-267)	0.4312
History of hypertension	153 (115-425)	227 (89-488)	0.9273	123 (82-220)	123 (56-233)	0.9452	133 (86-150)	113 (59-335)	0.977	121 (100-150)	129 (75-267)	>0.9999
History of DM	129 (89-168)	227 (94-488)	0.3273	120 (56-220)	125 (82-233)	0.8112	129 (59-150)	115 (86-335)	0.8626	131 (75-150)	127 (86-267)	>0.9999
CMV positive	266 (89-488)	168 (94-315)	0.9273	114 (56-220)	130 (82-233)	0.5338	109 (59-150)	133 (100-335)	0.2418	123 (75-150)	129 (86-267)	0.8751

Table 7. Correlation between continuous demographic variables and serum creatinine. R-values (95% confidence interval) represent a correlation co-efficient calculated using a two-tailed Spearman's rank correlation test, as datasets were assumed to be non-normally distributed. P-values significant at p<0.05.

	1 week creatinine		1 month creatinine		6 month creatinine		12 month creatinine	
	r (95% CI)	p-value	r (95% CI)	p-value	r (95% CI)	p-value	r (95% CI)	p-value
Donor demographics								
Age	-0.1545 (-0.7010 to 0.5062)	0.6538	-0.2473 (-0.7117 to 0.3676)	0.4151	-0.09021 (-0.6037 to 0.4761)	0.7582	0.06608 (-0.4947 to 0.5880)	0.8226
BMI	-0.02727 (-0.6296 to 0.5955)	0.9462	-0.4231 (-0.7967 to 0.1845)	0.1517	-0.396 (-0.7728 to 0.1872)	0.1611	-0.3987 (-0.7741 to 0.1842)	0.158
Recipient demographics								
Age	-0.2182 (-0.7330 to 0.4556)	0.5208	-0.2143 (-0.6941 to 0.3973)	0.4819	-0.1386 (-0.6339 to 0.4373)	0.6342	-0.04405 (-0.5734 to 0.5112)	0.8822
BMI	0.4273 (-0.2514 to 0.8243)	0.1928	0.4286 (-0.1781 to 0.7992)	0.146	0.319 (-0.2709 to 0.7348)	0.2642	0.3106 (-0.2796 to 0.7304)	0.2778
Transplant demographics								
Total CIT	0.3364 (-0.3483 to 0.7870)	0.3132	0.3407 (-0.2759 to 0.7586)	0.255	0.3784 (-0.2071 to 0.7644)	0.1818	0.2445 (-0.3442 to 0.6952)	0.3966
Duration of HMP	0.4636 (-0.2084 to 0.8383)	0.1546	0.2363 (-0.3776 to 0.7059)	0.4368	0.1342 (-0.4409 to 0.6312)	0.6452	0.01542 (-0.5321 to 0.5538)	0.9607
HMP as % of total CIT	0.3909 (-0.2918 to 0.8098)	0.2366	0.1813 (-0.4258 to 0.6759)	0.5537	0.0044 (-0.5399 to 0.5461)	0.9911	0.01542 (-0.5321 to 0.5538)	0.9607

Changes in metabolite concentrations and renal resistance during machine perfusion

Table 8 shows metabolite concentrations for the cohort at one hour, four hours and at the endpoint of machine perfusion. Figure 44 shows the increase in all anaerobic metabolite concentrations over each timepoint.

Table 8. Changes in metabolite concentrations and renal resistance over time. All metabolite concentrations units mmol/L unless otherwise stated. Median values (range) are reported for 1 hour, 4 hour sampling timepoints and Tend, the endpoint of perfusion period which varied for each kidney.

	1 hour	**4 hours**	**T End**
	Median (range)	Median (range)	Median (range)
3-Methylxanthine	0.0266 (0.023-0.033)	0.0269 (0.0236-0.0347)	0.0271 (0.0238-0.0364)
Acetate	0.21 (0.0398-0.388)	0.194 (0.0493-0.386)	0.172 (0.0511-0.345)
Adenine	5.8 (5.05-6.15)	5.55 (5.02-6.62)	5.78 (5.09-6.5)
Alanine	0.0672 (0.0273-0.11)	0.117 (0.07-0.26)	0.152 (0.0844-0.268)
Ethanolamine	7.07 (5.71-8.34)	7.18 (6.24-10.6)	7.55 (5.58-10.2)
Formate	0.182 (0.043-0.348)	0.199 (0.0422-0.402)	0.207 (0.0405-0.366)
Fumarate	0.0021 (0.00061-0.0060)	0.0039 (0.00092-0.0075)	0.00545 (0.002-0.0121)
Gluconate	76.4 (59.5-80.8)	78.1 (66.4-86.5)	79.7 (67.2-88.7)
Glutamate	0.303 (0.152-0.497)	0.943 (0.496-1.47)	1.61 (0.792-2.66)
Glutathione	1.34 (1.16-1.77)	0.767 (0.591-1.52)	0.554 (0.0476-0.924)
Glycine	0.57 (0-0.971)	1.85 (0.579-2.79)	3.02 (1.12-4.27)
Hippurate	0.00169 (0-1.34)	0.00361 (0-0.0149)	0.00391 (0-0.0118)
Hypoxanthine	0.104 (0-0.222)	0.175 (0.0972-0.447)	0.184 (0.0749-0.474)
Inosine	0.0207 (0-0.0889)	0.0301 (0-0.121)	0.0233 (0.00491-0.0832)
Isopropanol	0.0141 (0-0.0173)	0.0149 (0.0127-0.0201)	0.0158 (0.013-0.0246)
Lactate	0.829 (0.371-1.12)	1.3 (0.558-1.78)	1.58 (0.655-2.13)
Leucine	0.0079 (0.00322-0.0163)	0.0164 (0.00414-0.0333)	0.0144 (0.00261-0.043)
Oxypurinol	0.293 (0.257-0.35)	0.31 (0.274-0.378)	0.312 (0.262-0.431)
Ribose	1.59 (1.51-2.03)	1.59 (1.38-1.99)	1.64 (1.55-2.28)
Succinate	0.0177 (0.00813-0.0262)	0.0195 (0.0135-0.0382)	0.0254 (0.0155-0.0625)
Trimethylamine N-oxide	0 (0-0.0275)	0 (0-0.0411)	0.00813 (0-0.0783)
Tyrosine	0.00629 (0-0.292)	0.0099 (0-0.486)	0.0117 (0-0.424)
Valine	0.00821 (0.00399-0.016)	0.0129 (0.00767-0.0313)	0.015 (0.00952-0.0413)
Total concentration of lactate	0.937 (0.406-1.2)	1.54 (0.641-2.13)	1.91 (0.907-3.88)
Concentration of [U-^{13}C] lactate	0.0371 (0.0134-0.353)	0.149 (0.0835-0.962)	0.258 (0.163-2.14)
% [U-^{13}C] lactate	6.04 (1.26-30.7)	10.8 (5.54-47.1)	16.1 (8.7-55)
Total concentration of alanine	0.07 (0.027-0.11)	0.128 (0.073-0.278)	0.165 (0.098-0.279)
Concentration of [U-^{13}C] alanine	0 (0-0.012)	0.01 (0-0.047)	0.0125 (0.004-0.106)
% [U-^{13}C] alanine	0 (0-14)	7.13 (0-29.2)	8.26 (2.67-39.7)
POC lactate	1.4 (0.9-2.14)	2.05 (1.2-2.82)	2.4 (1.7-3.9)
POC glucose	9.15 (8.6-10)	8.6 (8-9.4)	8.44 (8-9.31)
POC pH	7.17 (7.07-7.23)	7.12 (7.02-7.18)	7.1 (6.97-7.14)
Renal Resistance (mmHg/ml/min)	0.21 (0.07-2)	0.215 (0.07-2)	0.22 (0.09-1.4)

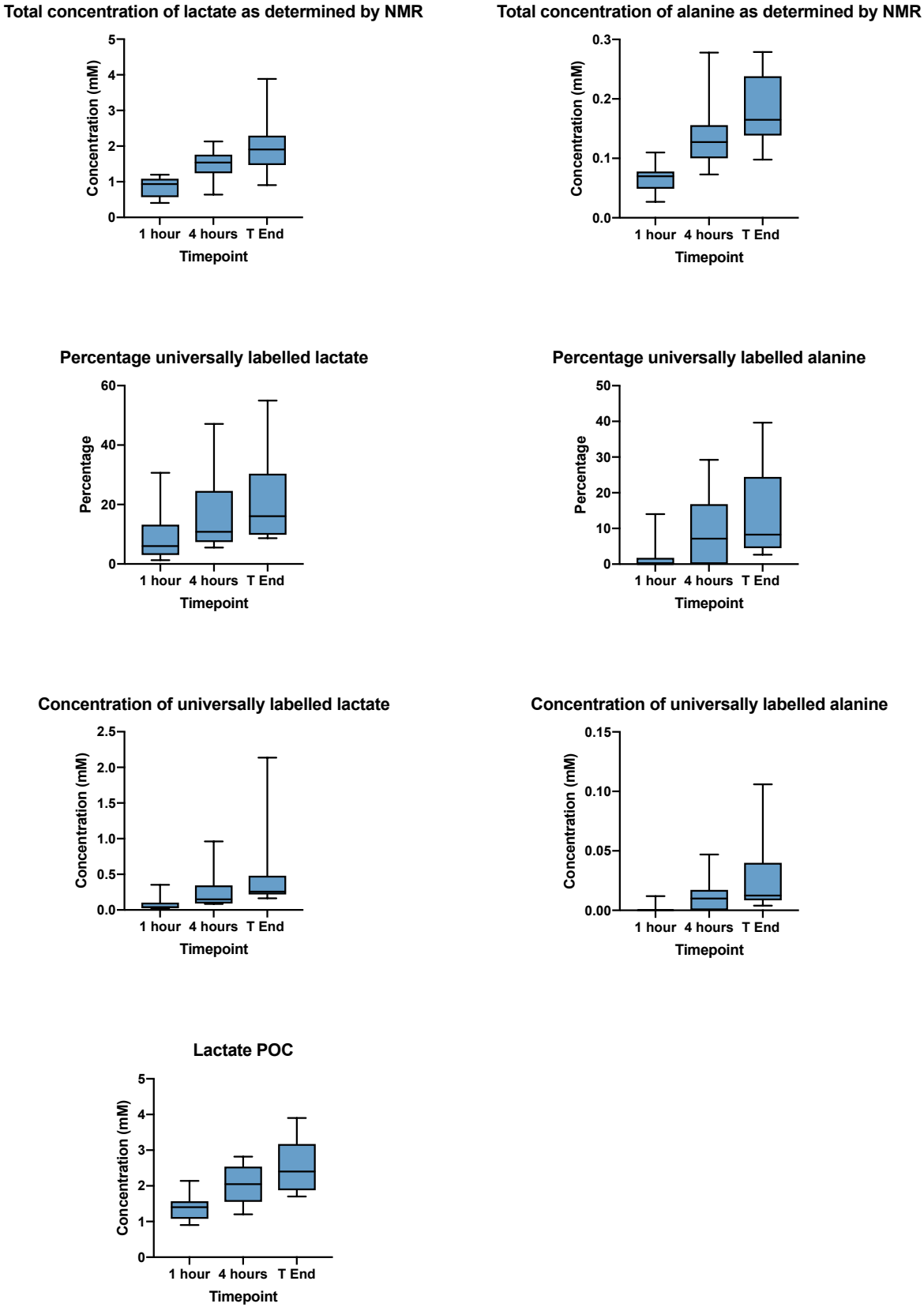

Figure 44. Graphs showing changes in the concentration of perfusate lactate and alanine during machine perfusion at 1 hour, 4 hours and T End. Median concentrations (mM) are shown along with interquartile range and range of values.

Associations between metabolite concentrations, renal resistance and clinical outcomes

No metabolite concentration was associated with the development of delayed graft function (Supplementary Information, Table 17). Multiple correlation analyses were performed to determine whether there was a consistent correlation between metabolite concentration and serum creatinine at 1 week (Supplementary Information, Table 18), 1 month (Supplementary Information, Table 19), 6 months (Supplementary Information, Table 20) and 12 months (Supplementary Information, Table 21).

A negative correlation was observed between both labelled and unlabelled anaerobic metabolite concentrations at 4 hours and perfusion endpoint, and serum creatinine at 1 month, 6 months and 12 months with such correlation investigated further with analysis according to DBD donor (Table 10) and DCD donor (Supplementary Information, Table 22) subtype. Further correlations between metabolite concentration and serum creatinine were identified but few were consistently statistically significant across sampled timepoints or serum creatinine values. Of these, formate concentrations at 1 hour, 4 hours and perfusion endpoint were negatively correlated with 12-month creatinine.

There was no correlation between change in oxygen levels over the perfusion period and point of care lactate ($p=0.924$), concentration of *de novo* [U-^{13}C] lactate ($p=0.727$) or total lactate concentration as demonstrated by NMR ($p=0.483$) at the end of the perfusion period.

Timing of machine perfusion

Duration of SCS prior to HMP, duration of HMP, total CIT and HMP as a % of CIT were not associated with renal resistance at the end of the perfusion period (Supplementary Information, Table 23). Of these 3 time periods relevant to the initiation of HMP, none were associated with perfusate concentration of anaerobic metabolites at 1 hour, 4 hours or T End (Supplementary Information; Table 25, Table 26, Table 27).

An analysis was performed to determine if correlations were present between endpoint metabolite concentrations and duration of SCS, duration of HMP and total CIT to determine whether metabolite concentrations increased as a result of an increase in each time period (Supplementary Information, Table 24). There was no correlation between any anaerobic metabolite concentration and duration of SCS, HMP or total CIT. Endpoint glutamate and glycine concentrations were positively correlated with duration of HMP whilst glutathione concentrations were negatively correlated with duration of HMP.

Differences between DBD and DCD donor kidneys

Analysis of labelled anaerobic metabolites yielded consistent differences between DBD and DCD kidneys. Significant differences in the proportion of U-^{13}C labelled alanine and U-^{13}C labelled lactate were evident as soon as 1 hour after commencing HMP (Table 9). This contributed to the observation that concentrations of U-^{13}C lactate and U-^{13}C alanine were proportionally higher in DCD kidneys at all timepoints, although differences were only significantly at T End (Figure 45). The same changes were not observed in ^{1}H-1D NMR alanine and lactate concentrations. POC lactate concentrations were higher in DCD vs DBD kidneys at all timepoints although the difference in concentrations did not reach statistical significance. Changes in anaerobic metabolite proportions and concentrations for each kidney in the cohort are displayed in Figure 46.

Following initial analysis suggesting a negative correlation between some anaerobic metabolites and serum creatinine, a sub-group analysis according to donor sub-type was performed to see if the relationship was consistent. On first appearance, there was a significant correlation between several anaerobic metabolite concentrations and serum creatinine with r-value suggesting *de novo* anaerobic metabolism correlates with lower serum Cr. However, on observation of data this observed trend was due to outlying Cr values for a single kidney. When removed, the same relationship did not exist.

Table 9. Differences in metabolite concentration and renal resistance between DBD and DCD donor kidneys. All metabolite concentrations units mmol/L unless otherwise stated. P-values are reported for Mann-Whitney tests. P-values significant at p<0.05.

	1 hour			4 hours			T End		
	DBD (n=10)	**DCD** (n=4)	p-value	**DBD** (n=10)	**DCD** (n=4)	p-value	**DBD** (n=10)	**DCD** (n=4)	p-value
3-Methylxanthine	0.02717	0.02571	0.3566	0.02793	0.02548	0.1988	0.02678	0.02747	0.8392
Acetate	0.2098	0.1853	0.9451	0.1942	0.172	0.9451	0.1723	0.1704	0.9181
Adenine	5.77	5.869	0.6354	5.495	5.727	0.3736	5.846	5.32	0.2398
Alanine	0.07014	0.05694	0.3736	0.1295	0.08073	**0.024***	0.1534	0.1132	0.1059
Ethanolamine	7.35	6.54	**0.024***	7.122	7.669	0.5395	7.532	7.776	0.5395
Formate	0.1824	0.1557	0.8392	0.1992	0.1769	0.9451	0.2066	0.1503	0.7333
Fumarate	0.001688	0.00376	0.2897	0.0033	0.005449	0.1778	0.004605	0.007521	0.0839
Gluconate	76.23	76.65	0.8392	76.98	78.94	0.8392	79.7	78.74	>0.9999
Glutamate	0.3031	0.3503	0.5395	0.9433	1.113	0.7333	1.518	2.033	0.4535
Glutathione	1.344	1.297	0.4535	0.8348	0.7477	0.6583	0.5757	0.1162	0.3037
Glycine	0.4302	0.7827	0.9451	1.543	2.149	0.5395	2.791	3.312	0.3736
Hippurate	0.003607	0	0.0509	0.004758	0.0006907	0.1279	0.009133	0	**0.033***
Hypoxanthine	0.1044	0.1013	0.7283	0.1753	0.2005	>0.9999	0.1838	0.1902	0.9451
Inosine	0.02617	0.01435	0.5395	0.03361	0.009977	0.1968	0.02448	0.005372	0.0719
Isopropanol	0.01412	0.01427	0.9161	0.01535	0.01481	0.4775	0.01566	0.01581	0.7572
Lactate	0.8852	0.6404	0.2398	1.348	1.009	0.1878	1.723	1.228	0.1878
Leucine	0.01005	0.005142	0.1878	0.01742	0.00112	0.1518	0.0188	0.01105	0.3736
Oxypurinol	0.2929	0.2828	0.5395	0.3218	0.3084	0.3906	0.3123	0.31	0.6354
Ribose	1.594	1.594	0.2498	1.594	1.594	0.999	1.594	1.723	0.5415
Succinate	0.01773	0.01757	0.7333	0.01803	0.02333	0.1878	0.02533	0.0254	0.8392
Trimethylamine N-oxide	0	0	0.5055	0	0	0.8801	0	0.03108	0.2797
Tyrosine	0.005986	0.0145	0.0519	0.0109	0.008826	0.2887	0.01167	0.0119	0.969
Valine	0.008365	0.007291	0.3966	0.01289	0.01151	0.5395	0.01504	0.01589	0.4346
Total concentration of lactate	0.9372	0.8463	>0.9999	1.528	1.787	0.5395	1.907	2.062	0.9451
Concentration of U-^{13}C lactate	0.03286	0.1536	0.0759	0.1444	0.6402	0.0939	0.232	0.8194	**0.024***
% U-^{13}C lactate	3.359	15.77	**0.036***	9.626	35.11	**0.008***	13.71	39.85	**0.002***
Total concentration of alanine	0.07014	0.06011	0.7333	0.1365	0.0955	0.2398	0.168	0.1542	0.5395
Concentration of U-^{13}C alanine	0	0.003169	0.2567	0.0055	0.0165	0.1159	0.01023	0.04097	**0.036***
% U-^{13}C alanine	0	4.437	0.2567	3.361	17.52	**0.023***	5.249	27.02	**0.008***
POC lactate	1.25	1.5	0.8551	1.8	2.475	0.3966	2.25	3.81	0.1768
POC glucose	8.895	9.48	0.0709	8.45	8.935	0.1129	8.3	8.75	0.1399
POC pH	7.164	7.173	0.9451	7.131	7.1	0.6354	7.121	7.036	0.5185
Renal Resistance (mmHg/ml/min)	0.215	0.195	0.5385	0.225	0.19	0.2877	0.225	0.21	0.6084

Table 10. Correlation between creatinine values and T End concentration of anaerobic metabolites for DBD kidneys. R-values represent a correlation co-efficient calculated using a two-tailed Spearman's rank correlation test for continuous data, as datasets were assumed to be non-normally distributed. P-values significant at p<0.05.

	1-week Cr		**1-month Cr**		**6-month Cr**		**12-month Cr**	
	r value	p-value	r value	p-value	r value	p-value	r value	p-value
Total concentration of lactate	-0.5667	0.1206	-0.5667	0.1206	-0.2675	0.4529	-0.4146	0.233
Concentration of U-^{13}C lactate	-0.5333	0.1475	-0.6667	0.0589	-0.7052	**0.0272***	-0.6464	**0.0485***
% U-^{13}C lactate	0.03333	0.9484	-0.15	0.7081	-0.4559	0.1864	-0.3171	0.3693
POC lactate	-0.4979	0.1763	-0.6667	0.057	-0.4616	0.1791	-0.5216	0.1244
Total concentration of alanine	-0.7	**0.0433***	-0.6667	0.0589	-0.383	0.2732	-0.5183	0.1283
Concentration of U-^{13}C alanine	-0.5774	0.1101	-0.5774	0.1101	-0.6728	**0.0374***	-0.6411	0.0502
% U-^{13}C alanine	-0.08333	0.8432	-0.1667	0.6777	-0.3283	0.3527	-0.2256	0.529

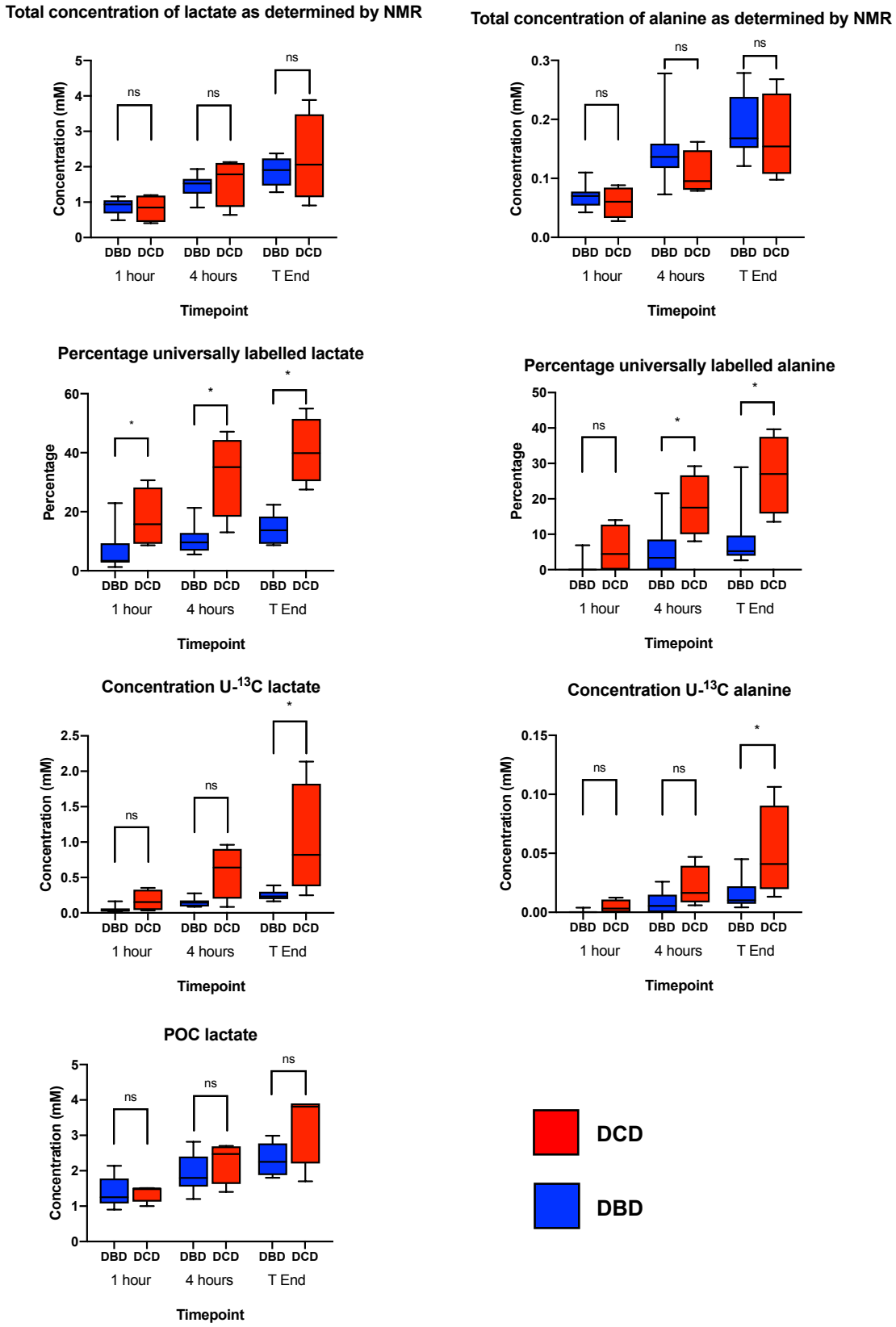

*Figure 45. Difference in anaerobic metabolites concentrations between DBD and DCD kidneys at 1 hour, 4 hours and T End. Median concentrations are shown along with interquartile range and range of values. *- indicates statistical significance where p-value <0.05*

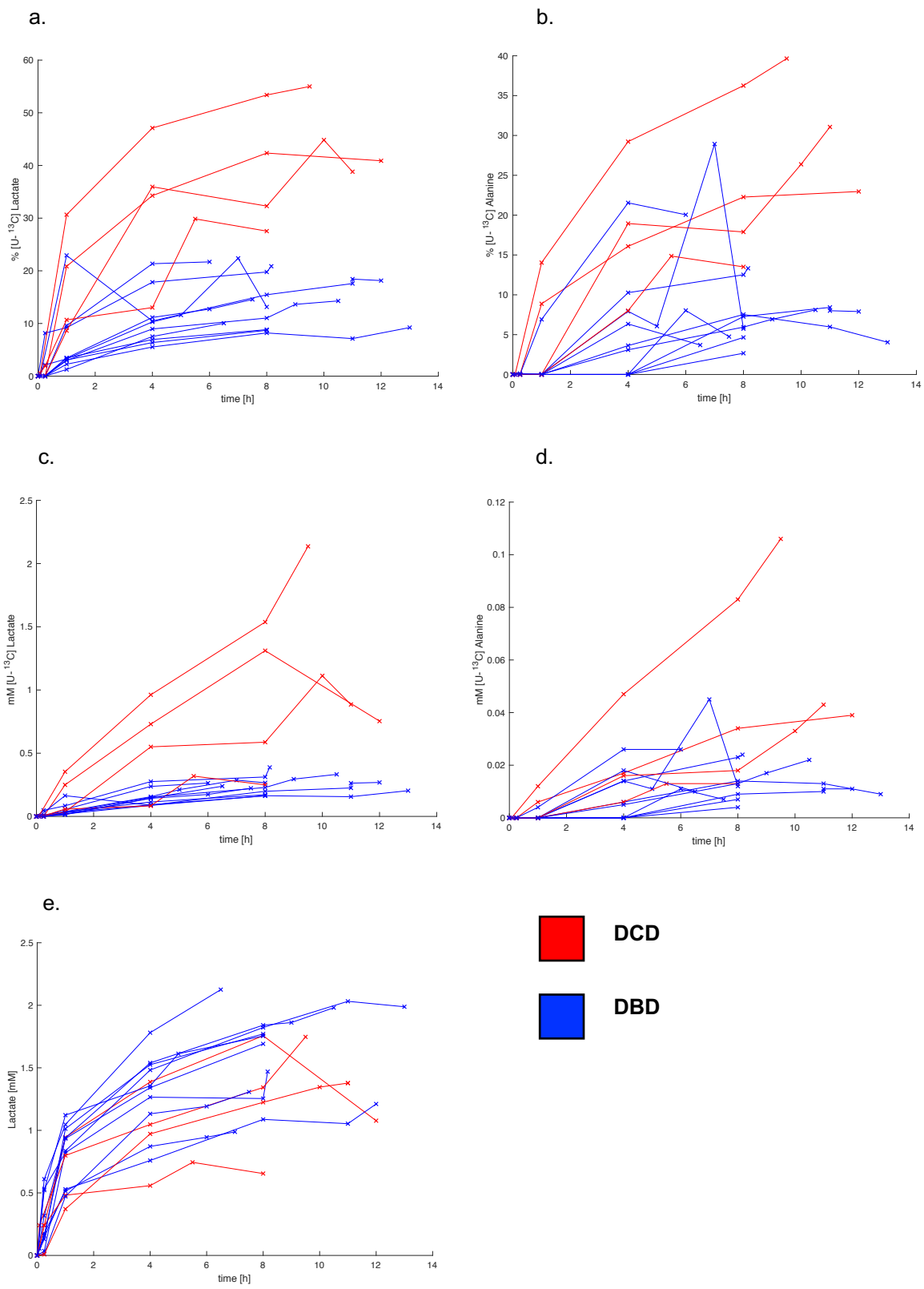

Figure 46. Changes in percentage U-^{13}C labelled lactate(a), absolute concentrations of U-^{13}C lactate(b), percentage concentration of U-^{13}C alanine(c), absolute concentration of U-^{13}C alanine(d) and 1D-^{1}H NMR lactate concentration(e) changes for each kidney for the duration of machine perfusion.

Biochemical assays

Preliminary analysis of donor variables and transplant timings were performed to determine whether these impacted on biochemical assay results (Table 11, Table 12). Male gender was significantly associated with LDH concentration at all timepoints. Donor BMI correlated with increasing LDH concentration at all sampling timepoints. However, LDH, GST-Pi and NGAL concentrations at any timepoint, were not associated with the development of DGF (Supplementary Information, Table 28) or serum creatinine values (Supplementary Information, Table 29).

NGAL concentration at 4 hours positively correlated with endpoint 1H 1D NMR lactate concentrations whilst NGAL concentrations 1 hour and 4 hours positively correlated with ^{1}H 1D alanine and total alanine concentrations (Table 13). On observation of the concentration of [U-^{13}C] metabolites, the converse was true and an inverse correlation was suggested. Both endpoint concentrations of [U-^{13}C] lactate and [U-^{13}C] alanine were negatively correlated with endpoint concentrations of NGAL.

Endpoints LDH concentrations were positively correlated with all anaerobic metabolite concentrations at all timepoint but only reached statistical significance for U-^{13}C lactate concentrations at 4 hours and at the endpoint of machine perfusion, in addition to total alanine concentrations at 1 hour and 4 hour (see Table 13). No consistent, or significant correlation was observed between GST-Pi concentrations and anaerobic metabolite concentrations.

Table 11. Association between donor categorical variables and biochemical assays. Data reported as Median (range), with p-value from Mann-Whitney test. P-values significant at p<0.05.

	1 hour			4 hours			T End		
	Yes Median (range)	No Median (range)	p-value	Yes Median (range)	No Median (range)	p-value	Yes Median (range)	No Median (range)	p-value
NGAL									
Male	4.55 (2.75-14.4)	2.69 (1.48-11)	0.2593	4.78 (3.85-18.9)	3.78 (2.58-11.5)	0.4452	4.77 (4.04-25.5)	7.18 (2.25-13.9)	>0.9999
DCD donor	3.65 (1.62-4.59)	3.81 (1.48-14.4)	0.6354	4.25 (2.95-5.11)	4.78 (2.58-18.9)	0.5035	4.4 (2.25-5.27)	6.28 (2.42-25.5)	0.1878
Traumatic brain injury	2.93 (2.69-4.16)	4.55 (1.48-14.4)	0.5549	4.23 (3.85-4.61)	4.78 (2.58-18.9)	0.641	7.18 (4.45-9.23)	4.77 (2.25-25.5)	0.5549
Hx of hypertension	2.75 (1.48-2.93)	4.55 (1.62-14.4)	0.1264	3.85 (2.71-3.94)	4.94 (2.58-18.9)	0.1119	4.04 (2.71-4.45)	5.38 (2.25-25.5)	0.1264
GST-Pi									
Male	33 (22.1-36.5)	28.1 (14.1-36.7)	0.2593	31.1 (28.8-32.2)	30.8 (21.6-32.1)	0.6282	28.4 (25.1-32.8)	28.8 (21.2-30)	0.5944
DCD donor	33.1 (28.1-36.5)	30.2 (14.1-36.7)	0.4535	30.9 (28.8-32.2)	31 (21.6-32.1)	0.8252	30.5 (25.4-31.2)	28.5 (21.2-32.8)	0.2278
Traumatic brain injury	29.1 (25.2-34.1)	33 (14.1-36.7)	>0.9999	31.3 (31-31.6)	30.7 (21.6-32.2)	0.7692	30 (28.8-32.8)	28.4 (21.2-31.2)	0.1209
Hx of hypertension	33.2 (14.1-34.1)	31.3 (19.6-36.7)	>0.9999	31.1 (21.6-31.6)	30.8 (27.2-32.2)	0.6923	31.2 (21.6-32.8)	28.5 (21.2-31.2)	0.3819
LDH									
Male	12.9 (12.3-32)	6.46 (1-11.7)	**0.0006***	23.5 (15.3-35.7)	14.2 (3.77-22.3)	**0.014***	27.5 (18.1-36.4)	15.9 (3.77-22.5)	**0.007***
DCD donor	19.7 (6.46-32)	10.7 (1-14.4)	0.1878	23.3 (15.7-35.7)	15.3 (3.77-28.9)	0.1483	25.4 (19-36.4)	17.6 (3.77-33.4)	0.0759
Traumatic brain injury	6.7 (5.13-12.9)	12.3 (1-32)	0.6593	18.6 (13.7-23.5)	17.7 (3.77-35.7)	0.9231	15.9 (9.07-28.2)	19 (3.77-36.4)	0.6593
Hx of hypertension	12.7 (1-12.9)	11.7 (3.01-32)	0.8846	19.4 (3.77-23.5)	16.7 (5.66-35.7)	0.8112	23.3 (3.77-28.2)	18.6 (8.48-36.4)	>0.9999

Table 12. Association between donor continuous variables and biochemical assays. R-values represent a correlation co-efficient calculated using a two-tailed Spearman's rank correlation test for continuous data, as datasets were assumed to be non-normally distributed. P-values significant at p<0.05.

	1 hour			4 hours			T End		
	r	95% CI	p-value	r	95% CI	p-value	r	95% CI	p-value
NGAL									
Donor Age	0.3099	-0.2803 to 0.7301	0.2806	0.1209	-0.4751 to 0.6408	0.696	0.03297	-0.5193 to 0.5659	0.9155
Donor BMI	0.2132	-0.3730 to 0.6777	0.4636	0.06593	-0.5169 to 0.6070	0.8347	-0.1297	-0.6284 to 0.4447	0.6595
SCS time prior to HMP	0.2088	-0.3770 to 0.6752	0.4731	0.3022	-0.3151 to 0.7398	0.3155	0.2615	-0.3281 to 0.7045	0.3656
HMP duration	0.3275	-0.2622 to 0.7391	0.253	0.2967	-0.3205 to 0.7371	0.3247	0.2659	-0.3238 to 0.7069	0.3573
Total CIT	0.2659	-0.3238 to 0.7069	0.3573	0.3132	-0.3041 to 0.7453	0.2975	0.3407	-0.2483 to 0.7457	0.2335
% HMP of total CIT	0.006593	-0.5383 to 0.5476	0.9879	-0.1154	-0.6375 to 0.4794	0.7097	-0.08132	-0.5979 to 0.4830	0.7849
GST-Pi									
Donor Age	0.4901	-0.07209 to 0.8160	0.0779	0.522	-0.05899 to 0.8388	0.0707	0.2838	-0.3064 to 0.7164	0.3226
Donor BMI	0.3582	-0.2294 to 0.7545	0.209	0.4451	-0.1583 to 0.8064	0.1299	0.297	-0.2933 to 0.7234	0.2999
SCS time prior to HMP	0.3187	-0.2713 to 0.7346	0.2666	-0.07692	-0.6139 to 0.5088	0.8064	0.1892	-0.3943 to 0.6640	0.5142
HMP duration	0.4637	-0.1060 to 0.8042	0.0973	0.3242	-0.2930 to 0.7506	0.28	0.4422	-0.1326 to 0.7945	0.1143
Total CIT	0.3758	-0.2101 to 0.7631	0.1862	0.1099	-0.4837 to 0.6342	0.7231	0.4466	-0.1272 to 0.7965	0.1104
% HMP of total CIT	0.1385	-0.4374 to 0.6338	0.6375	0.1044	-0.4879 to 0.6309	0.737	0.1078	-0.4623 to 0.6148	0.7122
LDH									
Donor Age	0.4769	-0.08919 to 0.8101	0.0872	0.4725	-0.1242 to 0.8182	0.1057	0.5297	-0.01873 to 0.8331	0.0544
Donor BMI	0.6396	0.1479 to 0.8777	**0.0161***	0.7143	0.2522 to 0.9111	**0.0079***	0.7363	0.3220 to 0.9139	**0.0037***
SCS time prior to HMP	0.178	-0.4041 to 0.6575	0.5423	0.1758	-0.4304 to 0.6728	0.5659	0.2044	-0.3809 to 0.6727	0.4827
HMP duration	0.1736	-0.4078 to 0.6549	0.5526	0.1923	-0.4164 to 0.6820	0.5293	0.0989	-0.4693 to 0.6092	0.7385
Total CIT	0.1516	-0.4265 to 0.6418	0.6051	0.04396	-0.5329 to 0.5929	0.8917	0.1121	-0.4589 to 0.6175	0.7043
% HMP of total CIT	-0.05055	-0.5777 to 0.5064	0.8676	-0.07143	-0.6105 to 0.5128	0.8207	-0.1648	-0.6497 to 0.4154	0.5733

Table 13. Association between key metabolites of interest and biochemical assays. R-values represent a correlation co-efficient calculated using a two-tailed Spearman's rank correlation test for continuous data, as datasets were assumed to be non-normally distributed. P-values significant at p<0.05.

	1 hour		4 hours		T End	
	r (95% CI)	p-value	r (95% CI)	p-value	r (95% CI)	p-value
NGAL						
1D lactate	0.4857 (-0.07783 to 0.8140)	0.0809	0.7088 (0.2418 to 0.9092)	**0.0086***	0.4681 (-0.1004 to 0.8062)	0.0938
Total NMR Lactate	0.3319 (-0.2576 to 0.7413)	0.2464	0.5385 (-0.03612 to 0.8455)	0.0611	0.1473 (-0.4302 to 0.6392)	0.6158
U-^{13}C lactate	-0.222 (-0.6827 to 0.3650)	0.4448	-0.3846 (-0.7793 to 0.2285)	0.1955	-0.5824 (-0.8550 to -0.05763)	**0.0318***
POC lactate	0.1569 (-0.4221 to 0.6450)	0.5895	0.1685 (-0.4366 to 0.6686)	0.5791	-0.07956 (-0.5968 to 0.4844)	0.7867
1D alanine	0.5429 (-0.0002240 to 0.8387)	**0.0479***	0.6703 (0.1715 to 0.8956)	**0.0147***	0.4813 (-0.08353 to 0.8121)	0.084
Total NMR alanine	0.5824 (0.05763 to 0.8550)	**0.0318***	0.6374 (0.1151 to 0.8836)	**0.0221***	0.3275 (-0.2622 to 0.7391)	0.253
U-^{13}C alanine	-0.1916 (-0.6654 to 0.3922)	0.5087	-0.3934 (-0.7833 to 0.2187)	0.1834	-0.5749 (-0.8519 to -0.04634)	**0.0341***
TMNO	0.2042 (-0.3811 to 0.6726)	0.4821	0.2568 (-0.3587 to 0.7167)	0.3956	0.2183 (-0.3684 to 0.6806)	0.4516
GST-Pi						
1D lactate	0.1253 (-0.4482 to 0.6257)	0.6706	0.3077 (-0.3096 to 0.7425)	0.3063	-0.1628 (-0.6485 to 0.4171)	0.5756
Total NMR Lactate	0.06374 (-0.4965 to 0.5865)	0.8319	0.1209 (-0.4751 to 0.6408)	0.696	-0.2354 (-0.6902 to 0.3527)	0.4145
U-^{13}C lactate	0.1912 (-0.3926 to 0.6652)	0.5121	-0.005495 (-0.5674 to 0.5599)	0.9929	0.1144 (-0.4570 to 0.6190)	0.6956
POC lactate	0.05525 (-0.5029 to 0.5808)	0.8517	0.1519 (-0.4502 to 0.6591)	0.6175	-0.2223 (-0.6829 to 0.3647)	0.4403
1D alanine	0.1648 (-0.4154 to 0.6497)	0.5733	0.2802 (-0.3366 to 0.7287)	0.3535	-0.2662 (-0.7070 to 0.3236)	0.3545
Total NMR alanine	0.2703 (-0.3196 to 0.7092)	0.3492	0.3297 (-0.2873 to 0.7533)	0.2715	-0.2596 (-0.7035 to 0.3299)	0.3673
U-^{13}C alanine	0.1233 (-0.4498 to 0.6245)	0.6726	-0.1018 (-0.6293 to 0.4899)	0.7402	0.002205 (-0.5415 to 0.5446)	0.9956
TMNO	0.2277 (-0.3598 to 0.6859)	0.4319	-0.07168 (-0.6106 to 0.5126)	0.82	0.1386 (-0.4373 to 0.6339)	0.6341
LDH						
1D lactate	0.3231 (-0.2667 to 0.7368)	0.2597	0.1813 (-0.4258 to 0.6759)	0.5537	0.244 (-0.3447 to 0.6949)	0.3998
Total NMR Lactate	0.4549 (-0.1170 to 0.8003)	0.1044	0.4451 (-0.1583 to 0.8064)	0.1299	0.4725 (-0.09482 to 0.8082)	0.0905
U-^{13}C lactate	0.4462 (-0.1278 to 0.7963)	0.1119	0.5604 (-0.004644 to 0.8542)	**0.0499***	0.5824 (0.05763 to 0.8550)	**0.0318***
POC lactate	0.4 (-0.1827 to 0.7747)	0.1564	0.4503 (-0.1519 to 0.8087)	0.1236	0.3956 (-0.1878 to 0.7726)	0.1614
1D alanine	0.4154 (-0.1648 to 0.7820)	0.1413	0.2912 (-0.3259 to 0.7343)	0.3342	0.2791 (-0.3110 to 0.7139)	0.3332
Total NMR alanine	0.6527 (0.1700 to 0.8828)	**0.0136***	0.5824 (0.02799 to 0.8628)	**0.0402***	0.5341 (-0.01260 to 0.8349)	0.0521
U-^{13}C alanine	0.3546 (-0.2333 to 0.7527)	0.2124	0.4512 (-0.1508 to 0.8091)	0.1228	0.4714 (-0.09630 to 0.8077)	0.0905
TMNO	0.4905 (-0.07156 to 0.8161)	0.0779	0.2748 (-0.3418 to 0.7260)	0.3623	0.1948 (-0.3894 to 0.6672)	0.503

Associations between pH and lactate concentrations

Anaerobic metabolite concentrations, labelled and unlabelled, were negatively correlated with pH (Table 14).

Table 14. Associations between pH and anaerobic metabolites. R-values represent a correlation co-efficient calculated using either a two-tailed Spearman's rank correlation test or Pearson's correlation co-efficient as specified. a- denotes use of Pearson's correlation co-efficient which was used when values were normally distributed. b- denotes use of Spearman's correlation test. P-values significant at p<0.05.

Metabolite	r value	95% CI	R squared	p-value
Lactate Point of Care[a]	-0.8974	-0.9337 to -0.8429	0.8054	<0.0001
1D Lactate[a]	-0.7045	-0.8019 to -0.5705	0.4963	<0.0001
Total concentration lactate using NMR[a]	-0.759	-0.8402 to -0.6446	0.5761	<0.0001
Concentration U^{13}C labelled lactate[b]	-0.6283	-0.7501 to -0.4653	0.3948	<0.0001
1D Alanine[b]	-0.6951	-0.7977 to -0.5533	0.4832	<0.0001
Total concentration alanine using NMR[a]	-0.7256	-0.8168 to -0.5989	0.5264	<0.0001
Concentration U^{13}C labelled alanine[b]	-0.6592	-0.7723 to -0.5057	0.4345	<0.0001

Composition of Neat KPS

For six kidneys, KPS-1 was sampled prior to commencing perfusion. The median concentration of constituent metabolites as detected by ^{1}H 1D-NMR is reported in Table 15.

Table 15. Metabolites contained within sampled Neat KPS-1 prior to commencing perfusion. Mean concentrations (mM) are reported along with standard deviation and standard error of mean.

	Mean (mM)	Standard Deviation	Standard error of mean
Known constituent			
Adenine	6.38	0.506	0.207
Gluconate	76.1	4.35	1.78
Glutathione	1.39	0.42	0.171
Ribose	1.56	0.0951	0.0388
Not known constituent			
3-Methylxanthine	0.027	0.00166	0.00068
Acetate	0.326	0.137	0.0559
Alanine	0.0134	0.00172	0.000701
Ethanolamine	6.63	0.422	0.172
Formate	0.258	0.107	0.0438
Fumarate	0.00046	0.000713	0.000291
Glutamate	0.0467	0.0562	0.0229
Glycine	0	0	0
Hippurate	0	0	0
Hypoxanthine	0	0	0
Inosine	0.009	0.0106	0.00431
Isopropanol	0.012	0.00161	0.000655
Lactate	0.011	0.00211	0.000861
Leucine	0	0	0
Oxypurinol	0.304	0.0131	0.00537
Succinate	0.0198	0.00341	0.00139
Trimethylamine N-oxide	0	0	0
Tyrosine	0.0947	0.147	0.0599
Valine	0	0	0

Precision of sample processing

In order to determine the precision of sample processing and analysis, six replicates of the same end-point sample for one kidney were processed and analysed as separate samples from the point of thawing. The mean concentration, standard deviation and standard error of the mean are reported in Table 16.

Table 16. Analysis of sample replicates. Mean concentrations (mM) are reported along with standard deviation and standard error of mean.

	Mean (mM)	Standard Deviation	Standard error of mean
% [U-^{13}C] lactate	12.6	0.073	0.0326
NMR Lactate total Concentration [U-^{13}C] labelled lactate	1.26 0.16	0.147 0.0194	0.0659 0.00869
% [U-^{13}C] alanine	5.58	1.54	0.689
NMR Alanine total Concentration [U-^{13}C] labelled alanine	0.129 0.00725	0.00313 0.00219	0.0014 0.00098
3-Methylxanthine	0.0258	0.000287	0.000128
Acetate	0.273	0.00355	0.00159
Adenine	6.08	0.853	0.381
Alanine	0.122	0.00103	0.000459
Ethanolamine	6.53	0.152	0.0678
Formate	0.267	0.0303	0.0136
Fumarate	0.0015	0.000128	0.0000574
Gluconate	80	0.361	0.161
Glutamate	0.826	0.00639	0.00286
Glutathione	0.792	0.0767	0.0343
Glycine	1	0.0441	0.0197
Hippurate	0.00792	0.00196	0.000874
Hypoxanthine	0.1	0.0629	0.0281
Inosine	0.0258	0.00347	0.00155
Isopropanol	0.0139	0.000128	0.0000574
Lactate	1.1	0.128	0.0571
Leucine	0.00976	0.000385	0.000172
Oxypurinol	0.297	0.00598	0.00267
Ribose	1.61	0.0356	0.0159
Succinate	0.0215	0.000168	0.0000752
Trimethylamine N-oxide	0.00089	0.00199	0.00089
Tyrosine	0.007	0.000385	0.000172
Valine	0.0116	0.000206	0.0000921

Discussion

Tracer based metabolism provides unequivocal evidence of *de novo* metabolism. These experiments apply such methodology to *ex vivo* cadaveric kidneys prior to transplantation in order to improve understanding of metabolism during the organ preservation period. Here we describe the first study to use tracer-based metabolism to describe *de novo* metabolism in human cadaveric kidneys prior to observation of clinical outcome following transplantation.

Metabolism

Overall kidneys underwent HMP for a median of 8.7 hours, a relatively short duration which contrasts with the 18-hour duration of HMP used in previous metabolomic studies in our group (175, 219, 220).

Increased durations of HMP correlated with decreasing glutathione concentrations likely reflecting its role as a scavenger of free radicals. Decreases in perfusate glutathione over time have been observed in several other studies (219, 220). The concentration of most labelled and unlabelled metabolites did not correlate significantly with duration of HMP, suggesting metabolite build up was not simply related to exposure of organs to metabolic substrate alone.

The absence of correlation between any endpoint anaerobic metabolite concentration and duration of SCS, HMP or total CIT suggests it is too simplistic to suggest anaerobic metabolism occurs at a consistent rate in all kidneys. Analysis of DBD and DCD subgroups suggest donor subtype is a dominant factor in the metabolic phenotype of kidneys undergoing HMP; even with such relatively short perfusion durations, stark differences in *de novo* metabolism were observed between DBD and DCD kidneys.

The concentration of [U-^{13}C] lactate was higher in DCD kidneys by a magnitude of 4.7, 4.4 and 3.5 at 1 hour, 4 hours and at the endpoint of machine perfusion although this only reached statistical significance for endpoint samples. The concentration of [U-^{13}C] alanine was also higher by a magnitude of 3.0 and 4.0 at 4 hours and at the endpoint of perfusion, although this also only reached statistical significance at T End. Differences are represented graphically in Figure 45. Such differences in T endpoint concentration of labelled metabolites may in part be accounted for by the increased duration of HMP in DCD vs DBD kidneys (10.8 vs 8.1hrs) resulting in longer perfusion period in which *de novo* metabolism can occur. However, changes in *de novo* metabolite composition and concentration were evident early in the perfusion period.

No labelled glutamate was observed in any perfusate sample in the study at any timepoint. This was unsurprising given the relatively short duration of HMP compared with previous studies in which [4,5-^{13}C] glutamate was observed (175, 219). In addition, porcine kidneys are larger and are retrieved from relatively young subjects compared with human kidneys included in this study. However, the absence of [4,5-^{13}C] glutamate does not evidence that *de novo* aerobic metabolism is not ongoing. In contrast to products of glycolysis which can appear within minutes, TCA cycle intermediates do not appear for several hours (249).

As differences in the concentration of U^{13}C lactate were evident as early as 1 hour after commencing machine perfusion, one would suspect that DCD kidneys are reliant on anaerobic metabolism, with a relative thirst for glucose to fuel such metabolism early in in the perfusion period, unsurprising given the yield of ATP per glucose molecule when cells utilise anaerobic vs aerobic metabolism. This may be due to depletion of intra-cellular glucose stores during organ retrieval and static storage. Such a difference in preference for anaerobic metabolism may be explained by exposure to warm ischaemia at the time

of organ retrieval. Such warm ischaemia results in a switch to anaerobic metabolism which likely continues once the organ is cooled, with anaerobic metabolism ongoing during HMP.

In comparison, one would suspect that DBD kidneys utilise both anaerobic and aerobic metabolism. Cold perfusion of DBD kidneys without preceding warm ischaemia may serve to slow the rate of aerobic metabolism, with anaerobic metabolism occurring following this due to lower oxygen availability during conditions of static storage.

If DCD kidneys are indeed reliant on anaerobic metabolism due to the manner in which they are retrieved, there may be a role for normothermic regional perfusion to revert organs to a state of aerobic metabolism prior to organ cooling.

As expected, a correlation was observed between increasing lactate concentrations and a decrease in pH suggesting changes in acid-base balance were a result of anaerobic metabolism (Table 14) A lower rate of anaerobic metabolism may be beneficial for cells as it results in less lactate accumulation, and maintenance of a more physiological pH.

Glutathione concentrations were negatively correlated with duration of HMP suggesting the anti-oxidant continued to scavenge free radicals during the perfusion period. Such change in concentration would suggest ongoing ischaemic injury during HMP despite the provision of metabolic substrate and washout of toxic metabolites.

Having identified differences between DBD and DCD groups, one would suspect that these differences in *de novo* metabolism may be responsible for the development of delayed graft function. Yet no metabolite was identified as predictive of DGF, perhaps reflecting the difference needed between groups to be statistically significant. Correlations observed between serum creatinine values and concentration of anaerobic metabolites

suggest a relationship between *de novo* metabolism and functional outcome. However, given the small sample size, such correlation proved to be spurious once data for one kidney was removed.

In a study using venous samples obtained via a cannulated renal vein and paired arterial following reperfusion, Wijermars et al demonstrated an association between continuing anaerobic metabolism in kidneys, evidenced by continuing lactate production on reperfusion, and the development of delayed graft function (234). The study did not investigate functional differences in DGF and IGF groups by means of observing creatinine values.

Demographics

Recruitment for the study was lower than expected resulting in a sample size of 14 kidneys. There was a stark contrast between donor and recipient ethnicity, with diverse local ethnicity reflected in the demographics of the cohort. Ethnicity was the only demographic variable to differ between DGF and IGF groups (Table 5). The higher incidence of DGF in non-Caucasians did not appear to be related to a higher prevalence of diabetes or hypertension with the association likely due to chance given the small sample size.

In the study population, kidneys underwent HMP for less than half of the total CIT with a median delay of 8.4 hours in initiating HMP during the preservation period. In conjunction with the extended total CIT observed in the cohort, a delay in the initiation of HMP, with kidneys remaining in static storage, is likely to limit its benefits as several beneficial mechanisms of action, such as preservation of endothelium via exertion of shear stress and delivery of glucose to tissues in order to fuel metabolism, do not occur during static

conditions. The delay in initiation contrasts with timings of the Machine Preservation Trial (70) and provides a small insight into the variation in delay in initiation of HMP in the UK. Such information was lacking from the NHSBT registry analysis discussed in Chapter 4.

Biochemical assays

Observed positive correlations between unlabelled alanine and lactate concentrations and NGAL concentration in perfusate may infer ongoing kidney damage leads to cell damage, and release of intra-cellular metabolites following cell death. In contrast, the negative correlation observed between endpoint NGAL concentrations and endpoint concentrations of U-^{13}C lactate and U-^{13}C alanine suggests preservation of organs is associated with higher *de novo* metabolism, albeit anaerobic.

An increase in LDH concentrations correlated with increasing concentrations of anaerobic metabolites at all timepoints suggesting increasing anaerobic metabolism is associated with cell death.

The search for a metabolic biomarker

Donor, recipient and transplant specific factors influence graft function following implantation (35, 70, 186). Most studies measuring changes in metabolites and protein levels (95, 96, 173, 247) aim to identify biomarkers of organ damage and consequently predict graft function. Despite the identification of more novel biomarkers in recent years including the lysosomal enzyme N-acetyl-D-glucosaminidase (96), granulocyte-macrophage colony-stimulating factor (GM-CSF) (250), leptin (250) and micro RNAs (251), no perfusate biomarker is routinely used in clinical practice. The complexities of transplantation are reflected in this inability for researchers to identify one sensitive and specific biomarker which predicts graft function post-transplantation. Indeed Ischaemia-

Reperfusion Injury inflicts much of the damage organs sustain during organ preservation and following reperfusion, with changes in metabolism playing a key role in such injury.

Number of variables

Small scale animal studies (212, 220, 252) are conducted in a controlled environment in which animals are of a similar age, same gender and often identical genetic strain. Whether auto-transplant, reperfusion model or benchtop set-up alone, the experimental design of these studies dictates that only one variable is examined in isolation. This is a stark contrast to the number of variables which cannot be controlled for in our 'real world' setting.

As such, the small sample size and large number of variables did not permit a multivariate analysis, limiting analyses to univariate analyses alone. The large number of statistical tests performed also increased the likelihood of both type 1 and type 2 errors occurring.

Limitations

There are several limitations of the study in addition to sample size and experimental methodology itself.

This non-interventional study is novel as patient care did not change as a result of the study and in the absence of taking renal biopsies, kidneys were in no way damaged as a result of the study. Original ethical approval was sought to include biopsies taken from machine perfused organs at the end of the period of HMP. However, biopsies pose a risk of damaging organs and it is not unit policy to perform routine tissue biopsies. At the time of commencing the study, a national study was under way which included a punch biopsy of renal cortex at organ retrieval (253). Several complications including bleeding and

formation of iatrogenic arterio-venous fistulae were attributed to these retrieval biopsies in other kidneys implanted in the centre thus biopsies were not taken from kidneys included in our study due to reluctance of transplant surgeons. Ideally punch biopsies would have been taken following the perfusion period enabling direct observation of renal cortex metabolites.

The sampling of circulating perfusate was non-invasive and can be performed frequently with biochemical assays and 1D ^{1}H NMR samples (172) processed and analysed within hours. However, as they are non-invasive several inferences must be made in order to draw conclusions regarding *de novo* metabolism within tissues themselves. Referring back to Chapter 6, a strong correlation was observed between end-point perfusate and renal cortex concentrations for the unlabelled metabolites alanine ($r=0.82$, $p=0.01$), lactate ($r=0.750$, $p=0.005$) and glutamate ($r=0.86$, $p<0.001$). Hence one limitation is the extent to which changes in perfusate mimic changes in metabolism within tissue.

With respect to clinical outcome measures, delayed graft function as a binary outcome was less useful for sub-group analysis given the small sample size. Large differences in measured outcomes were required to show differences in IGF and DGF groups. Serum creatinine was a better functional measure of outcome however, as an outcome measure this was influenced in the short-term by development of DGF. As creatinine values for patients requiring haemodialysis do not indicate graft function, those values were deemed ‘missing’ for purpose of analysis. However, kidneys which had regained graft function had a high creatinine value, skewing results.

Final comments

By the time of HMP initiation, DCD kidneys are likely to be starved of oxygen with the likelihood that intra-cellular glucose levels have been continually decreasing due to reliance on anaerobic metabolism in the hypoxic conditions of static storage.

Our data shows how donor sub-type is a key determinant of the extent of *de novo* anaerobic metabolism as evidenced by significantly higher proportions and absolute concentrations of U-^{13}C alanine and lactate in DCD kidneys compared with DBD kidneys at end timepoints. Importantly the same differences would not have been apparent without employment of a metabolic tracer.

Such description of *de novo* metabolism adds to our understanding of biological processes which continue during HMP in DCD kidneys and would not be possible without the use of tracer-based metabolism analysis. Anaerobic metabolism resulting in a higher lactate concentration contributes to higher rates of DGF in these kidneys in keeping with research showing anaerobic metabolism is higher in kidneys which experience DGF post-implantation (234). Subsequent studies should confirm this association with a larger sample size and aim to correlate increasing warm ischaemic time with the amount of anaerobic metabolism to see if such a dose response relationship is present.

If such an association is consistent amongst DCD kidneys, therapeutic efforts should seek to promote aerobic metabolism in near physiological conditions using normothermic regional perfusion prior to HMP. Alternatively, oxygenated HMP should be considered as a means of organ reconditioning by promoting aerobic metabolism as described in Chapter 6.

Supplementary tables

Table 17. Association between development of DGF and measured outcomes including metabolite concentration and renal resistance. All metabolite concentrations units mmol/L unless otherwise stated. Data reported as median (range), with p-value from Mann-Whitney test. P-values significant at p<0.05.

	1 hour			4 hours			T End		
	DGF (n=4)	IGF (n=10)	p-value	DGF (n=4)	IGF (n=10)	p-value	DGF (n=4)	IGF (n=10)	p-value
3-Methylxanthine	0.0273	0.0266	0.9151	0.0275	0.0267	0.969	0.0283	0.0268	0.6354
Acetate	0.185	0.21	0.8392	0.172	0.194	0.7333	0.168	0.172	0.972
Adenine	6.09	5.63	0.1878	5.7	5.5	0.5395	5.85	5.66	0.8392
Alanine	0.0599	0.0672	0.7333	0.116	0.129	0.4535	0.142	0.153	0.4535
Ethanolamine	6.87	7.23	0.4535	6.89	7.39	0.2398	7.26	7.77	0.5395
Formate	0.156	0.182	0.9451	0.177	0.199	>0.9999	0.15	0.207	0.9451
Fumarate	0.00238	0.00207	0.8142	0.00391	0.00353	>0.9999	0.00614	0.0046	0.3926
Gluconate	76.3	76.6	0.8392	79.8	76.3	0.3736	79.9	77.7	0.4535
Glutamate	0.324	0.303	0.9451	0.939	0.943	0.9451	1.35	1.61	0.6354
Glutathione	1.33	1.34	0.9451	0.767	0.817	0.9211	0.486	0.554	0.6354
Glycine	0.554	0.57	0.9451	1.46	1.85	0.8392	2.25	3.02	0.7333
Hippurate	0.00169	0.00215	0.9441	0.00384	0.00215	0.4505	0.0053	0.00391	0.8332
Hypoxanthine	0.125	0.104	0.7283	0.182	0.175	>0.9999	0.18	0.193	0.6354
Inosine	0.012	0.034	0.1059	0.0177	0.0348	0.2517	0.0145	0.0237	0.2278
Isopropanol	0.0136	0.0146	0.2008	0.0144	0.0158	0.4775	0.0147	0.0175	0.2258
Lactate	0.64	0.888	0.1878	1.09	1.37	0.1878	1.5	1.61	0.3736
Leucine	0.00545	0.0102	0.1419	0.0129	0.0174	0.5205	0.0122	0.0188	0.5395
Oxypurinol	0.297	0.293	0.9451	0.318	0.31	0.8152	0.319	0.312	0.9451
Ribose	1.59	1.59	0.7762	1.59	1.59	0.8342	1.64	1.67	0.9291
Succinate	0.0153	0.018	0.1878	0.0177	0.0226	0.3037	0.0216	0.0286	0.1878
Trimethylamine N-oxide	0	0	0.6703	0.0185	0	0.2567	0.028	0	0.4126
Tyrosine	0.00553	0.00668	0.8362	0.0099	0.0102	0.979	0.0103	0.0124	0.8142
Valine	0.00729	0.00837	0.3566	0.0122	0.0134	0.4535	0.014	0.0177	0.2897
NMR Total concentration of lactate	0.752	0.940	0.5395	1.36	1.56	0.3736	1.7	1.98	0.6354
Concentration of U-^{13}C lactate	0.044	0.037	0.9451	0.118	0.154	0.5395	0.236	0.276	0.6354
% U-^{13}C lactate	7.07	6.04	0.5395	12.1	10.4	0.7333	21	15.9	0.7333
NMR Total concentration of alanine	0.06	0.07	0.8651	0.118	0.137	0.5395	0.149	0.174	0.5395
Concentration of U-^{13}C alanine	0	0	0.6703	0.003	0.014	0.5504	0.01	0.017	0.7053
% U-^{13}C alanine	0	0	>0.9999	4.01	7.13	0.9471	9.13	8.26	0.7333
POC lactate	1.35	1.4	0.6124	1.95	2.1	0.9181	2.15	2.55	0.6623
POC glucose	9.4	8.995	0.4376	8.75	8.55	0.2567	8.55	8	0.7343
Renal Resistance (mmHg/ml/min)	0.28	0.21	0.9451	0.31	0.215	0.9211	0.31	0.22	0.975

Table 18. Association between metabolite concentration and serum creatinine 1 week following transplantation. R-values represent the correlation co-efficient calculated using a two-tailed Spearman's rank correlation test, reported alongside 95% confidence interval. P-values significant at p<0.05.

	1 hour		4 hours		End point	
	r (95% CI)	p-value	r (95% CI)	p-value	r (95% CI)	p-value
3-Methylxanthine	0.1048 (-0.5429 to 0.6743)	0.7601	-0.1636 (-0.7057 to 0.4993)	0.6337	0.05455 (-0.5776 to 0.6458)	0.8812
Acetate	-0.5455 (-0.8681 to 0.1012)	0.0876	-0.6091 (-0.8898 to 0.005963)	0.0519	-0.5455 (-0.8681 to 0.1012)	0.0876
Adenine	0.4909 (-0.1744 to 0.8485)	0.1294	0.01818 (-0.6013 to 0.6241)	0.9673	-0.04545 (-0.6404 to 0.5836)	0.9033
Alanine	-0.4273 (-0.8243 to 0.2514)	0.1928	-0.5727 (-0.8775 to 0.06179)	0.0708	-0.3818 (-0.8060 to 0.3016)	0.2483
Ethanolamine	-0.2909 (-0.7670 to 0.3918)	0.3863	-0.6818 (-0.9131 to -0.1185)	0.0251	-0.2636 (-0.7546 to 0.4165)	0.4348
Formate	-0.6091 (-0.8898 to 0.005963)	0.0519	-0.5636 (-0.8744 to 0.07515)	0.0761	-0.5545 (-0.8713 to 0.08829)	0.0818
Fumarate	-0.1364 (-0.6914 to 0.5199)	0.6937	-0.2733 (-0.7590 to 0.4078)	0.4128	0.2785 (-0.4031 to 0.7614)	0.4034
Gluconate	-0.2818 (-0.7629 to 0.4001)	0.4023	0.1091 (-0.5398 to 0.6767)	0.7545	-0.4455 (-0.8313 to 0.2302)	0.173
Glutamate	-0.1636 (-0.7057 to 0.4993)	0.6337	-0.3636 (-0.7985 to 0.3206)	0.2731	0.02727 (-0.5955 to 0.6296)	0.9462
Glutathione	-0.1364 (-0.6914 to 0.5199)	0.6937	0.164 (-0.4990 to 0.7059)	0.6278	-0.3091 (-0.7751 to 0.3747)	0.356
Glycine	-0.2455 (-0.7461 to 0.4324)	0.4684	-0.3636 (-0.7985 to 0.3206)	0.2731	-0.06364 (-0.6511 to 0.5715)	0.8603
Hippurate	0.07909 (-0.5609 to 0.6599)	0.8179	0.3107 (-0.3732 to 0.7758)	0.3489	0.1907 (-0.4779 to 0.7195)	0.5704
Hypoxanthine	-0.004598 (-0.6157 to 0.6099)	0.9948	-0.4364 (-0.8278 to 0.2409)	0.1826	-0.2273 (-0.7374 to 0.4479)	0.5034
Inosine	-0.4364 (-0.8278 to 0.2409)	0.1826	-0.4 (-0.8134 to 0.2819)	0.225	-0.1636 (-0.7057 to 0.4993)	0.6337
Isopropanol	-0.3371 (-0.7873 to 0.3475)	0.3082	-0.5968 (-0.8857 to 0.02525)	0.0569	-0.5 (-0.8518 to 0.1627)	0.1217
Lactate	-0.3091 (-0.7751 to 0.3747)	0.356	-0.2545 (-0.7503 to 0.4245)	0.4511	-0.4182 (-0.8207 to 0.2617)	0.203
Leucine	-0.2182 (-0.7330 to 0.4556)	0.5208	-0.3052 (-0.7734 to 0.3784)	0.3591	-0.1455 (-0.6962 to 0.5131)	0.6731
Oxypurinol	0.2364 (-0.4402 to 0.7417)	0.4854	-0.3508 (-0.7931 to 0.3338)	0.2886	0.009091 (-0.6071 to 0.6185)	0.9895
Ribose	0.3718 (-0.3122 to 0.8019)	**0.2639**	-0.3668 (-0.7998 to 0.3174)	0.271	0.143 (-0.5149 to 0.6949)	0.68
Succinate	-0.7909 (-0.9455 to -0.3456)	**0.0055**	-0.09091 (-0.6666 to 0.5527)	0.7964	0.2545 (-0.4245 to 0.7503)	0.4511
Trimethylamine N-oxide	0.1079 (-0.5407 to 0.6760)	0.7636	0.1156 (-0.5351 to 0.6803)	0.7333	0.4001 (-0.2818 to 0.8135)	0.224
Tyrosine	-0.2661 (-0.7557 to 0.4143)	0.4291	0.1093 (-0.5396 to 0.6768)	0.7487	-0.03189 (-0.6324 to 0.5925)	0.9302
Valine	-0.4055 (-0.8156 to 0.2759)	0.2159	-0.3182 (-0.7791 to 0.3660)	0.3415	-0.2961 (-0.7693 to 0.3869)	0.374
NMR Total concentration of lactate	-0.1182 (-0.6816 to 0.5333)	0.7345	-0.01818 (-0.6241 to 0.6013)	0.9673	-0.5727 (-0.8775 to 0.06179)	0.0708
Concentration of U-^{13}C lactate	0.3455 (-0.3392 to 0.7909)	0.2993	-0.1364 (-0.6914 to 0.5199)	0.6937	-0.1727 (-0.7104 to 0.4922)	0.6147
% U-^{13}C lactate	0.5091 (-0.1508 to 0.8551)	0.1142	0.1818 (-0.4851 to 0.7150)	0.595	0.2364 (-0.4402 to 0.7417)	0.4854
NMR Total concentration of alanine	-0.3818 (-0.8060 to 0.3016)	0.2483	-0.6909 (-0.9159 to -0.1354)	0.0226	-0.5182 (-0.8584 to 0.1387)	0.1072
Concentration of U-^{13}C alanine	0.2023 (-0.4687 to 0.7252)	0.5636	-0.5242 (-0.8606 to 0.1306)	0.1011	-0.2916 (-0.7673 to 0.3911)	0.3813
% U-^{13}C alanine	-0.1158 (-0.6804 to 0.5350)	0.7432	-0.3762 (-0.8037 to 0.3076)	0.255	0.03636 (-0.5896 to 0.6350)	0.9241
POC lactate	-0.4966 (-0.8506 to 0.1671)	0.1229	-0.4545 (-0.8348 to 0.2194)	0.1635	-0.1053 (-0.6746 to 0.5426)	0.7584
POC glucose	0.2621 (-0.4179 to 0.7538)	0.4341	-0.02278 (-0.6269 to 0.5984)	0.9516	0.1321 (-0.5231 to 0.6891)	0.6984
Renal Resistance	-0.09175 (-0.6671 to 0.5521)	0.7953	-0.07289 (-0.6564 to 0.5652)	0.8328	-0.05923 (-0.6485 to 0.5745)	0.8656

Table 19. Association between metabolite concentration and serum creatinine 1 month following transplantation. R-values represent the correlation co-efficient calculated using a two-tailed Spearman's rank correlation test, reported alongside 95% confidence interval. P-values significant at p<0.05.

	1 hour		4 hours		End point	
	r (95% CI)	p-value	r (95% CI)	p-value	r (95% CI)	p-value
3-Methylxanthine	-0.1018 (-0.6293 to 0.4899)	0.7403	-0.1953 (-0.6837 to 0.4139)	0.5198	-0.0989 (-0.6275 to 0.4921)	0.7506
Acetate	-0.456 (-0.8112 to 0.1448)	0.1198	-0.4725 (-0.8182 to 0.1242)	0.1057	-0.2558 (-0.7162 to 0.3596)	0.3959
Adenine	0.3901 (-0.2224 to 0.7818)	0.1889	0.1484 (-0.4532 to 0.6570)	0.6298	-0.2582 (-0.7174 to 0.3574)	0.3939
Alanine	-0.5055 (-0.8321 to 0.08128)	0.0812	-0.5549 (-0.8521 to 0.01262)	0.0525	-0.5824 (-0.8628 to -0.02799)	**0.0402***
Ethanolamine	-0.3516 (-0.7639 to 0.2644)	0.2392	-0.4011 (-0.7868 to 0.2100)	0.1759	-0.5769 (-0.8607 to -0.01972)	**0.0425***
Formate	-0.4176 (-0.7943 to 0.1910)	0.1574	-0.3681 (-0.7716 to 0.2467)	0.2167	-0.456 (-0.8112 to 0.1448)	0.1198
Fumarate	-0.5055 (-0.8321 to 0.08128)	0.0812	-0.4374 (-0.8031 to 0.1675)	0.1359	0.2562 (-0.3593 to 0.7164)	0.395
Gluconate	-0.2912 (-0.7343 to 0.3259)	0.3342	0.02198 (-0.5484 to 0.5784)	0.9493	-0.4725 (-0.8182 to 0.1242)	0.1057
Glutamate	-0.533 (-0.8433 to 0.04381)	0.0642	-0.6923 (-0.9034 to -0.2110)	**0.0109***	-0.3901 (-0.7818 to 0.2224)	0.1889
Glutathione	0.1374 (-0.4620 to 0.6506)	0.6561	0.4897 (-0.1021 to 0.8255)	0.0913	0.1264 (-0.4708 to 0.6441)	0.6827
Glycine	-0.7198 (-0.9130 to -0.2628)	**0.0073***	-0.6319 (-0.8815 to -0.1060)	**0.0236***	-0.2692 (-0.7231 to 0.3470)	0.3734
Hippurate	0.3448 (-0.2716 to 0.7606)	0.2482	0.4613 (-0.1383 to 0.8134)	0.114	0.2996 (-0.3177 to 0.7385)	0.3187
Hypoxanthine	-0.3945 (-0.7838 to 0.2175)	0.1836	-0.3846 (-0.7793 to 0.2285)	0.1955	-0.6593 (-0.8916 to -0.1523)	**0.0169***
Inosine	-0.3736 (-0.7742 to 0.2407)	0.2095	-0.2586 (-0.7176 to 0.3571)	0.3902	0.02751 (-0.5445 to 0.5821)	0.9311
Isopropanol	-0.3995 (-0.7861 to 0.2119)	0.176	-0.5041 (-0.8315 to 0.08309)	0.0812	-0.4292 (-0.7994 to 0.1774)	0.1439
Lactate	-0.4011 (-0.7868 to 0.2100)	0.1759	-0.4121 (-0.7918 to 0.1974)	0.1635	-0.4066 (-0.7893 to 0.2037)	0.1695
Leucine	-0.3681 (-0.7716 to 0.2467)	0.2167	-0.564 (-0.8556 to -0.0005061)	**0.0476***	-0.4066 (-0.7893 to 0.2037)	0.1695
Oxypurinol	0 (-0.5636 to 0.5636)	>0.9999	-0.3329 (-0.7549 to 0.2840)	0.2648	-0.1538 (-0.6602 to 0.4487)	0.6167
Ribose	0.5576 (-0.008835 to 0.8531)	**0.0493***	-0.08457 (-0.6187 to 0.5030)	0.7876	0.1445 (-0.4563 to 0.6548)	0.6363
Succinate	-0.5495 (-0.8499 to 0.02052)	0.0553	-0.3077 (-0.7425 to 0.3096)	0.3063	0.1703 (-0.4351 to 0.6697)	0.5786
Trimethylamine N-oxide	-0.01747 (-0.5754 to 0.5516)	0.9744	0.1745 (-0.4316 to 0.6720)	0.5719	0.0657 (-0.5171 to 0.6068)	0.8355
Tyrosine	-0.03867 (-0.5894 to 0.5366)	0.9055	-0.07153 (-0.6105 to 0.5128)	0.8166	-0.07703 (-0.6140 to 0.5087)	0.8025
Valine	-0.5427 (-0.8472 to 0.03013)	0.058	-0.5165 (-0.8366 to 0.06649)	0.0741	-0.5805 (-0.8621 to -0.02505)	**0.0406***
NMR Total concentration of lactate	-0.467 (-0.8159 to 0.1311)	0.1103	-0.4286 (-0.7992 to 0.1781)	0.146	-0.5714 (-0.8585 to -0.01152)	**0.0449***
Concentration of U-^{13}C lactate	0.1484 (-0.4532 to 0.6570)	0.6298	-0.5275 (-0.8411 to 0.05144)	0.0673	-0.456 (-0.8112 to 0.1448)	0.1198
% U-^{13}C lactate	0.3132 (-0.3041 to 0.7453)	0.2975	-0.08791 (-0.6208 to 0.5005)	0.7784	-0.03297 (-0.5857 to 0.5407)	0.9205
NMR Total concentration of alanine	-0.5557 (-0.8524 to 0.01151)	0.0514	-0.7418 (-0.9205 to -0.3061)	**0.0051***	-0.7363 (-0.9187 to -0.2951)	**0.0056***
Concentration of U-^{13}C alanine	-0.2489 (-0.7126 to 0.3660)	0.4184	-0.5679 (-0.8572 to -0.006280)	**0.046***	-0.3906 (-0.7821 to 0.2218)	0.1864
% U-^{13}C alanine	-0.52 (-0.8380 to 0.06174)	0.0714	-0.3149 (-0.7461 to 0.3024)	0.2941	-0.08242 (-0.6174 to 0.5046)	0.7926
POC lactate	-0.675 (-0.8973 to -0.1797)	**0.0135***	-0.6217 (-0.8778 to -0.08947)	**0.0261***	-0.5055 (-0.8321 to 0.08123)	0.0804
POC glucose	0.3292 (-0.2878 to 0.7531)	0.2705	0.1568 (-0.4462 to 0.6619)	0.6068	0.01376 (-0.5542 to 0.5729)	0.9677
Renal Resistance	0.1934 (-0.4155 to 0.6826)	0.5269	0.121 (-0.4750 to 0.6409)	0.6921	0.2149 (-0.3968 to 0.6944)	0.4778

Table 20. Association between metabolite concentration and serum creatinine 6 months following transplantation. R-values represent the correlation co-efficient calculated using a two-tailed Spearman's rank correlation test, reported alongside 95% confidence interval. P-values significant at p<0.05.

	1 hour		4 hours		End point	
	r (95% CI)	p-value	r (95% CI)	p-value	r (95% CI)	p-value
3-Methylxanthine	0.0871 (-0.4785 to 0.6017)	0.765	-0.0793 (-0.5966 to 0.4846)	0.7866	0.09901 (-0.4692 to 0.6093)	0.7351
Acetate	-0.4598 (-0.8025 to 0.1108)	0.0994	-0.4708 (-0.8074 to 0.09696)	0.091	-0.2775 (-0.7131 to 0.3126)	0.3335
Adenine	0.363 (-0.2242 to 0.7569)	0.2011	0.09681 (-0.4710 to 0.6079)	0.7413	-0.1672 (-0.6511 to 0.4133)	0.5653
Alanine	-0.352 (-0.7514 to 0.2361)	0.216	-0.2728 (-0.7106 to 0.3172)	0.3427	-0.3938 (-0.7718 to 0.1898)	0.1634
Ethanolamine	-0.08141 (-0.5980 to 0.4830)	0.7815	-0.4576 (-0.8015 to 0.1136)	0.1013	-0.5325 (-0.8343 to 0.01486)	0.0524
Formate	-0.3696 (-0.7601 to 0.2169)	0.1928	-0.3806 (-0.7654 to 0.2047)	0.1789	-0.418 (-0.7833 to 0.1617)	0.1375
Fumarate	-0.4119 (-0.7804 to 0.1689)	0.1434	-0.413 (-0.7809 to 0.1676)	0.1417	0.1876 (-0.3957 to 0.6631)	0.5163
Gluconate	-0.1628 (-0.6485 to 0.4171)	0.5757	0.2992 (-0.2911 to 0.7245)	0.2965	-0.286 (-0.7176 to 0.3042)	0.3191
Glutamate	-0.3366 (-0.7437 to 0.2525)	0.2376	-0.473 (-0.8084 to 0.09415)	0.0892	-0.2332 (-0.6890 to 0.3547)	0.4194
Glutathione	0.209 (-0.3768 to 0.6754)	0.47	0.2445 (-0.3442 to 0.6952)	0.396	0.09241 (-0.4744 to 0.6051)	0.7529
Glycine	-0.3784 (-0.7644 to 0.2071)	0.1818	-0.4202 (-0.7843 to 0.1591)	0.1351	-0.121 (-0.6231 to 0.4517)	0.6784
Hippurate	0.4906 (-0.07151 to 0.8162)	0.077	0.5936 (0.07467 to 0.8596)	**0.0279***	0.405 (-0.1769 to 0.7771)	0.1507
Hypoxanthine	-0.2819 (-0.7154 to 0.3083)	0.326	-0.1166 (-0.6203 to 0.4552)	0.6897	-0.473 (-0.8084 to 0.09415)	0.0892
Inosine	-0.3388 (-0.7448 to 0.2502)	0.2347	-0.0837 (-0.5995 to 0.4812)	0.7748	0.1498 (-0.4280 to 0.6407)	0.6061
Isopropanol	-0.3252 (-0.7379 to 0.2645)	0.2538	-0.2958 (-0.7227 to 0.2945)	0.3011	-0.3076 (-0.7289 to 0.2826)	0.2816
Lactate	-0.2882 (-0.7188 to 0.3021)	0.315	-0.165 (-0.6498 to 0.4152)	0.5701	-0.209 (-0.6754 to 0.3768)	0.47
Leucine	-0.3058 (-0.7280 to 0.2844)	0.2853	-0.2181 (-0.6805 to 0.3686)	0.4502	-0.1452 (-0.6379 to 0.4319)	0.6183
Oxypurinol	0.07921 (-0.4847 to 0.5966)	0.7878	0.02974 (-0.5217 to 0.5636)	0.9192	0.07261 (-0.4897 to 0.5923)	0.805
Ribose	0.5178 (-0.03511 to 0.8280)	0.0594	0.1109 (-0.4598 to 0.6168)	0.7057	0.2874 (-0.3029 to 0.7183)	0.3157
Succinate	-0.4532 (-0.7995 to 0.1191)	0.105	-0.2838 (-0.7164 to 0.3064)	0.3227	0.1804 (-0.4020 to 0.6589)	0.5344
Trimethylamine N-oxide	0.1868 (-0.3965 to 0.6626)	0.5266	0.1667 (-0.4138 to 0.6508)	0.5675	0.05404 (-0.5038 to 0.5800)	0.8558
Tyrosine	-0.03536 (-0.5675 to 0.5176)	0.9059	0.00882 (-0.5368 to 0.5492)	0.9774	-0.03084 (-0.5644 to 0.5209)	0.9176
Valine	-0.3863 (-0.7682 to 0.1983)	0.1715	-0.4092 (-0.7791 to 0.1720)	0.1466	-0.3932 (-0.7715 to 0.1905)	0.1632
NMR Total concentration of lactate	-0.4708 (-0.8074 to 0.09696)	0.091	-0.407 (-0.7781 to 0.1746)	0.1488	-0.4268 (-0.7874 to 0.1512)	0.1288
Concentration of U-^{13}C lactate	-0.1672 (-0.6511 to 0.4133)	0.5653	-0.5919 (-0.8588 to -0.07198)	**0.0282***	-0.5941 (-0.8597 to -0.07535)	**0.0276***
% U-^{13}C lactate	-0.07481 (-0.5937 to 0.4880)	0.7995	-0.3586 (-0.7547 to 0.2290)	0.2069	-0.3498 (-0.7503 to 0.2385)	0.2188
NMR Total concentration of alanine	-0.4366 (-0.7919 to 0.1395)	0.1191	-0.5787 (-0.8535 to -0.05197)	**0.0327***	-0.5765 (-0.8526 to -0.04868)	**0.0335***
Concentration of U-^{13}C alanine	-0.4439 (-0.7952 to 0.1306)	0.1186	-0.7024 (-0.9015 to -0.2576)	**0.0066***	-0.5667 (-0.8486 to -0.03422)	**0.037***
% U-^{13}C alanine	-0.6385 (-0.8773 to -0.1461)	**0.0163***	-0.4575 (-0.8014 to 0.1138)	0.1014	-0.3124 (-0.7314 to 0.2777)	0.2749
POC lactate	-0.6102 (-0.8662 to -0.1005)	**0.0227***	-0.5469 (-0.8403 to -0.005466)	**0.0453***	-0.5243 (-0.8308 to 0.02611)	0.0564
POC glucose	-0.06416 (-0.5867 to 0.4961)	0.8271	-0.01544 (-0.5538 to 0.5320)	0.9592	-0.1105 (-0.6165 to 0.4601)	0.7056
Renal Resistance	0.0884 (-0.4775 to 0.6025)	0.7633	0.04626 (-0.5096 to 0.5748)	0.8755	0.07718 (-0.4862 to 0.5952)	0.7917

Table 21. Association between metabolite concentration and serum creatinine 12 months following transplantation. R-values represent the correlation co-efficient calculated using a two-tailed Spearman's rank correlation test, reported alongside 95% confidence interval. P-values significant at p<0.05.

	1 hour		4 hours		End point	
	r (95% CI)	p-value	r (95% CI)	p-value	r (95% CI)	p-value
3-Methylxanthine	0.08609 (-0.4793 to 0.6010)	0.7678	-0.01544 (-0.5538 to 0.5320)	0.9593	0.2048 (-0.3805 to 0.6730)	0.4794
Acetate	-0.6388 (-0.8774 to -0.1466)	**0.0161***	-0.6454 (-0.8800 to -0.1576)	**0.0148***	-0.452 (-0.7989 to 0.1206)	0.1055
Adenine	0.5264 (-0.02322 to 0.8317)	0.0555	0.03084 (-0.5209 to 0.5644)	0.9183	-0.1167 (-0.6204 to 0.4551)	0.6896
Alanine	-0.2885 (-0.7189 to 0.3017)	0.3146	-0.3502 (-0.7505 to 0.2381)	0.2185	-0.4626 (-0.8037 to 0.1074)	0.0973
Ethanolamine	-0.2137 (-0.6780 to 0.3726)	0.4603	-0.7137 (-0.9057 to -0.2786)	**0.0054***	-0.4824 (-0.8126 to 0.08215)	0.0825
Formate	-0.5463 (-0.8401 to -0.004609)	**0.0458***	-0.5485 (-0.8410 to -0.007754)	**0.0448***	-0.5595 (-0.8456 to -0.02364)	**0.04***
Fumarate	-0.1841 (-0.6610 to 0.3988)	0.5244	-0.2326 (-0.6887 to 0.3553)	0.4192	0.3702 (-0.2163 to 0.7603)	0.1912
Gluconate	-0.2974 (-0.7235 to 0.2930)	0.2996	0.1938 (-0.3903 to 0.6667)	0.5037	-0.3326 (-0.7417 to 0.2568)	0.2437
Glutamate	-0.06608 (-0.5880 to 0.4947)	0.8226	-0.3392 (-0.7450 to 0.2498)	0.234	-0.1982 (-0.6692 to 0.3864)	0.4938
Glutathione	0.01982 (-0.5289 to 0.5568)	0.9486	0.28 (-0.3101 to 0.7144)	0.3287	0.1366 (-0.4390 to 0.6327)	0.6395
Glycine	-0.326 (-0.7383 to 0.2637)	0.2536	-0.3502 (-0.7505 to 0.2381)	0.2185	-0.1233 (-0.6245 to 0.4498)	0.6727
Hippurate	0.4168 (-0.1632 to 0.7827)	0.1385	0.6191 (0.1146 to 0.8697)	**0.0209***	0.3469 (-0.2416 to 0.7489)	0.2224
Hypoxanthine	-0.1333 (-0.6307 to 0.4417)	0.6474	-0.3128 (-0.7315 to 0.2773)	0.2742	-0.3546 (-0.7527 to 0.2333)	0.2124
Inosine	-0.5242 (-0.8308 to 0.02626)	0.0567	-0.2723 (-0.7103 to 0.3177)	0.3423	-0.086 (-0.6009 to 0.4794)	0.7681
Isopropanol	-0.415 (-0.7818 to 0.1652)	0.1399	-0.516 (-0.8272 to 0.03750)	0.0609	-0.5397 (-0.8373 to 0.004640)	**0.0486***
Lactate	-0.2643 (-0.7060 to 0.3254)	0.3583	-0.2577 (-0.7024 to 0.3317)	0.3709	-0.4251 (-0.7866 to 0.1533)	0.1304
Leucine	-0.2841 (-0.7166 to 0.3061)	0.3223	-0.2018 (-0.6712 to 0.3832)	0.4848	-0.1432 (-0.6367 to 0.4335)	0.6232
Oxypurinol	0.1476 (-0.4299 to 0.6394)	0.6124	-0.108 (-0.6150 to 0.4621)	0.7107	0.1498 (-0.4280 to 0.6407)	0.6069
Ribose	0.5366 (-0.008991 to 0.8360)	**0.0491***	0.009757 (-0.5361 to 0.5499)	0.9753	0.2843 (-0.3060 to 0.7167)	0.3211
Succinate	-0.6872 (-0.8959 to -0.2301)	**0.0082***	-0.2996 (-0.7247 to 0.2907)	0.2958	0.1035 (-0.4657 to 0.6121)	0.7237
Trimethylamine N-oxide	0.1318 (-0.4429 to 0.6297)	0.6589	0.2824 (-0.3078 to 0.7157)	0.3257	0.247 (-0.3419 to 0.6966)	0.3905
Tyrosine	-0.1571 (-0.6451 to 0.4219)	0.5888	0.05629 (-0.5021 to 0.5815)	0.8477	0.03087 (-0.5209 to 0.5644)	0.917
Valine	-0.3282 (-0.7394 to 0.2614)	0.2494	-0.3767 (-0.7635 to 0.2091)	0.1839	-0.3881 (-0.7690 to 0.1963)	0.1695
NMR Total concentration of lactate	-0.2687 (-0.7084 to 0.3212)	0.3501	-0.3392 (-0.7450 to 0.2498)	0.234	-0.6145 (-0.8679 to -0.1073)	**0.0217***
Concentration of U-13C lactate	0.1145 (-0.4569 to 0.6191)	0.6951	-0.4559 (-0.8007 to 0.1157)	0.1027	-0.4912 (-0.8164 to 0.07068)	0.0765
% U-13C lactate	0.2093 (-0.3765 to 0.6755)	0.4698	-0.152 (-0.6420 to 0.4262)	0.6016	-0.1278 (-0.6273 to 0.4462)	0.6615
NMR Total concentration of alanine	-0.3102 (-0.7302 to 0.2800)	0.2776	-0.5947 (-0.8600 to -0.07636)	**0.0274***	-0.5308 (-0.8336 to 0.01711)	0.0532
Concentration of U-^{13}C alanine	-0.07049 (-0.5909 to 0.4913)	0.8182	-0.5514 (-0.8422 to -0.01193)	**0.0435***	-0.4338 (-0.7906 to 0.1429)	0.1216
% U-^{13}C alanine	-0.3517 (-0.7512 to 0.2365)	0.2166	-0.3296 (-0.7402 to 0.2599)	0.2478	-0.1564 (-0.6447 to 0.4225)	0.591
POC lactate	-0.6574 (-0.8846 to -0.1779)	**0.0124***	-0.6071 (-0.8650 to -0.09554)	**0.0236***	-0.515 (-0.8268 to 0.03895)	0.0615
POC glucose	0.02769 (-0.5232 to 0.5622)	0.9254	0.05188 (-0.5054 to 0.5786)	0.8596	0.02212 (-0.5272 to 0.5584)	0.9423
Renal Resistance	-0.004138 (-0.5664 to 0.5608)	0.9908	0.0469 (-0.5307 to 0.5948)	0.879	-0.009669 (-0.5702 to 0.5570)	0.9765

Table 22. Correlation between creatinine values and T End concentration of anaerobic metabolites for DCD kidneys. R-values represent the correlation co-efficient calculated using a two-tailed Spearman's rank correlation test. P-values significant at p<0.05.

	1 month Cr		6 month Cr		12 month Cr	
	r value	p-value	r value	p-value	r value	p-value
Total concentration of lactate	-0.8	0.3333	-0.8	0.3333	-0.4	0.75
Concentration of U-^{13}C lactate	-0.8	0.3333	-0.8	0.3333	-0.8	0.3333
% U-^{13}C lactate	-1	0.0833	-1	0.0833	-0.8	0.3333
POC lactate	-0.9487	0.1667	-0.9487	0.1667	-0.3162	0.6667
Total concentration of alanine	-1	0.0833	-1	0.0833	-0.4	0.75
Concentration of U-^{13}C alanine	-0.8	0.3333	-0.8	0.3333	-0.8	0.3333
% U-^{13}C alanine	-0.8	0.3333	-0.8	0.3333	-0.8	0.3333

Table 23. Association between timings of HMP and renal resistance. R-values represent the correlation co-efficient calculated using a two-tailed Spearman's rank correlation test. P-values significant at p<0.05.

	Renal resistance	r	95% CI	p-value
Duration of SCS prior to HMP	RR at 1 hour	0.3113	-0.2789 to 0.7308	0.2785
	RR at 4 hours	0.286	-0.3042 to 0.7176	0.3191
	RR at Tend	0.37	-0.2165 to 0.7603	0.1921
Duration of HMP	RR at 1 hour	0.2627	-0.3270 to 0.7051	0.3636
	RR at 4 hours	0.4224	-0.1565 to 0.7853	0.1331
	RR at Tend	0.348	-0.2404 to 0.7494	0.2214
Total CIT	RR at 1 hour	0.2539	-0.3354 to 0.7003	0.3805
	RR at 4 hours	0.3388	-0.2502 to 0.7448	0.2347
	RR at Tend	0.3348	-0.2545 to 0.7428	0.2404
HMP as a % of CIT	RR at 1 hour	0.09492	-0.4724 to 0.6067	0.749
	RR at 4 hours	0.1826	-0.4001 to 0.6602	0.529
	RR at Tend	0.1079	-0.4622 to 0.6149	0.7122

Table 24. The influence of perfusion timing on endpoint metabolite concentration. R-values represent the correlation co-efficient as per two-tailed Spearman's rank correlation test, reported alongside 95% confidence interval. P-values significant at p<0.05.

	Duration of SCS prior to HMP			Duration of HMP			Total CIT		
	r	95% CI	p-value	r	95% CI	p-value	r	95% CI	p-value
3-Methylxanthine	0.1516	-0.4265 to 0.6418	0.6051	0.1824	-0.4002 to 0.6601	0.5321	0.1956	-0.3887 to 0.6677	0.5022
Acetate	-0.5721	-0.8508 to -0.04213	**0.0352***	-0.3168	-0.7336 to 0.2732	0.2679	-0.6755	-0.8915 to -0.2092	**0.0098***
Adenine	-0.3055	-0.7278 to 0.2848	0.2878	0.1385	-0.4374 to 0.6338	0.6375	-0.1824	-0.6601 to 0.4002	0.5321
Alanine	0.002198	-0.5415 to 0.5446	>0.9999	-0.04176	-0.5718 to 0.5129	0.8915	-0.09011	-0.6036 to 0.4762	0.7616
Ethanolamine	-0.2747	-0.7116 to 0.3153	0.3411	0.1824	-0.4002 to 0.6601	0.5321	-0.1297	-0.6284 to 0.4447	0.6595
Formate	-0.5956	-0.8604 to -0.07773	**0.0274***	-0.3275	-0.7391 to 0.2622	0.253	-0.7187	-0.9075 to -0.2881	**0.005***
Fumarate	0.3506	-0.2377 to 0.7507	0.2178	0.2249	-0.3624 to 0.6844	0.4363	0.4785	-0.08716 to 0.8108	0.0853
Gluconate	-0.244	-0.6949 to 0.3447	0.3998	0.04176	-0.5129 to 0.5718	0.8915	-0.2571	-0.7021 to 0.3323	0.374
Glutamate	0.3231	-0.2667 to 0.7368	0.2597	0.6747	0.2079 to 0.8912	**0.01***	0.5736	0.04446 to 0.8514	**0.0349***
Glutathione	-0.3187	-0.7346 to 0.2713	0.2666	-0.7143	-0.9059 to -0.2798	**0.0054***	-0.6615	-0.8862 to -0.1850	**0.0121***
Glycine	0.3055	-0.2848 to 0.7278	0.2878	0.5473	0.006029 to 0.8405	**0.0458***	0.5868	0.06428 to 0.8568	**0.0303***
Hippurate	-0.1371	-0.6330 to 0.4386	0.6401	-0.06968	-0.5904 to 0.4919	0.8155	-0.1281	-0.6275 to 0.4459	0.6626
Hypoxanthine	-0.04176	-0.5718 to 0.5129	0.8915	0.1648	-0.4154 to 0.6497	0.5733	0.05495	-0.5031 to 0.5806	0.8557
Inosine	0.1254	-0.4481 to 0.6258	0.6672	-0.297	-0.7234 to 0.2933	0.2998	0.0484	-0.5080 to 0.5763	0.8706
Isopropanol	0.1057	-0.4639 to 0.6135	0.7179	0.1894	-0.3941 to 0.6641	0.5137	0.185	-0.3980 to 0.6616	0.5237
Lactate	0.1033	-0.4658 to 0.6120	0.727	0.03297	-0.5193 to 0.5659	0.9155	0.1165	-0.4553 to 0.6203	0.693
Leucine	-0.01099	-0.5507 to 0.5352	0.9758	0.09011	-0.4762 to 0.6036	0.7616	0.08132	-0.4830 to 0.5979	0.7849
Oxypurinol	0.2615	-0.3281 to 0.7045	0.3656	0.1648	-0.4154 to 0.6497	0.5733	0.2791	-0.3110 to 0.7139	0.3332
Ribose	-0.04346	-0.5730 to 0.5116	0.884	0.3203	-0.2697 to 0.7354	0.2625	0.3546	-0.2334 to 0.7527	0.2125
Succinate	0.05934	-0.4998 to 0.5836	0.8438	0.1473	-0.4302 to 0.6392	0.6158	0.2352	-0.3529 to 0.6901	0.4175
Trimethylamine N-oxide	0.2699	-0.3200 to 0.7090	0.3491	0.3309	-0.2586 to 0.7408	0.247	0.3497	-0.2386 to 0.7502	0.22
Tyrosine	0.3322	-0.2572 to 0.7415	0.2441	0.07481	-0.4880 to 0.5937	0.7995	0.3476	-0.2408 to 0.7492	0.2221
Valine	-0.0132	-0.5523 to 0.5336	0.9669	0.2288	-0.3588 to 0.6865	0.4284	0.07481	-0.4880 to 0.5937	0.7995
Total concentration of lactate	0.2308	-0.3570 to 0.6876	0.4265	0.1648	-0.4154 to 0.6497	0.5733	0.244	-0.3447 to 0.6949	0.3998
Concentration of U-^{13}C lactate	0.1121	-0.4589 to 0.6175	0.7043	0.2615	-0.3281 to 0.7045	0.3656	0.05495	-0.5031 to 0.5806	0.8557
% U-^{13}C lactate	-0.08132	-0.5979 to 0.4830	0.7849	0.222	-0.3650 to 0.6827	0.4448	-0.03297	-0.5659 to 0.5193	0.9155
Total concn of alanine	0.08132	-0.4830 to 0.5979	0.7849	0.04176	-0.5129 to 0.5718	0.8915	-0.002198	-0.5446 to 0.5415	>0.9999
Concentration of U-^{13}C alanine	0.1209	-0.4518 to 0.6230	0.6818	0.1956	-0.3887 to 0.6677	0.5022	0.05055	-0.5064 to 0.5777	0.8676
% U-^{13}C alanine	0.0989	-0.4693 to 0.6092	0.7385	0.2791	-0.3110 to 0.7139	0.3332	0.1033	-0.4658 to 0.6120	0.727
POC lactate	0.1193	-0.4530 to 0.6220	0.6829	0.3072	-0.2830 to 0.7287	0.283	0.2122	-0.3739 to 0.6772	0.4634
POC glucose	-0.08609	-0.6010 to 0.4793	0.7723	-0.006623	-0.5477 to 0.5383	0.9879	-0.06402	-0.5866 to 0.4962	0.8312
POC pH	0.07277	-0.4896 to 0.5924	0.8047	-0.07718	-0.5952 to 0.4862	0.7929	0.1125	-0.4586 to 0.6178	0.7004

Table 25. Correlation between total CIT duration and T End anaerobic metabolite levels. R-values represent the correlation co-efficient calculated using a two-tailed Spearman's rank correlation test, reported alongside 95% confidence interval. P-values significant at p<0.05.

Metabolites	Timepoint	r	95% CI	p-value
1D lactate	1 hour	0.1165	-0.4553 to 0.6203	0.693
	4 hours	0.07692	-0.4864 to 0.5951	0.7966
	T End	0.1033	-0.4658 to 0.6120	0.727
POC Lactate	1 hour	-0.146	-0.6384 to 0.4312	0.6162
	4 hours	0.04626	-0.5096 to 0.5748	0.8763
	T End	0.1193	-0.4530 to 0.6220	0.6829
% U-^{13}C lactate	1 hour	0.156	-0.4228 to 0.6445	0.5944
	4 hours	0.01538	-0.5321 to 0.5538	0.9638
	T End	-0.08132	-0.5979 to 0.4830	0.7849
Total amount of lactate detected on NMR	1 hour	0.2132	-0.3730 to 0.6777	0.4636
	4 hours	0.3099	-0.2803 to 0.7301	0.2806
	T End	0.2308	-0.3570 to 0.6876	0.4265
Concentration U-^{13}C lactate	1 hour	0.2835	-0.3067 to 0.7163	0.3253
	4 hours	0.2264	-0.3610 to 0.6852	0.4356
	T End	0.1121	-0.4589 to 0.6175	0.7043

Table 26. Correlation between duration of HMP and T End anaerobic metabolite levels. R-values represent the correlation co-efficient calculated using a two-tailed Spearman's rank correlation test, reported alongside 95% confidence interval. P-values significant at p<0.05.

Metabolites	Timepoint	r	95% CI	p-value
1D lactate	1 hour	-0.07253	-0.5922 to 0.4898	0.8083
	4 hours	-0.002198	-0.5446 to 0.5415	>0.9999
	T End	0.03297	-0.5193 to 0.5659	0.9155
POC Lactate	1 hour	-0.2102	-0.6760 to 0.3757	0.4678
	4 hours	-0.03304	-0.5659 to 0.5193	0.9124
	T End	0.3072	-0.2830 to 0.7287	0.283
% U-^{13}C lactate	1 hour	0.1692	-0.4116 to 0.6523	0.5629
	4 hours	0.09011	-0.4762 to 0.6036	0.7616
	T End	0.222	-0.3650 to 0.6827	0.4448
Total amount of lactate detected on NMR	1 hour	0.06374	-0.4965 to 0.5865	0.8319
	4 hours	0.2659	-0.3238 to 0.7069	0.3573
	T End	0.1648	-0.4154 to 0.6497	0.5733
Concentration U-^{13}C lactate	1 hour	0.2703	-0.3196 to 0.7092	0.3492
	4 hours	0.1121	-0.4589 to 0.6175	0.7043
	T End	0.2615	-0.3281 to 0.7045	0.3656

Table 27. Correlation between period of SCS prior to HMP and T End anaerobic metabolite levels. R-values represent the correlation co-efficient calculated using a two-tailed Spearman's rank correlation test, reported alongside 95% confidence interval. P-values significant at p<0.05.

Metabolites	Timepoint	r	95% CI	p-value
1D lactate	1 hour	0.3363	-0.2529 to 0.7435	0.2399
	4 hours	0.05055	-0.5064 to 0.5777	0.8676
	T End	0.1033	-0.4658 to 0.6120	0.727
POC Lactate	1 hour	0.1637	-0.4163 to 0.6490	0.5734
	4 hours	0.1608	-0.4188 to 0.6473	0.5804
	T End	0.1193	-0.4530 to 0.6220	0.6829
% U-^{13}C lactate	1 hour	0.178	-0.4041 to 0.6575	0.5423
	4 hours	0.08132	-0.4830 to 0.5979	0.7849
	T End	-0.08132	-0.5979 to 0.4830	0.7849
Total amount of lactate detected on NMR	1 hour	0.4286	-0.1492 to 0.7882	0.1281
	4 hours	0.1868	-0.3964 to 0.6626	0.5221
	T End	0.2308	-0.3570 to 0.6876	0.4265
Concentration U-^{13}C lactate	1 hour	0.367	-0.2198 to 0.7588	0.1974
	4 hours	0.3846	-0.2002 to 0.7674	0.1755
	T End	0.1121	-0.4589 to 0.6175	0.7043

Table 28. Association between biochemical assay concentrations and development of DGF. Data reported as Median (range), with p-value from Mann-Whitney test. P-values significant at p<0.05.

		All (n=14)	DGF (n=4)	IGF (n=10)	p-value
NGAL (ng/ml)	1 hour	3.81 (1.48-14.4)	3.65 (1.48-14.4)	3.81 (1.62-11.0)	0.9451
	4 hours	4.61 (2.58-18.9)	4.52 (2.71-18.9)	4.61 (2.58-11.5)	0.9399
	T End	5.02 (2.25-25.5)	5.33 (2.25-13.9)	4.40 (2.71-25.5)	0.8392
GST Pi (ng/ml)	1 hour	32.1 (14.1-36.7)	33.0 (14.1-33.2)	30.2 (19.6-36.7)	0.8392
	4 hours	31.0 (21.6-32.2)	31.6 (27.2-32.2)	29.6 (21.6-31.1)	0.0755
	T End	28.7 (21.2-32.8)	26.9 (21.6-31.2)	28.9 (21.2-32.8)	0.4725
LDH (Nmol)	1 hour	12.0 (1.00-32.0)	12.5 (1.00-32.0)	13.3 (3.01-26.8)	0.8392
	4 hours	17.7 (3.77-35.7)	17.4 (3.77-35.7)	17.7 (5.66-28.9)	0.9399
	T End	18.8 (3.77-36.4)	20.7 (3.77-36.4)	18.8 (8.48-33.4)	0.9451

Table 29. Association between biochemical assay concentrations and serum creatinine. R-values represent the correlation co-efficient calculated using a two-tailed Spearman's rank correlation test, reported alongside 95% confidence interval. P-values significant at p<0.05.

	1 week Cr		1 month Cr		6 month Cr		12 month Cr	
	r (95% CI)	p-value	r (95% CI)	p-value	r (95% CI)	p-value	r (95% CI)	p-value
NGAL (ng/ml)								
1 hour	-0.2182 (-0.7330 to 0.4556)	0.5208	-0.3462 (-0.7613 to 0.2702)	0.2471	-0.1518 (-0.6419 to 0.4263)	0.6018	-0.1079 (-0.6149 to 0.4622)	0.7123
4 hours	-0.2485 (-0.7298 to 0.5029)	0.4918	-0.2727 (-0.7409 to 0.3738)	0.3912	-0.008253 (-0.5692 to 0.5580)	0.9822	-0.1129 (-0.6361 to 0.4813)	0.7122
T End	0.1 (-0.5463 to 0.6717)	0.7759	0.07692 (-0.5088 to 0.6139)	0.8064	0.143 (-0.4337 to 0.6366)	0.6233	0.1189 (-0.4534 to 0.6218)	0.6838
GST Pi (ng/ml)								
1 hour	0.01818 (-0.6013 to 0.6241)	0.9673	-0.03297 (-0.5857 to 0.5407)	0.9205	0.07041 (-0.4914 to 0.5908)	0.8113	0.1167 (-0.4551 to 0.6204)	0.6896
4 hours	0.06667 (-0.7919 to 0.3843)	0.8651	0.02797 (-0.5681 to 0.6048)	0.9388	-0.09078 (-0.6225 to 0.4983)	0.768	-0.1846 (-0.6777 to 0.4231)	0.5432
T End	0.4273 (-0.2514 to 0.8243)	0.1928	0.5254 (-0.05423 to 0.8402)	0.0679	0.4427 (-0.1320 to 0.7947)	0.1137	0.366 (-0.2209 to 0.7583)	0.1966
LDH (Nmol)								
1 hour	-0.1818 (-0.7150 to 0.4851)	0.595	-0.456 (-0.8112 to 0.1448)	0.1198	-0.3894 (-0.7697 to 0.1948)	0.1684	-0.1762 (-0.6564 to 0.4056)	0.5439
4 hours	-0.297 (-0.7037 to 0.5420)	0.4069	-0.5035 (-0.8416 to 0.1181)	0.0989	-0.6025 (-0.8705 to -0.05884)	0.0323	-0.4298 (-0.7997 to 0.1767)	0.1435
T End	-0.3727 (-0.8023 to 0.3112)	0.2608	-0.4231 (-0.7967 to 0.1845)	0.1517	-0.4532 (-0.7995 to 0.1191)	0.105	-0.3282 (-0.7394 to 0.2614)	0.2503

Chapter 8 : Discussion

The French surgeon Alexis Carrel, considered the father of solid organ transplantation, made significant contributions to the field of organ preservation (254). In his sentinel paper entitled ‘the preservation of tissues and its applications in surgery’ published in 1912, he stated ‘a tissue is in latent life when its metabolism becomes so slight that it can hardly been detected, and also when its metabolism is completely suspended’ (255). As a hypothermic modality of preservation, such reduction in metabolism is a key mechanism by which hypothermic machine perfusion acts. Additional mechanisms include simple mechanistic amelioration of vasospasm, protective endothelial pathways and a limited role of resuscitation including the reversal of ischaemia reperfusion injury.

Research conducted forming the contents of this thesis adds to current understanding of the clinical utility and metabolic mechanisms by which HMP is beneficial in addition to discussing one method of optimisation of cadaveric kidneys during hypothermic machine perfusion. Exploration of such metabolism with employment of [U-^{13}C] glucose as a metabolic tracer forms the basis of work contained in this thesis.

However, given the lack of explicit guidance for its usage and a lack of clinical trials within the UK showing any benefit to the use of HMP, the first aim of the thesis addressed in Chapter 4 was to determine whether HMP does in fact influence clinical outcomes in this population via registry analysis of a national cohort of patients. Such examination of outcomes for DBD and DCD kidneys was important given the results of the only UK based RCT for DCD kidneys contradicted the results of the Machine Preservation Trial. Results showed a reduction in the incidence of DGF for recipients of DCD kidneys which underwent HMP with the suggestion of a slight improvement in serum creatinine at 1 year.

Importantly, the study highlighted graphically for DCD kidneys how the incidence of DGF changes for kidneys undergoing HMP with increasing durations of CIT.

With the suggestion clinical outcomes differ between kidneys stored in HMP and SCS, as a preliminary study, the aim of the study described in Chapter 5 was to determine changes in metabolism between HMP and SCS conditions using 1D-^{1}H NMR. This chapter along with Chapter 6 utilises an established porcine DCD model with significant advantages but also inherent limitations.

With limitations associated with non-utilisation of tracer-based metabolism, it was still evident that metabolism differed in those organs undergoing HMP compared those stored using SCS alone. It was evident that such differences could and should indeed be investigated with use of a metabolic tracer; research has shown tracer-based metabolism using 2D NMR spectroscopy has a role in describing *de novo* metabolism in discarded human cadaveric kidneys and porcine kidneys during HMP (175). Chapter 3 describes refinements in NMR methodology which permit a more accurate determination of isotopomers in a shorter time period using ^{13}C spectral filters and J-coupling based splitting enhancement in 2D-NMR spectra.

Given that hypoxia initiates IRI, and with changes in metabolism central to ongoing ischaemic insult during the preservation period, supplemental oxygenation during HMP may serve to reduce injury. Using a multi-modality approach, the aim of Chapter 6 was to determine the changes effected by supplementation of circulating perfusion fluid with oxygen. Results showing a greater degree of aerobic metabolism and higher ATP levels in kidneys undergoing oxygenated HMP compared with aerated HMP suggest oxygenation has a limited role in resuscitation during HMP although the results of clinical studies addressing the use of such technology are awaited.

Application of tracer-based NMR and MS methodology to human cadaveric kidneys during HMP prior to transplantation allows for description of *de novo* metabolism during the ischaemic phase of IRI. However, such methodology has never been applied to human kidneys prior to transplantation. The results of the CHAMPION study described in Chapter 7 showed stark differences in *de novo* metabolism with DCD kidneys displaying higher rates of anaerobic metabolism. The extent of anaerobic metabolism may be associated with duration of initial warm ischaemic insult. Such changes in metabolism for DCD organs are perhaps unsurprising but provide an explanation of why the incidence of DGF is higher in DCD kidneys and provides a focus for resuscitation of such organs.

Optimal duration

The benefits of HMP in the wider context are due to hypothermia, but in comparison to static storage, benefits are due to changes in metabolism as a driving force for reduction of IRI, simple mechanistic amelioration of vasospasm and upregulation of protective endothelial pathways.

The duration of HMP after which each of these mechanisms of action exerts clinical benefit is likely to differ. For example, endothelial protective methods likely occur as a result of upregulation of protective endothelial pathways such as KLF-2 and eNOS, some of which also result in vasodilation. Such pathways are unlikely to be upregulated within minutes, and likely require several of hours of HMP to take effect. Similarly, in Chapter 6, deviation from anaerobic metabolism as a result of oxygenation seemed to occur at 8 hours. Simple mechanistic amelioration of vasospasm which occurs during hypothermia is likely to occur within the first hour of machine perfusion and it is this mechanism which is likely responsible for the change in perfusion parameters in the first instance. As such, the question of which duration of HMP is beneficial is a difficult question to answer. The

duration is likely to differ per mechanism of action and also for each kidney according to donor subtype amongst other variables.

The resuscitative potential of HMP

The basic principle of hypothermic modalities of organ preservation is a reduction in the rate of metabolic reactions. Whilst this reduces organ damage otherwise seen in warm ischaemia, it seems rational that the extent to which organs can be resuscitated swiftly is limited as deviation towards a different metabolic phenotype is also limited by hypothermia. For example, even with oxygenated HMP, 8 hours of perfusion were required before differences in *de novo* metabolites in circulating perfusate were evident. However, technologies such as oxygenation (212) alongside the addition of additives such as haemoglobin (256) have shown promise in organ resuscitation.

The limited role of standard HMP in the resuscitation of kidneys is evidenced by the predominance of CIT as an independent risk factor for adverse long-term outcomes regardless of hypothermic preservation modality in several studies (70, 186, 187, 200).

Normothermic modalities of organ preservation

The results of the CHAMPION study (Chapter 7) suggested DCD organs rely on anaerobic metabolism compared to DBD organs. Such a switch to anaerobic metabolism likely occurs due to initial warm ischaemic insult. Normothermic regional perfusion has the potential to reduce this initial warm ischaemic insult *in situ* prior to cold-flush and subsequent preservation in hypothermic conditions.

Restoration of blood in DCD donors following asystole using the patient's own blood circulated through an extra-corporeal is the premise behind normothermic regional

perfusion, considered a form of pre-conditioning as organs remain *in situ* whilst perfusion is commenced. A study by Antoine et al (257) described clinical outcomes of uncontrolled DCD donors in France where uncontrolled DCD donors form part of the donor pool, unlike the UK. In this study, organs perfused using NRP displayed lower rates of PNF compared with those cooled *in situ*.

Ex vivo normothermic perfusion (EVNP), first described by Carrel and Lindbergh in 1935 (50), attempts to simulate the *in vivo* environment by supplementing explanted organs with oxygenated blood whilst maintaining homeostasis. Similar to hypothermic perfusion, normothermic perfusion aims to preserve organs *ex vivo* whilst also providing opportunities to assess viability and repair damage. However, whilst hypothermic conditions aim to reduce metabolic processes, both types of normothermic perfusion preserve and facilitate these processes.

The benefits of EVNP, whilst shown to be promising in preliminary animal studies (258) and those in discarded human kidneys (259), are yet to be reported in randomised trials although one such trial is currently underway.

Future studies and technologies

Future studies relating to this thesis should explore the relationship between warm ischaemia and predominance of anaerobic metabolism further. If, as suggested by data in Chapter 7, warm ischaemic insult determines the extent of anaerobic metabolism, there may be a greater role for resuscitative technologies in such organs such as oxygenated hypothermic machine perfusion and normothermic regional perfusion.

Tracer-based metabolism should easily be applied to the setting of *ex vivo* normothermic perfusion in order to guide its usage and optimise outcome. The results of such studies are likely to show a greater degree of aerobic metabolism.

Recently, the role of mesenchymal stem cells has been explored within the field of renal transplantation (260) with evidence that the infusion of such cells has the potential to promote an immunomodulatory effect (258, 261, 262) in addition to promoting angiogenesis (263) and improving the function of glomeruli and tubuli (264). Studies should continue to investigate the role of mesenchymal stem cell infusion on organ regeneration.

Final comments

Regardless of the method of preservation, the primary aim is to preserve structure and function of the kidney with secondary aims of resuscitation and assessment of donor kidneys prior to implantation. The organ preservation period is a crucial period in which cadaveric kidneys lie dormant, classically in static hypoxic ischaemic conditions. However, hypothermic machine perfusion is an alternative established, dynamic method of preserving kidneys with observed clinical benefits in well-designed major randomised control trials. This thesis aids understanding of its clinical utility and mechanism of action with reference to metabolism in addition to showing the benefits of oxygenating circulating perfusion fluid.

Appendices

Appendix A: Published abstract for oral presentation at the 18th Annual Congress of the European Society of Transplantation 2017 (Barcelona)

Conclusion: Our data suggest that treating kidneys with MitoQ during cold preservation ameliorates the detrimental effects of IRI and can potentially improve graft and patient outcomes after kidney transplantation.

Translational Kidney Ischemia-reperfusion and preservation

OS331 HYPOTHERMIC MACHINE PERFUSION FOLLOWING STATIC COLD STORAGE IN DONATION AFTER CARDIAC DEATH CADAVERIC KIDNEYS: A UK POPULATION-BASED COHORT STUDY

Kamlesh Patel, James Hodson, Adnan Sharif, Melanie Field, Jay Nath, Nick Inston, Andrew Ready

Queen Elizabeth Hospital Birmingham, United Kingdom

Background: Previous systematic reviews have demonstrated the reduction in delayed graft function (DGF) rates when hypothermic machine perfusion (HMP) is used to preserve kidneys prior to transplantation. However, heterogeneity in design of randomised controlled trials, such as the timing of the start of HMP, may explain why reduction in DGF rates in a Eurozone population were not demonstrated in a UK study in Donation after Cardiac Death (DCD) donors.

The aim was to assess the outcome of DCD donor kidneys which undergo a period of HMP following SCS compared to those which are preserved with SCS alone.

Methods: A population based cohort study was performed using prospectively collected data from the National Health Service Blood and Transplant service in the United Kingdom. All adult recipients of single organ DCD kidneys transplanted between 2007 and 2015 were included.

Results: A total of 4529 DCD kidneys were included in the study with HMP used in 19.1% of cases ($N = 864$). HMP usage was found to be in decline over the period of the study ($p < 0.001$), from 25.6% of transplants in 2007–2010, to 14.4% of transplants in 2014–2015. Cases where HMP was used had significantly longer CIT than SCS organs (median: 14.8 vs. 14.1 h, $p < 0.001$), and HMP was most commonly used in organs that were re-perfused with the recipients' blood during the daytime (8:00–16:59, $p < 0.001$).

The rate of DGF was found to be significantly lower in organs where HMP was used, compared to SCS (34.2% vs. 41.9%, $p < 0.001$). This remained significant after accounting for potentially confounding factors in a multivariable analysis, with an odds ratio of 0.64 (95% CI: 0.53–0.78, $p < 0.001$) for HMP vs. SCS. Neither patient ($p = 0.610$) nor graft ($p = 0.664$) survival were found to differ significantly between the HMP and SCS cohorts.

Discussion: Our UK population-based study demonstrates the incidence of delayed graft function can be significantly reduced by a period of HMP in DCD kidneys, even after a period of SCS.

OS332 EVALUATION OF OUTCOMES IN RENAL TRANSPLANTATION USING MACHINE PERFUSION FOR THE PRESERVATION OF KIDNEYS FROM EXPANDED CRITERIA DONORS

Emilie Savoye[1], Marie-Alice Macher[1], Michel Videcocq[2], P Gatault[3], M. Hazzan[4], I Abboud[5], Antoine Thierry[6], Isabelle Etienne[7], S Drouin[8], J Sayegh[9], Olivier Bastien[1], Christian Lamotte[1], Hélène Logerot[1], Camille Legeai[1], Corinne Antoine[1]

[1]Agence De La Biomédecine, France; [2]Chu Nantes, France; [3]Chu Tours, France; [4]Chu Lille, France; [5]Chu Saint Louis Paris, France; [6]Chu Poitier, France; [7]Chu Rouen, France; [8]Chu La Pitié Salpétrière Paris, France; [9]Chu Anger, France

Introduction: The shortage of kidney grafts led to retrieve organs from old donors with one or more co-morbidities, considered as "expanded criteria donors" (ECD). In France, since 2012, the Agency of biomedicine (ABM) has recommended the use of machines perfusion (MP) to preserve kidneys from this donor population to improve kidney preservation and the transplantation outcomes, with the creation of a specific lump sum financing the additional costs of this strategy. This study evaluates the impact of MP vs. cold storage (CS), for the period 2011–2014 with kidneys from ECD.

Methods: From the ABM database (Cristal), the effect of MP on the delayed graft function (DGF) was analyzed using a multivariate logistic model excluding pre-emptive transplants and primary non functions (PNF). In addition, transplants from the same donor, whose one kidney preserved by MP and the other by CS (population of twins), were analyzed using a mixed model.

Results: Co-morbidities of recipients are more frequent and the age of donors and recipients is significantly higher for kidney preserved by MP ($n = 801$) vs. CS ($n = 3515$). With 16% of DGF for MP vs. 29% for CS, MP has a protective effect on the DGF (OR adjusted = 0.45, CI [0.36, 0.56]). In the population of the twins (84 pairs, 168 grafts), we observed 7% of DGF for MP vs. 33% for CS and an adjusted OR 0.19 (CI [0.06; 0.58]). The durations of hospitalization and dialysis after transplantation are shorter with fewer sessions of dialysis.

Discussion: Our results confirm the reduction in the incidence of the DGF of ECD kidneys preserved by machines, with 2.2 times less risk despite a population more at risk in this group, and a lower 5.2 times risk in the population of the kidneys "twins". It remains to assess the impact of the DGF in the long term survival and measure the cost effectiveness of this strategy.

Clinical Kidney Ischemia-reperfusion and preservation

OS333 EXTENDED EX-VIVO NORMOTHERMIC HUMAN KIDNEY PERFUSION USING AN ARTIFICIAL OXYGEN CARRIER

Fermin Fontan, Mohamed Aburawi, Negin Karimian, Heidi Yeh, Korkut Uygun, James Markmann

Harvard Medical School Massachusetts General Hospital, United States

Background: Hypothermic machine perfusion (HMP) is commonly used in kidney preservation, providing some advantage over static cold storage. However, the low temperature offers little opportunity to improve organ quality or to obtain functional data. We therefore established an oxygenated normothermic machine perfusion (NMP) system to investigate the possibility of rescuing discarded kidneys.

Methods/materials: Pressure and temperature controlled NMP with an enriched media and Hemopure (bovine hemoglobin-based oxygen carrier) was used to perfuse 9 human kidneys deemed un-transplantable by all transplant centers. The average cold ischemia time (CIT) was 21 h. The grafts were discarded for different reasons, including poor performance on the HMP pump, concerning biopsy results, poor flush, fail to allocate the organ, and surgical damage to the hilum. Organs from donation after circulatory and brain death were accepted. Kidneys were perfused for up to 12 hrs. Different metabolic markers, functional parameters and macroscopic assessment measurements were recorded throughout the perfusion session.

Results: Renal artery flow/resistance showed a sustained improvement throughout the perfusion period. The maintenance of a relatively physiologic pH/bicarbonate level and the arterio-venous oxygen difference showed evidence of significant metabolic activity. Only the last three kidneys in our series produced significant amounts of urine; this correlated with removing the albumin aiming to assess the implications of decreasing the oncotic pressure of the perfusate.

Conclusions: Our ongoing series results are notable for a significant metabolic activity, favorable functional parameters and macroscopic characteristics; in addition to urine production suggesting that some of these kidneys could have been used for transplantation. ATP and pathology results are pending, which will likely add more information for us to more accurately catalog these grafts and theorize which ones could be implanted.

Translational Kidney Ischemia-reperfusion and preservation

OS334 DEVELOPMENT OF AN AUTOMATIC REGULATED NORMOTHERMIC KIDNEY PRESERVATION DEVICE FOR LONG-TERM PERFUSION

Annemarie Weissenbacher[1], Letizia Lo Faro[2], Olga Boubriak[3], James Hunter[1], Rutger Ploeg[1], Nikolay Mikov[4], Andrew Cook[4], Daniel Voyce[4], Constantin Coussios[3], Peter Friend[1]

[1]Oxford Transplant Centre Nuffield Department of Surgical Sciences, United Kingdom; [2]Oxford Transplant Centre, Nuffield Department of Surgical Sciences, Oxford University, United Kingdom; [3]Institute of Biomedical Engineering Department of Engineering Science University of Oxford, United Kingdom; [4]Organox Limited Oxford Science Park Magdalen Centre, United Kingdom

Background: Normothermic kidney perfusion for a period of 24 h or longer could offer significant clinical advantages. It would enable clinicians to investigate the condition of renal parenchyma during the warm preservation period and provide a platform for repairing kidneys that are currently discarded. This would enlarge the donor pool and enable more successful renal transplants.

Methods: We have established an automated closed circuit normothermic kidney perfusion (NKP) prototype, with the objective of perfusing human kidneys for 24 h.

Results: Twenty-one discarded human kidneys from DBD (donation after brain death) and DCD (donation after cardiac death) donors were perfused and functional parameters were proven stable and physiological. Median perfusion time was 15 h (1.5–24.4). Eight kidneys were perfused for 24 h. Cold ischemia time (CIT) was significantly longer in DCD compared to DBD; $p = 0.033$. Median CIT was 25.3 h (8.1–106). DCD kidneys (601.7 $\pm$ 150 ml) produced more urine than DBDs (285 $\pm$ 95.74 ml) but this was not significant; $p = 0.17$. Urinary output was significantly correlated with warm ischemia time in DCD; $p = 0.018$. Measured biochemical parameters included glucose, lactate, NGAL, KIM-1 and L-FABP. All but one perfused kidneys showed clear

Appendix B: Champion study NRES Ethical Approval REC reference 15/EM/0328

NRES Committee East Midlands - Leicester
The Old Chapel
Royal Standard Place
Nottingham
NG1 6FS

Telephone: 0115 8839436

07 September 2015

Mr Jay Nath
Queen Elizabeth Hospital
Mindelsohn Way
Edgbaston, Birmingham
B15 2WB

Dear Mr Nath

Study title:	**A study to determine the metabolic effects of machine perfusion on cadaveric kidneys for transplantation.**
REC reference:	**15/EM/0328**
Protocol number:	**1**
IRAS project ID:	**184195**

Thank you for your letter of 28 August 2015, responding to the Committee's request for further information on the above research and submitting revised documentation.

The further information has been considered on behalf of the Committee by the Chair.

We plan to publish your research summary wording for the above study on the HRA website, together with your contact details. Publication will be no earlier than three months from the date of this favourable opinion letter. The expectation is that this information will be published for all studies that receive an ethical opinion but should you wish to provide a substitute contact point, wish to make a request to defer, or require further information, please contact the REC Assistant, Joanne Unsworth, nrescommittee.eastmidlands-leicester@nhs.net. Under very limited circumstances (e.g. for student research which has received an unfavourable opinion), it may be possible to grant an exemption to the publication of the study.

Confirmation of ethical opinion

On behalf of the Committee, I am pleased to confirm a favourable ethical opinion for the above research on the basis described in the application form, protocol and supporting documentation as revised, subject to the conditions specified below.

Conditions of the favourable opinion

The favourable opinion is subject to the following conditions being met prior to the start of the study.

Management permission or approval must be obtained from each host organisation prior to the start of the study at the site concerned.

Management permission ("R&D approval") should be sought from all NHS organisations involved in the study in accordance with NHS research governance arrangements.

Guidance on applying for NHS permission for research is available in the Integrated Research Application System or at http://www.rdforum.nhs.uk.

Where a NHS organisation's role in the study is limited to identifying and referring potential participants to research sites ("participant identification centre"), guidance should be sought from the R&D office on the information it requires to give permission for this activity.

For non-NHS sites, site management permission should be obtained in accordance with the procedures of the relevant host organisation.

Sponsors are not required to notify the Committee of approvals from host organisations

Registration of Clinical Trials

All clinical trials (defined as the first four categories on the IRAS filter page) must be registered on a publically accessible database. This should be before the first participant is recruited but no later than 6 weeks after recruitment of the first participant.

There is no requirement to separately notify the REC but you should do so at the earliest opportunity e.g. when submitting an amendment. We will audit the registration details as part of the annual progress reporting process.

To ensure transparency in research, we strongly recommend that all research is registered but for non-clinical trials this is not currently mandatory.

If a sponsor wishes to request a deferral for study registration within the required timeframe, they should contact hra.studyregistration@nhs.net. The expectation is that all clinical trials will be registered, however, in exceptional circumstances non registration may be permissible with prior agreement from the HRA. Guidance on where to register is provided on the HRA website.

It is the responsibility of the sponsor to ensure that all the conditions are complied with before the start of the study or its initiation at a particular site (as applicable).

Ethical review of research sites

NHS sites

The favourable opinion applies to all NHS sites taking part in the study, subject to management permission being obtained from the NHS/HSC R&D office prior to the start of the study (see "Conditions of the favourable opinion" below).

Non-NHS sites

Approved documents

The final list of documents reviewed and approved by the Committee is as follows:

Document	*Version*	*Date*
Covering letter on headed paper [Covering letter explaining changes to PIS]		26 August 2015
IRAS Checklist XML [Checklist_08072015]		08 July 2015

IRAS Checklist XML [Checklist_28082015]		28 August 2015
Participant consent form [Consent form]	1	01 June 2015
Participant consent form [Revised consent form]	V1.1	20 August 2015
Participant information sheet (PIS) [Information Sheet]	1	01 June 2015
Participant information sheet (PIS) [Revised PIS]	V1.1	20 August 2015
Participant information sheet (PIS) [PIS with changes explained]		20 August 2015
REC Application Form [REC_Form_08072015]		08 July 2015
Research protocol or project proposal [Protocol]	1	01 June 2015
Summary CV for Chief Investigator (CI) [CV Jay Nath]	1	06 July 2015
Summary CV for student [CV Jay Nath]	1	06 July 2015
Summary CV for supervisor (student research) [CV Supervisor]	1	06 July 2015
Summary, synopsis or diagram (flowchart) of protocol in non technical language [Protocol Flowsheet]	1	01 June 2015

Statement of compliance

The Committee is constituted in accordance with the Governance Arrangements for Research Ethics Committees and complies fully with the Standard Operating Procedures for Research Ethics Committees in the UK.

After ethical review

Reporting requirements

The attached document *"After ethical review – guidance for researchers"* gives detailed guidance on reporting requirements for studies with a favourable opinion, including:

- Notifying substantial amendments
- Adding new sites and investigators
- Notification of serious breaches of the protocol
- Progress and safety reports
- Notifying the end of the study

The HRA website also provides guidance on these topics, which is updated in the light of changes in reporting requirements or procedures.

User Feedback

The Health Research Authority is continually striving to provide a high quality service to all applicants and sponsors. You are invited to give your view of the service you have received and the application procedure. If you wish to make your views known please use the feedback form available on the HRA website:
http://www.hra.nhs.uk/about-the-hra/governance/quality-assurance/

HRA Training

We are pleased to welcome researchers and R&D staff at our training days – see details at http://www.hra.nhs.uk/hra-training/

15/EM/0328	Please quote this number on all correspondence

With the Committee's best wishes for the success of this project.

Yours sincerely

pp.

Mr Ken Willis
Chair

Email:nrescommittee.eastmidlands-leicester@nhs.net

Copy to: *Mr Jay Nath*
Dr Chris Counsell, Research and Development Office

Appendix C: Champion study R&D approval, University Hospitals Birmingham NHS Foundation Trust

(RPAv41)

Mr N. Inston
Consultant Surgeon
Department of Renal Transplantation & Nephrology
Queen Elizabeth Hospital
UHB

UHB Research Governance Office
1st Floor, Institute of Translational Medicine
Heritage Building
Queen Elizabeth Hospital Birmingham
Mindelsohn Way
Edgbaston
Birmingham B15 2WG
Tel. 0121 371 4185
Fax 0121 371 4204

Research Project Authorisation

Project reference:**RRK 5478**

Main Ethics Committee Reference: 15/EM/0328
IRAS Project ID:

24 November 2015

Dear Mr Inston

A Study to Determine the Metabolic effects of Machine Perfusion on Cadaveric Kidneys for Transplantation

Thank you for submitting details of your proposed research project, which I am happy to authorise on behalf of University Hospitals Birmingham. The following main document versions were reviewed (note this is not a complete list of all documents submitted):

Protocol - version: V1 01/06/15
Participant information sheet (main) - version: V1 20/08/15
Participant consent form (main) - version: V1 20/08/15

Acv2/12

Sponsorship
University Hospitals Birmingham NHS Trust has agreed to act as sponsor for this study. We believe this is a single site study. If you wish to include sites outside University Hospitals Birmingham then you must provide details of potential sites to the R&D Office, the main research ethics committee, and if necessary to the regulatory authorities. Note, however, that sites outside University Hospitals Birmingham must not start recruiting into the study until there has been formal authorisation from the R&D Office at University Hospitals Birmingham. We will require a copy of the approval letter from the R&D Department of the relevant Trust. If the study is a clinical trial of a medicine then we will also require a signed clinical trial agreement which we will draw up between UHB and the other Trust; for other types of study a clinical study agreement would not normally be required.

Indemnity arrangements.
Researchers who hold substantive or honorary contracts with University Hospital Birmingham (UHBT) will be covered against claims of negligence by patients of UHBT under the Clinical Negligence Scheme for Trusts (CNST). This scheme does not cover 'no fault' compensation and the Trust is precluded from taking out separate insurance to cover this. Any patient or volunteer taking part in the study is entitled to know that if they suffered injury as a result of

participating in the study they would first have to prove negligence in a court of law before they could gain compensation.

If the study involves patients of any other Trust or healthcare organisation, you will need to confirm the indemnity arrangements with that organisation.

Pharmacy
If your study involves Pharmacy then you must ensure that they are ready to initiate the study before the first patients are recruited.

Medical Devices
Any medical devices used specifically for this study, whether purchased, loaned or borrowed must be registered with the Medical Engineering Department. Equipment must not be used until it has completed formal acceptance testing by Medical Engineering. A calibration and maintenance schedule must be drawn up and agreed with Medical Engineering in accordance with the manufacturer's recommendations. There should be a formal maintenance contract in place if maintenance is to be carried out by external contractors (including the equipment manufacturers). If, at the end of the study, the equipment is transferred or disposed of, details must be sent to Medical Engineering to amend the equipment asset register.

Reporting Adverse Events
If this study involves an intervention in the treatment of patients then you must ensure that any serious adverse events, **regardless of whether you believe the event is related to the research or the intervention**, are reported according to the Trust's policy on reporting research-related adverse events. Please see attached memo. Note that you must also follow any SAE reporting requirements stipulated by the sponsor.

A copy of the Trust policy may be obtained from the R&D office and is also available on the R&D section of the Trust's intranet and internet sites. A copy of a blank SAE form is enclosed, this may be used if it is not possible to report the event through the Trust's online reporting system.

Drugs and Treatment outside the study
Approval for the study to commence cannot be taken to imply approval for the same form of treatment to continue beyond the end of the study, or for patients who are not part of the study. If it is likely that continuing treatment is required at the end of the study, then it is the Principal Investigator's responsibility to ensure that study participants are fully aware of the types of treatment that would be available to them.

Research Governance
You should ensure that you and your research team abide by the Trust policies on research governance. These are available from the R&D Office and on the R&D section of the Trust's intranet and internet sites (www.uhb.nhs.uk/research)

Study Files
You must set up and maintain a study file containing the essential documents needed to facilitate a full audit of the conduct of the study. The minimum requirements for the content and layout of the study file are set out in the enclosed documents. This file may be audited at short notice by the R&D Office, the sponsor, or regulatory authorities.

R&D Office
Head of R&D Governance: Dr Christopher Counsell
Head of R&D Operations: Joanne Plumb
R&D Office, 1st Floor, ITM, Heritage Building, Queen Elizabeth Hospital Birmingham, Edgbaston Birmingham B15 2WG
Tel: 0121 371 4185 *Fax:*0121 371 4204 *Email:* R&D@uhb.nhs.uk
Website: www.research.uhb.nhs.uk
Projects database: //uhb/userdata/R & D/R&D database/distributed database 2002.mdb

Delegated Duties Log
You must maintain a list of all those people who have responsibility for delivering any study-related tasks set out in the protocol. The log must list the names of the individuals, their roles and responsibilities, the date they started working on the study, and, if appropriate, the date they finished. Each entry must be signed by the person accepting the responsibilities. Note that anyone who is involved in the direct care of patients must hold a substantive or honorary contract with University Hospitals Birmingham.

Accrual Records
It is essential that you maintain up-to-date and accurate records of recruitment and participation in your study. You will be asked to provide these figures as part of the annual reporting and on request at other times during the year. For studies registered on the UKCRN portfolio, you are expected to provide regular accrual data to the Chief Investigator who will submit them to the UKCRN. You should keep an anonymised record, with dates, of patients approached, consented, screened, recruited, completed, and dropped out as appropriate.

PICS
Research studies are now listed on a separate research tab on the trust's Prescribing, Information and Communication System (PICS). When a participant is screened or recruited into this study you must ensure that this is promptly recorded on PICS. If you have any queries about how to do this please contact the PICS training team (PICSTrainingTeam@uhb.nhs.uk)

Annual Reports
The R&D Office will request information about progress with the study in 6 months, 12 months and annually thereafter. Approval for this study may be withdrawn if you do not complete and return reports when requested.

Protocol Breaches
Serious protocol breaches must be reported to the R&D office as soon as possible and must be notified to the Chief Investigator and Sponsor immediately you become aware of them. If you are the Chief Investigator you must notify the Ethics Committee within 7 days and, for CTIMP studies, you must notify the MHRA within 7 days. A serious breach is one that is likely to affect to a significant degree the mental or physical integrity of the research participants or the scientific value of the study. A report of a serious breach should identify measures taken to correct the consequences of the breach and measures to prevent future similar breaches (a so-called 'CAPA' log). Minor protocol breaches should be recorded in your study file.

Urgent Safety Measure
If necessary, appropriate urgent safety measure to protect clinical trial subjects from any immediate hazard to their health and safety can be taken immediately without waiting for Ethics Committee, Regulatory Authority or R&D approval. However you must inform the R&D Office, Chief Investigator, Sponsor, Ethics Committee and MHRA, as appropriate, in writing within 3 days.

Protocol Amendments
Trust approval will usually automatically cover minor protocol amendments but you must send details to the R&D office for information. Details of all substantial amendments must be sent to the R&D Office for authorisation together with copies of the ethics approval and/or regulatory approval for the amendments and any revised documentation. The R&D office will acknowledge all amendments. A substantial amendment is defined by NRES (the National Research Ethics Service) and would include any change that could affect the safety, conduct or the resource implications of the study.

R&D Office
Head of R&D Governance: Dr Christopher Counsell
Head of R&D Operations: Joanne Plumb
R&D Office, 1st Floor, ITM, Heritage Building, Queen Elizabeth Hospital Birmingham, Edgbaston Birmingham B15 2WG
Tel: 0121 371 4185 *Fax:*0121 371 4204 *Email:* R&D@uhb.nhs.uk
Website: www.research.uhb.nhs.uk
Projects database: //uhb/userdata/R & D/R&D database/distributed database 2002.mdb

Duration
It is expected that the study will begin at University Hospital Birmingham within 12 months of Trust authorisation. If there is a long delay in starting the study, the Trust may consider withdrawing authorisation for the study. Unless explicitly withdrawn, Trust approval lasts for as long as the study has valid ethics committee and regulatory approval.

End of Study
According to information you have provided, this study is expected to end in **August 2018** and the minimum recruitment target is **75**. The R&D Office will request a final report shortly after this date. If the study ends for any reason before this date you must notify the R&D Office. Note that the Chief Investigator for the whole study is required to provide an end of study report to the main research ethics committee and regulatory authorities.

Archiving
For studies designated as a Clinical Trial of an Investigational Medicinal Product (CTIMP), it is a **legal** requirement to retain essential documents for at least **5 years** after the declared end of the study. The sponsor or regulatory authorities may insist on a longer retention period for a particular study. For all other types of study there are no statutory requirements but generally accepted good practice guidelines recommend that documents are retained for at least 5 years. Documents must be archived in a way such that they can be readily accessed (24 hours notice) if required for audits or regulatory purposes. The costs of archiving is borne by the Principal or Lead Investigator and should be taken into account when applying for research grants or seeking other forms of funding. For CTIMPs, there must be a named archivist, approved by the sponsor, who is responsible for setting up and controlling the archive.

Health Records Labelling
The Health Records of study subjects are retained according to the Trust's "*Health Records Management Policy*"; for patients in research studies the retention period is 15 years after the last treatment or consultation related to the study. The Principal Investigator must ensure that all records for patients involved in a study are clearly labelled to ensure that the retention policy can be followed.

Cover for absence
If the Principal Investigator is likely to be absent and out of contact for a prolonged period (> 2 weeks), the PI must either explicitly suspend patient recruitment and patient-related activity in the study, or explicitly delegate the responsibilities of Principal Investigator to a named deputy. The PI must be satisfied that their deputy is sufficiently qualified through education, training and experience to take on the role of PI. These periods of absence and delegation must be recorded in the study file.

Website entry
Basic details of your study will be made available on the Trust's website at
http://www.research.uhb.nhs.uk/trials/RRK5478

Guidance Tool
The Trust R&D Office has developed a Powerpoint-based tool summarising some of the regulations relevant to clinical research. This is available at \\uhb\userdata\R & D\R&D Shared Docs\Guide to Responsibilities\Guide to Investigator Responsibilities.ppsx (requires access to the Trust's network)

Yours sincerely,

24 November 2015

R&D Office
Head of R&D Governance: Dr Christopher Counsell
Head of R&D Operations: Joanne Plumb
R&D Office, 1st Floor, ITM, Heritage Building, Queen Elizabeth Hospital Birmingham, Edgbaston Birmingham B15 2WG
Tel: 0121 371 4185 *Fax:*0121 371 4204 *Email:* R&D@uhb.nhs.uk
Website: www.research.uhb.nhs.uk
Projects database: //uhb/userdata/R & D/R&D database/distributed database 2002.mdb

Dr Christopher Counsell
Head of R&D Governance

Enclosed: Sample study file layout
Incident Reporting & Serious Adverse Event Form

Copies to: Dr Nath
Relevant Service Departments
Division B Manager, Lynn Willetts

R&D Office
Head of R&D Governance: Dr Christopher Counsell
Head of R&D Operations: Joanne Plumb
R&D Office, 1st Floor, ITM, Heritage Building, Queen Elizabeth Hospital Birmingham, Edgbaston Birmingham B15 2WG
Tel: 0121 371 4185 *Fax:*0121 371 4204 *Email:* R&D@uhb.nhs.uk
Website: www.research.uhb.nhs.uk
Projects database: //uhb/userdata/R & D/R&D database/distributed database 2002.mdb

Appendix D: Champion study Consent form

University Hospitals Birmingham NHS
NHS Foundation Trust

CONSENT FORM FOR RESEARCH STUDY

Effects of Machine Perfusion on Cadaveric Kidneys for Transplantation

Name of researchers: Mr Nicholas Inston,,Mr Jay Nath, Mr Kamlesh Patel

Please initial to confirm

- I confirm that I have read and understood the information sheet version ……..…Date……..…….. **Effects of Machine Perfusion on Cadaveric Kidneys for Transplantation.** ☐
- I have had the opportunity to consider the information, ask questions and have had these answered satisfactorily. ☐
- I understand that my participation is voluntary and that I am free to withdraw at any time, without giving any reason, without my medical care or legal rights being affected. ☐
- I understand that relevant sections of any of my medical notes and data collected during the study may be looked at by researchers, from regulatory authorities or from the NHS Trust, where it is relevant to my taking part in the research. I give permission for these individuals to have access to my records. ☐
- I agree to take part in the above research study ☐

Name of Patient	Date	Signature
Name of Person taking consent (if different from the researcher)	Date	Signature
Researcher	Date	Signature

Appendix E: Champion study Patient Information Sheet

PARTICIPANT INFORMATION SHEET
KIDNEY PERFUSION STUDY

The following information describes a study which we are inviting you to take part in, the results of which will be used in part towards a PhD qualification for the lead researcher.

What is the study?

It has been standard practice to flush transplant kidneys with fluid using a specialised machine for over five years and is recommended in national guidelines. We are undertaking this research to help us understand how the flushing process benefits the kidney at a metabolic level.

To better understand this, one of the components of the fluid used to flush the kidney (glucose) will be labelled or 'chemically dyed'. This labelled glucose is a safe, naturally occurring substance and is identical to the unlabelled version with regards to kidney biology.

Why are you doing it?

We hope that by better understanding what happens in the kidney during this flushing process, we will be able to improve their function. This could lead to an increase in the number of kidneys available for transplant in the future.

What would I have to do?

We need your permission to take part in the study. This will include using labelled fluid to flush through the transplant kidney, taking a small sample (biopsy) of the kidney at the end of flushing for research, taking a sample of your urine after your operation and recording the results of your blood tests and how well your kidney is working and any problems you might have. Medical records and data may be accessed by researchers, regulatory authorities or the NHS trust. There are no extra blood tests or extra appointments.

Will being in the study change my treatment at all?

Whether you take part in the study or not will not influence the treatment you receive in any way. You are free to stop being in the study at any point and your treatment will remain exactly the same.

Potential Harm or Benefit to Participants

There are no harmful effects of using labelled fluids during this flushing process. The risk associated with kidney biopsy is very small and is a test performed routinely for non-research purposes. We have had no serious problems with this type of biopsy in this hospital and estimate the risk of serious harm to be less than 1:1000. No extra tests are carried out following your operation.

Can I get the results of the study?

If you are interested in the results of the study a summary can be sent to you once all of the analyses are complete.

Funding

This study is funded by University Hospitals Birmingham Charities and Organ Recovery Systems and has been approved by the relevant ethics committee.

What do I need to do if I want to be in the study?

All you need to do to take part is to agree and sign the consent form. It is important to take the time to read this information and ask any questions you have. Once you have agreed to be in the study the information will be collected. At the end of the study, any personal data is kept securely for 12 months and then destroyed.

Thank you very much for reading this information and we hope you will be part of the study. Feel free to ask any questions.

If you would like general, impartial advice on taking part in research studies we would suggest contacting the PALS office on 0121 371 2550

Mr. Inston (Consultant Surgeon)
Mr. Nath (Research Registrar)
Mr. K Patel (Research Registrar)
0121 371 5851

References

1. Agarwal R. Defining end-stage renal disease in clinical trials: a framework for adjudication. Nephrol Dial Transplant. 2016;31(6):864-7.
2. Stevens PE, Levin A, for the Kidney Disease: Improving Global Outcomes Chronic Kidney Disease Guideline Development Work Group M. Evaluation and management of chronic kidney disease: Synopsis of the kidney disease: improving global outcomes 2012 clinical practice guideline. Annals of Internal Medicine. 2013;158(11):825-30.
3. Jaar BG, Chang A, Plantinga L. Can we improve quality of life of patients on dialysis? Clin J Am Soc Nephrol. 2013;8(1):1-4.
4. Mollaoğlu. Quality of Life in Patients Undergoing Hemodialysis: IntechOpen; 2013 [Available from: https://www.intechopen.com/books/hemodialysis/quality-of-life-in-patients-undergoing-hemodialysis.
5. Neipp M, Karavul B, Jackobs S, Meyer zu Vilsendorf A, Richter N, Becker T, et al. Quality of life in adult transplant recipients more than 15 years after kidney transplantation. Transplantation. 2006;81(12):1640-4.
6. Fiebiger W, Mitterbauer C, Oberbauer R. Health-related quality of life outcomes after kidney transplantation. Health Qual Life Outcomes. 2004;2:2.
7. Abecassis M, Bartlett ST, Collins AJ, Davis CL, Delmonico FL, Friedewald JJ, et al. Kidney transplantation as primary therapy for end-stage renal disease: a National Kidney Foundation/Kidney Disease Outcomes Quality Initiative (NKF/KDOQITM) conference. Clin J Am Soc Nephrol. 2008;3(2):471-80.
8. Oniscu GC, Brown H, Forsythe JL. Impact of cadaveric renal transplantation on survival in patients listed for transplantation. J Am Soc Nephrol. 2005;16(6):1859-65.
9. Ojo AO, Port FK, Wolfe RA, Mauger EA, Williams L, Berling DP. Comparative mortality risks of chronic dialysis and cadaveric transplantation in black end-stage renal disease patients. Am J Kidney Dis. 1994;24(1):59-64.
10. Schnuelle P, Lorenz D, Trede M, Van Der Woude FJ. Impact of renal cadaveric transplantation on survival in end-stage renal failure: evidence for reduced mortality risk compared with hemodialysis during long-term follow-up. J Am Soc Nephrol. 1998;9(11):2135-41.
11. Port FK, Wolfe RA, Mauger EA, Berling DP, Jiang K. Comparison of survival probabilities for dialysis patients vs cadaveric renal transplant recipients. JAMA. 1993;270(11):1339-43.
12. Ansell D, O'Neil J, Johnson R, Collett D, Dudley C. Transplantation of older pateints does not improve survival compated with those wait listed. Analysis of 9,700 wait listed patients in the UK: 900. Transplantation. 2008;86(2S):314.
13. Oniscu GC, Brown H, Forsythe JL. How great is the survival advantage of transplantation over dialysis in elderly patients? Nephrol Dial Transplant. 2004;19(4):945-51.
14. Laupacis A, Keown P, Pus N, Krueger H, Ferguson B, Wong C, et al. A study of the quality of life and cost-utility of renal transplantation. Kidney Int. 1996;50(1):235-42.
15. Howard K, Salkeld G, White S, McDonald S, Chadban S, Craig JC, et al. The cost-effectiveness of increasing kidney transplantation and home-based dialysis. Nephrology (Carlton). 2009;14(1):123-32.
16. Cost-Effectiveness of Transplantation Factsheet 7. Available online at www.organdonation.nhs.uk/newsroom/fact_sheets/Organ_Donation_Registry_Fact_Sheet_7_21337.pdf: NHS Blood and Transplant; 2009 25/09/2018.
17. Guild WR, Harrison JH, Merrill JP, Murray J. Successful homotransplantation of the kidney in an identical twin. Trans Am Clin Climatol Assoc. 1955;67:167-73.
18. Shrestha B, Haylor J, Raftery A. Historical perspectives in kidney transplantation: an updated review. Progress in transplantation (Aliso Viejo, Calif). 2015;25(1):64-9, 76.
19. Annual Report on Kidney Transplantation: Report for 2017/2018. Available online at https://nhsbtdbe.blob.core.windows.net/umbraco-assets-corp/12256/nhsbt-kidney-transplantation-annual-report-2017-2018.pdf: NHS Blood and Transplant; 2018 September 2018.
20. Dunne K, Doherty P. Donation after circulatory death. Continuing Education in Anaesthesia Critical Care & Pain. 2011;11(3):82-6.
21. Kootstra G, Daemen JH, Oomen AP. Categories of non-heart-beating donors. Transplant Proc. 1995;27(5):2893-4.
22. Thuong M, Ruiz A, Evrard P, Kuiper M, Boffa C, Akhtar MZ, et al. New classification of donation after circulatory death donors definitions and terminology. Transpl Int. 2016;29(7):749-59.
23. Suntharalingam C, Sharples L, Dudley C, Bradley JA, Watson CJ. Time to cardiac death after withdrawal of life-sustaining treatment in potential organ donors. Am J Transplant. 2009;9(9):2157-65.
24. Oniscu G FJ, Fung J eds. Abdominal Organ Retrieval and Transplantation Bench Surgery: John Wiley & Sons; 2013.
25. Minambres E, Rubio JJ, Coll E, Dominguez-Gil B. Donation after circulatory death and its expansion in Spain. Curr Opin Organ Transplant. 2018;23(1):120-9.
26. Matillon X, Danjou F, Petruzzo P, Thaunat O, Rimmele T, Delsuc C, et al. Hypothermic pulsatile preservation of kidneys from uncontrolled deceased donors after cardiac arrest - a retrospective study. Transpl Int. 2017;30(12):1284-91.

27. Gagandeep S, Matsuoka L, Mateo R, Cho YW, Genyk Y, Sher L, et al. Expanding the donor kidney pool: utility of renal allografts procured in a setting of uncontrolled cardiac death. Am J Transplant. 2006;6(7):1682-8.
28. Summers DM, Watson CJ, Pettigrew GJ, Johnson RJ, Collett D, Neuberger JM, et al. Kidney donation after circulatory death (DCD): state of the art. Kidney Int. 2015;88(2):241-9.
29. Transplantation From Donors After Deceased Circulatory Death. Available at http://bts.org.uk/wp-content/uploads/2016/09/15_BTS_Donors_DCD.pdf: British Transplantation Society; July 2015 25/09/2018.
30. Nishikido M, Noguchi M, Koga S, Kanetake H, Matsuya F, Hayashi M, et al. Kidney transplantation from non-heart-beating donors: analysis of organ procurement and outcome. Transplant Proc. 2004;36(7):1888-90.
31. Teraoka S, Nomoto K, Kikuchi K, Hirano T, Satomi S, Hasegawa A, et al. Outcomes of kidney transplants from non-heart-beating deceased donors as reported to the Japan Organ Transplant Network from April 1995-December 2003: a multi-center report. Clin Transpl. 2004:91-102.
32. Patel AR, Eggener SE. Warm ischemia less than 30 minutes is not necessarily safe during partial nephrectomy: every minute matters. Urol Oncol. 2011;29(6):826-8.
33. Port FK, Bragg-Gresham JL, Metzger RA, Dykstra DM, Gillespie BW, Young EW, et al. Donor characteristics associated with reduced graft survival: an approach to expanding the pool of kidney donors. Transplantation. 2002;74(9):1281-6.
34. Johnson RJ, Bradbury LL, Martin K, Neuberger J, Registry UKT. Organ donation and transplantation in the UK-the last decade: a report from the UK national transplant registry. Transplantation. 2014;97 Suppl 1:S1-S27.
35. Watson CJ, Johnson RJ, Birch R, Collett D, Bradley JA. A simplified donor risk index for predicting outcome after deceased donor kidney transplantation. Transplantation. 2012;93(3):314-8.
36. Mallon DH, Summers DM, Bradley JA, Pettigrew GJ. Defining delayed graft function after renal transplantation: simplest is best. Transplantation. 2013;96(10):885-9.
37. McCaughan JA, Courtney AE. The clinical course of kidney transplant recipients after 20 years of graft function. Am J Transplant. 2015;15(3):734-40.
38. Bond M, Pitt M, Akoh J, Moxham T, Hoyle M, Anderson R. The effectiveness and cost-effectiveness of methods of storing donated kidneys from deceased donors: a systematic review and economic model. Health Technol Assess. 2009;13(38):iii-iv, xi-xiv, 1-156.
39. Nath J, Hodson J, Canbilen SW, Al Shakarchi J, Inston NG, Sharif A, et al. Effect of cold ischaemia time on outcome after living donor renal transplantation. Br J Surg. 2016;103(9):1230-6.
40. Watson CJ, Wells AC, Roberts RJ, Akoh JA, Friend PJ, Akyol M, et al. Cold machine perfusion versus static cold storage of kidneys donated after cardiac death: a UK multicenter randomized controlled trial. Am J Transplant. 2010;10(9):1991-9.
41. Yarlagadda SG, Coca SG, Formica RN, Jr., Poggio ED, Parikh CR. Association between delayed graft function and allograft and patient survival: a systematic review and meta-analysis. Nephrol Dial Transplant. 2009;24(3):1039-47.
42. Ojo AO, Wolfe RA, Held PJ, Port FK, Schmouder RL. Delayed graft function: risk factors and implications for renal allograft survival. Transplantation. 1997;63(7):968-74.
43. Tapiawala SN, Tinckam KJ, Cardella CJ, Schiff J, Cattran DC, Cole EH, et al. Delayed graft function and the risk for death with a functioning graft. J Am Soc Nephrol. 2010;21(1):153-61.
44. Locke JE, Segev DL, Warren DS, Dominici F, Simpkins CE, Montgomery RA. Outcomes of kidneys from donors after cardiac death: implications for allocation and preservation. Am J Transplant. 2007;7(7):1797-807.
45. Singh RP, Farney AC, Rogers J, Zuckerman J, Reeves-Daniel A, Hartmann E, et al. Kidney transplantation from donation after cardiac death donors: lack of impact of delayed graft function on post-transplant outcomes. Clin Transplant. 2011;25(2):255-64.
46. Summers DM, Johnson RJ, Hudson A, Collett D, Watson CJ, Bradley JA. Effect of donor age and cold storage time on outcome in recipients of kidneys donated after circulatory death in the UK: a cohort study. Lancet. 2013;381(9868):727-34.
47. Summers DM, Johnson RJ, Allen J, Fuggle SV, Collett D, Watson CJ, et al. Analysis of factors that affect outcome after transplantation of kidneys donated after cardiac death in the UK: a cohort study. Lancet. 2010;376(9749):1303-11.
48. van der Vliet JA, Warle MC, Cheung CL, Teerenstra S, Hoitsma AJ. Influence of prolonged cold ischemia in renal transplantation. Clin Transplant. 2011;25(6):E612-6.
49. van der Vliet JA, Warle MC. The need to reduce cold ischemia time in kidney transplantation. Curr Opin Organ Transplant. 2013;18(2):174-8.
50. Carrel A, Lindbergh CA. The Culture of Whole Organs. Science. 1935;81(2112):621-3.
51. Belzer FO, Kountz SL. Preservation and transplantation of human cadaver kidneys: a two-year experience. Ann Surg. 1970;172(3):394-404.
52. Opelz G, Dohler B. Multicenter analysis of kidney preservation. Transplantation. 2007;83(3):247-53.
53. Collins GM, Bravo-Shugarman M, Terasaki PI. Kidney preservation for transportation. Initial perfusion and 30 hours' ice storage. Lancet. 1969;2(7632):1219-22.
54. Collins GM, Halasz NA. Letter: Composition of intracellular flush solutions for hypothermic kidney storage. Lancet. 1975;1(7900):220.
55. Dreikorn K, Horsch R, Rohl L. 48- to 96-hour preservation of canine kidneys by initial perfusion and hypothermic storage using the Euro-Collins solution. Eur Urol. 1980;6(4):221-4.

56. de Boer J, De Meester J, Smits JM, Groenewoud AF, Bok A, van der Velde O, et al. Eurotransplant randomized multicenter kidney graft preservation study comparing HTK with UW and Euro-Collins. Transpl Int. 1999;12(6):447-53.
57. Ploeg RJ, van Bockel JH, Langendijk PT, Groenewegen M, van der Woude FJ, Persijn GG, et al. Effect of preservation solution on results of cadaveric kidney transplantation. The European Multicentre Study Group. Lancet. 1992;340(8812):129-37.
58. Morariu AM, Vd Plaats A, W VO, NA TH, Leuvenink HG, Graaff R, et al. Hyperaggregating effect of hydroxyethyl starch components and University of Wisconsin solution on human red blood cells: a risk of impaired graft perfusion in organ procurement? Transplantation. 2003;76(1):37-43.
59. van der Plaats A, t Hart NA, Morariu AM, Verkerke GJ, Leuvenink HG, Ploeg RJ, et al. Effect of University of Wisconsin organ-preservation solution on haemorheology. Transpl Int. 2004;17(5):227-33.
60. t Hart NA, van der Plaats A, Leuvenink HG, Wiersema-Buist J, Olinga P, van Luyn MJ, et al. Initial blood washout during organ procurement determines liver injury and function after preservation and reperfusion. Am J Transplant. 2004;4(11):1836-44.
61. Mosbah IB, Franco-Gou R, Abdennebi HB, Hernandez R, Escolar G, Saidane D, et al. Effects of polyethylene glycol and hydroxyethyl starch in University of Wisconsin preservation solution on human red blood cell aggregation and viscosity. Transplant Proc. 2006;38(5):1229-35.
62. O'Callaghan JM, Knight SR, Morgan RD, Morris PJ. Preservation solutions for static cold storage of kidney allografts: a systematic review and meta-analysis. Am J Transplant. 2012;12(4):896-906.
63. Southard JH, Belzer FO. Organ preservation. Annu Rev Med. 1995;46:235-47.
64. Wahlberg JA, Southard JH, Belzer FO. Development of a cold storage solution for pancreas preservation. Cryobiology. 1986;23(6):477-82.
65. Bretschneider HJ. Myocardial protection. Thorac Cardiovasc Surg. 1980;28(5):295-302.
66. Maathuis MH, Leuvenink HG, Ploeg RJ. Perspectives in organ preservation. Transplantation. 2007;83(10):1289-98.
67. St Peter SD, Imber CJ, Friend PJ. Liver and kidney preservation by perfusion. Lancet. 2002;359(9306):604-13.
68. Wszola M, Kwiatkowski A, Diuwe P, Domagala P, Gorski L, Kieszek R, et al. One-year results of a prospective, randomized trial comparing two machine perfusion devices used for kidney preservation. Transpl Int. 2013;26(11):1088-96.
69. Machine perfusion systems and cold static storage of kidneys from deceased donors. Available online at https://www.nice.org.uk/guidance/ta165/: National Institute of Health and Care Excellence; 2009 29/11/2017.
70. Moers C, Smits JM, Maathuis MH, Treckmann J, van Gelder F, Napieralski BP, et al. Machine perfusion or cold storage in deceased-donor kidney transplantation. N Engl J Med. 2009;360(1):7-19.
71. Moers C, Pirenne J, Paul A, Ploeg RJ, Machine Preservation Trial Study G. Machine perfusion or cold storage in deceased-donor kidney transplantation. N Engl J Med. 2012;366(8):770-1.
72. Guy A, McGrogan D, Inston N, Ready A. Hypothermic machine perfusion permits extended cold ischemia times with improved early graft function. Exp Clin Transplant. 2015;13(2):130-7.
73. Patel SK, Pankewycz OG, Weber-Shrikant E, Zachariah M, Kohli R, Nader ND, et al. Effect of increased pressure during pulsatile pump perfusion of deceased donor kidneys in transplantation. Transplant Proc. 2012;44(7):2202-6.
74. Berne RM, Koeppen BM, Stanton BA. Berne & Levy physiology. 6th ed., updated ed. ed. Philadelphia, PA: Mosby/Elsevier; 2010.
75. Belzer FO, Glass NR, Sollinger HW, Hoffmann RM, Southard JH. A new perfusate for kidney preservation. Transplantation. 1982;33(3):322-3.
76. Manekeller S, Leuvenink H, Sitzia M, Minor T. Oxygenated Machine Perfusion Preservation of Predamaged Kidneys With HTK and Belzer Machine Perfusion Solution: An Experimental Study in Pigs. Transplantation Proceedings. 2005;37(8):3274-5.
77. Lindell SL, Compagnon P, Mangino MJ, Southard JH. UW solution for hypothermic machine perfusion of warm ischemic kidneys. Transplantation. 2005;79(10):1358-61.
78. Gage F, Leeser DB, Porterfield NK, Graybill JC, Gillern S, Hawksworth JS, et al. Room temperature pulsatile perfusion of renal allografts with Lifor compared with hypothermic machine pump solution. Transplant Proc. 2009;41(9):3571-4.
79. De Deken J, Kocabayoglu P, Moers C. Hypothermic machine perfusion in kidney transplantation. Curr Opin Organ Transplant. 2016;21(3):294-300.
80. Yuan X, Theruvath AJ, Ge X, Floerchinger B, Jurisch A, Garcia-Cardena G, et al. Machine perfusion or cold storage in organ transplantation: indication, mechanisms, and future perspectives. Transpl Int. 2010;23(6):561-70.
81. Jochmans I, O'Callaghan JM, Pirenne J, Ploeg RJ. Hypothermic machine perfusion of kidneys retrieved from standard and high-risk donors. Transpl Int. 2015;28(6):665-76.
82. Gallinat A, Efferz P, Paul A, Minor T. One or 4 h of "in-house" reconditioning by machine perfusion after cold storage improve reperfusion parameters in porcine kidneys. Transpl Int. 2014;27(11):1214-9.
83. Gracia-Sancho J, Villarreal G, Jr., Zhang Y, Yu JX, Liu Y, Tullius SG, et al. Flow cessation triggers endothelial dysfunction during organ cold storage conditions: strategies for pharmacologic intervention. Transplantation. 2010;90(2):142-9.
84. Tullius SG, Garcia-Cardena G. Organ procurement and perfusion before transplantation. N Engl J Med. 2009;360(1):78-80.

85. Parmar KM, Larman HB, Dai G, Zhang Y, Wang ET, Moorthy SN, et al. Integration of flow-dependent endothelial phenotypes by Kruppel-like factor 2. J Clin Invest. 2006;116(1):49-58.
86. Sebzda E, Zou Z, Lee JS, Wang T, Kahn ML. Transcription factor KLF2 regulates the migration of naive T cells by restricting chemokine receptor expression patterns. Nat Immunol. 2008;9(3):292-300.
87. Chatauret N, Coudroy R, Delpech PO, Vandebrouck C, Hosni S, Scepi M, et al. Mechanistic analysis of nonoxygenated hypothermic machine perfusion's protection on warm ischemic kidney uncovers greater eNOS phosphorylation and vasodilation. Am J Transplant. 2014;14(11):2500-14.
88. Jochmans I, Moers C, Smits JM, Leuvenink HG, Treckmann J, Paul A, et al. The prognostic value of renal resistance during hypothermic machine perfusion of deceased donor kidneys. Am J Transplant. 2011;11(10):2214-20.
89. Fukae K, Tominaga R, Tokunaga S, Kawachi Y, Imaizumi T, Yasui H. The effects of pulsatile and nonpulsatile systemic perfusion on renal sympathetic nerve activity in anesthetized dogs. J Thorac Cardiovasc Surg. 1996;111(2):478-84.
90. Divonin AL, Mishchenko BP, Loginova LI, Mikhailova ML. [Changes in the liver circulation and kidney function during pulsatile and non-pulsatile perfusion]. Anesteziol Reanimatol. 1991(3):36-40.
91. Dutkowski P, Schonfeld S, Odermatt B, Heinrich T, Junginger T. Rat liver preservation by hypothermic oscillating liver perfusion compared to simple cold storage. Cryobiology. 1998;36(1):61-70.
92. Maathuis MH, Manekeller S, van der Plaats A, Leuvenink HG, t Hart NA, Lier AB, et al. Improved kidney graft function after preservation using a novel hypothermic machine perfusion device. Ann Surg. 2007;246(6):982-8; discussion 9-91.
93. Lee CY, Mangino MJ. Preservation methods for kidney and liver. Organogenesis. 2009;5(3):105-12.
94. Kaminski J, Delpech PO, Kaaki-Hosni S, Promeyrat X, Hauet T, Hannaert P. Oxygen Consumption by Warm Ischemia-Injured Porcine Kidneys in Hypothermic Static and Machine Preservation. J Surg Res. 2019;242:78-86.
95. Bhangoo RS, Hall IE, Reese PP, Parikh CR. Deceased-donor kidney perfusate and urine biomarkers for kidney allograft outcomes: a systematic review. Nephrol Dial Transplant. 2012;27(8):3305-14.
96. Moers C, Varnav OC, van Heurn E, Jochmans I, Kirste GR, Rahmel A, et al. The value of machine perfusion perfusate biomarkers for predicting kidney transplant outcome. Transplantation. 2010;90(9):966-73.
97. Hall IE, Bhangoo RS, Reese PP, Doshi MD, Weng FL, Hong K, et al. Glutathione S-transferase iso-enzymes in perfusate from pumped kidneys are associated with delayed graft function. Am J Transplant. 2014;14(4):886-96.
98. de Vries EE, Hoogland ER, Winkens B, Snoeijs MG, van Heurn LW. Renovascular resistance of machine-perfused DCD kidneys is associated with primary nonfunction. Am J Transplant. 2011;11(12):2685-91.
99. Mozes MF, Skolek RB, Korf BC. Use of perfusion parameters in predicting outcomes of machine-preserved kidneys. Transplant Proc. 2005;37(1):350-1.
100. Groen H, Moers C, Smits JM, Treckmann J, Monbaliu D, Rahmel A, et al. Cost-effectiveness of hypothermic machine preservation versus static cold storage in renal transplantation. Am J Transplant. 2012;12(7):1824-30.
101. Gomez V, Galeano C, Diez V, Bueno C, Diaz F, Burgos FJ. Economic impact of the introduction of machine perfusion preservation in a kidney transplantation program in the expanded donor era: cost-effectiveness assessment. Transplant Proc. 2012;44(9):2521-4.
102. Hameed AM, Pleass HC, Wong G, Hawthorne WJ. Maximizing kidneys for transplantation using machine perfusion: from the past to the future: A comprehensive systematic review and meta-analysis. Medicine (Baltimore). 2016;95(40):e5083.
103. O'Callaghan JM, Morgan RD, Knight SR, Morris PJ. Systematic review and meta-analysis of hypothermic machine perfusion versus static cold storage of kidney allografts on transplant outcomes. Br J Surg. 2013;100(8):991-1001.
104. Zorgdrager M, Krikke C, Hofker SH, Leuvenink HG, Pol RA. Multiple Renal Arteries in Kidney Transplantation: A Systematic Review and Meta-Analysis. Ann Transplant. 2016;21:469-78.
105. Jochmans I, Moers C, Smits JM, Leuvenink HG, Treckmann J, Paul A, et al. Machine perfusion versus cold storage for the preservation of kidneys donated after cardiac death: a multicenter, randomized, controlled trial. Ann Surg. 2010;252(5):756-64.
106. Treckmann J, Moers C, Smits JM, Gallinat A, Maathuis MH, van Kasterop-Kutz M, et al. Machine perfusion versus cold storage for preservation of kidneys from expanded criteria donors after brain death. Transpl Int. 2011;24(6):548-54.
107. Keeler J. Understanding NMR spectroscopy. 2nd ed. ed. Oxford: Wiley; 2010.
108. Levitt MH. Spin dynamics : basics of nuclear magnetic resonance. 2nd ed. ed. Hoboken, N.J.: Wiley ; Chichester : John Wiley [distributor]; 2008.
109. Fukushima E, Roeder SBW. Experimental pulse NMR : a nuts and bolts approach. Reading, Mass. ; London: Addison-Wesley; 1981.
110. Heude C, Nath J, Carrigan JB, Ludwig C. Nuclear Magnetic Resonance Strategies for Metabolic Analysis. Adv Exp Med Biol. 2017;965:45-76.
111. Ellis Ha, Mahadevan Va. Clinical anatomy : applied anatomy for students and junior doctors. Thirteenth edition. / Harold Ellis, Vishy Mahadevan. ed.
112. Simmons MN, Schreiber MJ, Gill IS. Surgical renal ischemia: a contemporary overview. J Urol. 2008;180(1):19-30.

113. Rolfe DF, Brown GC. Cellular energy utilization and molecular origin of standard metabolic rate in mammals. Physiol Rev. 1997;77(3):731-58.
114. Kramer K, Thurau K, Deetjen P. [Hemodynamics of kidney medullary substance. Part I. Capillary passage time, blood volume, circulation, tissue hematocrit and oxygen consumption of kidney medullary substance in situ]. Pflugers Arch Gesamte Physiol Menschen Tiere. 1960;270:251-69.
115. Kramer K, Deetjen P. [Relation of renal oxygen consumption to blood supply and glomerular filtration during variations of the blood pressure]. Pflugers Arch Gesamte Physiol Menschen Tiere. 1960;271:782-96.
116. Salway JG. Metabolism at a glance. 3rd ed. ed. Malden, Mass. ; Oxford: Blackwell; 2004.
117. Berg JM, Tymoczko JL, Stryer L. Biochemistry. 5th ed. / Jeremy Berg, John Tymoczko, Lubert Stryer / web content by Neil D. Clarke. ed. New York: W. H. Freeman and Co. ; [Basingstoke : Palgrave] [distributor], 2001; 2002.
118. Owen OE, Kalhan SC, Hanson RW. The key role of anaplerosis and cataplerosis for citric acid cycle function. J Biol Chem. 2002;277(34):30409-12.
119. Collard CD, Gelman S. Pathophysiology, clinical manifestations, and prevention of ischemia-reperfusion injury. Anesthesiology. 2001;94(6):1133-8.
120. Schroppel B, Legendre C. Delayed kidney graft function: from mechanism to translation. Kidney Int. 2014;86(2):251-8.
121. Kosieradzki M, Rowinski W. Ischemia/reperfusion injury in kidney transplantation: mechanisms and prevention. Transplant Proc. 2008;40(10):3279-88.
122. Sugiyama S, Hanaki Y, Ogawa T, Hieda N, Taki K, Ozawa T. The effects of SUN 1165, a novel sodium channel blocker, on ischemia-induced mitochondrial dysfunction and leakage of lysosomal enzymes in canine hearts. Biochem Biophys Res Commun. 1988;157(2):433-9.
123. Schumacher CA, Baartscheer A, Coronel R, Fiolet JW. Energy-dependent transport of calcium to the extracellular space during acute ischemia of the rat heart. J Mol Cell Cardiol. 1998;30(8):1631-42.
124. Eltzschig HK, Eckle T. Ischemia and reperfusion--from mechanism to translation. Nat Med. 2011;17(11):1391-401.
125. Poli G, Leonarduzzi G, Biasi F, Chiarpotto E. Oxidative stress and cell signalling. Curr Med Chem. 2004;11(9):1163-82.
126. Kalogeris T, Bao Y, Korthuis RJ. Mitochondrial reactive oxygen species: a double edged sword in ischemia/reperfusion vs preconditioning. Redox Biol. 2014;2:702-14.
127. Fridovich I. Biological effects of the superoxide radical. Arch Biochem Biophys. 1986;247(1):1-11.
128. Liochev SI, Fridovich I. The role of O2.- in the production of HO.: in vitro and in vivo. Free Radic Biol Med. 1994;16(1):29-33.
129. Bonora M, Pinton P. The mitochondrial permeability transition pore and cancer: molecular mechanisms involved in cell death. Front Oncol. 2014;4:302.
130. Marchi S, Patergnani S, Missiroli S, Morciano G, Rimessi A, Wieckowski MR, et al. Mitochondrial and endoplasmic reticulum calcium homeostasis and cell death. Cell Calcium. 2018;69:62-72.
131. Salvadori M, Rosso G, Bertoni E. Update on ischemia-reperfusion injury in kidney transplantation: Pathogenesis and treatment. World J Transplant. 2015;5(2):52-67.
132. Faller DV. Endothelial cell responses to hypoxic stress. Clin Exp Pharmacol Physiol. 1999;26(1):74-84.
133. Collard CD, Lekowski R, Jordan JE, Agah A, Stahl GL. Complement activation following oxidative stress. Mol Immunol. 1999;36(13-14):941-8.
134. Carden DL, Granger DN. Pathophysiology of ischaemia-reperfusion injury. J Pathol. 2000;190(3):255-66.
135. Panes J, Perry M, Granger DN. Leukocyte-endothelial cell adhesion: avenues for therapeutic intervention. Br J Pharmacol. 1999;126(3):537-50.
136. Devarajan P. Update on mechanisms of ischemic acute kidney injury. J Am Soc Nephrol. 2006;17(6):1503-20.
137. Taylor M. Biology of cell survival in the cold: The Basis for Biopreservation of Tissues and Organs. 2006.
138. Boutilier RG. Mechanisms of cell survival in hypoxia and hypothermia. Journal of Experimental Biology. 2001;204(18):3171-81.
139. Dausmann KH, Glos J, Ganzhorn JU, Heldmaier G. Physiology: hibernation in a tropical primate. Nature. 2004;429(6994):825-6.
140. Hochachka PW. Defense strategies against hypoxia and hypothermia. Science. 1986;231(4735):234-41.
141. Plesnila N, Muller E, Guretzki S, Ringel F, Staub F, Baethmann A. Effect of hypothermia on the volume of rat glial cells. J Physiol. 2000;523 Pt 1:155-62.
142. van Breukelen F, Krumschnabel G, Podrabsky JE. Vertebrate cell death in energy-limited conditions and how to avoid it: what we might learn from mammalian hibernators and other stress-tolerant vertebrates. Apoptosis : an international journal on programmed cell death. 2010;15(3):386-99.
143. Rauen U, de Groot H. Mammalian cell injury induced by hypothermia- the emerging role for reactive oxygen species. Biol Chem. 2002;383(3-4):477-88.
144. Singbartl K, Green SA, Ley K. Blocking P-selectin protects from ischemia/reperfusion-induced acute renal failure. FASEB J. 2000;14(1):48-54.
145. Salmela K, Wramner L, Ekberg H, Hauser I, Bentdal O, Lins LE, et al. A randomized multicenter trial of the anti-ICAM-1 monoclonal antibody (enlimomab) for the prevention of acute rejection and delayed onset of

graft function in cadaveric renal transplantation: a report of the European Anti-ICAM-1 Renal Transplant Study Group. Transplantation. 1999;67(5):729-36.
146. de Vries DK, Lindeman JH, Ringers J, Reinders ME, Rabelink TJ, Schaapherder AF. Donor brain death predisposes human kidney grafts to a proinflammatory reaction after transplantation. Am J Transplant. 2011;11(5):1064-70.
147. Anaise D, Ramsammy L, Lane B, Waltzer WC, Rapaport FT. The pathophysiology of the no-reflow phenomenon in cold-stored kidneys. Transplant Proc. 1987;19(1 Pt 2):1348-52.
148. Moeckel GW. Pathologic Perspectives on Acute Tubular Injury Assessment in the Kidney Biopsy. Semin Nephrol. 2018;38(1):21-30.
149. Dettmer K, Aronov PA, Hammock BD. Mass spectrometry-based metabolomics. Mass Spectrometry Reviews. 2007;26(1):51-78.
150. Patel S, Ahmed S. Emerging field of metabolomics: big promise for cancer biomarker identification and drug discovery. J Pharm Biomed Anal. 2015;107:63-74.
151. Fiehn O. Metabolomics--the link between genotypes and phenotypes. Plant Mol Biol. 2002;48(1-2):155-71.
152. Roberts LD, Souza AL, Gerszten RE, Clish CB. Targeted metabolomics. Curr Protoc Mol Biol. 2012;Chapter 30:Unit 30 2 1-24.
153. Pan Z, Raftery D. Comparing and combining NMR spectroscopy and mass spectrometry in metabolomics. Anal Bioanal Chem. 2007;387(2):525-7.
154. t'Kindt R, Scheltema RA, Jankevics A, Brunker K, Rijal S, Dujardin JC, et al. Metabolomics to unveil and understand phenotypic diversity between pathogen populations. PLoS Negl Trop Dis. 2010;4(11):e904.
155. Halouska S, Zhang B, Gaupp R, Lei S, Snell E, Fenton RJ, et al. Revisiting Protocols for the NMR Analysis of Bacterial Metabolomes. J Integr OMICS. 2013;3(2):120-37.
156. Bingol K, Bruschweiler R. Two elephants in the room: new hybrid nuclear magnetic resonance and mass spectrometry approaches for metabolomics. Curr Opin Clin Nutr Metab Care. 2015;18(5):471-7.
157. Kim IY, Suh SH, Lee IK, Wolfe RR. Applications of stable, nonradioactive isotope tracers in in vivo human metabolic research. Exp Mol Med. 2016;48:e203.
158. Chong M, Jayaraman A, Marin S, Selivanov V, de Atauri Carulla PR, Tennant DA, et al. Combined Analysis of NMR and MS Spectra (CANMS). Angew Chem Int Ed Engl. 2017;56(15):4140-4.
159. Peng B, Li H, Peng XX. Functional metabolomics: from biomarker discovery to metabolome reprogramming. Protein Cell. 2015;6(9):628-37.
160. Wishart DS. Metabolomics: a complementary tool in renal transplantation. Contrib Nephrol. 2008;160:76-87.
161. Ziegler A, Koch A, Krockenberger K, Grosshennig A. Personalized medicine using DNA biomarkers: a review. Hum Genet. 2012;131(10):1627-38.
162. Serkova N, Fuller TF, Klawitter J, Freise CE, Niemann CU. H-NMR-based metabolic signatures of mild and severe ischemia/reperfusion injury in rat kidney transplants. Kidney Int. 2005;67(3):1142-51.
163. Foxall PJ, Mellotte GJ, Bending MR, Lindon JC, Nicholson JK. NMR spectroscopy as a novel approach to the monitoring of renal transplant function. Kidney Int. 1993;43(1):234-45.
164. Hauet T, Gibelin H, Godart C, Eugene M, Carretier M. Kidney retrieval conditions influence damage to renal medulla: evaluation by proton nuclear magnetic resonance (NMR) pectroscopy. Clin Chem Lab Med. 2000;38(11):1085-92.
165. Kostidis S, Bank JR, Soonawala D, Nevedomskaya E, van Kooten C, Mayboroda OA, et al. Urinary metabolites predict prolonged duration of delayed graft function in DCD kidney transplant recipients. Am J Transplant. 2019;19(1):110-22.
166. Rush D, Somorjai R, Deslauriers R, Shaw A, Jeffery J, Nickerson P. Subclinical rejection--a potential surrogate marker for chronic rejection--may be diagnosed by protocol biopsy or urine spectroscopy. Ann Transplant. 2000;5(2):44-9.
167. Blydt-Hansen TD, Sharma A, Gibson IW, Mandal R, Wishart DS. Urinary metabolomics for noninvasive detection of borderline and acute T cell-mediated rejection in children after kidney transplantation. Am J Transplant. 2014;14(10):2339-49.
168. Sowemimo-Coker SO. Red blood cell hemolysis during processing. Transfusion medicine reviews. 2002;16(1):46-60.
169. Yucel D, Dalva K. Effect of in vitro hemolysis on 25 common biochemical tests. Clinical chemistry. 1992;38(4):575-7.
170. Yin P, Peter A, Franken H, Zhao X, Neukamm SS, Rosenbaum L, et al. Preanalytical aspects and sample quality assessment in metabolomics studies of human blood. Clinical chemistry. 2013;59(5):833-45.
171. Hene RJ, van der Grond J, Boer WH, Mali WP, Koomans HA. Pre-transplantation assessment of renal viability with 31P magnetic resonance spectroscopy. Kidney Int. 1994;46(6):1694-9.
172. Bon D, Billault C, Thuillier R, Hebrard W, Boildieu N, Celhay O, et al. Analysis of perfusates during hypothermic machine perfusion by NMR spectroscopy: a potential tool for predicting kidney graft outcome. Transplantation. 2014;97(8):810-6.
173. Guy AJ, Nath J, Cobbold M, Ludwig C, Tennant DA, Inston NG, et al. Metabolomic analysis of perfusate during hypothermic machine perfusion of human cadaveric kidneys. Transplantation. 2015;99(4):754-9.
174. Nath J, Guy A, Smith TB, Cobbold M, Inston NG, Hodson J, et al. Metabolomic perfusate analysis during kidney machine perfusion: the pig provides an appropriate model for human studies. PLoS One. 2014;9(12):e114818.

175. Nath J, Smith T, Hollis A, Ebbs S, Canbilen SW, Tennant DA, et al. (13)C glucose labelling studies using 2D NMR are a useful tool for determining ex vivo whole organ metabolism during hypothermic machine perfusion of kidneys. Transplant Res. 2016;5:7.
176. Bohra R, Klepacki J, Klawitter J, Klawitter J, Thurman JM, Christians U. Proteomics and metabolomics in renal transplantation-quo vadis? Transpl Int. 2013;26(3):225-41.
177. Ludwig C, Gunther UL. MetaboLab--advanced NMR data processing and analysis for metabolomics. BMC Bioinformatics. 2011;12:366.
178. Delaglio F, Grzesiek S, Vuister GW, Zhu G, Pfeifer J, Bax A. NMRPipe: a multidimensional spectral processing system based on UNIX pipes. J Biomol NMR. 1995;6(3):277-93.
179. Kazimierczuk K, Orekhov VY. Accelerated NMR spectroscopy by using compressed sensing. Angew Chem Int Ed Engl. 2011;50(24):5556-9.
180. Orekhov VY, Jaravine VA. Analysis of non-uniformly sampled spectra with multi-dimensional decomposition. Prog Nucl Magn Reson Spectrosc. 2011;59(3):271-92.
181. Smith SA, Levante TO, Meier BH, Ernst RR. Computer Simulations in Magnetic Resonance. An Object-Oriented Programming Approach. Journal of Magnetic Resonance, Series A. 1994;106(1):75-105.
182. Wishart DS, Tzur D, Knox C, Eisner R, Guo AC, Young N, et al. HMDB: the Human Metabolome Database. Nucleic Acids Res. 2007;35(Database issue):D521-6.
183. Hiller K, Hangebrauk J, Jager C, Spura J, Schreiber K, Schomburg D. MetaboliteDetector: comprehensive analysis tool for targeted and nontargeted GC/MS based metabolome analysis. Anal Chem. 2009;81(9):3429-39.
184. Hissin PJ, Hilf R. A fluorometric method for determination of oxidized and reduced glutathione in tissues. Anal Biochem. 1976;74(1):214-26.
185. Smith TB, Patel K, Munford H, Peet A, Tennant DA, Jeeves M, et al. High-Speed Tracer Analysis of Metabolism (HS-TrAM). Wellcome Open Res. 2018;3:5.
186. Patel K, Nath J, Hodson J, Inston N, Ready A. Outcomes of donation after circulatory death kidneys undergoing hypothermic machine perfusion following static cold storage: A UK population-based cohort study. American Journal of Transplantation. 2018;18(6):1408-14.
187. Kox J, Moers C, Monbaliu D, Strelniece A, Treckmann J, Jochmans I, et al. The Benefits of Hypothermic Machine Preservation and Short Cold Ischemia Times in Deceased Donor Kidneys. Transplantation. 2018;102(8):1344-50.
188. Kootstra G, van Heurn E. Non-heartbeating donation of kidneys for transplantation. Nat Clin Pract Nephrol. 2007;3(3):154-63.
189. Watson C. CArdiac Death kidney Machine Perfusion trial 2011 [28/03/2019]. Available from: http://www.isrctn.com/ISRCTN50082383.
190. Yarlagadda SG, Coca SG, Garg AX, Doshi M, Poggio E, Marcus RJ, et al. Marked variation in the definition and diagnosis of delayed graft function: a systematic review. Nephrol Dial Transplant. 2008;23(9):2995-3003.
191. Nicholson ML, Wheatley TJ, Horsburgh T, Edwards CM, Veitch PS, Bell PR. The relative influence of delayed graft function and acute rejection on renal transplant survival. Transpl Int. 1996;9(4):415-9.
192. Koning OH, van Bockel JH, van der Woude FJ, Persijn GG, Hermans J, Ploeg RJ. Risk factors for delayed graft function in University of Wisconsin solution preserved kidneys from multiorgan donors. European Multicenter Study Group on Organ Preservation. Transplant Proc. 1995;27(1):752-3.
193. Boom H, Mallat MJ, de Fijter JW, Zwinderman AH, Paul LC. Delayed graft function influences renal function, but not survival. Kidney Int. 2000;58(2):859-66.
194. Zeraati AA, Naghibi M, Kianoush S, Ashraf H. Impact of slow and delayed graft function on kidney graft survival between various subgroups among renal transplant patients. Transplant Proc. 2009;41(7):2777-80.
195. Cosio FG, Pelletier RP, Falkenhain ME, Henry ML, Elkhammas EA, Davies EA, et al. Impact of acute rejection and early allograft function on renal allograft survival. Transplantation. 1997;63(11):1611-5.
196. Barry JM, Shively N, Hubert B, Hefty T, Norman DJ, Bennett WM. Significance of delayed graft function in cyclosporine-treated recipients of cadaver kidney transplants. Transplantation. 1988;45(2):346-8.
197. Turkowski-Duhem A, Kamar N, Cointault O, Lavayssiere L, Ribes D, Esposito L, et al. Predictive factors of anemia within the first year post renal transplant. Transplantation. 2005;80(7):903-9.
198. Benson K, Hartz AJ. A comparison of observational studies and randomized, controlled trials. Am J Ophthalmol. 2000;130(5):688.
199. Concato J, Shah N, Horwitz RI. Randomized, controlled trials, observational studies, and the hierarchy of research designs. N Engl J Med. 2000;342(25):1887-92.
200. Gill J, Dong J, Eng M, Landsberg D, Gill JS. Pulsatile perfusion reduces the risk of delayed graft function in deceased donor kidney transplants, irrespective of donor type and cold ischemic time. Transplantation. 2014;97(6):668-74.
201. Hosgood SA, Mohamed IH, Bagul A, Nicholson ML. Hypothermic machine perfusion after static cold storage does not improve the preservation condition in an experimental porcine kidney model. Br J Surg. 2011;98(7):943-50.
202. Matos ACC, Requiao Moura LR, Borrelli M, Nogueira M, Clarizia G, Ongaro P, et al. Impact of machine perfusion after long static cold storage on delayed graft function incidence and duration and time to hospital discharge. Clinical Transplantation. 2018;32(1):e13130.
203. Arrhenius S. Quantitative Laws in Biological Chemistry. 1st ed. London: G. Bell; 1915 1915.

204. Lindell SL, Muir H, Brassil J, Mangino MJ. Hypothermic Machine Perfusion Preservation of the DCD Kidney: Machine Effects. J Transplant. 2013;2013:802618.
205. Pereira-Sampaio MA, Favorito LA, Sampaio FJ. Pig kidney: anatomical relationships between the intrarenal arteries and the kidney collecting system. Applied study for urological research and surgical training. J Urol. 2004;172(5 Pt 1):2077-81.
206. Khamanarong K, Prachaney P, Utraravichien A, Tong-Un T, Sripaoraya K. Anatomy of renal arterial supply. Clin Anat. 2004;17(4):334-6.
207. Lunney JK. Advances in swine biomedical model genomics. Int J Biol Sci. 2007;3(3):179-84.
208. Hannon JP, Bossone CA, Wade CE. Normal physiological values for conscious pigs used in biomedical research. Lab Anim Sci. 1990;40(3):293-8.
209. Merrifield CA, Lewis M, Claus SP, Beckonert OP, Dumas ME, Duncker S, et al. A metabolic system-wide characterisation of the pig: a model for human physiology. Mol Biosyst. 2011;7(9):2577-88.
210. Nielsen KL, Hartvigsen ML, Hedemann MS, Laerke HN, Hermansen K, Bach Knudsen KE. Similar metabolic responses in pigs and humans to breads with different contents and compositions of dietary fibers: a metabolomics study. Am J Clin Nutr. 2014;99(4):941-9.
211. Gallinat A, Paul A, Efferz P, Luer B, Kaiser G, Wohlschlaeger J, et al. Hypothermic reconditioning of porcine kidney grafts by short-term preimplantation machine perfusion. Transplantation. 2012;93(8):787-93.
212. Darius T, Gianello P, Vergauwen M, Mourad N, Buemi A, De Meyer M, et al. The effect on early renal function of various dynamic preservation strategies in a preclinical pig ischemia-reperfusion autotransplant model. Am J Transplant. 2019;19(3):752-62.
213. Minor T, Paul A, Efferz P, Wohlschlaeger J, Rauen U, Gallinat A. Kidney transplantation after oxygenated machine perfusion preservation with Custodiol-N solution. Transplant International. 2015;28(9):1102-8.
214. Kaths JM, Cen JY, Chun YM, Echeverri J, Linares I, Ganesh S, et al. Continuous Normothermic Ex Vivo Kidney Perfusion Is Superior to Brief Normothermic Perfusion Following Static Cold Storage in Donation After Circulatory Death Pig Kidney Transplantation. American Journal of Transplantation. 2017;17(4):957-69.
215. He N, Li JH, Jia JJ, Xu KD, Zhou YF, Jiang L, et al. Hypothermic Machine Perfusion's Protection on Porcine Kidney Graft Uncovers Greater Akt-Erk Phosphorylation. Transplantation Proceedings. 2017;49(8):1923-9.
216. Metcalfe MS, Waller JR, Hosgood SA, Shaw M, Hassanein W, Nicholson ML. A paired study comparing the efficacy of renal preservation by normothermic autologous blood perfusion and hypothermic pulsatile perfusion. Transplant Proc. 2002;34(5):1473-4.
217. Sachs DH. The pig as a potential xenograft donor. Vet Immunol Immunopathol. 1994;43(1-3):185-91.
218. Hayes JD, Flanagan JU, Jowsey IR. Glutathione transferases. Annu Rev Pharmacol Toxicol. 2005;45:51-88.
219. Patel K, Smith TB, Neil DAH, Thakker A, Tsuchiya Y, Higgs EB, et al. The Effects of Oxygenation on Ex Vivo Kidneys Undergoing Hypothermic Machine Perfusion. Transplantation. 2019;103(2):314-22.
220. Nath J, Smith TB, Patel K, Ebbs SR, Hollis A, Tennant DA, et al. Metabolic differences between cold stored and machine perfused porcine kidneys: A (1)H NMR based study. Cryobiology. 2017;74:115-20.
221. Hosgood SA, Nicholson HF, Nicholson ML. Oxygenated kidney preservation techniques. Transplantation. 2012;93(5):455-9.
222. O'Callaghan JM, Pall KT, Pengel LHM, Consortium for Organ preservation in E. Supplemental oxygen during hypothermic kidney preservation: A systematic review. Transplant Rev (Orlando). 2017;31(3):172-9.
223. Gallinat A, Paul A, Efferz P, Luer B, Swoboda S, Hoyer D, et al. Role of oxygenation in hypothermic machine perfusion of kidneys from heart beating donors. Transplantation. 2012;94(8):809-13.
224. Thuillier R, Allain G, Celhay O, Hebrard W, Barrou B, Badet L, et al. Benefits of active oxygenation during hypothermic machine perfusion of kidneys in a preclinical model of deceased after cardiac death donors. J Surg Res. 2013;184(2):1174-81.
225. Suszynski TM, Rizzari MD, Scott WE, 3rd, Tempelman LA, Taylor MJ, Papas KK. Persufflation (or gaseous oxygen perfusion) as a method of organ preservation. Cryobiology. 2012;64(3):125-43.
226. Treckmann J, Nagelschmidt M, Minor T, Saner F, Saad S, Paul A. Function and quality of kidneys after cold storage, machine perfusion, or retrograde oxygen persufflation: results from a porcine autotransplantation model. Cryobiology. 2009;59(1):19-23.
227. Treckmann JW, Paul A, Saad S, Hoffmann J, Waldmann KH, Broelsch CE, et al. Primary organ function of warm ischaemically damaged porcine kidneys after retrograde oxygen persufflation. Nephrol Dial Transplant. 2006;21(7):1803-8.
228. Hendry WF, Struthers NW, Duguid WP, Hopkinson WI. Twenty-four-hour storage of kidneys. Lancet. 1968;1(7554):1221-5.
229. Snell ME, Hopkinson WI. Studies on the preservation of kidneys under hyperbaric oxygen after significant warm ischemia. Transplant Proc. 1974;6(3):275-7.
230. Ravaioli M, Baldassare M, Vasuri F, Pasquinelli G, Laggetta M, Valente S, et al. Strategies to Restore Adenosine Triphosphate (ATP) Level After More than 20 Hours of Cold Ischemia Time in Human Marginal Kidney Grafts. Ann Transplant. 2018;23:34-44.
231. Hoyer DP, Gallinat A, Swoboda S, Wohlschlager J, Rauen U, Paul A, et al. Subnormothermic machine perfusion for preservation of porcine kidneys in a donation after circulatory death model. Transpl Int. 2014;27(10):1097-106.

232. Thuillier R, Dutheil D, Trieu MT, Mallet V, Allain G, Rousselot M, et al. Supplementation with a new therapeutic oxygen carrier reduces chronic fibrosis and organ dysfunction in kidney static preservation. Am J Transplant. 2011;11(9):1845-60.
233. Fontes P, Lopez R, van der Plaats A, Vodovotz Y, Minervini M, Scott V, et al. Liver preservation with machine perfusion and a newly developed cell-free oxygen carrier solution under subnormothermic conditions. Am J Transplant. 2015;15(2):381-94.
234. Wijermars LG, Schaapherder AF, de Vries DK, Verschuren L, Wust RC, Kostidis S, et al. Defective postreperfusion metabolic recovery directly associates with incident delayed graft function. Kidney Int. 2016;90(1):181-91.
235. Minor T, Sitzia M, Dombrowski F. Kidney transplantation from non-heart-beating donors after oxygenated low-flow machine perfusion preservation with histidine-tryptophan-ketoglutarate solution. Transpl Int. 2005;17(11):707-12.
236. Buchs JB, Lazeyras F, Ruttimann R, Nastasi A, Morel P. Oxygenated hypothermic pulsatile perfusion versus cold static storage for kidneys from non heart-beating donors tested by in-line ATP resynthesis to establish a strategy of preservation. Perfusion. 2011;26(2):159-65.
237. Stuehr DJ. Enzymes of the L-arginine to nitric oxide pathway. J Nutr. 2004;134(10 Suppl):2748S-51S; discussion 65S-67S.
238. Kellum JA, Fuhrman DY. The handwriting is on the wall: there will soon be a drug for AKI. Nat Rev Nephrol. 2019;15(2):65-6.
239. 2019 [30/03/2019]. Available from: http://cope-eu.com/work%20programme/trials.html.
240. Patel K, Smith TB, Neil DA, Thakker A, Tsuchiya Y, Higgs EB, et al. The effects of oxygenation on ex vivo kidneys undergoing Hypothermic Machine Perfusion. Transplantation. 2018.
241. de Vries B, Snoeijs MG, von Bonsdorff L, Ernest van Heurn LW, Parkkinen J, Buurman WA. Redox-active iron released during machine perfusion predicts viability of ischemically injured deceased donor kidneys. Am J Transplant. 2006;6(11):2686-93.
242. McMahon BA, Koyner JL, Murray PT. Urinary glutathione S-transferases in the pathogenesis and diagnostic evaluation of acute kidney injury following cardiac surgery: a critical review. Curr Opin Crit Care. 2010;16(6):550-5.
243. Schmidt-Ott KM, Mori K, Kalandadze A, Li JY, Paragas N, Nicholas T, et al. Neutrophil gelatinase-associated lipocalin-mediated iron traffic in kidney epithelia. Curr Opin Nephrol Hypertens. 2006;15(4):442-9.
244. Mori K, Lee HT, Rapoport D, Drexler IR, Foster K, Yang J, et al. Endocytic delivery of lipocalin-siderophore-iron complex rescues the kidney from ischemia-reperfusion injury. J Clin Invest. 2005;115(3):610-21.
245. Haase-Fielitz A, Bellomo R, Devarajan P, Bennett M, Story D, Matalanis G, et al. The predictive performance of plasma neutrophil gelatinase-associated lipocalin (NGAL) increases with grade of acute kidney injury. Nephrol Dial Transplant. 2009;24(11):3349-54.
246. Jochmans I, Lerut E, van Pelt J, Monbaliu D, Pirenne J. Circulating AST, H-FABP, and NGAL are early and accurate biomarkers of graft injury and dysfunction in a preclinical model of kidney transplantation. Ann Surg. 2011;254(5):784-91; discussion 91-2.
247. Parikh CR, Hall IE, Bhangoo RS, Ficek J, Abt PL, Thiessen-Philbrook H, et al. Associations of Perfusate Biomarkers and Pump Parameters With Delayed Graft Function and Deceased Donor Kidney Allograft Function. Am J Transplant. 2016;16(5):1526-39.
248. MRC guidelines for good clinical practice in clinical trials. London: Medical Research Council; 1998.
249. Buescher JM, Antoniewicz MR, Boros LG, Burgess SC, Brunengraber H, Clish CB, et al. A roadmap for interpreting (13)C metabolite labeling patterns from cells. Curr Opin Biotechnol. 2015;34:189-201.
250. Hall IE. Can Preservation Fluid Biomarkers Predict Delayed Graft Function in Transplanted Kidneys? Clinical journal of the American Society of Nephrology : CJASN. 2017;12(5):715-7.
251. Gomez-Dos-Santos V, Ramos-Munoz E, Garcia-Bermejo ML, Ruiz-Hernandez M, Rodriguez-Serrano EM, Saiz-Gonzalez A, et al. MicroRNAs in Kidney Machine Perfusion Fluid as Novel Biomarkers for Graft Function. Normalization Methods for miRNAs Profile Analysis. Transplant Proc. 2019;51(2):307-10.
252. Hoyer DP, Gallinat A, Swoboda S, Wohlschlaeger J, Rauen U, Paul A, et al. Influence of oxygen concentration during hypothermic machine perfusion on porcine kidneys from donation after circulatory death. Transplantation. 2014;98(9):944-50.
253. Kaisar M, van Dullemen L, Charles P, Akhtar ZM, Thezenas ML, Huang H, et al. Subclinical Changes in Deceased Donor Kidney Proteomes Are Associated With 12-month Allograft Function Posttransplantation-A Preliminary Study. Transplantation. 2019;103(2):323-8.
254. Aida L. Alexis Carrel (1873-1944): visionary vascular surgeon and pioneer in organ transplantation. J Med Biogr. 2014;22(3):172-5.
255. Carrel A. The Preservation of Tissues and its Applications in Surgery. JAMA. 1912;LIX(7):523-7.
256. Kasil A, Giraud S, Couturier P, Amiri A, Danion J, Donatini G, et al. Individual and Combined Impact of Oxygen and Oxygen Transporter Supplementation during Kidney Machine Preservation in a Porcine Preclinical Kidney Transplantation Model. Int J Mol Sci. 2019;20(8).
257. Antoine C, Savoye E, Gaudez F, Cheisson G, Badet L, Videcoq M, et al. Kidney transplant from uncontrolled donation after circulatory death: contribution of normothermic regional perfusion. Transplantation. 2019.

258. Blum MF, Liu Q, Soliman B, Dreher P, Okamoto T, Poggio ED, et al. Comparison of normothermic and hypothermic perfusion in porcine kidneys donated after cardiac death. The Journal of surgical research. 2017;216:35-45.
259. Weissenbacher A, Lo Faro L, Boubriak O, Soares MF, Roberts IS, Hunter JP, et al. Twenty-four–hour normothermic perfusion of discarded human kidneys with urine recirculation. American Journal of Transplantation. 2019;19(1):178-92.
260. Pool M, Leuvenink H, Moers C. Reparative and Regenerative Effects of Mesenchymal Stromal Cells-Promising Potential for Kidney Transplantation? Int J Mol Sci. 2019;20(18).
261. Liu L, Yu Y, Hou Y, Chai J, Duan H, Chu W, et al. Human umbilical cord mesenchymal stem cells transplantation promotes cutaneous wound healing of severe burned rats. PLoS One. 2014;9(2):e88348.
262. Luo G, Cheng W, He W, Wang X, Tan J, Fitzgerald M, et al. Promotion of cutaneous wound healing by local application of mesenchymal stem cells derived from human umbilical cord blood. Wound repair and regeneration : official publication of the Wound Healing Society [and] the European Tissue Repair Society. 2010;18(5):506-13.
263. Watt SM, Gullo F, van der Garde M, Markeson D, Camicia R, Khoo CP, et al. The angiogenic properties of mesenchymal stem/stromal cells and their therapeutic potential. British medical bulletin. 2013;108:25-53.
264. Baulier E, Favreau F, Le Corf A, Jayle C, Schneider F, Goujon JM, et al. Amniotic fluid-derived mesenchymal stem cells prevent fibrosis and preserve renal function in a preclinical porcine model of kidney transplantation. Stem Cells Transl Med. 2014;3(7):809-20.